INFORMATION TO USERS

This manuscript has been reproduced from the microfilm master. UMI films the text directly from the original or copy submitted. Thus, some thesis and dissertation copies are in typewriter face, while others may be from any type of computer printer.

The quality of this reproduction is dependent upon the quality of the copy submitted. Broken or indistinct print, colored or poor quality illustrations and photographs, print bleedthrough, substandard margins, and improper alignment can adversely affect reproduction.

In the unlikely event that the author did not send UMI a complete manuscript and there are missing pages, these will be noted. Also, if unauthorized copyright material had to be removed, a note will indicate the deletion.

Oversize materials (e.g., maps, drawings, charts) are reproduced by sectioning the original, beginning at the upper left-hand corner and continuing from left to right in equal sections with small overlaps.

ProQuest Information and Learning
300 North Zeeb Road, Ann Arbor, MI 48106-1346 USA
800-521-0600

THE SIGNIFICANCE OF THE CRITICAL POTENTIAL IN THE KOLBE REACTION

BY

B. E. CONWAY and M. DZIECIUCH

Reprinted from Proceedings of the Chemical Society
March 1962, page 121

LONDON:
THE CHEMICAL SOCIETY
BURLINGTON HOUSE, W.1

(*Reprinted from Nature, Vol.* 189, *No.* 4768, *pp.* 914–915, *March* 18, 1961)

Delayed Gas Evolution from Passive Films formed in the Kolbe Reaction

DURING the course of electrochemical kinetic studies on the Kolbe reaction, we have observed a remarkable phenomenon, the details of which are recorded here. The classical Kolbe reaction involves the anodic electrolytic synthesis of hydrocarbons from solutions of salts of appropriate aliphatic carboxylic acids. As a model system for preliminary investigations of the electrochemical kinetics of this reaction, we have examined the anodic reaction which occurs in the electrolysis of a solution of potassium formate in pure anhydrous formic acid; in this case 1 mole of carbon dioxide is evolved in the passage of two Faradays.

During steady-state electrolysis of the above solution at platinum, gold and palladium electrodes, the only gas evolved is carbon dioxide. The overall reaction is hence formally[1]:

$$2HCOO^- \rightarrow HCOOH + CO_2 + 2e$$

On interrupting the current at platinum and gold electrodes, the gas evolution ceases immediately in the normal way. However, on interrupting the current at a palladium electrode, the gas evolution initially ceases, but is then followed by a further burst of gas from the surface after a delay period of up to 5 sec., this gas evolution occurring in the complete absence of current-flow. The effect at palladium is quite reproducible and is best observed at a current density greater than 10^{-1} amp./cm.^{2} in 5-*M* solutions of potassium formate in formic acid (pre-saturated

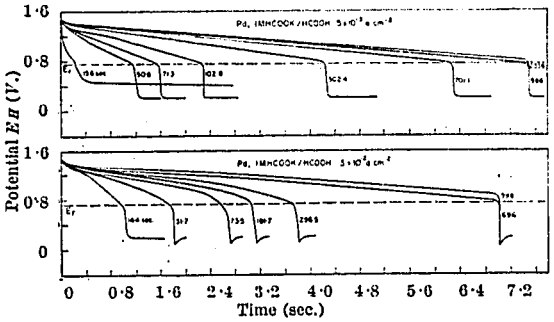

Fig. 1. Open-circuit e.m.f. decay curves taken on an oscilloscope at two current densities of prior polarization for the indicated times (sec.).

with carbon dioxide) at 5° C. Although carbon dioxide is evolved at platinum and gold with the same current efficiency (about 90 per cent) as at palladium, the delayed gas evolution is not observed, and the effect hence arises from some property of the palladium anode. No hydrogen is evolved as might be expected by analogy with the coupling reaction occurring with acetic and other aliphatic acids, but this is understandable since any H radicals generated by the anodic decarboxylation will ionize rapidly at a rate of at least 10^{10} amp./cm.^{2} at the high anodic potentials (about 1·2 V. with respect to the hydrogen electrode in the same acid solution) required for significant rates of electrolysis of the formic acid. Hence it is improbable that hydrogen produced in the decarboxylation step and taken up into the surface regions of the palladium is responsible for the effect, and in fact the coulombic yields of carbon dioxide gas by continuous and repeatedly interrupted polarization are identical within experimental error and no hydrogen is detectable by chemical or gas chromatographic means under either set of conditions of polarization.

Rapid ciné-photography of the palladium surface with a simultaneous recording of the moment when current stops flowing has enabled the delay-times in gas evolution in interrupted polarization experiments to be measured with some precision to about 0·1 sec. The delay-time in the gas evolution after the current stops is found to be a function of the time of previous anodic electrolysis up to periods of about 5 min. This suggests that the anodic electrolysis

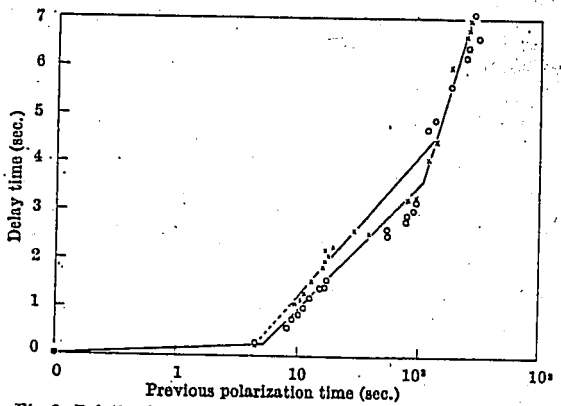

Fig. 2. Relationship of both the delay in open-circuit gas evolution (from ciné photography) and the potential delay to the period of prior anodic polarization at 10^{-2} amp./cm.$^{-2}$. O, delayed gas evolution; ×, potential delay; 5 *M* HCOOK/HCOOH

forms a relatively thick film of a surface palladium formate (possibly non-stoichiometric[2,3]) at the electrode, and, after net current ceases to flow, this film breaks down auto-catalytically with evolution of carbon dioxide. The formation of this film appears to be analogous to that of passive films formed anodically, for example, in aqueous solutions at nickel and iron. Determinations of the galvanostatic charging and open-circuit decay curves, using a cathode ray oscilloscope, for the polarized palladium and platinum electrodes indicate the formation of surface films as shown in Fig. 1. The pseudo-capacity associated with the film at palladium is much greater (10–50 times) than that at platinum; and this is evidently the reason why the delayed decomposition is observable at the former metal although it may still occur but not be visible at platinum or gold. We believe that the effect is larger at palladium than at the other metals since palladium is less noble than gold or platinum, so that palladium has a greater susceptibility to anodic oxidation. The delay in the open-circuit decay trace of e.m.f. as a function of time is found to depend on the time of previous anodic polarization, as also observed with the delay in visible gas evolution on open-circuit. The delay in the e.m.f. decay curve, in fact, is directly related to the delay in the open circuit gas evolution as shown in Fig. 2; both effects appear to be related to the thickness of the anodically formed layer. Less spectacular self-discharge effects with non-delayed evolution of oxygen occurring over much longer periods of time are known in oxide electrode systems and have been treated in detail in some of our previous papers[2–4]. Visible delayed gas evolution effects are not observed when the true Kolbe coupling reaction is proceeding, for example, in the electrolysis of trifluoroacetic acid, although galvanostatic charging curves again indicate formation of surface films but of thicknesses much less than those found at palladium in the formic acid solutions.

B. E. Conway
M. Dzieciuch

Department of Chemistry,
University of Ottawa,
Ottawa, Ontario.

[1] Baur, E., *Helv. Chim. Acta*, 11, 372 (1928).
[2] Conway, B. E., and Bourgault, P. L., *Can. J. Chem.*, 37, 292 (1959).
[3] Bourgault, P. L., and Conway, B. E., *ibid.*, 38, 1557 (1960).
[4] Bourgault, P. L., and Conway, B. E., *J. Electroanalytical Chem.*, 1, 8 (1959).

Printed in Great Britain by Fisher, Knight & Co., Ltd., St. Albans.

Reprinted from Proceedings of the Chemical Society, March, 1962, page 121

The Significance of the Critical Potential in the Kolbe Reaction

By B. E. Conway and M. Dzieciuch

(Department of Chemistry, University of Ottawa, Ottawa, Canada)

The yield of Kolbe products R_2 from an aliphatic acid $R{\cdot}CO_2H$ has been found[1–3] to be a critical function of potential, and the reaction occurs significantly only above a certain limiting value of the electrode potential, *e.g.*, that for appreciable rates of oxygen evolution[1,2] in the absence of the carboxylic acid. The exact significance of these potentials has been little discussed.

We have found that at platinum, gold, or palladium in pure anhydrous trifluoroacetic acid containing potassium trifluoroacetate as electrolyte and saturated with carbon dioxide, high Faradaic yields (96%) are obtained of the Kolbe coupled product C_2F_6 (cf. ref. 4) and no detectable oxygen evolution. This reaction is thus specially suitable for quantitative electrochemical kinetic study. Current–potential curves (see Fig. 1) indicate that a critical potential is

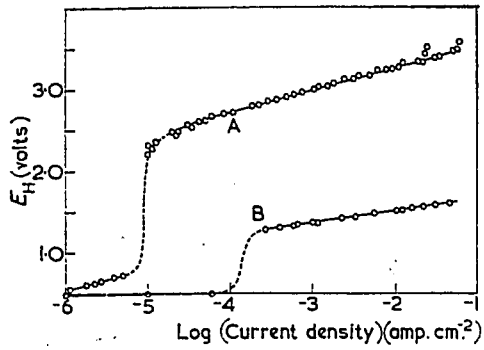

Fig. 1. *Current–potential curves (Tafel lines) for anodic polarisation of the platinum electrode in* (A) M-$CF_3{\cdot}CO_2K$ *in pure* $CF_3{\cdot}CO_2H$ (b = 0·26) *and* (B) M-$H{\cdot}CO_2K$ *in pure* $H{\cdot}CO_2H$ (b = 0·14), *at* 5°.

reached at a limiting current density of about 10^{-5} a. cm.$^{-2}$ in N-potassium trifluoroacetate in pure trifluoroacetic acid, and 10^{-4} a. cm.$^{-2}$ in N-potassium formate in pure formic acid or in water. The significance of the break in the curve and of the associated critical potential has been examined by the observation of galvanostatic potential transients on anodic polarisation and reverse cathodic discharge (Fig. 2). Both types of measurements indicate the formation of a surface film of intermediates. The charge associated with the arrest region in Fig. 2 corresponds, for a one-electron transfer, to formation of a layer having a fractional coverage of 0·3—0·1 (based on true surface area[5]) depending upon current density. The pseudo-capacity of the film at platinum varies from about 30 to 125 μF cm.$^{-2}$ depending on current density. Films of 10—100 molecular layers are formed at palladium (depending on the time of previous polarisation) when anodic decarboxylation of formate ions in formic acid is occurring, and pseudo-capacities are between 700 and 4300 μF cm.$^{-2}$; similar current–potential curves are observed (Fig. 1). The inflections in Figs. 1 and 2 are not due to depolarisers and are also observed in anodic oxide film formation, *e.g.*, in passivation of metals (cf. the Flade potential). We suggest, therefore, that the critical potentials previously mentioned

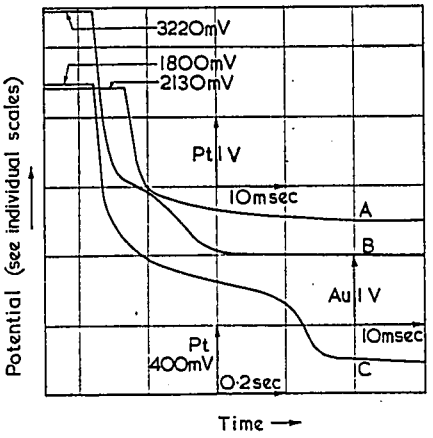

Fig. 2. *Galvanostatic cathodic discharge curves following prior anodic polarisation for the indicated conditions*: (A) Pt,M-$CF_3{\cdot}CO_2K$–$CH_3{\cdot}CO_2H$, 6·1 × 10^{-3} a. cm.$^{-2}$, 310 *sec. anodic, followed by cathodic transient.* (B) Au,M-$CF_3{\cdot}CO_2K$–$CF_3{\cdot}CO_2H$, 7·2 × 10^{-3} a. cm.$^{-2}$, 304 *sec. anodic, etc.*; (C) Pd,M-$H{\cdot}CO_2K$–$H{\cdot}CO_2H$, 5·9 × 10^{-3} a. cm.$^{-2}$, 314 *sec. anodic, etc.*

involve formation of passive films of a metal "carboxylate" on the electrode and that the transition region in Figs. 1 and 2 corresponds to formation and removal,[6] respectively, of this film which is then a pre-

[1] Glasstone and Hickling, *J.*, 1934, 1878; 1936, 820.
[2] Pande and Shukla, *Electrochim. Acta*, 1961, 4, 215.
[3] Preuner and Ludlam, *Z. phys. Chem.*, 1907, 59, 682; Shukla and Walker, *Trans. Faraday Soc.*, 1931, 27, 727; Vasilev *Doklady Akad. Nauk U.S.S.R.*, 1960, 134, 879.
[4] Swarts, *Bull. Soc. chim. belges*, 1933, 42, 102.
[5] Bockris and Conway, *J. Chem. Phys.*, 1958, 28, 707.
[6] Conway and Dzieciuch, *Nature*, 1961, 189, 914.

requisite for subsequent steady-state occurrence of the Kolbe decarboxylation, but it must be noted that $C_2F_6^{\cdot}$ is still a product of the reaction below the transition region. The critical potentials are observed in aqueous as well as non-aqueous formate and trifluoroacetate solutions and are hence not related to a critical condition for discharge of hydroxyl from water or OH^- ions to form hydrogen peroxide[1] or alkyl oxidation products. Also, since the anodic reaction in aqueous formate solution is only a decarboxylation, the critical potential is not itself specially related to hydrocarbon formation in the coupling reaction.

Calculations of the relevant reversible potentials for decarboxylation of aqueous formic and acetic acid show that the critical potentials cannot be identified with the corresponding reversible potentials and in fact exceed them by some 0·6—1·0v.

(*Received, December 16th*, 1961.)

SC

NEW APPROACHES TO THE STUDY OF ELECTROCHEMICAL DECARBOXYLATION AND THE KOLBE REACTION

by

Matthew A. Dzieciuch

A thesis submitted in partial fulfillment
of the requirements for the degree of
Doctor of Philosophy in the
Department of Chemistry, University of Ottawa,
Ottawa, Canada.

Matthew A. Dzieciuch
Candidate

B.E. Conway
Professor of Chemistry
Research Supervisor.

October, 1962.

TABLE OF CONTENTS

CHAPTER III - RESULTS

PREFACE

The present work was undertaken in order to attempt to elucidate some aspects of the electrochemical kinetics and mechanism of the Kolbe reaction and the related model reaction of formate decarboxylation which involves no coupling step. Despite numerous applications of the Kolbe reaction in synthetic organic chemistry, the reaction is outstanding in regard to the lack, in previous work, of applications of basic electrochemical methods of experimental kinetic study and of critical development of electrochemical kinetic theory in regard to the probable consecutive steps in the reaction. Previous work has been mainly characterised by attempts to explain the variety of products which are normally observed when the reaction is carried out in aqueous solution where irrelevant side oxidation reactions are observed and associated with simultaneous oxygen evolution. Very little previous work has been described where the behavior of adsorbed intermediates in the reaction has been considered although this is obviously a basic requirement in the study of such reactions where several possible radical intermediates must be involved in the consecutive steps.

In the present work, an attempt has been made to consider only simple model reactions where the electrochemical kinetics of mainly single overall reactions can be examined.

Emphasis has been made in quantitatively evaluating the electrochemical behavior in terms of current-potential curves, d.c. and open-circuit transients. These can lead, when used in appropriate complementary ways, to a quantitative elucidation of the reaction mechanism and the behavior of adsorbed intermediates including knowledge of their isotherm for adsorption at the electrode and the associated potential dependent pseudo-capacitance. These approaches are supported by a detailed theoretical electrochemical analysis of the kinetic consequences of various reaction schemes involving intermediates adsorbed according to Langmuir or Temkin isotherms. In these respects, we claim to have carried the study of the Kolbe and the related formate decarboxylation reaction much further than has been done in previous more qualitative approaches to the problem.

A general critical introduction to the problem is presented first, followed by an examination of theories of film growth which was undertaken since the present studies involve some new aspects of growth of anodic films in non-aqueous media. A resumé of some of the experimental methods of approach which have been brought to bear on the present problem in a complementary way is then presented followed by the usual account of experimental procedures and results.

All the work described in the present thesis has been prepared for publication in seven papers (five papers and two communications). All the papers except the last listed below, which was submitted only recently, have either been published

or accepted for publication (see attached reprints, etc.) The papers resulting from the thesis are as follows:

1) The Phenomenon of Delayed Gas Evolution from Passive Films in the Kolbe Reaction, Nature, 189, 914 (1961).

2) The Significance of the Critical Potential in the Kolbe Reaction, Proc. Chem. Soc., 121 (1962).

3) New Approaches to the Study of Electrochemical Decarboxylation and the Kolbe Reaction. Part I. The Model Reaction with Formate, Can. J. Chem., Accepted for publication.

4) New Approaches to the Study of Electrochemical Decarboxylation and the Kolbe Reaction. Part II. The Model Reaction with Trifluoroacetate: Comparison with Aqueous Solution Behavior, Can. J. Chem., Accepted for publication.

5) New Approaches to the Study of Electrochemical Decarboxylation and the Kolbe Reaction. Part III. Quantitative Analysis of Decay and Discharge Transients and the Role of Adsorbed Intermediates. Can. J. Chem., Accepted for publication.

6) Theory and Analysis of Adsorption Pseudo-Capacitance Curves from E.M.F. Decay and Polarisation Curves; Applications to a Decarboxylation Reaction, (with E. Gileadi) Electrochimica Acta. Accepted for publication 1962.

7) Periodic Phenomena, Surface Coverage and Pseudo-Capacitance in Electrochemical Decarboxylation Reactions. Can. J. Chem., in course of publication.

ACKNOWLEDGMENT

The author wishes to express his deepest gratitude to Professor B.E. Conway under whose direction and constant encouragement this work was made possible. Throughout the course of the research and preparation of the thesis Professor Conway was always prepared to give freely of his time and energy to guide and assist whenever difficulties arose.

LIST OF TABLES

LIST OF FIGURES

ABSTRACT

A critical review of previous work on the Kolbe reaction is given where it is shown that very few applications of modern electrochemical techniques and no applications of recent electrochemical kinetic theory have been made previously to this reaction. No work on the electrochemical kinetics of formate decarboxylation has been carried out previously.

The kinetics of electrochemical decarboxylation of formate ions in pure anhydrous formic acid have been studied in detail for the first time as a model reaction for examination of the decarboxylation and radical coupling reactions that occur with higher aliphatic acids. Current-potential relations (Tafel slopes) have been obtained which show a sharp transition, not diffusion controlled, which is characteristic of passivation phenomena. The behavior is observed at platinum, palladium, gold and palladium-gold alloy electrodes. Tafel slopes are derived for "Langmuir" and "Temkin" conditions of surface coverage. Reversible potentials and exchange currents have been evaluated for the reaction.

Galvanostatic charging, cathodic discharge and open circuit decay transients have been obtained for the decarboxylation of formate in formic acid which indicate the formation of films and are interpreted quantitatively in terms of the adsorption of reaction intermediates on the electrode

surface. These intermediates are surmised to be $HCOO^{\bullet}$ radicals, and the transition regions in the Tafel plots are identified with the formation of this adsorbed layer. Extended anodic polarisation at platinum and particularly at palladium leads to the formation of films of an anodic product which are considerably thicker than a monolayer, but at gold the film thickness does not exceed that of a monolayer. Following relatively long times (> 100 sec.) of anodic polarisation, film growth obeys the inverse logarithmic rate law deduced by Mott and Cabrera.

During the course of the work, an interesting and evidently unique phenomenon of delayed gas evolution was discovered during studies of the formate decarboxylation reaction at palladium electrodes. The electrochemistry of this phenomenon has been studied in some detail and the delayed gas evolution is shown to be associated with attainment of a critical potential in the self-discharge process on open-circuit e.m.f. decay. The thick films formed at palladium are believed to be responsible, upon autocatalytic decomposition, for the delayed gas evolution phenomenon observed at this metal.

A new method for deduction of adsorption pseudo-capacitance and charge associated with the adsorbed layer from open-circuit decay transients and Tafel parameters is used to obtain the pseudo-capacitance and charge associated

with the transition region in the current-potential relationships for the formate decarboxylation. It is shown that this region corresponds to filling of the surface with adsorbed intermediates formed in the reaction.

Possible reaction mechanisms are proposed and are examined in relation to the observed experimental results. The galvanostatic results enable distinctions to be made between some of the possible reaction mechanisms proposed.

In the aqueous formate systems, current-potential relationships have been obtained which also exhibit transition regions; multilayer formation is indicated, including deposition of layers of different species corresponding to different potential arrest regions in the galvanostatic discharge transients. Reversible potentials and exchange currents have been evaluated for the reaction. Experimental results in the non-aqueous and aqueous formate systems are compared; It is suggested that the layers formed in the aqueous system may consist of oxide and discharged carboxylate and that the transition behavior and critical currents in the Kolbe reaction correspond to conditions for passivation of the metal by oxide and discharged carboxylate species.

Electrochemical kinetic studies on the Kolbe reaction have been carried out with potassium trifluoroacetate in trifluoroacetic acid (100%). High yields of the Kolbe product

C_2F_6 and CO_2 are obtained and current-potential plots exhibiting transition behavior and linear Tafel regions are found. Tafel slopes are deduced for "Langmuir" and "Temkin" surface coverage conditions by surface intermediates and compared with experimental results. Plausible reaction mechanisms are proposed, which are supported by galvanostatic discharge transients; the latter indicate that the coverage by adsorbed intermediates in the trifluoroacetate reaction approaches a monolayer.

CHAPTER I

INTRODUCTION

A. GENERAL

The study of electrode processes has been the subject of intensive investigation since the beginning of the 19th century when the electrolysis of water was first reported (1). Electrochemical kinetic work has been largely limited to studies of hydrogen and oxygen evolution and in recent years to metal deposition or electro-crystallisation. The broad field of electro-organic chemistry is, from an electrochemical point of view, less well developed or understood and for several of the simplest electro-organic reactions, the elementary electrochemical steps have not yet been satisfactorily formulated nor the mechanisms clearly elucidated.

The anodic decarboxylation of carboxylic acids (the Kolbe and related reactions), which is the subject of the present investigation, has been extensively studied by organic chemists interested in the synthetical applications of this reaction. On the basis of these investigations the scope and limitations of the reaction have been defined. However, in many cases, percentage yields, experimental conditions etc., have not been clearly indicated and in view of the results of more recent studies, many of the reported reactions must be reinvestigated under more rigorous electrochemical control,

e.g. of the potential and current density. Usually both electrodes were placed in solution and the products subsequently analysed; as a result, a diversity of reactions can be envisaged as occurring not only with respect to the original starting material, but also between the products at either the anode or cathode. The most important variable in the kinetics of electrode processes, the potential of the working electrode, has not often been clearly defined or controlled in this kind of work.

Electrochemical investigations have resulted in several proposals regarding the mechanisms of the reaction. However, owing to the lack of reproducible measurements and varying experimental techniques between different workers, considerable controversy has arisen amongst the proponents of the various theories.

In the present investigation, systems have been chosen in which a minimal number of side reactions can occur, so that modern electrochemical approaches can be applied to obtain information of least ambiguity on the nature of the basic electrochemical processes occurring at the metal-solution interface in these decarboxylation reactions. Previous work, to be described below, has usually been complicated by the occurrence of many simultaneous oxidation reactions which have obscured the electrochemical significance of the main decarboxylation and coupling reaction.

B. KOLBE REACTION

(a) General

The classical work of Kolbe (2) constituted the first detailed study of the anodic reaction involving carboxylic acids and their anions in which it was shown that electrolysis of an aqueous solution of an alkali metal carboxylate, led to the production of carbon dioxide and a hydrocarbon. The overall anodic reaction can be written

$$2\ RCOO^- \longrightarrow 2CO_2 + R\text{-}R + 2\ e$$

where R is an aliphatic alkyl or substituted alkyl residue. The above reaction is known as the Kolbe electrosynthesis.

This reaction has subsequently been the subject of extensive investigation and has not only been found to constitute a valuable and remarkably simple method for the synthesis of many organic compounds but also has been employed as an aid in structure determination (3,4). The reaction may be carried out in either aqueous or non-aqueous solvents not only with straight chain fatty acids, but also with half-esters of dicarboxylic acids, unsaturated acids, some aromatic acids, substituted acids and mixtures of carboxylic acids. The Kolbe electrosynthesis may hence be defined more generally as an anodic reaction involving a carboxylate structure, producing carbon dioxide together with a hydrocarbon or derivative of a hydrocarbon. As several excellent reviews and bibliographies

are available on the organic chemistry of the reaction [the reader is referred to references 5,6,7 for detailed information on the products of electrolysis of individual acids], only a brief review will be given of the more important features of the reaction, but particular emphasis will be placed on the physical chemistry involved.

Various detailed studies have been made in order to establish the optimum conditions for the formation of ethane from acetate in aqueous (8) and non-aqueous (9) solvents and the conclusions which can be drawn from these investigations are, in general, applicable to most other examples of the Kolbe reaction. In aqueous solutions, the nature of the anode is of great importance, and in previous work coupling is found to occur to an appreciable extent only with smooth platinum or iridium anodes. The reaction is also favoured by using a high current density ($> 10^{-2}$ amps.cm.$^{-2}$), a high carboxylate concentration ($>$ 1M) in an acidic medium and relatively low temperatures ($< 50^{\circ}C$). In non-aqueous solvents, conditions for optimum yields are less critical than in aqueous media; thus, the nature of the anode material, temperature and concentration have relatively little effect on the yield of coupled products under such conditions. Low current densities promote the formation of olefins and paraffins (CH_4 in the acetate case) possessing only half the number of carbon atoms required for the coupled product (10). Another side reaction

frequently encountered is the formation of alcohols. This is generally referred to as the Hofer-Moest reaction (11) and is favoured by an alkaline medium in the presence of such inorganic salts as perchlorates, bicarbonates and persulphates. Little is known about the formation of alcohols in the electrolysis of carboxylic acids. Other by-products which may be formed include esters of the starting acid with the corresponding alcohol and ketones. The extent to which side reactions occur is governed both by experimental conditions and by the structure of the acid itself.

(b) Organic Chemical Studies: Scope and Limitations

Experimentally it has been observed that there are three important limitations in the choice of reactants for synthetic applications. The three structures which suppress the Kolbe reaction are (a) α-β or β-γ unsaturation in the reactant acid (12); (b) α-alkyl substituents and cycloalkyl structures (13) and (c) aromatic groups (ArCOOH) (14). Electrolysis of compounds possessing these structures usually results in oxygen evolution as the major reaction with the production of numerous degradation (oxidation) products. The effect of unsaturation is, however, limited; thus, two or more methylene groups between the carboxyl group and the point of unsaturation removes the inhibiting effect (15, 16) and coupling proceeds normally. The inhibitory effects of

α-substituents and cycloalkyl residues, when removed to other positions in the acid molecule, exert no adverse effects (17), however, more recent investigations have shown that the Kolbe reaction with α-substituted acids is no longer adversely affected if the solvent is changed from an aqueous to a non-aqueous medium (18, 19). Similarly, with aromatic acids, if the phenyl ring is removed further than the β-position, electrolysis will give the expected Kolbe dimer (16, 19). When the phenyl ring is vicinal to the COOH group, as in benzoic acid, benzene is the main product.

Studies in non-aqueous solvents have been undertaken by numerous investigators, and the most comprehensive early work has been that by Glasstone and Hickling (9) using ethylene glycol as the solvent. The results show that current efficiencies for the production of the coupled product both in aqueous or non-aqueous solvents are similar, with values, for example, for ethane formation in acetate electrolysis only being appreciable (ca. 90%) at the highest current densities in the absence of foreign ions.

Electrolysis of several anhydrous fatty acids containing the corresponding alkali-metal salt as electrolyte has been shown to give results which are almost identical with those obtained in the corresponding aqueous solution (14, 20- 26).

(c) Electrochemical Aspects

The experimental conditions used in the earlier work

cannot be considered ideal in relation to modern techniques available for the investigation of electrode processes.

Measurements of electrode potentials over a range of current densities have been carried out by several investigators (8,25,27-29) for the acetate case and for higher homologues and plots of anode potential versus log current-density have in all cases shown breaks in the curves, corresponding to a sudden increase in the anode potential at a particular current density. Analysis of products over the current density range has shown that in acidic solutions (23-29) (for a series of alkali-metal salts and/or corresponding acids from acetic to heptanoic), the major product at low current densities was oxygen together with a variety of oxidative degradation products. As a critical current density and associated potential is approached, the yields of carbon dioxide and the Kolbe product begin to become appreciable, while the rate of production of oxygen decreases. At, and above, the critical current density, the major products were as expected for the Kolbe electrosynthesis together with negligible amounts, if any, of oxygen. In alkaline solutions, Hofer and Moest (11) have shown that methyl alcohol is formed instead of ethane during the electrolysis of acetates.

The range of critical potentials in aqueous solution lies in the region 2.1-2.2 volts (with respect to the potential of the normal hydrogen electrode). In non-aqueous solutions Glasstone and Hickling (9) have shown that the critical

potential for the electrolysis of acetates and/or acetic acid was similar to that observed (viz. 2.14 v.) for aqueous solutions (8), and that the current efficiencies for ethane production were quantitatively similar in the two types of system.

The potential at which the Kolbe electrosynthesis occurs in aqueous solution presents a seemingly anomalous situation. Oxygen evolution in aqueous acid solutions normally occurs significantly at a much lower potential (ca. 1.7 v., but the reversible potential is at 1.23 v E_H, under standard conditions) than that required for the Kolbe reaction (2.1-2.2 v.), yet in the presence of dischargeable carboxylates the Kolbe reaction occurs preferentially at higher potentials with suppression of oxygen evolution. The role of oxygen evolution has received rather little attention; qualitatively all that can at present be said is that when the Hofer-Moest reaction is occurring (basic solutions) at the anode, oxygen is one of the major products*, but when the Kolbe

---

* From a chemical kinetic point of view, this situation is actually not unexpected. When the electrochemical rate constants for the competing reactions of carboxylate ion discharge, oxygen evolution and radical coupling are such that the oxygen evolution rate and the corresponding rate of production of oxidising radicals (e.g. OH or O, which are involved in that reaction) are appreciable, any simultaneously discharged $RCOO^-$ ions will be subject to oxidation by the intermediates involved in the oxygen producing reaction, so that the normal coupling reaction will be inhibited. Thus, Hofer-Moest products will be expected as a direct result of the kinetic situation which allows under certain conditions, significant competitive rates of oxygen evolution from OH^- or H_2O in aqueous media.

reaction occurs, little, if any, oxygen is present in the mixture of reaction products. (The significance of these older observations is examined in more detail in the "Discussion"). In a theory proposed by Glasstone and Hickling (8), to be discussed in more detail below it is suggested that hydroxyl radicals (arising from the anodic discharge of OH^- ions which normally leads to oxygen evolution) combine to form hydrogen peroxide, which then reacts with the acetate ion to form either peracetic acid or acetate radicals, eventually yielding the Kolbe product.

The suggestion has also been made (34,61) that acetate ions are preferentially adsorbed on the anode surface, so that water molecules cannot approach the surface to be discharged. However, it is difficult to envisage this occurring, especially when at potentials below the critical potential for the Kolbe reaction, oxygen evolution is already a major reaction; it is hence not clear why preferential adsorption should suddenly arise at a critical current density and associated potential, leading to almost exclusive occurrence of the Kolbe reaction.

Thiessen (35) has envisaged a situation in which the anode is covered with a hydroxyl free-radical layer, acetate ions then being adsorbed on the hydroxyl radical layer. Electron transfer from the carboxyl oxygen is then regarded as occurring through the hydrogen bond formed by the hydroxyl proton and

the carboxylate oxygen; electron rearrangement then occurs and the $^{\bullet}R - CO_2$ bond cleaves to give the alkyl radical and carbon dioxide.

This mechanism is evidently not general since MOH species cannot normally arise from non-aqueous solutions where the Kolbe reaction can proceed efficiently with the same products and, as we show in the present research, also with associated critical potentials.

(d) Proposed Mechanisms

Numerous theories have been proposed for the mechanism of the Kolbe electrosynthesis, and three have received serious consideration in recent years. These will now be reviewed briefly.

i) The Acyl Peroxide Theory

This was originally proposed by Schall (36) and subsequently developed by Fichter (37,38). Initially Fichter (38), in agreement with Schall, postulated that active oxygen liberated at the anode oxidized the carboxylic acid anion which then decomposed through an acyl peroxide intermediate to give the characteristic Kolbe products. Subsequently, Fichter (37) proposed that the primary step was the discharge of the carboxylic acid anion. The resulting discharged ions were then regarded as forming a diacyl peroxide intermediate, (cf. Glasstone and Hickling (8,9)) which then decomposed with the formation of the characteristic Kolbe products. The reaction can be

written:

$$2\ RCOO^- \longrightarrow 2\ RCOO^\bullet + 2\ e$$

$$2\ RCOO^\bullet \longrightarrow R\text{-}\overset{O}{\overset{\|}{C}}\text{-}O\text{-}O\text{-}\overset{O}{\overset{\|}{C}}\text{-}R$$

$$R\text{-}\overset{O}{\overset{\|}{C}}\text{-}O\text{-}O\text{-}\overset{O}{\overset{\|}{C}}\text{-}R \longrightarrow 2\ R^\bullet + 2CO_2$$

$$R^\bullet + R^\bullet \longrightarrow R\text{-}R.$$

Side reactions were explained in terms of the hydrolysis of the intermediate diacyl peroxide and formation of the peracid, which then was considered to undergo decarboxylation forming the alcohol:

$$R\text{-}\overset{O}{\overset{\|}{C}}\text{-}O\text{-}O\text{-}\overset{O}{\overset{\|}{C}}\text{-}R + H_2O \longrightarrow RCOOH + RCOO\text{-}OH$$

$$RCOO\text{-}OH \longrightarrow ROH + CO_2$$

In alkaline media, the hydrolysis of the peroxide was regarded as the principal reaction so that the alcohol ROH could be the major product (Hofer-Moest reaction (11)). In acid solutions, it is stated, the alcohols so formed can be dehydrated to form olefins, (we believe, however, that this is chemically unlikely in the dilute acids used) or react with the free acid to form esters. It must be stated that under the experimental conditions existing during electrolysis, it is difficult to conceive how either of these reactions can occur to any appreciable extent.

Fichter (37,39) has regarded the following observations as proof of the peroxide theory: (a) the similarity of products obtained by electrolysis and by thermal decomposition of the corresponding diacyl peroxides, and (b) the formation of glycolaldehyde during the electrolysis of acetate and of monomethyl malonate, and the thermal decomposition of the corresponding diacyl peroxides in ethylene glycol solutions. The glycolaldehyde, it is stated, is formed in both cases by oxidation of ethylene glycol by diacyl peroxides.

Diacyl peroxides* are, however, known to decompose relatively slowly when present in solution at low concentrations; hence if diacyl peroxides are formed during the electrolysis reaction in the way envisaged in the work referred to above, easily detectable amounts should be present.

Numerous attempts have been made to detect the peroxide at the anode. Positive results were obtained only under very special experimental conditions (low temperatures and streaming electrolyte) when the diacyl peroxide was detected (40,41) in very small amounts.

Further, it has been shown (42,43,44) that aliphatic acyloxy radicals, resulting from the decomposition of diacyl

---

* It is desirable to distinguish between the slow decomposition of diacyl peroxides in solution and the violent explosions which occur readily with the bulk material. The latter effect arises from the sensitivity of diacyl peroxides to shock and the large amount of energy liberated per gram in their decomposition.

peroxides in solution, lose CO_2 rapidly to give alkyl radicals. Hence it is rather unlikely and inconsistent with other known radical reactions in solution (45) and the gas phase (46) that two acyloxy radicals would first combine to form the peroxide intermediate which then decomposed via the same acyloxy radical again to give alkyl radicals and CO_2. A heterogeneous direct first order decomposition of the acyloxy radicals formed from the discharge of the carboxylate anions seems much more probable.

Goldschmidt et al. (47) have made a detailed study of the products of electrolysis of propionates in anhydrous propionic acid and compared them with the products of decomposition of dipropionyl peroxide. The good parallel between products of the Kolbe reaction and those of the decomposition of the corresponding diacyl peroxides, Goldschmidt states, (48) suggests more that the two processes have common paths (i.e. the decomposition and electrolysis reactions proceed through a free-radical intermediate) than that diacyl peroxides are directly involved as intermediates in the Kolbe reaction. This view point seems the most satisfactory one in regard to the problem of the validity of the "peroxide" mechanism in the Kolbe reaction.

ii) The Hydrogen Peroxide Theory

This was proposed by Glasstone and Hickling (8,9,30)

and is based on the assumption that hydrogen peroxide, formed by the anodic discharge of hydroxyl ions, initiates the decomposition of the carboxylate ion. The reaction is formulated in the following manner for acetate decomposition:

$$2\ OH^- \longrightarrow 2\ OH^\bullet + 2\ e$$

$$2\ OH^\bullet \longrightarrow H_2O_2$$

followed by

either $H_2O_2 + 2CH_3COO^- \longrightarrow 2\ CH_3COO^\bullet + 2\ OH^-$

or $OH^\bullet + CH_3COO^- \longrightarrow CH_3COO^\bullet + OH^-$

The acyloxy radicals may possibly combine to form diacyl peroxide - the intermediate according to Fichter's theory - which can then decompose to give the Kolbe products:

$$CH_3COO^\bullet \longrightarrow [CH_3COO]_2 \longrightarrow 2\ CO_2 + C_2H_6$$

or decompose directly, as below:

$$2\ CH_3COO^\bullet \longrightarrow C_2H_6 + 2\ CO_2$$

a reaction which is kinetically probably not a single step.

When either hydrogen peroxide or the acetate concentration is low at the anode, hydrogen peroxide is considered to react with acetate ions or acetic acid to form peracetic acid which then is regarded as decomposing to give carbon dioxide and methanol, viz.

$$H_2O_2 + CH_3COOH \longrightarrow CH_3COOOH + H_2O$$

$$CH_3COOOH \longrightarrow CH_3OH + CO_2.$$

This reaction is regarded as occurring whenever conditions are not favourable for the Kolbe reaction.

Numerous criticisms have been raised against this mechanism of the role of oxygen in the reaction, the most serious being that the addition of concentrated hydrogen peroxide to acetate solutions produces only trace amounts of hydrocarbon (8,30); furthermore, attempts to detect even trace amounts of hydrogen peroxide during and following electrolysis have not been successful (29). Failure of the reaction to occur homogeneously has been ascribed by Glasstone and Hickling to the fact that conditions in chemical experiments are quite different from those which exist at the anode where heterogeneous conditions prevail. More recent investigations have failed to detect even trace amounts of hydrogen peroxide during and following electrolysis (39,53) and at most noble metal electrodes hydrogen peroxide would be catalytically decomposed.

In several publications (51,52) it is denied that hydrogen peroxide is formed in anodic oxygen evolution and only in cathodic oxygen reduction (31) is hydrogen peroxide postulated as an intermediate. Thus, hydroxyl radicals formed as intermediates in anodic discharge from OH^- or H_2O evidently do not combine significantly to give desorbable products, except O_2 itself, although adsorbed metal peroxide intermediates have been

suggested (32,33) and may exist on the surface.

Tests for peracids have also been negative (29). The formation of olefins or saturated hydrocarbons containing one carbon atom less than the original acid also cannot be accounted for on the basis of the hydrogen peroxide mechanism.

The hydrogen peroxide theory also requires that hydroxyl ions or water molecules be present and hence is only applicable to aqueous solutions. It has been remarked (5) that the Kolbe reaction in anhydrous ethylene glycol occurs at an anode potential* almost identical with that for aqueous media (9) and that this would hardly be expected if the primary processes in anhydrous and aqueous media differed radically.

The general scheme discussed above, is seen to be similar to that proposed by Fichter (37), except that Glasstone and Hickling regard the oxidation steps as involving hydrogen peroxide (i.e. an oxidation-reduction reaction), rather than the peroxy-intermediate formed by coupling of acetate free radicals arising from the discharge of the corresponding anions.

For non-aqueous solvents, the mechanism postulated by Glasstone and Hickling (9,30) is similar to that proposed by Fichter (37).

---

* In point of fact, this agreement is probably coincidental since no comparison between potentials in water and any other solvent can, in principle, be made and such comparisons have no thermodynamic significance in the present case.

Glasstone and Hickling attach great importance to the fact that the Kolbe reaction occurs at potentials much higher than that required for oxygen evolution. They assumed that hydrogen peroxide, formed at the anode by the discharge of OH^- ions gives rise to the formation of radicals which are capable of establishing a much higher potential than that required for oxygen evolution. The high anode potentials observed in the Kolbe reaction are not surprising as the oxygen overvoltage itself can be increased considerably (at a given current density) as has been shown by Bockris (49) in the anodic evolution of oxygen in the presence of acetic acid at platinum (the Kolbe reaction in this case being "poisoned" by H_2SO_4). It has also been shown by Russian workers (50) that the presence of $SO_3^=$ ions also increases the oxygen overvoltage. Apparently under conditions existing when the Kolbe reaction is occurring, the discharge of carboxylate ions is energetically favored compared with that of hydroxyl ions (or water) in the oxygen evolution reaction.

iii) <u>The Discharged Ion or Free Radical Mechanism</u>

This was originally proposed by Crum-Brown and Walker (54) and supported by Walker and co-workers (25,55). The important steps in the proposed mechanisms are the direct electrochemical oxidation of the carboxylate ions and subsequent decomposition of the radicals formed. The reaction can be

written as

$$2\ RCOO^- \longrightarrow 2\ RCOO^\bullet + 2\ e$$

$$2\ RCOO^\bullet \longrightarrow 2\ R^\bullet + 2\ CO_2$$

$$R^\bullet + R^\bullet \longrightarrow RR.$$

Although each of the above proposed mechanisms is postulated as occurring through several steps, no mention is made by the authors concerning which step may be rate-determining nor what current-potential behavior would be associated with each step.

In more recent years, some insight into the mechanism of the anodic oxidation of carboxylic acids has been achieved in investigations by Clusius and co-workers (56,57,58) and in the kinetic studies of Wilson and Lippincott (53) which tend to favour the free radical mechanism (see below).

The mechanisms of some of the side reactions were elucidated by conducting electrolysis of acetates and deutero-acetates in deuterium oxide and water respectively (56,57). Electrolysis of the acetates was found to give ethane above a critical current density or potential and methane at low current densities, the composition of both products depending only on the isotopic structure of the acetate ion and not on that of the solvent. This is consistent with the view that methyl radicals are formed and that these either dimerise to give ethane or, when present in low concentrations, abstract hydrogen from an acetate ion (or another methyl radical)* to

* This could also lead to the production of olefins which is often observed. Similar radical processes occurring in the gas phase have been discussed by Steacie (46) and in solution by several other authors (42,45,47,48).

give methane thus

$$CH_3COO^- \longrightarrow CH_3COO^\bullet + e$$
$$CH_3COO^\bullet \longrightarrow CH_3^\bullet + CO_2$$

Above the critical potential the recombination

$$2\ CH_3^\bullet \longrightarrow C_2H_6$$

is regarded as occurring and below the critical potential, H abstraction according to the reaction

$$CH_3^\bullet + CH_3COO^-/D_2O \rightleftharpoons CH_4 + {}^\bullet CH_2CO_2^-$$

The molecular residue is then decomposed by oxygen (co-deposited at low current densities) to give carbon dioxide and water. Bauld (59) has shown recently that further oxidation of the electrolytically produced radicals can yield carbonium ions which then attack the solvent. It seems reasonable that ethers, esters and alcohols which arise as by-products in the Kolbe reaction can arise in this manner. Experimentally, this kind of process is favored by alkaline solutions and the presence of various inorganic ions (45).

The production of olefins on electrolysis of propionates and butyrates was shown (58) to arise from the intermediate alkyl free radicals by elimination of hydrogen from the carbon atom originally β to the carbonyl group. The formation of ethanol in the electrolysis of α,α-dideutero-propionates in acidic solution was shown (60) to occur by β-oxidation of the alkyl function in the carboxylic acids.

Additional evidence favouring the free radical mechanism has been obtained by Wilson and Lippincott (53) from a kinetic study of the formation of free radicals, using a variable frequency square wave current (cf. the rotating sector technique in photolysis reactions). The authors argue that if the reaction follows first order kinetics, the current efficiency (or yield) should be independent of frequency* (since the yield will not depend on the number of radicals produced per cycle, but on the total number produced per unit time). However, if the reaction is second order, the yield will be frequency dependent, being higher at low frequencies than at high frequencies. On this basis kinetic expressions are derived assuming that the radicals formed at the electrode can react to form products by a series of consecutive reactions, only one of which is slow and that this slow step is either first or second order.

The formation of ethane in the electrolysis of acetates in both aqueous and glacial acetic acid was shown to be frequency independent, or to follow first order kinetics. This suggests strongly that the mechanism is the same in both solvents and is strong evidence against the hydrogen peroxide

* A slight dependence of yield on frequency will be observed due to the time required to charge the double-layer during each cycle.

theory postulated by Glasstone and Hickling (8,30). Also the addition of concentrated hydrogen peroxide during electrolysis, in fact, results in a sharp decrease in the ethane yield, so that hydrogen peroxide is hence not a likely intermediate in this reaction. With the same kinetic treatment, the acyl peroxide theory requires that the reaction be second order in the concentration of radicals produced at the electrode. On the basis of this theory, the data of Wilson and Lippincott would indicate that the slow step is the first order decomposition of acetoxy radicals.

Olefin formation in the electrolysis of propionates was observed to follow second order kinetics in the radicals produced at the electrode. Wilson and Lippincott on the basis of their kinetic studies, coupled with the experimental results of Clusius et al. (56,57), (who showed that in the electrolysis of β,β,β-trideuteropropionic and α,α-dideuteropropionic acid, the same ethylenic compound, 1,1-dideuteroethylene was formed in both cases) have suggested a reaction involving two propionoxy radicals, one extracting a β-hydrogen atom from the other. The biradical thus formed is regarded as decomposing to yield ethylene and carbon dioxide. The reaction of two propionoxy radicals, in the light of the above results argues against the formation of an acyl peroxide intermediate, as the peroxide would not be expected to yield the same

ethylenic compound, nor to yield ethylene exclusively at an electrode surface.

Additional evidence in support of an (adsorbed) acetoxy intermediate (in the acetate case) is that when anisole is added to an aqueous solution undergoing electrolysis acetoxyanisole is isolated in good yield (62).

Pande and Shukla, (39) in a recent paper supporting the discharged ion theory, have proposed mechanisms for the formation of the various anode products; however, the authors have overlooked the excellent work of Clusius (56,57) on the mechanism of the side-reactions, as well as the kinetic studies of Wilson and Lippincott (53). As a result, several of the proposed mechanisms appear to be incorrect. (This will be discussed more fully in the "Discussion"). Although Pande and Shukla have also shown potential vs. current plots, they failed to discuss the proposed mechanisms logically in terms of Tafel equations; instead, the proposed mechanisms were based solely on the observed reaction products. Somewhat similar comments may be made about the recent work of Dickenson and Wynne-Jones (122). Further discussion of their approach will, however, be made in Chapter IV.

There is little doubt that free alkyl radicals are produced in the Kolbe reaction; thus Fieser, Clapp and Daudt (63) have shown that trinitrotoluene can be methylated in the anode compartment of an aqueous solution of acetate. That both acetoxy and methyl free radicals are produced has been demonstrated by electrolysis of acetate solutions in the presence of both butadiene and isoprene. Examination of products

indicated the addition of both methyl and acetoxy free radicals to the acceptor molecule (64). When electrolysis was carried out in the presence of vinyl acetate, methyl methacrylate or vinyl chloride, the respective polymers were pbtained in the anode compartment. Use of potassium acetate-2, C^{14} in the presence of either vinyl acetate or methyl methacrylate produced C^{14}-radioactive polymers. These results indicate that acetoxy or methyl free radicals produced during electrolysis serve as polymerization initiators (65).

Oxygen normally exerts a considerable inhibitory effect on the free radical polymerization of vinyl acetate (65), yet polymerization initiated by free radicals produced by electrolysis yields a polymer similar to that produced by other means. Thus, while the intervention of oxygen as an electrolytic by-product cannot be ruled out completely, it seems to play no significant role in determining the course of "electrochemically initiated" polymerization.

Most features of the Kolbe reaction can be most satisfactorily explained qualitatively by the free radical mechanism and are consistent with other known radical processes. Thus, in a solution containing carboxylate ions, acyloxy radicals can be formed and subsequently decompose to give alkyl radicals which may then either dimerise to give the coupled product, or react with another acyloxy radical to form esters; alternatively the

alkyl radical may either react with the solvent as in aqueous basic solutions to yield alcohols, or be further oxidized to carbonium ions which then attack the solvent. The formation of some non-dimeric hydrocarbons, particularly at low current densities, could arise from either disproportionation or hydrogen abstraction from the solvent, as discussed previously.

A summary of proposed mechanisms and their kinetic consequences is given on pp. 25-27 below.

C. ANODIC PROCESSES

(a) General

With the study of anodic processes are associated characteristic experimental difficulties which are absent in most cathodic processes. Thus, under anodic conditions, most metals either undergo "anodic dissolution" at low current densities or are themselves subject to "anodic oxidation". When a metal dissolves anodically a number of difficulties arise, the more important being:

(i) The total real area may change somewhat with time; hence the measured apparent current density may differ significantly from the true value at the electrode surface.

(ii) The measured electrode potential can be a "mixed potential" due to anodic dissolution of the metal and anodic oxidation of a component of the electrolyte; satisfactory separation of this mixed electrode process into components for each electrode process can only be achieved by coulombic

Summary of Proposed Mechanisms

Mechanism	Steps	Characteristic Predictions (as claimed by authors)	Evidence (as stated by authors)
i) Acyl Peroxide Mechanism Fichter (37)	$2RCOO^- \rightarrow 2RCOO^\bullet + 2e$ $2RCOO^\bullet \rightarrow RC(=O)-O-O-C(=O)-R$ $RC(=O)-O-O-C(=O)-R \rightarrow 2R^\bullet + 2CO_2$ $R^\bullet + R^\bullet \rightarrow R-R.$	Discharge of carboxylate anion. Three intermediates postulated: i) discharged anions ii) diacyl peroxide iii) alkyl radicals. Side reactions-intermediate peroxides hydrolyse to form peracids, which subsequently decarboxylate to form alcchols. Alcohols can be dehydrated to form olefins or combine with the free acid to form esters.	In streaming solutions and at low temperatures, diacyl peroxides and peracids detected in traces. Based mainly on similarity of products obtained by chemical decomposition of diacyl peroxides in solution to those obtained by electrolysis

(continued on next page)

(Summary - Continued)

ii) Hydrogen Peroxide Mechanism Glasstone and Hickling [8,9]	$2OH^- \longrightarrow 2OH^{\bullet} + 2e$ $2OH^{\bullet} \longrightarrow H_2O_2$ followed by either $H_2O_2 + 2RCOO^- \longrightarrow 2RCOO^{\bullet} + 2OH^-$ or $OH^{\bullet} + RCOO^- \longrightarrow RCOO^{\bullet} + OH^-$ then either $2RCOO^{\bullet} \longrightarrow RR + CO_2$ or $2RCOO^{\bullet} \longrightarrow R\overset{O}{\overset{\|}{C}}-O-O-\overset{O}{\overset{\|}{C}}-R$ $R\overset{O}{\overset{\|}{C}}-O-O-\overset{O}{\overset{\|}{C}}-R \longrightarrow RR + 2CO_2$	Hydrogen peroxide intermediate initiates decarboxylation and coupling reaction. Tenable in aqueous solution only. Followed by i) discharged ion and ii) diacyl peroxide intermediates. In non-aqueous solvents direct discharge of carboxylate anion, followed by same steps as in aqueous media. Side reactions - due to low concentrations of either hydrogen peroxide or carboxylate ions, hydrogen peroxide or active oxygen formed by its decomposition reacts with the acid to form the per-acid, which then decompose to the alcohol and carbon dioxide.	Addition of foreign cations which react with hydrogen peroxide chemically, results in a decrease of the Kolbe product and favours alcohol formation. Effect of pH on yield of the main product related to increased stability of hydrogen peroxide in acidic solutions. Importance attached to the fact that the coupling reaction occurs above the oxygen evolution potential.

(Summary - Continued)

iii) Discharged Ion or Free Radical Mechanism Crum-Brown and Walker (54)	$2RCOO^- \longrightarrow 2RCOO^\bullet + 2e$ $2RCOO^\bullet \longrightarrow 2R^\bullet + 2CO_2$ $R^\bullet + R^\bullet \longrightarrow R\text{-}R.$	Direct discharge of carboxylate ions. Mechanism tenable in all solvents. Two intermediates i) acyloxy radicals and ii) alkyl radicals. Consistent with other known radical processes in solution. Side reactions: alcohol formation due to β-oxidation of alkyl radical, ester formation due to coupling of alkyl and acyloxy radicals. Olefin formation due to hydrogen abstraction or disproportionation in alkyl radical.	Anodic methylation and acetoxylation reactions and polymerization initiation confirm presence of radicals. Mechanism of abstraction reactions-i.e. olefin formation, characterized by isotopic labelling. Alcohol formation characterized by isotopic labelling. Interrupted polarisation experiments (53) indicate first order decomposition step, i.e. $RCOO^\bullet \longrightarrow R^\bullet + CO_2$ -the second step in the above reaction scheme.

current efficiency studies. Under most conditions one or the other of these processes tends to predominate. However, the investigation of many anodic processes at low current densities has been limited to the noble metals on account of difficulties involved with side reactions involving metal dissolution.

When anodic oxidation of the electrode occurs without dissolution, the film formed on the metal presents a new surface to the solution, and the subsequent behavior of the anode will then depend largely on the electrical and chemical properties of this film. If this film behaves as a good electronic conductor, and the anodic oxidation of electrolyte at the film-electrolyte occurs at a higher potential, accounting for practically all the charge passing, little further change of the metal occurs and the metal is anodically passivated. If, however, the film is a poor electronic conductor, or no discharge process can occur at the film-electrolyte interface, passage of charge across the film can only occur by ionic transport through the film with the result that more metal continues to be oxidised to the surface compound and continuous anodic oxidation or film growth occurs.

Although combinations of the above phenomena can occur, one of the above processes is usually predominant and

can be experimentally distinguished from one another.

Since an important new conclusion from the present work is that both the anodic passivation and anodic film growth processes mentioned above are involved in the Kolbe reaction and formic acid decarboxylation, a brief survey of the principal factors involved in these two phenomena will be given as a basis for the discussion of the results to be presented subsequently.

(b) Anodic Passivation

Passivity of a metal may be said to have occurred when metal cations cease significantly to emerge from the metal lattice i.e. further dissolution of the metal is inhibited in spite of the potential being substantially anodic to the relevant metal metal-ion reversible potential.

Passivity produced either "chemically" or by anodic polarisation is considered in one school of thought (66) to be due to the formation of an oxide film of appreciable thickness; others, however, prefer to associate the primary process of passivation with the formation of an adsorbed monolayer of molecules, atoms or ions of, or containing, oxygen (67). The adherents of the oxide film theory cite as evidence that a metal, once passive, is covered with an oxide film. The classical experiments of Evans (68) provide the best experimental evidence for the solid film theory,

in which very thin oxide films stripped from anodically passivated iron may be visibly demonstrated. While neither view can be proven unequivocally, as various kinetic results can readily be interpreted in terms of either theory, more recent views may resolve the situation.

More recently, several investigators (67,69) have expressed the view that the film and adsorption theories do not contradict each other but are, in fact, complementary. Evans (69) has suggested that whether or not passivity will occur may well be determined at the stage of an adsorbed film, but that, once passivity has set in, there is always an actual oxide film, a view also held by Kolotyrkin (69).

Theories of passivity are still controversial owing to the fact that much remains to be discovered about the chemical and physical structure of the surface films which are present under different conditions, and also to uncertainty concerning the energetic factors which determine the processes of metal dissolution into the solution or into a surface film.

The onset of anodic passivation is readily indicated by electrical measurements in which a rapid rise of anode potential at constant current density, or a sudden fall in current density at an anode maintained at constant potential, occurs when passivation sets in. Passivation is not limited to metal oxidation processes but is also observed in hydrogen ionisation at platinum (67). The general anode potential-current

density relationships for passivation are shown schematically in Figures Ia and Ib.

If the current density i is held constant at a series of increasing values of i along AB (Figure Ia), a sudden potential rise BC occurs at the onset of passivation. Thereafter, as the current is increased along CD, the potential rises further, CD being the current-potential relationship for the anodic oxidation of a component of the electrolyte. When the current is lowered, this reaction can proceed along DCE, until a sudden fall in potential EF indicates a return to an "active" condition of the metal surface, and the renewal of anodic dissolution in some cases. The hysteresis effect CEF before activation is usually attributed to the thin passivating film remaining stable at current densities lower than those required to form it. If the anode potential is adjusted and held constant by means of a potentiostat, the potential-current relationship takes the course (Fig. Ib) $A'B'E'C'D'$, $A'B'$ indicating the active condition of the electrode. Passive electrodes can sustain an anodic process not involving production of metal cations at the film-solution interface for long periods without undergoing any visible change. In general, a steady passive film thickness is reached depending on the potential and specific electrical properties of the film. The potential (E_F in Figure Ic) at which full passivity starts or disappears (in the case of iron) is usually known as the

Figure I

Potential-current density relations

(a) Current-density constant: potential measured.

(b) Electrode potential constant, current measured.

(c) Potential-time relationship current density constant.

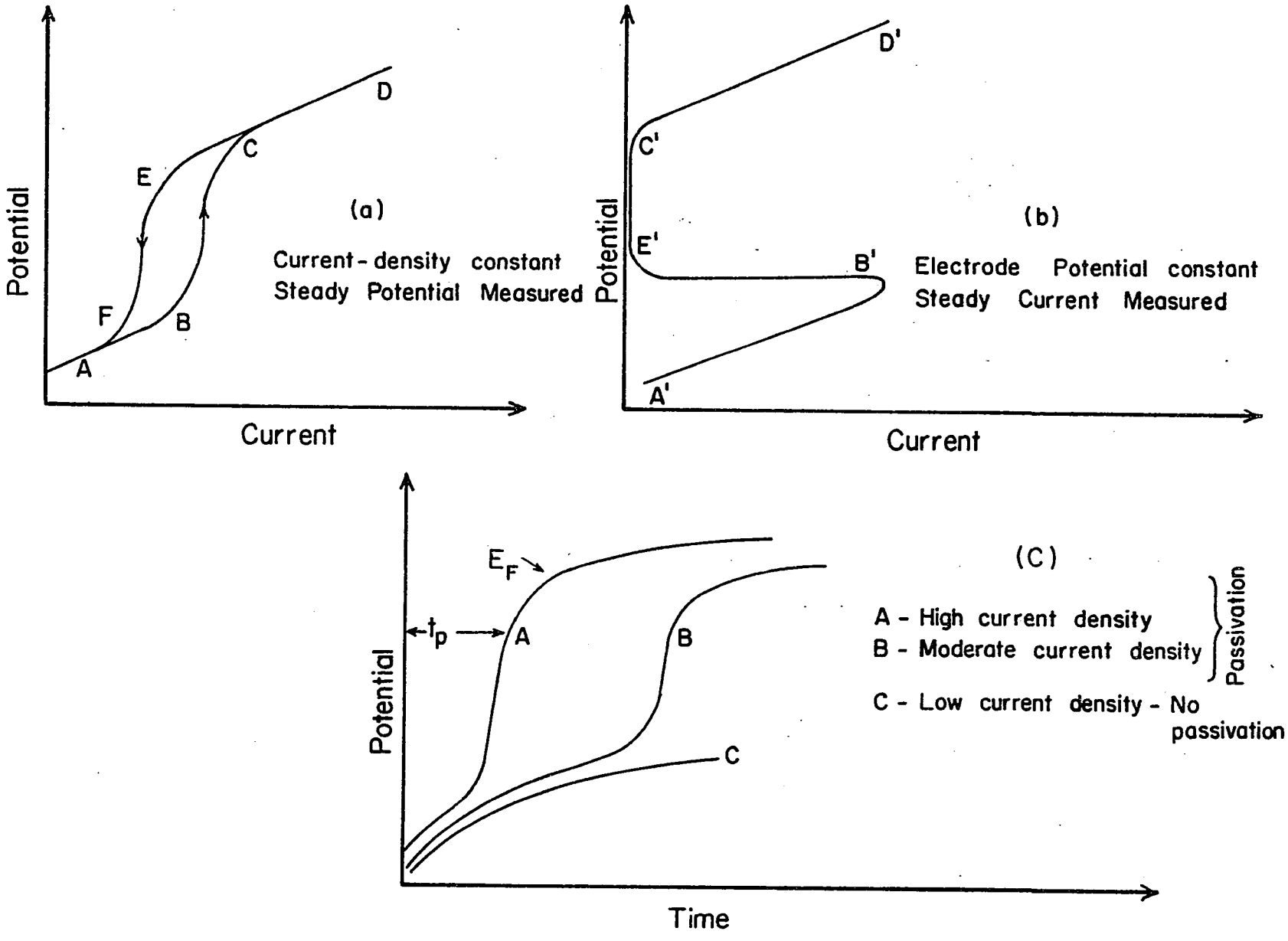
Potential
Current
A
B
C
D
E
F
(a)
Current - density constant
Steady Potential Measured
Potential
Current
A'
B'
C'
D'
E'
(b)
Electrode Potential constant
Steady Current Measured
Potential
Time
E_F
t_p
A
B
C
(C)
A - High current density
B - Moderate current density
Passivation
C - Low current density - No passivation

Flade potential (70); the Flade potential does not correspond to the equilibrium potential of any known oxide but is probably a potential associated with the species constituting the film.

Under galvanostatic conditions at current densities around B, the time lapse t_p required before passivation occurs, decreases with increase of current-density. The general anode potential-time relationship is shown in Figure Ic. Under constant current conditions it is often found that passivity is reached after a transition time t_p^* which depends on current density i according to

$$t_p (i - i_L) = \text{constant.}$$

where i_L is the limiting current density and depends upon experimental conditions (98).

The arrest of potential which occurs during passivation at constant current density, or the sharp decrease of current density in corresponding potentiostatic investigations, is usually attributed to the formation of insoluble compounds or protective films on the metal surface. These arrest potentials sometimes agree within a few millivolts with those calculated from thermodynamic equilibrium data for anticipated compounds (i.e. oxides); that may be reasonably expected to be formed

---

* This transition time is not to be confused with that for diffusion controlled processes in solution.

at the metal. However, it is generally dangerous to regard the surface films as having properties comparable with known bulk phases, since often the films may be only several monolayers thick.

In the transition from an active to a passive state periodic fluctuations in potential are often observed (71-75) (and were also found in the present work). According to various theories proposed, there can be two possible states of the film and the system oscillates between them (73,74,75) with corresponding potential fluctuations; or the periodic fluctuations can be ascribed to alternate operation of activation and diffusion controlled processes (71,72).

Periodic phenomena have been investigated rather little and as a result the cause of this behaviour is still ill understood. It is evident that one of the requirements is a current potential curve showing a maximum in current at a critical potential, i.e. the same magnitude of current can flow at two widely different potentials. The critical conditions required for periodic phenomena to arise have been discussed by Franck in terms of unstable steady states and irreversible thermodynamics (75).

(c) Film Growth

The study of electrochemical oxidation on the surface of film-covered electrodes has received rather little attention, although oxygen evolution studies (76) have usually

been conducted under such conditions, since metal oxide formation usually precedes oxygen evolution (77). Generally studies are conducted on initially bare metals, hence care is taken to remove any films that may be present; alternatively, as mentioned previously, reactions are normally investigated in such a manner as to minimize film growth. It is clear, however, that the presence of a film can markedly influence the oxidation process occurring at the surface by affecting the energetics of the reaction at the double-layer, or by imposing a barrier to charge transfer through the film, or both.

The kinetics of anodic film growth have not been extensively investigated, and experimental data is limited to only a few metals (78). Most of the detailed studies have been limited to the "valve metals" Zr or Ta which give practically useful capacitative films of ZrO_2 or Ta_2O_5.

Several theories have been proposed according to which the formation current density should be dependent exponentially or linearly on the electric field across the oxide. The kinetics of growth of thin films have been discussed in detail by Mott and Cabrera (79,80), primarily in regard to the formation of oxide films by reaction with oxygen ("tarnishing reaction"), and subsequently applied to anodically formed films. The essential difference between anodic film growth and the tarnishing reaction is

that in anodic oxidation only ions need cross the film for growth to occur, whilst in tarnishing reactions both ions and electrons must move across the film. In anodic film growth reactions, ionic transport is usually rate-determining for thick films (78) but in steady state anodic reactions proceeding on the film, electron transport through the film is then necessary and in some cases (81) can determine the rate of the surface electrochemical reaction. The anodic metal oxidation process is also more convenient for investigation than the gas-solid oxidation reaction as the rate of film growth can be controlled by controlling the current through the oxide.

Theories of film growth which have been proposed all assume the oxide to be of stoichiometric composition and to contain mobile metal ions, whose motions are unimpeded by other mobile ions, and which are in thermal equilibrium with the oxide lattice. The energy diagram normally used to represent the situation is shown in Figure II. Such a potential energy diagram applies, in principle, to any oxidation process involving the formation of a film, regardless of the detailed mechanism of oxidation or whether the process occurs under "high field" or "low field" conditions - the field referring to the electrostatic field across the barrier layer film. In Figure IIa is represented the potential energy of a mobile metal ion as it leaves the metal and passes

Figure II

Potential Energy of mobile ions as a function of distance

(a) ion entering oxide from the metal

(b) applied field.

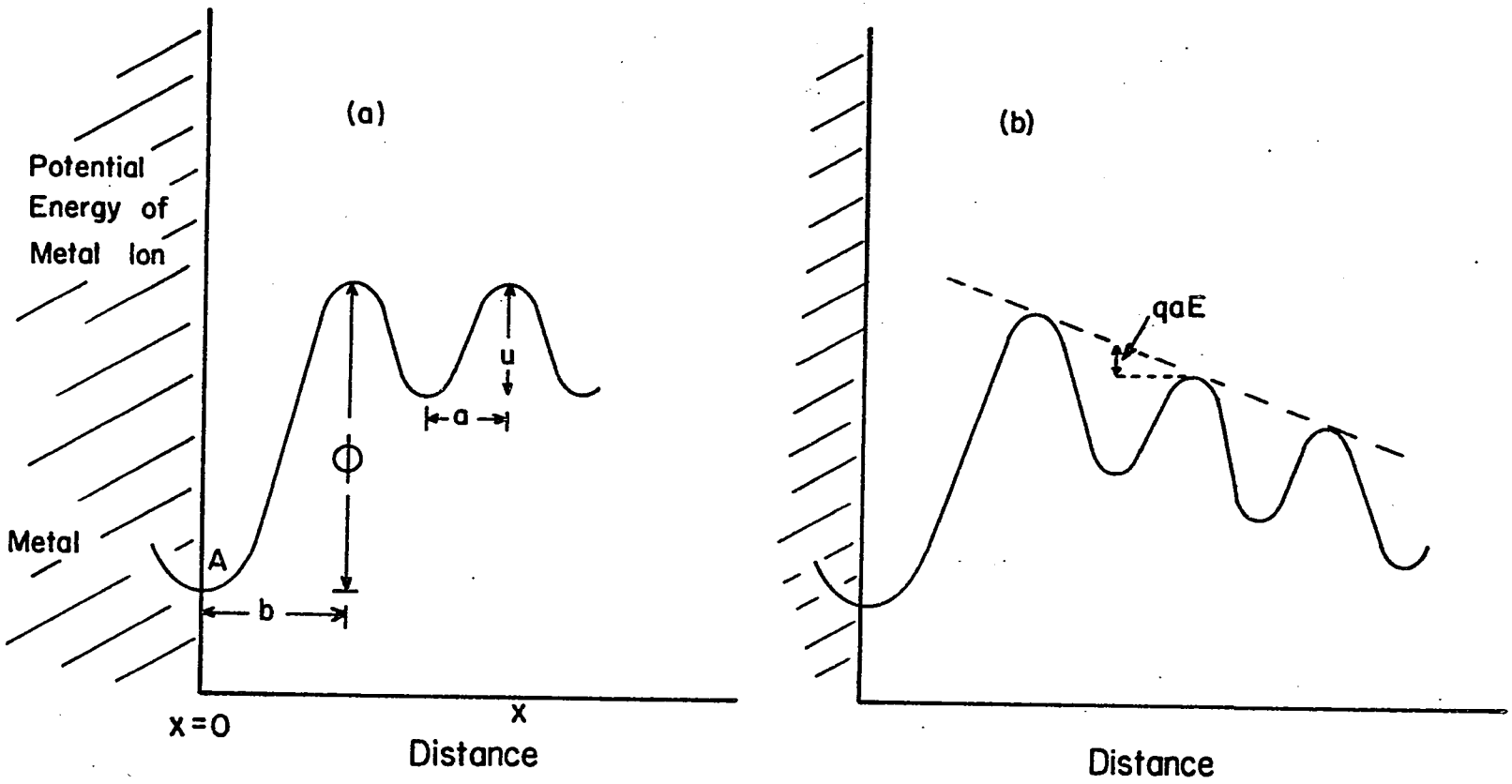
(a)
Potential
Energy of
Metal Ion
Metal
A
b
Φ
u
a
x=0
x
Distance
(b)
qaE
Distance

into and through the oxide in the absence of an external field. The point marked A represents the position of an ion in the metal and the point B represents an interstitial site; ϕ is the activation energy which must be surmounted to move the ion from the metal to an interstitial site and U is the energy required to move the metal ion between interstitial sites. The presence of a field lowers the barrier by an amount qaE (see Figure IIb) where E is the field, q the charge on the ion and a the "half-jump" distance. This representation is similar to that used in the absolute rate theory of electronic or ionic conductance.

The total ionic current density at a point x in the oxide (see Figure II) is assumed to be given by

$$i = 2\,a\nu n q \exp.- \left[\frac{U-qaE}{kT}\right] - 2\,a\nu n \exp.- \left[\frac{U+qaE}{kT}\right] \qquad [1]$$

$$= 4\,a\nu n q \exp.- \left[\frac{U}{kT}\right] \sinh \frac{qaE}{kT} \qquad [2]$$

where a = half-jump distance for the ions (2a = distance between interstitial sites)

ν = vibration frequency of ions at x

n = concentration of ions at x

U = activation energy for motion between interstitial sites

q = charge on the mobile ion

E = the electric field at x

k = Boltzmann constant

and

T = absolute temperature.

The first term in equation [1] refers to ions moving in a direction down the field and the second to ions moving against the field. For low fields or thick films ($qaE \ll kT$), the following approximation can be made

$$\sinh \frac{qaE}{kT} \simeq \frac{qaE}{kT} ;$$

hence equation [2] can be written as

$$i = \frac{4\, a^2 n\nu qE}{kT} \exp- [U/kT] \qquad [3]$$

which corresponds to ohmic* behaviour.

In the high field approximation, applicable to thin films, it is assumed that the reverse current can be neglected, so that equation [2] can be written

$$i = 2\, a\nu n q \exp- \left[\frac{U-qaE}{kT}\right] \qquad [4]$$

giving non-ohmic behaviour.

In the original treatment by Mott and Cabrera (79,80) for low fields, they assumed that: (a) regions of space charge at the two interfaces can be neglected and (b) the rate of growth is controlled by the rate of diffusion of metal ions across the oxide layer. For these conditions, the rate of growth can be written

$$\frac{dx}{dt} = \frac{4\, a^2 n\nu \Omega V q}{kT\, x} \exp- [U/kT] \qquad [5]$$

where V is the potential across a film of thickness x ($E = V/x$)

---

* It is of interest to note that, of course, ohm's law is a special case of activation controlled transport of charge carriers near equilibrium.

and Ω the volume of oxide per metal ion;

or

$$\frac{dx}{dt} = \frac{k_p}{x} \qquad [5]$$

where

$$k_p = \frac{4\, a^2 n \nu \Omega V q}{kT} \exp - [U/kT] \qquad [6]$$

Integration of equation [6] gives

$$x^2 = k_p t + C \qquad [7]$$

i.e., a parabolic equation for the rate of oxidation in terms of film thickness x.

In the case of thin films, i.e. with the high field donditions applying, Mott and Cabrera (79) assumed (a) the rate-determining step to be the initial transfer of ions from the metal to the oxide over the barrier ϕ, at which there is a surface concentration of ions and (b) that space charge effects were negligible so that the electric field was constant. In this high field approximation they assumed that every metal ion escaping from the metal would be swept through the oxide by the high field so that conduction through the oxide would not be an activated process. On this model the density of current across the film is given by

$$i = N_s \nu_s q \exp.- \left[\frac{\phi - qbE}{kT}\right] \qquad [8]$$

where N_s = number of ions per square centimeter of metal surface at the metal/oxide interface

ν_s = their vibrational frequency normal to the barrier

b = half-jump distance.

The Tafel slope for the ion transfer process at the metal-film barrier is given by differentiating [8] so that

$$\left(\frac{dE}{d \ln i}\right) = \frac{kT}{bq} \qquad [9]$$

giving a slope which is proportional to the absolute temperature; this result is to be expected when a single barrier determines the rate* and when no limit is placed on the concentration of ions in the initial state of the barrier transfer step at the metal-oxide interface.

The rate of oxidation can be written from [8] as

$$\frac{dx}{dt} = N_s \nu_s \Omega \quad \text{exp.} - \left[\frac{\phi - bqE}{kT}\right] \qquad [10]$$

where x is the thickness of the film at time t and Ω the volume of oxide per metal ion.

Equation [10] can be written as

$$\frac{dx}{dt} = u \quad \text{exp.} \quad \left[\frac{x_1}{x}\right] \qquad [11]$$

---

* The Tafel equation for an activation controlled electrode process is analogous and the associated logarithmic current-potential slope is, of course, of the same form as that given in equation [9]. Accordingly, the slopes involved in film growth processes, defined by equation [9] are also sometimes referred to as "Tafel slopes".

where $x_1 = \frac{qbV}{kT}$ and $u = N_s \nu_s \Omega \exp.- [\frac{\phi}{kT}]$

Equation [11] leads to the conclusion that for a constant potential V_1 below a critical temperature, a "limiting" film thickness is predicted, i.e. when the film growth rate corresponds (arbitrarily) to less than one layer of atoms added in 10^5 seconds (79).

An approximate integration of [11] for $x \ll x_1$ gives

$$\frac{x_1}{x} = \ln \left(\frac{x_1 u}{x_L^2}\right) + \ln (t + C) \qquad [12]$$

where C is a constant of integration, x_L the limiting thickness and x the film thickness at time t.

Rewriting equation [12] in the form

$$\frac{x_1}{x} = A - \ln (t + C); \quad A = \ln \left(\frac{x_1 u}{x_L^2}\right) \qquad [13]$$

gives an inverse logarithmic relationship between time and film thickness in the growth process. The Mott-Cabrera theory for the electrolytic oxidation was tested by Vermilyea (82) for high field (i.e. thin film) conditions. The experimental "Tafel" slopes were found to be temperature independent contrary to the Mott-Cabrera theory (this will be referred to as the "Tafel slope anomaly"). From equation [8] we can write

$$\ln i = \ln (N_s \nu_s q) - \frac{\phi}{kT} + \frac{bqE}{kT} \qquad [14]$$

which predicts that the field E is a linear function of the

absolute temperature T with a slope dependent on ln i, whereas Vermilyea found that the field was a linear function of the reciprocal temperature 1/T with a slope independent of ln i but with an intercept dependent on ln i, a result also subsequently observed by Young (83).

Vermilyea (84) rejected the existence of any space charge effects and postulated the creation of vacancies (or interstitial ions); the diffusion of such ions to the metal-oxide interface and the migration of mobile metal ions to the oxide-solution interface, involves a dual-barrier which can determine the rate. This view was rejected by Dewald (85) who subsequently put forward a theory (86) to account for the Tafel slope anomaly. The treatment is developed on the same kinetic basis as that in the theory of Mott and Cabrera, but allows for dual control by diffusion barriers for ion transfer both into, and through, the oxide; also space charge effects are introduced on the assumption that the space charge is due entirely to metal ions in transit, which are assumed to be stoichiometric "excess" ions (i.e. either interstitials or substitutionals).

Dewald has shown that the field at any point x in the oxide is given by

$$E = E_o + \frac{1}{\beta} \ln (1 + \beta\gamma n_o x). \qquad [15]$$

where $\beta = aq/kT$, $\gamma = 4\pi q/\epsilon$, ϵ is the dielectric constant

of the oxide and n_o the number of ions per cubic centimeter at x = o (cf. Figure II). This equation states that the field at any point x is composed of two parts, a surface charge contribution E_o and a space charge term. The surface charge contribution is given by

$$E_o = \frac{kT}{bq} \ln \left[\frac{i_o}{m_s \nu_s q}\right] + \frac{U}{bq} \qquad [16]$$

and

$$n_o = \left(\frac{m_s \nu_s}{2a\nu}\right)^{a/b} i_o^{(1-a/b)} \exp. \left[\frac{U - \frac{a\phi}{b}}{kT}\right]$$

where m_s and ν_s are the surface density of metal ions and their vibration frequency, i_o the current across the film-electrolyte interface and ν the vibration frequency of the ion in an interstitial position.

The average field $\bar{E}$, which is experimentally accessible, is obtained by evaluating

$$\bar{E} = \frac{V}{x} = \frac{1}{x} \int_o^x E \, dx \qquad [17]$$

where V is the voltage drop across a film of thickness x. Substituting equation [15] into [17] for E and integrating gives

$$\bar{E} = E_o + \frac{1}{\beta}\left[\left(1 + \frac{1}{\delta}\right) \ln (1 + \delta) - 1\right] \qquad [18]$$

where

$$\delta = \beta\gamma n_o x = \left[\frac{2\pi q^2}{\nu \epsilon kT} (m_s \nu_s)^{a/b}\right] \exp. \left[\frac{U - \frac{a\phi}{b}}{kT}\right] xi^{(1-a/b)}. \qquad [19]$$

Equation [18] gives the dependence of the average field on three variables, current density (through E_o and n_o), thickness of the film x and temperature (through E_o, β and δ). The second term in equation [18] is the space charge contribution to the average field.

The dimensionless quantity δ determines the importance of space charge. If δ is much less than one, the space charge is negligible and the equation reduces to that obtained by Mott and Cabrera. However, if δ is of the order of one or larger, space charge effects are important and the rate of oxidation is determined entirely by the bulk properties of the film. Expanding the $\ln (1 + \delta)$ term in equation [18] gives

$$\ln (1 + \delta) = \delta - \frac{\delta^2}{2} + \cdots$$

for small δ, or

$$\ln (1 + \delta) = \ln \delta + \ln (1 + 1/\delta)$$
$$= \ln \delta + 1/ \quad - \frac{1}{2\delta^2} + \cdots$$

for large δ. Neglecting second order and higher terms, the two limiting cases are given by:

$$\bar{E} \simeq E_o = \frac{kT}{bq} \ln \left(\frac{i}{m_s \nu_s}\right) + \frac{\phi}{bq} \qquad [20]$$

when $\delta \ll 1$

and

$$\bar{E} \simeq \frac{kT}{aq} \ln \left(\frac{2\pi q^2}{\epsilon \nu kT}\right) xi + \frac{U}{aq} \qquad [21]$$

when $\delta \gg 1$.

For both high and low values of δ , the field is logarithmic in current density and in both cases the Tafel slope $[(\frac{dE}{d \ln i})_T]$ is proportional to the absolute temperature. For low values of δ , the Tafel slope is given by kT/bq, while for high values of δ it is given by kT/aq.

Dewald's formulation has been based on the behaviour of thin films formed at constant current; hence, in the steady state, the concentration of mobile ions in the film is assumed to be constant. If the current is suddenly changed to a higher value, it is frequently observed that the potential "overshoots", that is the potential passes through a maximum and then sometimes a minimum before approaching a final steady state condition. (Behaviour such as this is observed in the present work in the decarboxylation kinetics) This is shown schematically in Figure III. The essential reason for this behaviour is that the variation of the concentration of charge carriers lags behind the variation of the field when the current is suddenly changed, that is the concentration of mobile ions changes relatively slowly during the rapid change of potential. The subsequent approach to the steady state beyond the minimum, then corresponds to normal film growth, i.e. a readjustment of the thickness to the new potential.

The effects of surface films on surface oxidation kinetics have been discussed (81) for two cases using a dual barrier model. In the first case, it has been assumed that

Figure III

Schematic representation of voltage transients observed on suddenly:

(a) increasing current density - (potential "overshoot"),

(b) decreasing current density - (potential "undershoot).

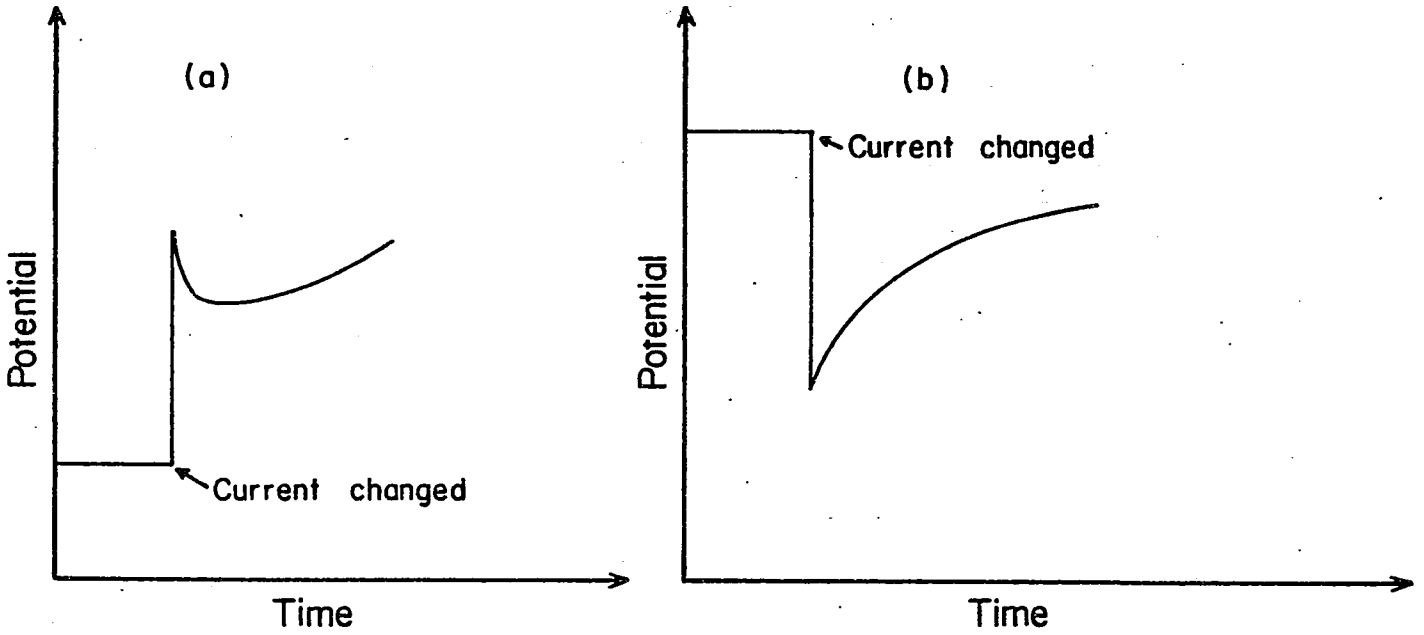
(a)
Potential
Current changed
Time
(b)
Potential
Current changed
Time

two potential dependent reactions are occurring at equal rates, one corresponding to film growth and the other to an electrochemical surface oxidation reaction and it was shown that in the usual overall rate equation

$$i = i_o \exp. \left[\frac{\alpha V_t F}{RT}\right] \qquad [22]$$

the transfer coefficient α in this equation is given by

$$\alpha = \frac{\alpha_f \alpha_s}{\alpha_f + \alpha_s} \qquad [23]$$

where α_f and α_s are the transfer coefficients for the film and surface oxidation reactions, respectively.

Hence the Tafel slope is given by

$$\frac{d\, V_t}{d \ln i} = \frac{RT}{F} \left[\frac{\alpha_f + \alpha_s}{\alpha_s \alpha_f}\right] \qquad [24]$$

where V_t is the total potential across the metal-film-solution interface and is the sum of the potential V_f across the film and the potential drop V_s across the double layer*.

The second case is that which arises when one of the reactions is essentially at equilibrium. If the process involving transfer of charge carriers in the film (as in a normal metal) is essentially at equilibrium, then the normal rate expression for the surface reaction will hold giving

---

* Gohr and Lange (121) were the first, it appears, to recognize the importance of the inhomogeneous field in the metal film-ionic-double layer region at film covered electrodes. This viewpoint was subsequently developed, as above, by Meyer (81).

a Tafel slope:

$$\frac{dV_t}{d \ln i} = \frac{dV_s}{d \ln i} = \frac{RT}{\alpha_s F} \qquad [25]$$

It is therefore possible, on the basis of the dual barrier model, to account for fractional and high values of the Tafel slopes without resorting to unusual adsorption isotherms or improbable values of the surface charge transfer symmetry factor when only the reaction at the surface double-layer is considered, as has been sometimes the case previously.

The postulate of two barriers seems quite reasonable on film-covered electrodes but conclusive direct experimental data is lacking to support this model. MacDonald and Conway (87) have given indirect evidence in support of the dual barrier process in oxygen evolution kinetics at gold electrodes by relating Tafel behaviour and open-circuit e.m.f. decay kinetics. The mechanism of charge transfer through these films is still speculative as little is known concerning the structure or semiconducting properties of these films.

D. EXPERIMENTAL APPROACHES FOR THE INVESTIGATION OF THE ELECTRODE PROCESSES INVOLVED IN ELECTROCHEMICAL DECARBOXYLATION

a) General

Previous experimental approaches to the study of the Kolbe reaction and the formate decarboxylation reaction have

been largely qualitative and based on analysis of products as a function of electrode potential, solvent, co-anions and other conditions. Such studies have been oriented along these directions of approach largely on account of the variety of products which can arise from the aqueous Kolbe reaction by side oxidation processes.

Despite the fact that more quantitative and theoretically significant approaches have been made to other electrochemical reactions, e.g. those of hydrogen and oxygen evolution, particularly over the past fifteen years, these approaches have not been made to elucidate the mechanism of electrochemical decarboxylation reactions. While the complexity of reaction products often observed in the Kolbe reaction has, no doubt, deterred authors from making such quantitative approaches to the kinetic study of the reaction, the present work described here is concerned with two reactions where the complexity of products is minimised.

The experimental approaches which have been used have hence been chosen as those which can lead to the most quantitative and least ambiguous discussion of reaction mechanism. For example, the question of the magnitudes of Tafel slopes and the electrochemical behaviour of adsorbed intermediates has virtually never previously been discussed quantitatively in relation to possible reaction mechanisms, and modern methods for the study of electrode processes have

hardly been applied at all to this type of reaction. In the present work, various complementary methods have been used for the purpose of elucidation of the rate-determining step in each of the reactions studied, the role of surface films and the concentration and role of adsorbed intermediates. We hence review briefly the methods which have been employed in the present work.

The classical approach for studying electrode reactions has been through current-potential measurements (direct method), in which the rate is measured directly in terms of current as a function of potential. Under limiting conditions of surface coverage ($\theta \rightarrow 0$; $\theta \rightarrow 1$)* by possible adsorbed reaction intermediates, limiting values of the Tafel slope can be deduced and compared with experiment and in many cases are characteristic of the reaction mechanism (32,88).

Additional information on the reaction mechanism can be obtained from galvanostatic d.c. charging potential-time relationships (89-92). The type of relationship obtained between potential and time (during the passage of a constant current) which is proportional to the quantity of electricity passed during charging up of the double-layer at the metal/solution interface, depends on the rate-determining step.

---

* In the Discussion, we examine cases where θ can have intermediate values, neither limitingly near zero nor unity.

If the double-layer capacity is independent of potential, and hence independent of the concentration of possible surface intermediates, the rate will depend on the potential difference between the electrode and adsorbed ions about to undergo reaction. However, if the overall double-layer capacity is potential dependent, e.g. owing to potential-dependent surface coverage by products of the ionic discharge reaction (corresponding to an adsorption pseudo-capacitance), this factor will enter into the rate expression for the charging process and the rate will then depend not only on the potential difference between the metal and adsorbed intermediates but also on the variation of degree of surface coverage with potential during charging.

The type of relation between potential and time, (viz. the e.m.f. decay) following interruption of the current is also characteristic of the surface concentration of intermediates, and depends on the kinetics of the rate-determining step and the potential dependence of any adsorption pseudo-capacitance (89,90,92-95).

Unless reaction products are unambiguous and obvious, the determination of current efficiencies for product formation and the characterization of products must normally be carried out before attempts are made to correlate the overall current and the reaction velocity since, in many cases, the current efficiency can be less than unity (8,9). In those reactions

where the reaction products are unambiguous (as in the hydrogen and oxygen evolution reaction under most conditions, but not for example with base metals in acidic solutions where metal dissolution or corrosion is usually a parallel process), such determinations are unnecessary.

b) Product Characterization

Before commencing any detailed measurements, the products of electrolysis and coulombic efficiencies should normally be determined. If changes of Tafel slope or critical limiting current densities are observed, then product characterization studies must be carried out, if possible, in each linear region of the Tafel plot. The total charge passed during electrolysis can easily be measured accurately by means of a coulometer and the products can be identified by appropriate analytical procedures. In the present work, products were identified by vapor-phase chromatography, based on previous calibration runs with known gas mixtures on a suitably chosen column which gave complete separation of all reaction products.

c) Direct Method

Measurement of the potential dependence of the overall rate of reaction can be made by a direct comparison of the potential of the working electrode with that of some standard reversible electrode as a function of measured current density. The basic kinetic equation relating current density and electrode potential while a reaction is proceeding

at the metal/solution interface is given by:

$$i_a = i_o' (1 - \theta) \exp - [\alpha \eta F/RT] = i_o \exp - [\alpha \eta F/RT] \qquad [26]$$

where i_a is the anodic current density; i_o' the "exchange current", that is the current at $\eta = 0$ corrected to zero coverage*; η, the overpotential defined by $\eta = E - E_r$, is the value of the metal-solution potential E when the reaction at the metal-solution interface is at thermodynamic equilibrium; α is the transfer coefficient determining the dependence of rate upon potential and is a parameter whose magnitude depends upon the mechanism of the reaction and the extent of coverage of the electrode by reaction intermediates; θ is the fraction of electrode surface covered with intermediates produced in the ionic discharge reaction and the remaining terms have their usual significance (96,97).

Taking logarithms and rearranging equation [26] gives

$$\eta = a + b \ln i_a; \; a = \frac{RT}{\alpha z F} \ln [i_o'(1 - \theta)], \; b = \frac{RT}{\alpha z F} \qquad [27]$$

which is the familiar Tafel equation.

---

* Here we use the expression for the current including a coverage term $1-\theta$ which may or may not be potential dependent. This expression and corresponding definition of i_o' differs from that usually used (viz. $i_a = i_o \exp - [\alpha \eta F/RT]$) which includes the coverage term in i_o. The expression [26] suggested by Devanathan and Selvaratnam (110) is to be preferred on account of its greater generality.

The Tafel parameters i_o and $RT/\alpha zF$ (or b) are readily evaluated from experimental logarithmic current-potential curves if the reversible potential for the reaction can be established experimentally or calculated from appropriate thermodynamic data (as actually carried out in the present work). The experimentally determined values of α, for limitingly low or high coverage of the surface by possible intermediates can be characteristic of the reaction mechanism (32,88,97). The degree of coverage θ can be estimated from galvanostatic charging or discharging data (77, 99,100,101) when it is significant (e.g. > 0.1), i.e. when the rate-determining step is not the initial ionic discharge reaction.

The applicability of direct d.c. polarization studies for the determination of the Tafel slope b, and hence the transfer coefficient α, is, however limited to ranges of current density where errors due to solution resistance, local heating effects, diffusion control, etc. can be minimized. In practice, this means that the upper limit of current density for reactant concentrations expressed as normality N is $i_{max} \doteqdot 0.1$ N. A more fundamental difficulty arises when the surface condition of the electrode changes with time on account of the formation of surface films. This is particularly important in anodic processes where the degree of surface oxidation of the electrode may have a direct bearing on the reaction mechanism and/the relation between electrode potential (103)

and current density.

Under the latter conditions, the use of a galvanostatic charging or discharging technique, provides information complementary to that given by the Tafel equation parameters, for example, information on the double-layer capacity, the concentration of adsorbed surface intermediates and the extent of surface film formation in the reaction. This technique must be regarded as complementary to the direct steady state current-potential method.

d) Galvanostatic Potential-Time Relationships

(i) General

In the reactions investigated in the present work, significant adsorption of acyloxy and/or CF_3 radicals was anticipated if the initial ion-discharge step was not rate determining. Several types of non-steady state measurements were hence made which can give information concerning the electrochemical behaviour of such intermediates in the respective overall reactions. Such knowledge is of primary importance in elucidation of any reaction mechanisms involving more than one step. The principles of such non-steady state measurements will now be briefly described.

Changes in electrode potential with time at constant current are controlled by two factors: (i) the charging or discharging of the ionic double-layer capacity, and (ii) the

alteration of composition and other conditions (such as the extent of adsorption of intermediates, formation or change of surface films) at the electrode/solution interface. The potential dependence of surface coverage by intermediates and the formation of surface films is reflected in the dependence of the overall double-layer capacity on potential* and provides an important diagnostic criterion for establishing the extent of adsorption of intermediates in the electrode reaction, e.g. an adsorption pseudo-capacity which increases with increasing (anodic) potential has been shown (119) to correspond to low coverage conditions while a capacity which decreases with increasing potential corresponds to high coverage conditions.

The total current, i_t, flowing across a metal/solution interface is normally composed of two components: (i) the non-Faradaic current i_c used to charge the double layer (including charging of any adsorption pseudo-capacity) and (ii) the current i_f corresponding to the Faradaic processes; i.e.

$$i_t = i_c + i_f \qquad [28]$$

At sufficiently high overpotentials ($\eta \gg RT/F$) the Faradaic current for an anodic process is given by

---

* Further discussion of this matter will be given in Chapter IV; a detailed analysis of this problem is in press elsewhere (102).

$$i_f = i_o \exp [\alpha \eta F/RT]^* \qquad [29]$$

From electrostatic theory, we can write the non-Faradaic current, for constant capacity as

$$i_c = C \, d\eta/dt \qquad [30]$$

Hence, the total current can be written as

$$i_t = i_o \exp [\alpha\eta F/RT] + C \, d\eta/dt \qquad [31]$$

which is the basic equation for galvanostatic conditions (89-93, 99, 104). As we have mentioned previously, C may itself be a function of η and a more complex expression for the non-steady Faradaic current may then be derived.

(ii) E.M.F. Build-up or Charging Relations

The double-layer capacity can be obtained from charging curves (99) if the Faradaic current is either negligible or if corrections can be made for it. Then if $i_f \simeq 0$, $i_t = i_c$, which is valid for very short times only. From equation [31] we can write

$$i_c = C_{d.l.} \, d\eta/dt \qquad [32]$$

Thus for constant capacity, the observed potential should increase linearly with time (77,105). If the potential is not linear with time, the assumption of constant capacity

---

* Here, for simplicity, we use the normal i_o (cf. p. 54).

(that is capacity independent of potential) is not valid, provided that i_f is small. Appreciable variation of capacity with potential (other than near the potential of zero charge where, in any case, the ionic double-layer capacity varies with potential) is generally attributed to the adsorption of reaction intermediates (95,105,106,107). This capacitance is the (parallel) sum of the double-layer capacity and a "pseudo-capacitance" due to the potential dependence of the adsorption of discharged ionic intermediates. The charging curve will then exhibit a plateau region, the length of which is dependent upon the degree of coverage, before the potential attains a steady value. The calculated capacity over such a region may be potential-dependent, or independent, since the concentration of adsorbed surface intermediates can depend upon the potential either linearly or exponentially in limiting cases. The origin of potential-dependent and potential-independent pseudo-capacity has been thoroughly examined theoretically by Conway and Gileadi (102) elsewhere.

(iii) Open-Circuit Decay

When the potential has attained a "steady state" value, the double-layer is normally fully charged at that potential, so that only the Faradaic current passes at the metal/solution interface. If the current is now suddenly interrupted, i.e. $i_t = 0$, the charge on the double-layer

capacitance will decrease with time on account of self-discharge by continuation of the rate-determining process* on open-circuit. From equation [31] we can then write the kinetic equation for self-discharge and e.m.f. decay as

$$- C \frac{d\eta}{dt} = i_o \exp. [\alpha \eta F/RT] \qquad [33]$$

where C may, or may not be potential dependent. The significance of studies of e.m.f. decay has been discussed elsewhere in a previous publication (119) and thesis (94) and we shall hence only note the principal conclusions from this analysis which are relevant to the present work. Integration and rearrangement of equation [33] gives:

(a) an e.m.f. decay slope b_1^- $(= d\eta/d \ln [t + \phi])$ in logarithmic time t which is <u>numerically equal</u> to the Tafel slope b_2 for the rate controlling step in the self-discharge reaction (which is normally identical with the rate controlling step in the overall reaction) when C is a constant. The integration constant ϕ, discussed in detail elsewhere (93,119), can be used to estimate the capacity C. It is frequently observed that an exponential relationship exists between the electrode potential and the capacitance. Under these conditions, two important further cases can be distinguished as discussed

---

* This is normally the process at any <u>real</u> electrode. However, at an "ideal polarised electrode", the e.m.f. decay process must be quite different since, by definition, no Faradaic process can occur. At such an ideal electrode, e.m.f. decay can only occur by relaxation of the ionic and electronic space charge at the two electrode interfaces in the polarising circuit.

by Conway and Bourgault (33,94).

(b) When C is an adsorption pseudo-capacity having the limiting form

$$C = C_o \exp \eta F/RT \qquad [34]$$

or

$$C = C_o \exp \eta/b_3$$

at low coverage (119), the e.m.f. decay slope is

$$d\eta/d \ln (t + \phi) = \frac{b_2 b_3}{b_3 - b_2} \qquad [35]$$

and ϕ is now related to C_o, b_2 and b_3.

(c) When C is an adsorption pseudo-capacitance having the limiting form

$$C = C_o \exp - \eta F/RT \qquad [36]$$

or

$$C = C_o \exp - \eta/b_3$$

at high coverage by the relevant intermediates, the e.m.f. decay slope is

$$d\eta/d \ln (t + \phi) = - \frac{b_2 b_3}{b_3 + b_2} \qquad [37]$$

Hence, high or low conditions of coverage by adsorbed intermediates produced in a non-rate-determining initial ion discharge step can be distinguished by comparison of e.m.f. decay slopes with logarithmic current-potential (Tafel) slopes.

Several authors (76,77,92,94,102,105,108,109) have discussed the variation of adsorption pseudo-capacitance with potential and have shown that this variation is connected with the potential dependence of coverage by adsorbed discharged intermediates on the electrode surface.

The behaviour of the adsorption capacity is conveniently considered for certain limiting conditions of surface coverage. Thus, if the surface coverage is approaching zero or unity, the pseudo-capacitance due to adsorbed intermediates will approach zero, and the overall capacitance will be determined by the ionic double-layer capacity. Hence, we can expect the capacitance to remain essentially constant and approximately independent of potential in these regions. Under conditions of fairly low, but significant, coverage ($0 < \theta < 0.5$), the pseudo-capacitance can be potential dependent and will initially increase with increasing potential reaching a maximum at half-coverage, then decreasing to zero as $\theta \longrightarrow 1$. In the potential region associated with high coverage ($0.5 < \theta < 1$), the capacitance will decrease with increasing potential, and as full coverage is approached, the capacity will again approach the ionic double-layer capacity (94). When coverage effects on the activation energies of the electrochemical reactions are considered, Conway and Gileadi (102) have shown that a region of appreciable, but potential-independent, pseudo-capacity will arise over a range of

electrode potentials determined by the extent of variation of adsorption energy of the relevant intermediates with coverage.

(e) Degree of Coverage

The extent of coverage (or film thickness for cases where $\theta \gg 1$) can be estimated directly from an analysis of galvanostatic charging curves; the method was originated in principle by Bowden (99) and since used by a number of other investigators (77, 92, 99,100,101,105). A typical cathodic galvanostatic charging curve is shown in Figure (IV) for an anodic process, and consists of three portions: 1-2 an initial region in which adsorbed intermediates formed in the anodic reaction are removed, 2-3 a region of more rapid potential change due to change of charge held in the ionic double-layer and 3-4 a region where adsorption of intermediates now formed in the cathodic reaction occurs. If adsorbed intermediates are not present, region 1-2 will, of course, be absent. The curve shown is typical for the behaviour of intermediates in the oxygen and hydrogen evolution reactions.

The concentration of surface intermediates expressed in terms of the number of coulombs q required to remove the adsorbed intermediates, can be calculated from the length of the plateau region; the associated pseudo-capacity can be obtained from the slope $dq/d\eta$ in this region. The degree of coverage can then be calculated after taking into account the roughness factor of the electrode surface and the appropriate

Figure IV

Schematic galvanostatic charging curve.

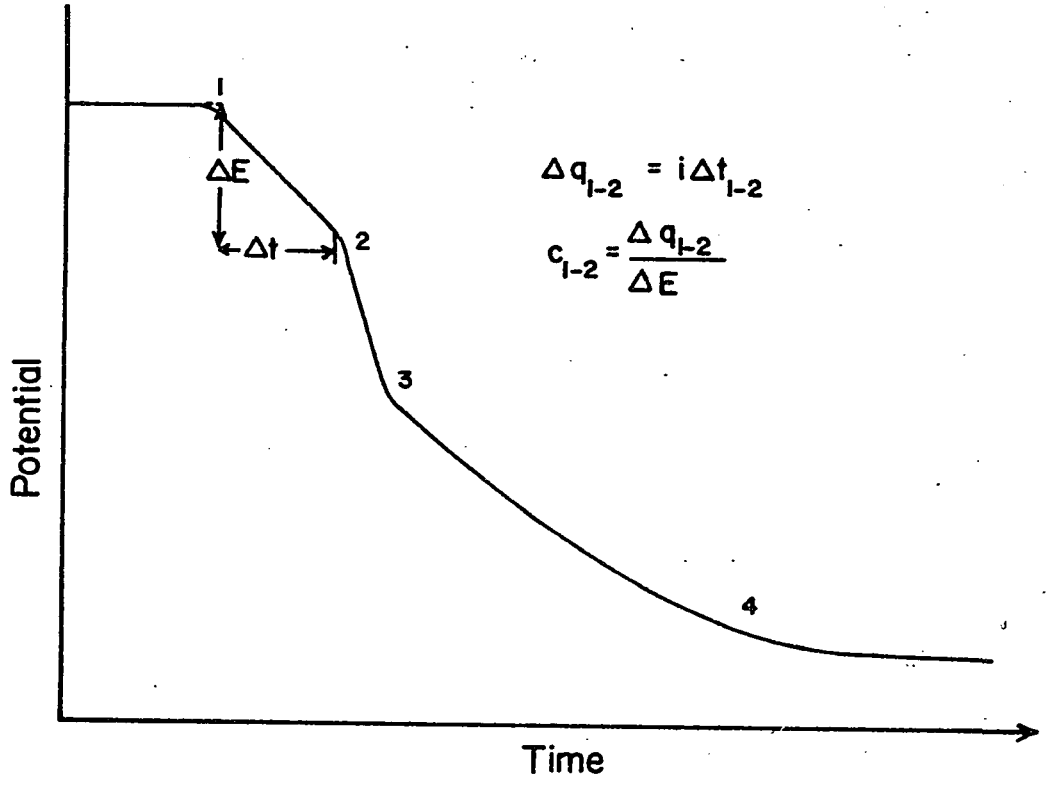

$$\Delta q_{1-2} = i\Delta t_{1-2}$$

$$c_{1-2} = \frac{\Delta q_{1-2}}{\Delta E}$$

dimensions of the adsorbed intermediates and their Faradaic valence*. This has been treated by several authors (77,89,92,99,100,101,105) and the experimental results for maximum coverage have been essentially in agreement with theoretical predictions for a monolayer of adsorbed intermediates.

This method can only be successfully applied if there is a considerable difference of potential between the completion of the first cathodic process (e.g. reduction of the initially adsorbed intermediate in the region 1-2) and the commencement of any succeeding cathodic process in the region 3-4. If these processes overlap, the potential region associated with adsorption or desorption of a particular species in the respective electrode process becomes difficult to define and the galvanostatic charging method cannot be applied in a direct manner. A method by which such difficulties can be overcome in principle by use of a double-charging technique has been described by Devanathan, Bockris and Mehl (95,110). The galvanostatic charging curve is obtained in the usual manner, then a compensation curve is obtained by starting a charging curve at a potential at which no adsorbed intermediates of the relevant process are (assumed to be)present. The subtraction

---

* That is, the number of electrons required per radical to form the adsorbed layer of intermediates.

of the current due to the irrelevant overlapping process from the total current gives the current due to the relevant process, so that the amount of adsorbed intermediates and hence the degree of coverage can be calculated. This method has, however, recently been criticised (102) since an incorrect allowance for the current due to the second process was made. That there was some error in the method is evident from the fact that at appreciable cathodic potentials at Ni, the extent of H coverage was found to be many times that corresponding to a monolayer, a result which is quite unrealistic.

In the present work, the normal single charging method is adequate since removal of the ad-species formed in the decarboxylation reactions occurs at a potential much more anodic than the range of potentials over which (cathodic) deposition adsorbed hydrogen could occur. Extents of coverage and anode film thickness can hence be obtained in the present work with much less ambiguity than corresponding estimates of extents of H-adsorption in the hydrogen evolution reaction discussed in other work (95,100).

After conclusion of the present experimental work, Dickenson and Wynne-Jones (122) published results obtained in the aqueous acetate system using experimental methods similar, in principle, to those applied in the present investigation. However, our preliminary description (123) of the application of the methods to be described in the experimental section

(Chapter II p. 81) to anodic decarboxylation was, in fact, published prior to the submission of their papers and described earlier (124). These approaches were evidently made independently and at about the same time.

Dickenson and Wynne-Jones (122) support the discharged ion theory qualitatively and, on the basis of galvanostatic measurements, recognise the importance of adsorbed intermediates (in agreement with the present investigation and our earlier publications (123,124,131)) in the Kolbe reaction. However, no quantitative information on the behavior of the intermediates was deduced in their work.

The present investigation differs from that of Dickenson and Wynne-Jones in the choice of systems studied and in the theoretical approaches made in the interpretation of our results. In the present case, systems were chosen so as to minimize undesirable side reactions so that the electrochemical kinetics of a single reaction could be studied with least ambiguity. The results of Dickenson and Wynne-Jones serve to demonstrate the additional complexity of the reaction when carried out in aqueous solution where oxide film growth and oxygen evolution are concomitant processes.

In the present work, the kinetics of the "model" anodic decarboxylation reactions and effects of surface coverage by adsorbed intermediates have been treated much more quantitatively, and in greater detail than in the papers of

Dickenson and Wynne-Jones who have given only a qualitative interpretation of their observations.

Further discussion of their conclusions will be presented in Chapter IV.

CHAPTER II

EXPERIMENTAL

A. INTRODUCTION

The experimental procedures used in the present work have consisted of: (i) steady state d,c. polarisation measurements for elucidation of the current-potential behaviour; (ii) examination of galvanostatic charging and discharging transients for elucidation of the role of adsorbed intermediates and anodic film formation; (iii) open-circuit decay measurements, which are complementary to the procedures mentioned in (i) and (ii), and (iv) coulombic efficiency determinations and related gas analyses to characterise chemically the electrode processes. In this section, these procedures will be described in detail but a general account of essential experimental technique for solution and gas purification, electrode preparation, cell design, etc, will first be given. The experimental techniques to be described have been applied to the Kolbe reaction with trifluoroacetate in both water and pure trifluoroacetic acid as solvents and, as a model system for examination of a "simple" decarboxylation reaction, i.e. one not involving at the same time radical coupling, the decarboxylation of formate ions in both water and pure formic acid has been kinetically examined.

B. SOLUTIONS

(a) Standard Purification Techniques

(i) Formic Acid

Formic acid (98-100%) was first given a preliminary drying over anhydrous cupric sulphate for two or three days and then distilled under vacuum at room temperature. Only the middle fraction was retained, the initial and final distillates being discarded. Final traces of water were removed by allowing the acid to remain in contact with boric anhydride for a minimum period of one week. The mixture was stirred continuously to ensure intimate contact between the formic acid and boric anhydride. The acid was then vacuum distilled at room temperature prior to use.

Purity of the acid was checked by determination of its freezing point; the freezing point of the acid was 8.2(3)°C compared with the literature value of 8.2(5)°C (111).

(ii) Trifluoroacetic Acid

Trifluoroacetic acid (b.p. 70-72°C) was first gently refluxed over phosphorous pentoxide* for one hour, and distilled (112). A second distillation from fresh phosphorous pentoxide

---

* The formation of the anhydride is minimised by keeping the temperature of the mixture as low as possible. In any case it is readily separated in the subsequent distillation.

was then carried out and only the fraction distilling at 71.1°C was kept for use in the experiments. The acid was stored in glass-stoppered vessels until required. Immediately prior to use in a run, the acid was again distilled from fresh phosphorous pentoxide.

(iii) Potassium Formate

Reagent grade potassium formate was further purified by dissolving the salt in hot conductivity water and filtering through decolorizing charcoal. The salt was then recrystallized twice from conductivy water at 0°C, washed with ethanol, dried at 120°C under vacuum and stored in brown tightly capped bottles.

(iv) Potassium Trifluoroacetate

Potassium trifluoroacetate was prepared by neutralizing previously purified trifluoroacetic acid with potassium hydroxide. The salt was then recrystallized twice from conductivity water, washed with ethanol and dried under vacuum at 100°C. The salt was then stored in tightly capped bottles.

(v) Potassium Hydroxide

Potassium hydroxide was prepared by electrolysis of analytical grade potassium hydroxide over triple distilled mercury. The potassium amalgam was then decomposed in conductivity water to form an aqueous solution of potassium hydroxide.

(b) Preparation of Solutions

Solutions of potassium formate in formic acid were prepared by drying the salt for twenty-four hours under vacuum

at 120°C. Formic acid was freshly distilled from boric anhydride under vacuum at room temperature. The purified acid was then transferred to a known weight of the salt to give the concentration desired. Solutions of potassium trifluoroacetate in trifluoroacetic acid were prepared in a similar manner; the salt was dried for twenty-four hours under vacuum at 100°C before use and the acid was freshly distilled from phosphorous pentoxide under vacuum at room temperature, as mentioned above.

Aqueous solutions were prepared by distilling conductivity water under hydrogen into a flask containing a known weight of salt. Basic aqueous solutions were prepared by diluting the concentrated potassium hydroxide solution to the required concentration and adding to it a known weight of potassium formate or potassium trifluoroacetate to give the desired concentration.

In all experimental measurements, pre-electrolysis of solutions was carried out for a minimum of twenty-four hours at a current density of 10^{-2} amps. $cm.^{-2}$ at a sacrificial electrode which was removed from the solution before the kinetic runs were commenced.

C. GASES

(a) Hydrogen

Hydrogen was rigorously purified before use. The purification train was similar to that previously described (113).

The train consisted of: (a) molecular sieve (Linde Co., type 13x), (b) calcium chloride, (c) magnesium perchlorate, (d) hopcalite, (e) palladized asbestos at 400°C, (f) copper turnings at 450°C, (g) two liquid nitrogen traps and (h) two charcoal traps maintained at liquid nitrogen temperatures.

(b) Carbon Dioxide

Medical grade carbon dioxide free from hydrogen sulphide, carbon monoxide and sulphur dioxide was further purified by passing the gas through a purification train consisting of: (a) molecular sieve (type 13x), (b) copper oxide furnace at 400°C, (c) saturated copper II-sulphate, (d) potassium bicarbonate and finally through (e) two traps at -60°C (chloroform-CO_2 slush bath).

The use of the train was discontinued when experimental results showed no significant differences when the highly purified gas was substituted by that passed through the molecular sieve material only.

(c) Nitrogen

Nitrogen gas was purified by passing the gas through a train identical with that described previously for the purification of hydrogen.

D. ELECTRODES

Reproducibility of measurements was obtained by adopting a standardized method of electrode preparation. The

electrodes were prepared from spectroscopically pure wires of gold, platinum and palladium (0.5 mm. diameter). The wire electrodes were first allowed to soak in alcoholic potassium hydroxide, washed in conductivity water and dried with redistilled acetone. Electrodes were then sealed under oxygen-free nitrogen in glass bulbs following the procedure outlined by Bockris, Conway and Mehl (114). Electrodes of larger area were cut from sheets of foil, spot welded to a wire of the same type of metal; subsequent purification was as described above.

E. CELLS

(a) Polarisation Cell

The cell used for galvanostatic and polarisation studies was constructed of pyrex glass. The cell consisted of three compartments which were separated from each other by "solution-seal" stopcocks. The anode and reference electrode compartments were provided with cooling coils, provision in each compartment being made to allow the appropriate gas to be bubbled through the solution. The cell is shown schematically in Figure V in which A, C and R are the anode, cathode and reference compartments, respectively.

(b) Coulombic Efficiency Cell

Coulombic efficiency studies were carried out in an all-glass pyrex cell consisting of two compartments separated by a solution-seal stopcock. The cathode compartment was vented directly to the atmosphere while the anode compartment

Figure V

Experimental cell used for polarization and potential-time measurements.

Polarisation Cell

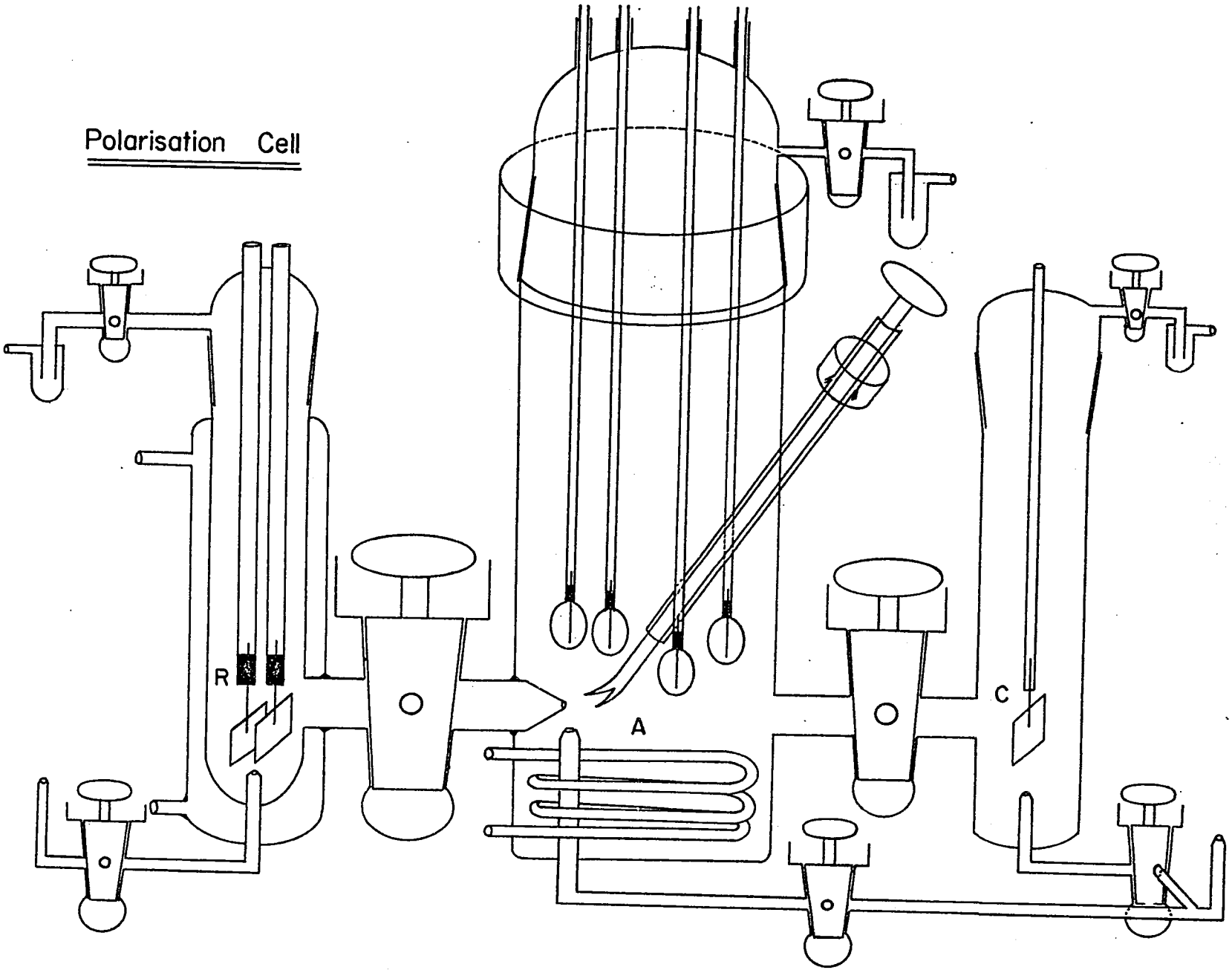

could be vented either to the atmosphere, or to a gas collecting system. (see below). Provision was also made to allow an appropriate gas to be bubbled through each compartment to pre-saturate the solutions. The cell is shown schematically in Figure VI in which A and C are the anode and cathode compartments, respectively. In Figure VII a photograph is shown of the apparatus used in coulombic volume measurements.

F. REFERENCE ELECTRODES

(a) Preparation

Hydrogen reference electrodes were used in these studies and were prepared by cleaning the electrodes in ten percent potassium dichromate in sulphuric acid solution followed by washing thoroughly in conductivity water. Two such electrodes were then suspended in the platinizing solution containing three grams of platinic chloride in one-hundred milliliters of conductivity water and connected to a reversing switch and d.c. power supply. The current was adjusted to approximately 5 ma. $cm.^{-2}$ so that there was only a moderate evolution of gas (H_2 and Cl_2) and its direction was reversed every thirty seconds by an automatic switching device. The current was allowed to pass until a moderately thick coating of platinum was obtained. The coating was greyish-black and velvety in appearance. The electrodes were then washed repeatedly with water and kept in distilled water until required for use.

Figure VI

Experimental cell used for coulombic efficiency measurements and apparatus for measurements of volumes of gaseous products.

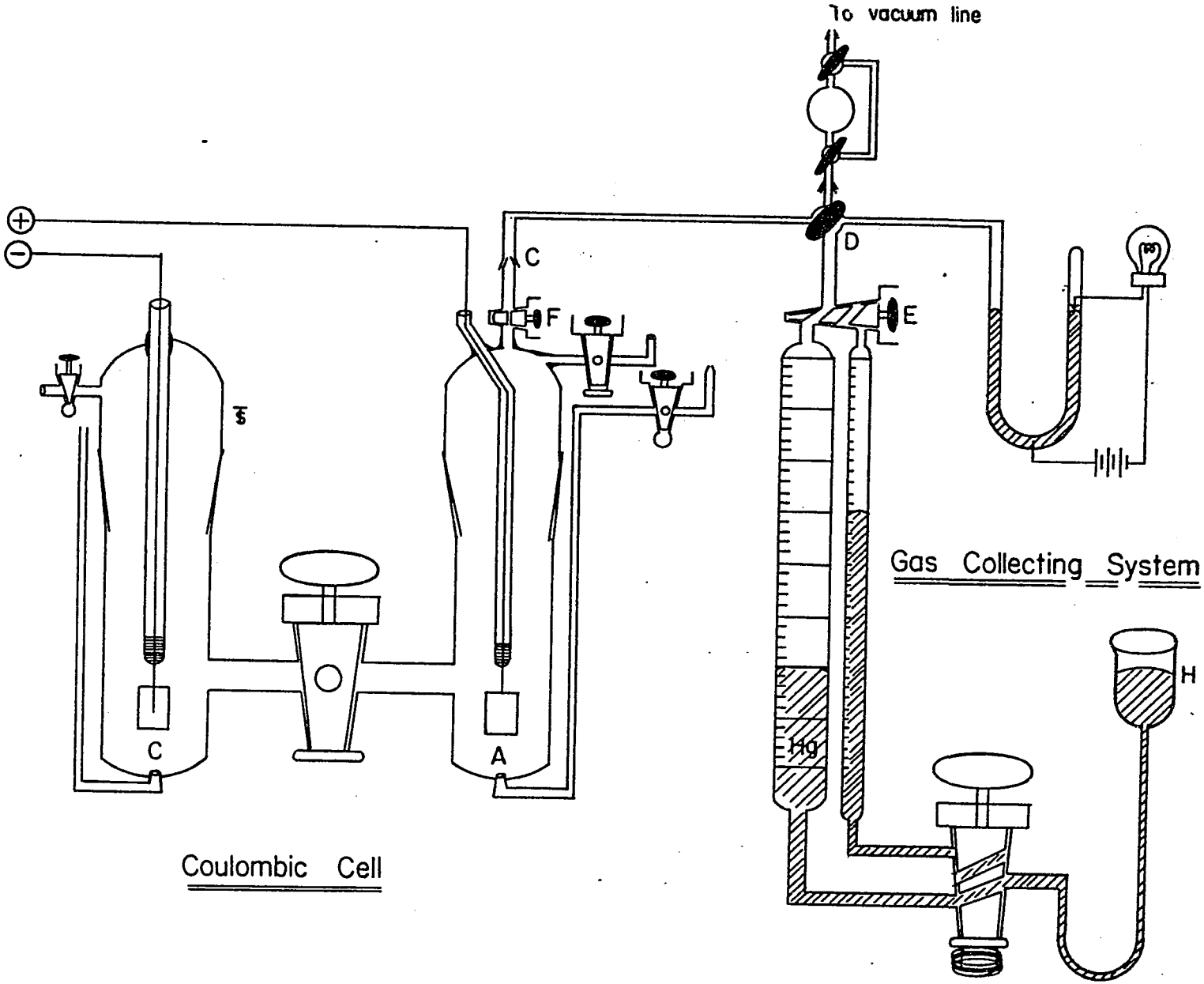
To vacuum line
C
F
D
E
S
C
A
Hg
H
Coulombic Cell
Gas Collecting System

Figure VII

Photograph of apparatus used in coulombic efficiency measurements.

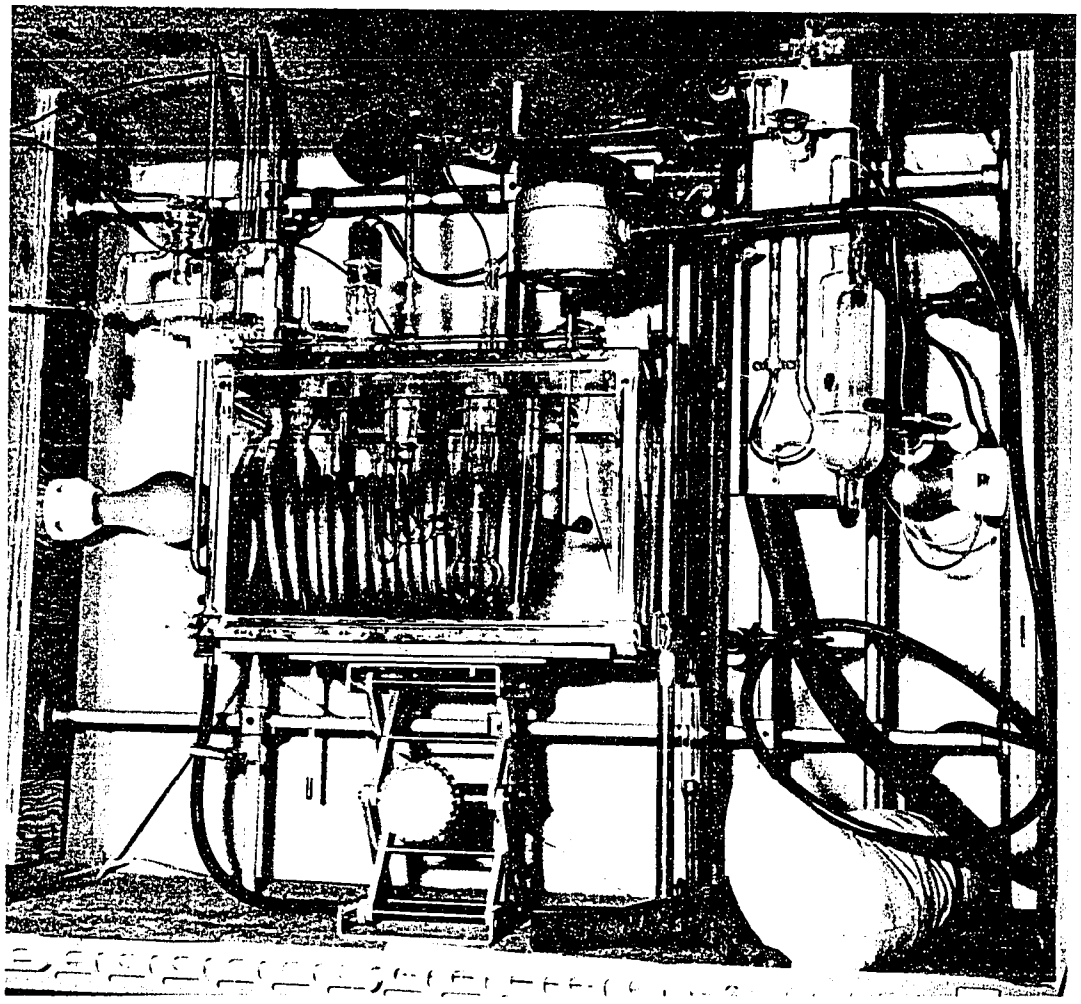

(b) Verification of Reversibility and Reproducibility

Before beginning measurements, the potential of the hydrogen electrode used was compared against that of another hydrogen electrode; if the potentials were consistent to within a half-millivolt, measurements on the test electrode were carried out. If the comparison was not consistent or if the potentials approached equilibrium slowly, the electrodes were removed and a new set of hydrogen electrodes was prepared before any measurements were attempted. Electrodes which are not behaving reversibly rarely give identical potentials nor do they give steady time-independent values of potential. Hydrogen electrodes are known to behave satisfactorily in non-aqueous solvents of the kind used in the present work (115) and they gave no problems in the systems studied.

G. CURRENT SUPPLY AND MEASUREMENTS

(a) Constant Current Supply

The polarization circuit shown in Figure VIII consisted of ten series-connected, twelve volt batteries to give 120 volts. The current was controlled by a series of resistors mounted on a rotary switch which could be set to give the desired current, a resistance (1 MΩ) higher than that of the cell always remained in the circuit to ensure that the current remained constant and the cell resistance relatively negligible. The current supply had a range of 10^{-6} to 10^{-2} amps.

Figure VIII

Constant current polarization circuit.

Constant Current Polarisation Circuit

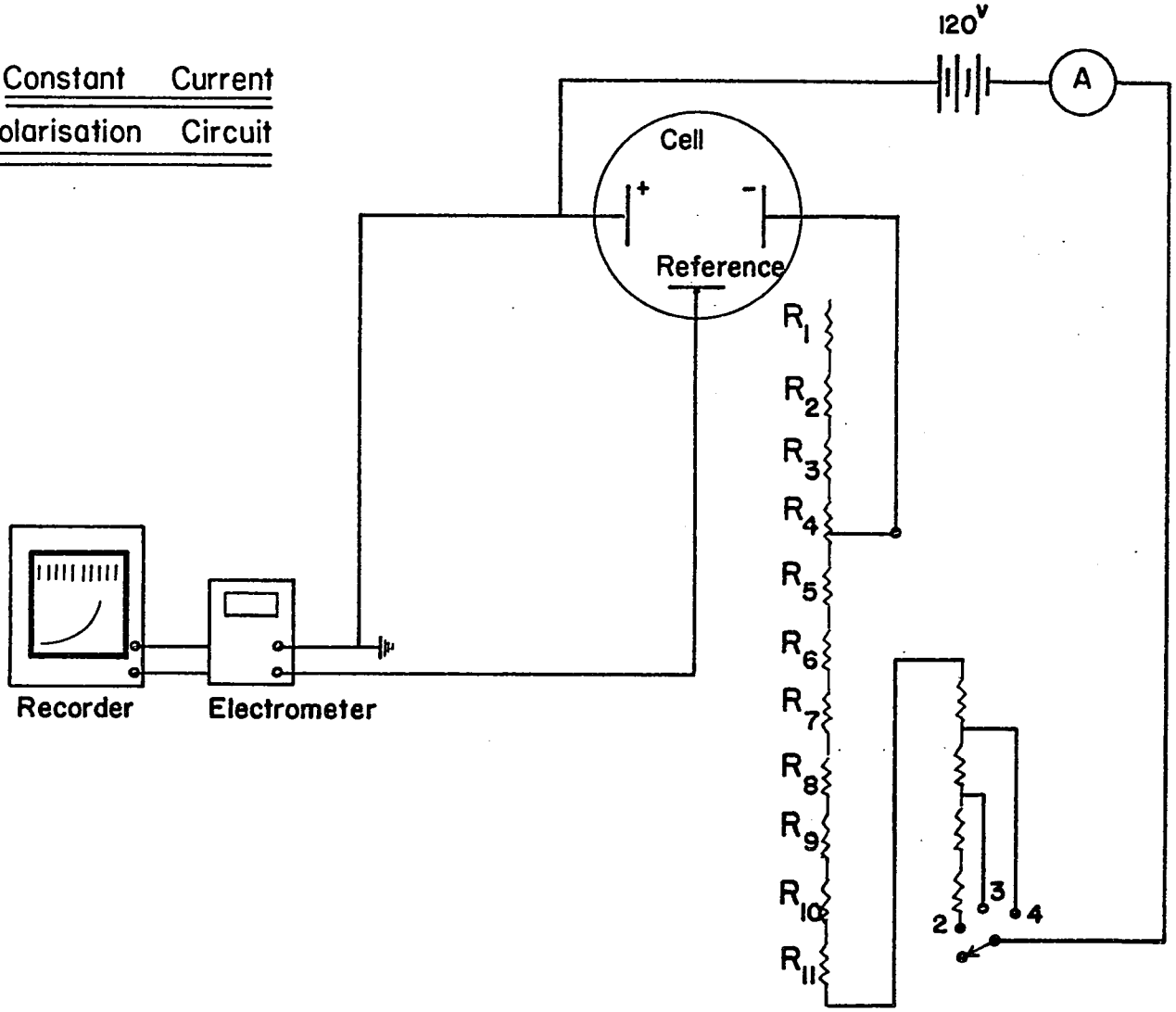

(b) Galvanostatic Circuit

The galvanostatic circuit was so designed that it could be used for charging, open-circuit decay or forced decay studies. The circuit consisted of a four-position mercury wetted contact vacuum relay (C.P. Clare model HG2A-1004) the contacts of which were activated by an internal electromagnet. The circuit is shown in Figure IX. For study of the charging curves, the output from the constant current supply was connected to positions two and five (see Fig. IX), and the cell electrodes were then connected to positions three and six. The relay was activated by depressing the micro-switch M and the current was immediately impressed on the electrodes.

For study of open-circuit decay curves, the constant current supply was connected to positions two and five (see Fig. IX) while the cell was connected to positions one and four.

Forced decay curves were obtained by applying the constant current supply at positions one and four, and position six was connected to position one and position four to position three; the cell was then connected to positions two and five. Upon depressing the microswitch M, the relay was activated and the current passing through the cell was reversed in direction in a switching time of less than 5×10^{-6} seconds.

Potential-time relationships at the test electrode (the potential of which was referred to that of the hydrogen electrode) were registered on an oscilloscope (Hewlett-Packard

Figure IX

Galvanostatic circuit for

(i) open circuit decay

(ii) charging curves

and

(iii) driven decay measurements.

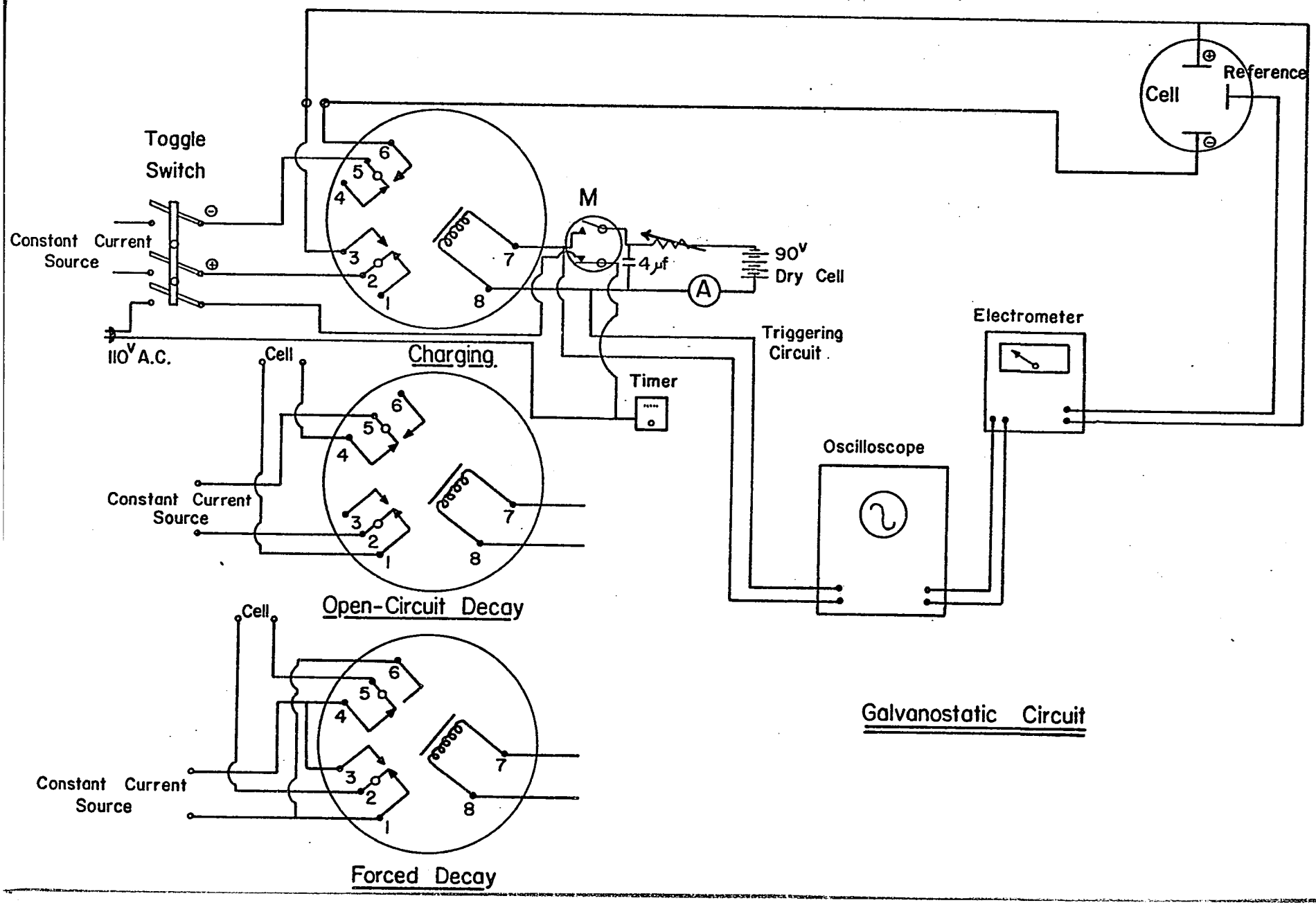
Toggle
Switch
Constant Current
Source
110V A.C.
Cell
Reference
M
4μf
90V
Dry Cell
A
Charging
Timer
Triggering
Circuit
Electrometer
Oscilloscope
Cell
Constant Current
Source
Open-Circuit Decay
Cell
Constant Current
Source
Forced Decay
Galvanostatic Circuit

Model 130A) using a Keithly electrometer (input impedance> 10^{14} ohms) between the test electrode and oscilloscope as an impedance converter to prevent significant current drain from the test electrode and hence to eliminate spurious time dependence of potential. The oscilloscope was automatically triggered when the microswitch M was depressed. Transients on the oscilloscope were recorded photographically by means of a Polaroid camera having a short focus attachment (f = 1.9). Photographs of the transients were then enlarged at a magnification of 8 times. A timer was also incorporated into the circuit to time the length of previous anodic polarization of the test electrode prior to current interruption.

(c) Current Measurements

The current applied to the test electrode was measured by means of a Sensitive Research milliameter (Model S) having a series of calibrated ranges from 0.01 to 1000 milliamps full scale. The accuracy of the instrument was certified by the manufacturer as 0.5% of full scale deflection.

(d) Potential Measurements

Measurements of the potential of the test electrode compared with that of the hydrogen electrode were made by one of the following procedures: (i) Potentials were read directly from a recording potentiometer (Phillips model PR2210A), with a high input impedance (> 10^{14} ohms) electrometer (Keithly model 610A) in series between the recorder and test electrode to

prevent significant current drain from the test electrode. (ii) Alternatively, potential measurements were made by means of a manual potentiometer (Radiometer model PHM-4b or a Doran m.V.-pH meter) equipped with an electrometer input circuit (impedance 10^{13} ohms). (iii) Potential variations over short times (1 m sec. to 1 sec.) were recorded on the oscilloscope using the electrometer as an input stage. The y-axis of the oscilloscope was calibrated by means of a potentiometer acting as a calibrated source of potential. The x-axis was calibrated by means of an electronic time marker.

H. COULOMBIC MEASUREMENTS IN CURRENT EFFICIENCY DETERMINATIONS

(a) Coulometer

The number of coulombs passed during electrolysis was evaluated by arranging a copper coulometer in series with the gas-collection coulombic efficiency cell. The copper coulometer was chosen as it is most suitable for repeated measurements and is more convenient for measurements of appreciable amounts of electricity than for example the iodine or silver coulometer (116). The increase in weight of a small cathode of platinum is measured after electrolysis between a pair of pure copper anodes in a copper sulphate solution. After electrolysis, the cathode is rinsed several times in distilled water, rinsed with acetone and dried at 100°C for a few minutes, allowed to cool and then weighed. One coulomb deposits 0.3292 mg. of copper.

The electrolyte was prepared by adding 125 g. copper sulphate ($CuSO_4 \cdot 5H_2O$) to a liter of tenth normal sulphuric acid. Fifty ml. of ethanol was added as an "additional agent" to improve the cohesion and structure of the deposit.

(b) Coulombic Efficiency Studies

Solutions and electrodes were prepared as previously described (page 70). The cell was filled with solution, saturated with carbon dioxide and allowed to come to thermal equilibrium at 5°C. The flow of gas through the solution was then stopped, and the solution electrolysed for approximately thirty minutes at the required current density, the gas evolved being vented to the atmosphere. This procedure ensured that the system was saturated with the desired product gases. Experimental measurements were then undertaken by placing the copper coulometer in the electrolysis circuit, and connecting the cell to the gas collecting burette. The gas was then collected by displacement of mercury at constant pressure and temperature.

(c) Volume Measurements

The apparatus designed to collect the evolved gas is shown diagramatically in Figure VI; a photograph of the entire apparatus is shown in Figure VII. The coulombic cell was connected at C (see Fig. VI) and the system evacuated to a pressure of less than 10^{-4} mm. Hg. The cell was connected to a graduated pipette by capillary tubing, the volume of which had

been previously determined. The gas was collected by displacement of mercury at constant temperature and pressure. At the commencement of electrolysis, the evolved gas was allowed to accumulate in the anode compartment until a sufficient pressure was reached that the solution would not be sucked into the evacuated gas collecting system when stopcock F was opened. Stopcock D was so adjusted that the gas could pass into the gas collecting burettes and at the same time a constant pressure manometer could be made to communicate with the system. The gas was kept at constant pressure by lowering the mercury reservoir H until constancy of pressure was indicated by an electric circuit incorporated into the constant pressure manometer. When a sufficient volume of gas had been collected and the electrolysis terminated, stopcock F was closed, the manometer adjusted and the volume of gas recorded and corrected to S.T.P. after allowance for the vapor pressure of the solvent.

(d) Gas Analysis

Carbon dioxide was determined by passing the gas in the burette through a 40% solution (by weight) of potassium hydroxide contained in an Orsat type absorption pipette. Remaining gases were then transferred to a gas sampling bulb at constant pressure and volume and analysed by gas-phase chromatography (Perkin-Elmer Model 154) using a silica gel or a molecular sieve (Linde Type 13x) column. Accurate analysis was achieved by preparing a series of calibration curves for

H_2, O_2, CF_4 and C_2F_6. The fractograms of the unknown mixture could then be compared against these and the quantity of unknown gases determined by comparing either peak heights or half widths.

I. EXPERIMENTAL PROCEDURE

(a) Polarization Measurements

After the solution had been prepared (as described previously) and transferred to the cell, the solution was cooled at $5^{o}C$ by circulating coolant from a low temperature thermostat through glass coils in the solution. Carbon dioxide was then bubbled through the non-aqueous and aqueous solutions and nitrogen through the basic aqueous solutions containing KOH. Pre-electrolysis was then commenced on a sacrificial electrode and continued for a minimum of twenty-four hours. Pre-electrolysis was interrupted by raising the pre-electrolysis electrode above the level of the solution. Potential measurements were then carried out by lowering one of the encapsulated electrodes under the solution and shattering the glass capsule surrounding the electrode by means of a glass probe. The electrode was then adjusted carefully against a Luggin capillary, and potential measurements were conducted over the current density range of 10^{-7} to 10^{-2} amps. $cm.^{-2}$ This procedure was repeated with the five other electrodes in the same solution. The potentials measured were with respect to the hydrogen electrode which had

been checked previously against another hydrogen electrode. Potentials were either recorded on a recording potentiometer or obtained manually on a balancing potentiometer as previously described.

Potential measurements were conducted by either the rapid method (117) in which the potential was measured (beyond the period of double layer charging) as quickly as possible after setting the current to successive desired values or by waiting until the potential has reached a steady value; the latter method was used only near the transition region of the current-potential curve, i.e. near and at the critical current density where there is a discontinuity in the current potential curves (see below).

(b) Galvanostatic Measurements

Galvanostatic transient studies were carried out in the same cell as that used for the steady-state potential measurements.

Electrodes, solutions and pre-electrolysis were carried out as previously described. When pre-electrolysis was terminated, one of the glass bulbs containing an electrode was broken under the solution and placed carefully against the Luggin capillary. On this electrode overpotential measurements were first carried out over the current density range of 10^{-7} to 10^{-2} amps.cm^{-2}. These measurements were necessary as

a criterion of purity of the solution. If the potential measurements were unsatisfactory, galvanostatic measurements were not carried out, and pre-electrolysis was continued for a further period or a fresh solution was prepared until satisfactory η -log[i] relations were obtained indicating a satisfactory degree of removal of impurities and depolarizers from the solutions.

Potential-time relationships, for the d.c. charging process, open-circuit decay and d.c. forced decay were then obtained in each case by breaking a further clean unused electrode under the solution, placing it against the Luggin capillary and allowing the test electrode to attain its rest potential. In each series of measurements the solutions were freshly prepared and treated as previously described to attain the required purity.

Galvanostatic charging curves were obtained by previously setting the current at the desired value, and impressing it on the test electrode by activating the relay. The resulting transient was then recorded photographically on the oscilloscope.

Potential-time relationships for the decay process were obtained by either polarizing the test electrode at the desired current density until a steady potential was reached or by polarizing the electrode for several controlled increments of time (1-300 secs.). The current was then terminated by

activating the relay and the resulting transient was recorded.

Galvanostatic forced decay studies were carried out by polarizing the test electrode at the desired current density for the controlled intervals of time (1-300 secs.), and then reversing the current by activating the relay, as described above, and recording the resulting transient on the oscilloscope.

In all the galvanostatic studies the test electrode was allowed to return to within 5-10 mV of its original rest potential before further measurements were undertaken on the same electrode. The current-potential curves for the non-aqueous decarboxylation reactions showed little hysteresis so that it was legitimate to make several transient measurements on the same electrode. In each solution, four or five separate electrodes could be studied successively.

J. TEMPERATURE CONTROL

The temperature of the solution in the polarisation cell was maintained constant by circulating a coolant through a cooling coil specially sealed in the anode compartment and through a water jacket around the reference electrode compartment. The coolant was kept at $5^{\circ}C$ by means of two low-temperature thermostats (Wilkins Anderson Company, Model 882). The low-temperature baths were capable of maintaining the temperature constant to within about $0.03^{\circ}C$. The cell temperature could be maintained at $5 \pm 0.1^{\circ}C$. This temperature was used for all the runs in order to minimise attack of the noble metals under anodic

conditions in the non-aqueous solutions.

The gas collecting system was maintained at 30 ± 0.5°C by enclosing the whole system in a box constructed of insulating material. Temperature control was effected through the use of a red-top thermoregulator and relay connected to a 40 watt bulb. A fan mounted in the box ensured good air circulation and maintenance of constant temperature throughout the air thermostat box.

The coulombic efficiency cell was cooled to 5 ± 0.1°C by placing the cell in a water bath cooled to 5°C by circulating water at 5°C through it by means of a copper coil. The water was cooled to 5°C by the same low-temperature baths as used for controlling the temperature of the polarization cell.

CHAPTER III

RESULTS

A. CURRENT-POTENTIAL RELATIONSHIP AND COULOMBIC YIELDS

(a) General

We have discussed in Chapter I in the section on experimental approaches for the elucidation of reaction mechanisms how the Tafel parameters under certain limiting conditions of surface coverage can provide valuable diagnostic criteria for the assignment of the reaction mechanism, provided that knowledge of reaction products is available and some kinetic scheme of the consecutive reactions has been formulated.

In the following section, experimental results are first presented for product analysis and coulombic yields; potential-current relationships (Tafel plots) for platinum, palladium and gold obtained in the anhydrous formate-formic acid and anhydrous trifluoroacetate-trifluoroacetic acid systems are then described. Results are also given for the same metals in aqueous formate and trifluoroacetate, and aqueous formate to which has been added KOH to stabilise the pH.

(b) Product Analysis and Coulombic Yields

The products of electrolysis were identified by gas-phase chromatography and chemical methods. Coulombic yields were determined in each linear Tafel region, and the experimental

results are given in Table [I]. In the anhydrous formate-formic acid solutions, the only product observed was carbon dioxide, the coulombic efficiency being high at high current densities, and falling appreciably in the lower Tafel region, where significant attack of the anode metal occurred. Almost quantitative yields, in terms of hexafluoroethane and carbon dioxide, (see Table II) were obtained in the trifluoroacetate-trifluoroacetic acid system at high current densities. With decreasing current densities, efficiencies for the coupling reaction fell somewhat and tetrafluoromethane was also detected in small amounts ($< 2\%$). At quite low current densities some attack of the metal was again visible.

In aqueous formate solutions, the yield of carbon dioxide was fairly high (see Table III) in the high current density upper Tafel region (see below). However, oxygen was also detected, the amount increasing as the current density was lowered as shown in Table [III]. In some exploratory experiments in basic aqueous solutions of 1 M potassium formate, carbon dioxide could still be identified as one of the reaction products but oxygen was now the major gaseous product observed, since most of the CO_2 formed would be absorbed in the basic solution.

(c) Experimental Electrode Potential-Current Density Relationships

In order to study the mechanisms of the decarboxy-

Table I

Coulombic Efficiencies for CO_2 Production in the Anodic Decarboxylation in Formic Acid

1 M HCOOK/HCOOH, 5°C.

Electrode	Current Density amps. cm^{-2}	Products	Coulombic Yield % CO_2
Pt	1×10^{-2}	CO_2	86
	2.5×10^{-3}	CO_2	79
	5×10^{-4}	CO_2	65
Pd	1×10^{-2}	CO_2	84
	1.2×10^{-3}	CO_2	75
	5×10^{-4}	CO_2	56
Au	1×10^{-2}	CO_2	86
	1×10^{-3}	CO_2	62
	5×10^{-4}	CO_2	55

Table II

Coulombic Efficiencies for CO_2 and C_2F_6 Production in the Trifluoroacetate Kolbe Reaction (100% trifluoroacetic acid 5°C)

Electrode	Current Density amps.cm.$^{-2}$	Coulombic Yield $\%CO_2$	Coulombic Yield $\%C_2F_6$
Pt	1×10^{-2}	94	96
	2.5×10^{-3}	93	92
	5×10^{-4}	93	85
Pd	1×10^{-2}	96	95
	2.5×10^{-3}	94	91
	5×10^{-4}	93	83
Au	1×10^{-2}	91	92
	2.5×10^{-3}	90	89
	5×10^{-4}	89	80

Note: at low current densities ($< 10^{-3}$ amp.cm.$^{-2}$), traces of CF_4 were identified in amounts less than 1-2% of the total volume of gas evolved and analysed.

Table III

Coulombic Efficiencies for CO_2 and O_2 Production in the Anodic Decarboxylation in Aqueous Potassium Formate

1 M HCOOK, 5°C.

Electrode	Current Density amps.cm.$^{-2}$	Coulombic Yields % CO_2	% O_2
Pt	1×10^{-1}	93	6
	2.5×10^{-2}	72	24
	5×10^{-3}	65	33
Pd	1×10^{-1}	74	21
	2.5×10^{-2}	63	27
	5×10^{-3}	52	33
Au	2.5×10^{-2}	24	55
	3.1×10^{-3}	22	38

lation reactions and to investigate the processes involved in the overall anodic reaction, current-potential measurements were made, in which the overall rate was measured in the usual way directly in terms of current as a function of potential (measured vs. the hydrogen electrode in the same solution). The experimental procedures used have been described in Chapter II (p. 83). All measurements were carried out at 5°C. in order to minimise attack of the metal anode which occurs significantly at room and higher temperatures, as was discussed above.

(i) The Formate-100% Formic Acid System at Platinum, Palladium and Gold

Potential-current relationships for this system were obtained by the so called "rapid method", (117) in which the electrode potential is recorded as rapidly as possible after the current density* has been adjusted to the desired value. Comparison with results obtained by the "steady state" or slow (117) method indicated no change of the Tafel slopes but the transition region (see below) from a lower to an upper Tafel line appeared at lower current densities in the slow method. This is to be expected since, as we show below, the transition region is associated with changes of the condition of anodic

* That is at current densities sufficient for the non-Faradaic ionic double-layer charging process to be terminated within 10-20 seconds.

surface films and these have more time to be formed under "slow" conditions near to the critical current.

Experimental Tafel plots for platinum, palladium, and gold over the current density range 10^{-7}-10^{-1} amps.cm.$^{-2}$ for the concentrations 0.1, 1 and 5M potassium formate in formic acid are shown in Figures [X, XI, XII]. In all these experiments, the data presented are based on runs on at least twelve electrodes studied in at least two separately prepared solutions. A typical assembly of points is shown for one series of runs in Figure XII but in the other figures referred to above, the data are shown as the best straight lines drawn over the linear regions of the V-log [i] plots. In most cases very satisfactory reproducibility was observed and it was unnecessary to make statistical calculations of the lines of best fit.

In each case, there are two ranges of potential over which Tafel behavior is observed, the transition from the lower to the upper region occurring over a narrow range of current densities or effectively at some critical current density. As will be recalled from the discussion on film growth (Chapter I), this is a typical phenomenon exhibited by many metals during the onset of anodic passivation. In the upper potential region, both platinum and palladium (Figures X, XI) show single linear regions with Tafel slopes of 0.14 and 0.10 volts per decade of current density, respectively. Gold

Figure X

Tafel plots for formate decarboxylation on Pt in 0,1, 1 and 5 M HCOOK/HCOOH.

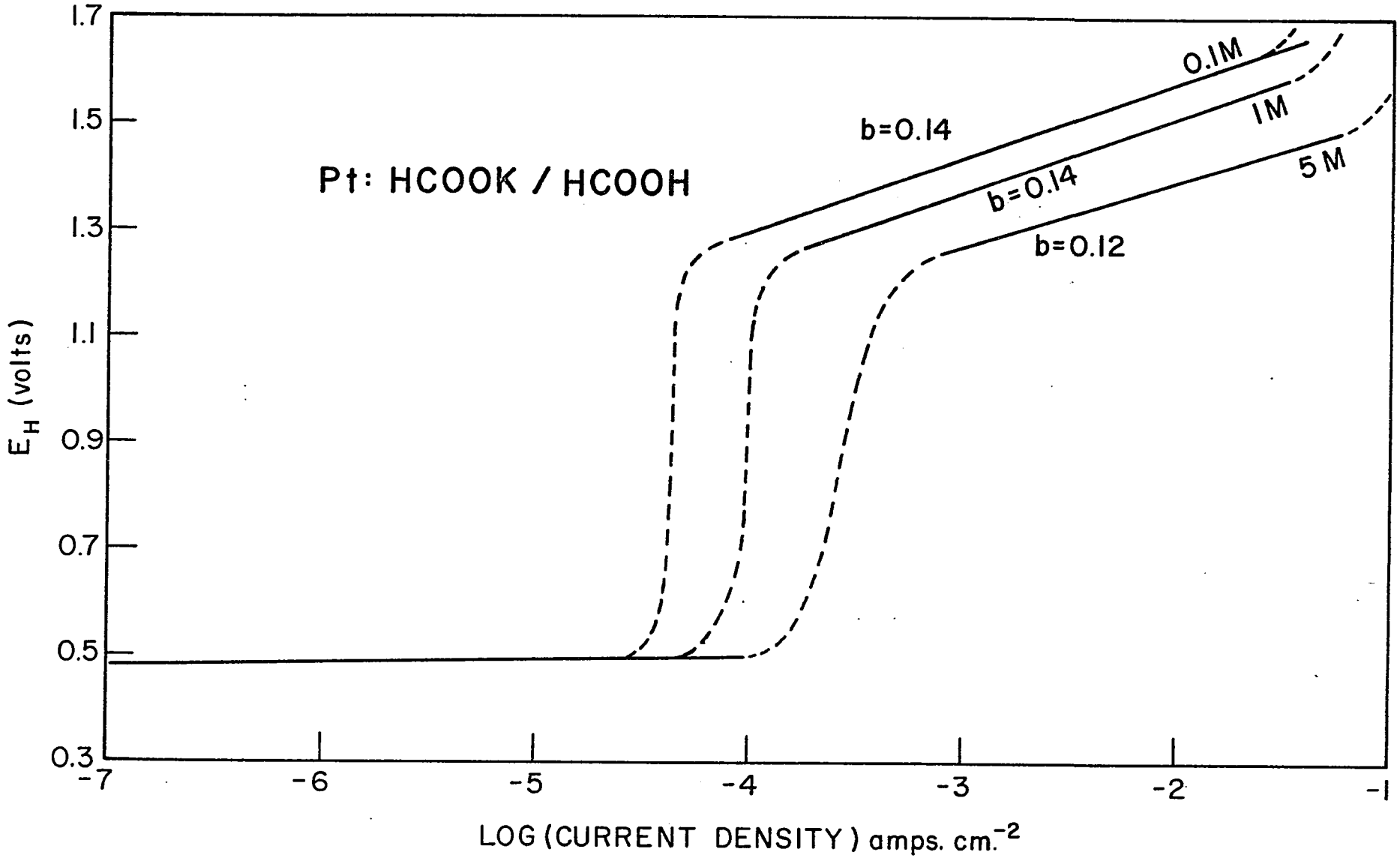
Pt: HCOOK / HCOOH
0.1M
b=0.14
1M
b=0.14
5 M
b=0.12
E_H (volts)
1.7
1.5
1.3
1.1
0.9
0.7
0.5
0.3
-7
-6
-5
-4
-3
-2
-1
LOG (CURRENT DENSITY) amps. cm.$^{-2}$

Figure XI

Tafel plots for formate decarboxylation on Pd in 0.1, 1 and 5 M HCOOK/HCOOH.

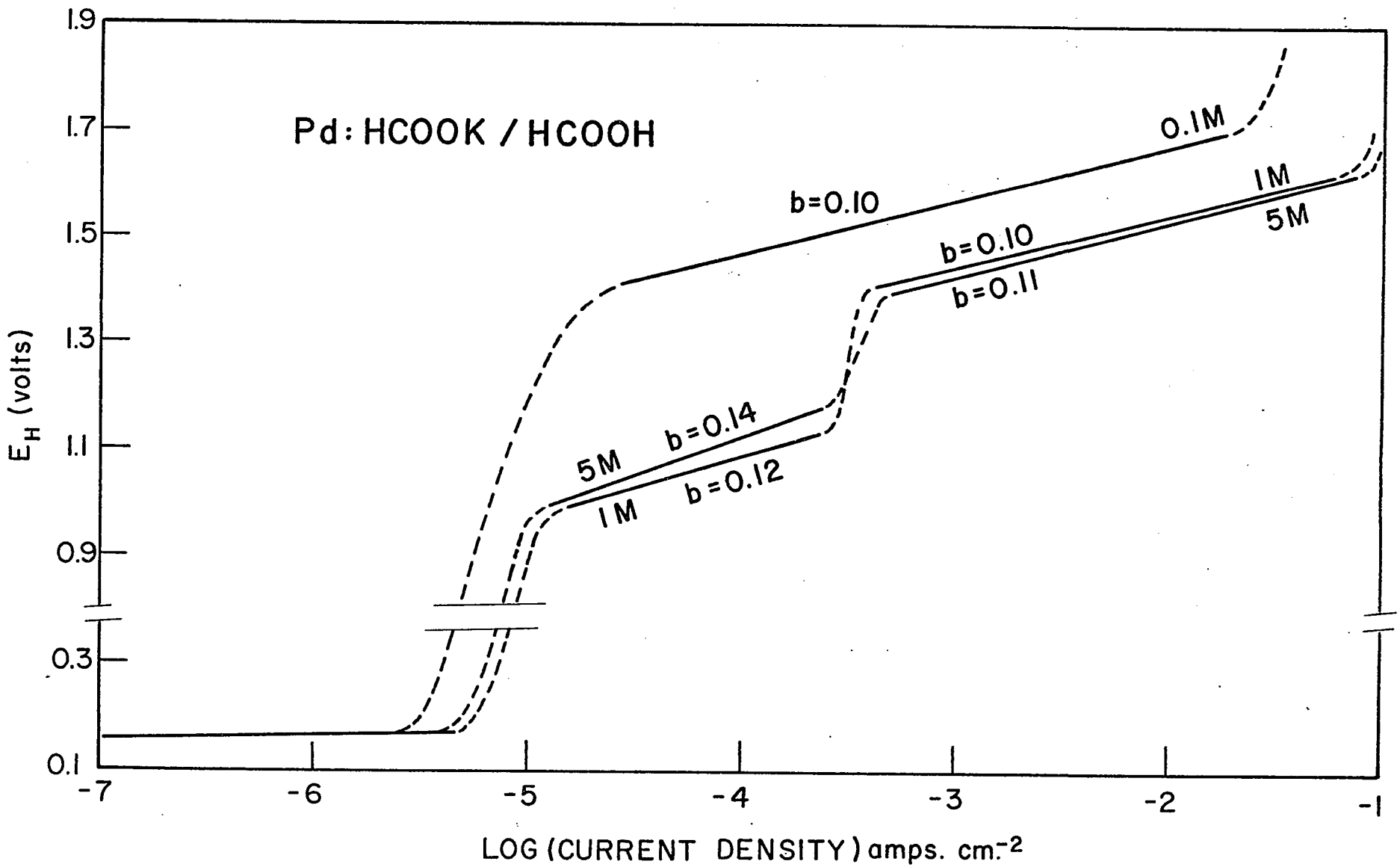
Pd: HCOOK / HCOOH
0.1M
b=0.10
1M
5M
b=0.10
b=0.11
5M b=0.14
1M b=0.12
1.9
1.7
1.5
1.3
1.1
0.9
0.3
0.1
E_H (volts)
-7
-6
-5
-4
-3
-2
-1
LOG (CURRENT DENSITY) amps. cm.$^{-2}$

Figure XII

Tafel plots for formate decarboxylation on Au in 0.1, 1 and 5 M HCOOK/HCOOH.

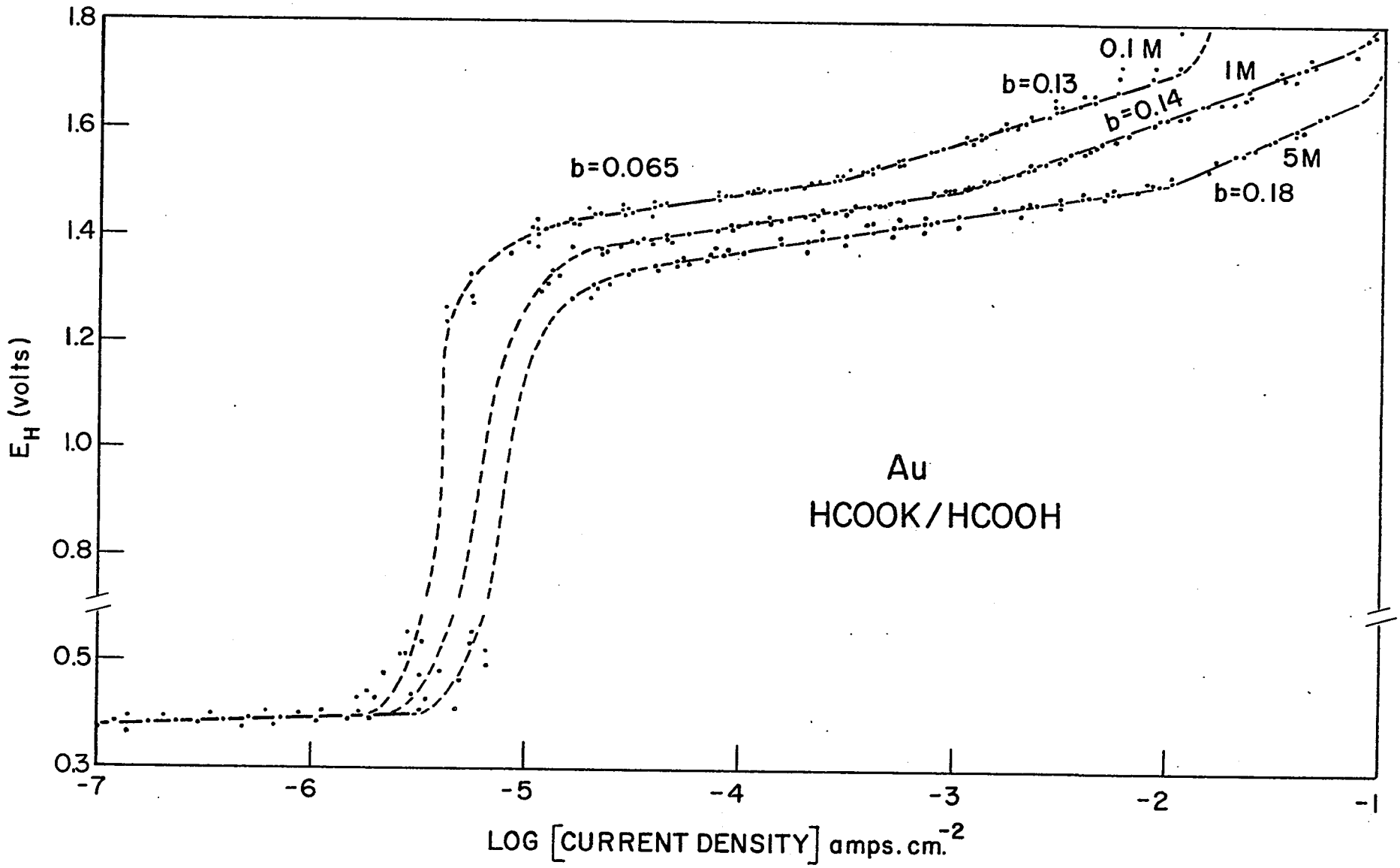
1.8
1.6
1.4
1.2
1.0
0.8
0.5
0.3
E_H (volts)
0.1 M
b=0.13
1M
b=0.14
5M
b=0.18
b=0.065
Au
HCOOK/HCOOH
-7
-6
-5
-4
-3
-2
-1
LOG [CURRENT DENSITY] amps. cm.$^{-2}$

(Figure XII) on the other hand shows two characteristic slopes of 0.065 and 0.14 volts per decade in the upper potential region, which, as pointed out in Chapter I, can be indicative (see Chapter IV) of a change in the reaction mechanism or of surface coverage conditions at the metal/solution interface. The corresponding exchange currents for these linear Tafel regions have been calculated and are presented in the Discussion section, where the corresponding reversible potentials for the reactions examined are derived.

At each metal, increasing formate concentration results in a decrease of overpotential in the upper Tafel region; however, no effect was observed in the lower Tafel region. The Tafel slopes at platinum and palladium remain sensibly constant with increasing formate concentration. At gold, the initial linear region in the upper Tafel region extends over a larger current density range with increasing formate concentration, but the Tafel slopes remain more or less constant, however, with changing concentration.

(ii) Palladium-Gold Alloys in the Formate-Formic Acid (100%) Acid System

In Chapter I, it was pointed out that the nature of the anode material was an important factor determining the efficiency and kinetics of the Kolbe reaction. The possible dependence of electronic configuration of the metal d-band on the kinetics of the formate decarboxylation reaction was

also investigated in the present work using a series of palladium-gold alloys. Analogous work has recently been carried out for the oxygen evolution reaction at the same alloys (87) and for the hydrogen evolution reaction at copper-nickel alloys (118). In Figures [XII, XIV, XV] experimental results are shown for three concentrations of potassium formate (0.1, 1 and 5M) in anhydrous formic acid. In the gold-rich alloy (22.6% Pd-Au)* (Figure XIII) the Tafel slopes are seen to be similar to those observed at pure gold (Figure XII); with increasing palladium content, the Tafel slopes approach the values obtained for pure palladium (see Figure (XI)).

As with the pure metals, critical current densities were observed corresponding to a transition region between the upper and lower Tafel lines. Increasing the formate concentration resulted in the displacement of the Tafel lines towards lower values of overpotential** (higher exchange currents - see Figures [XIII-XV]). The initial linear-region was observed to increase in length with increasing formate concentration, as observed at pure gold electrodes (Figure [XII]). The Tafel constants are given in Table [IV].

---

* The percentages given refer to the weight percent Pd in the Pd-Au alloy.

** The overpotentials and related exchange currents are deduced and examined in Chapter IV in relation to the relevant reversible potentials for the reactions examined.

Figure XIII

Tafel plots for formate decarboxylation on the 22,6% Pd-Au alloy in 0,1, 1 and 5M HCOOK/HCOOH.

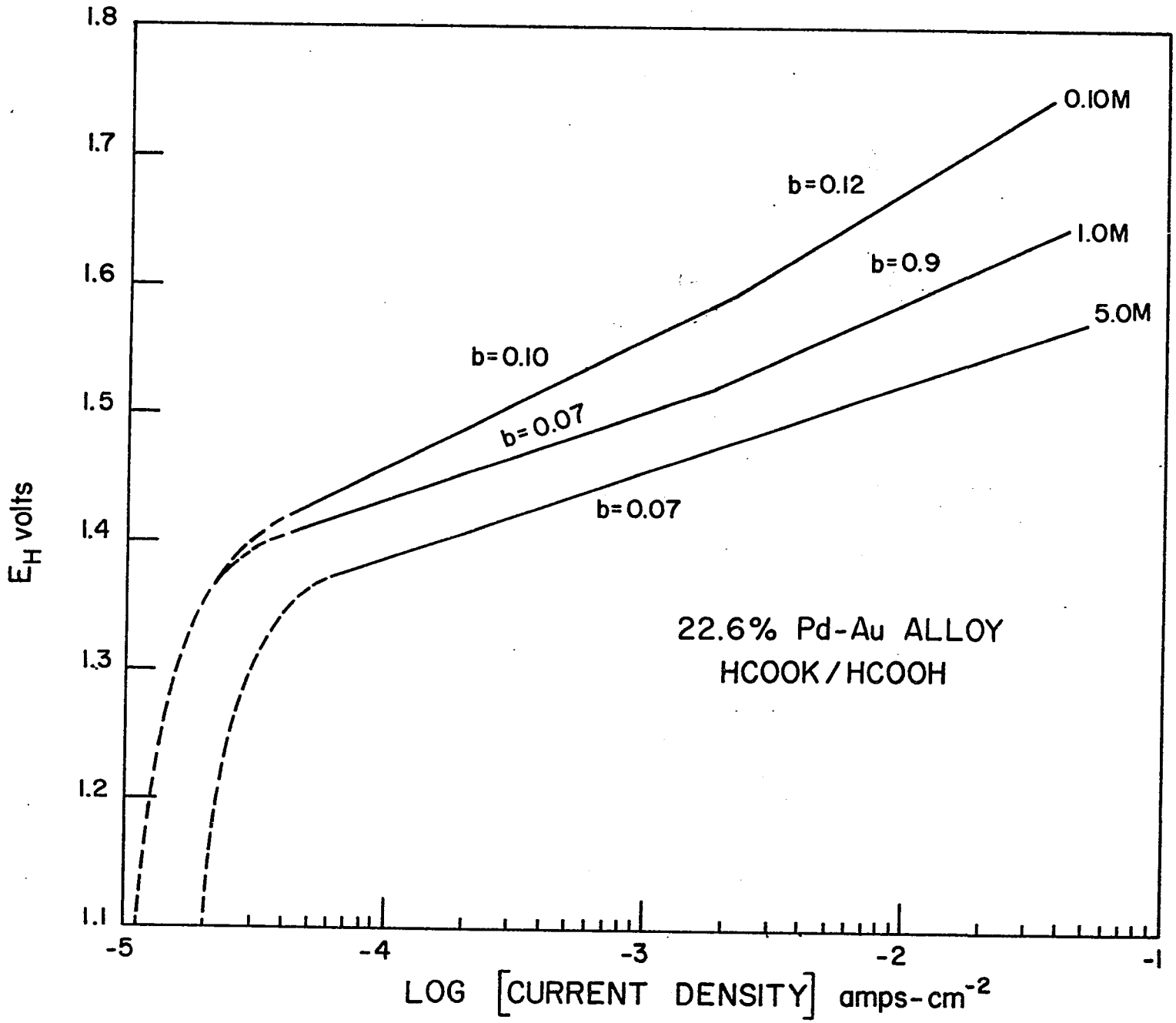
1.8
1.7
1.6
1.5
1.4
1.3
1.2
1.1
E_H volts
-5
-4
-3
-2
-1
LOG [CURRENT DENSITY] amps-cm^{-2}
0.10M
1.0M
5.0M
b=0.12
b=0.9
b=0.10
b=0.07
b=0.07
22.6% Pd-Au ALLOY
HCOOK / HCOOH

Figure XIV

Tafel plots for formate decarboxylation on the 44.8% Pd-Au alloy in 0.1, 1 and 5M HCOOK/HCOOH.

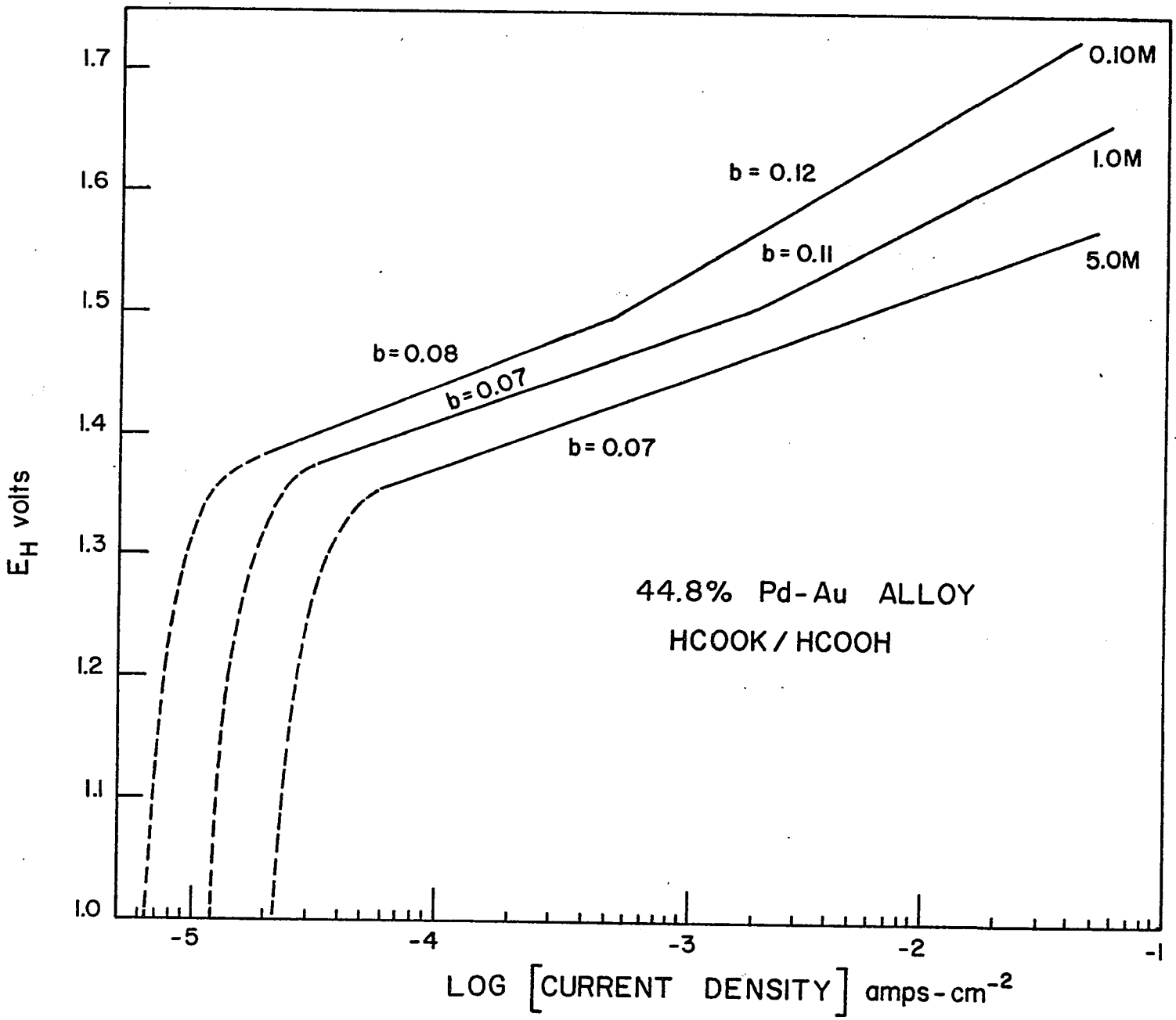
1.7
1.6
1.5
1.4
1.3
1.2
1.1
1.0
E_H volts
0.10M
1.0M
5.0M
b = 0.12
b = 0.11
b = 0.08
b = 0.07
b = 0.07
44.8% Pd-Au ALLOY
HCOOK / HCOOH
-5
-4
-3
-2
-1
LOG [CURRENT DENSITY] amps-cm^{-2}

Figure XV

Tafel plots for formate decarboxylation on the 61.8% Pd-Au alloy in 0.1, 1 and 5M HCOOK/HCOOH.

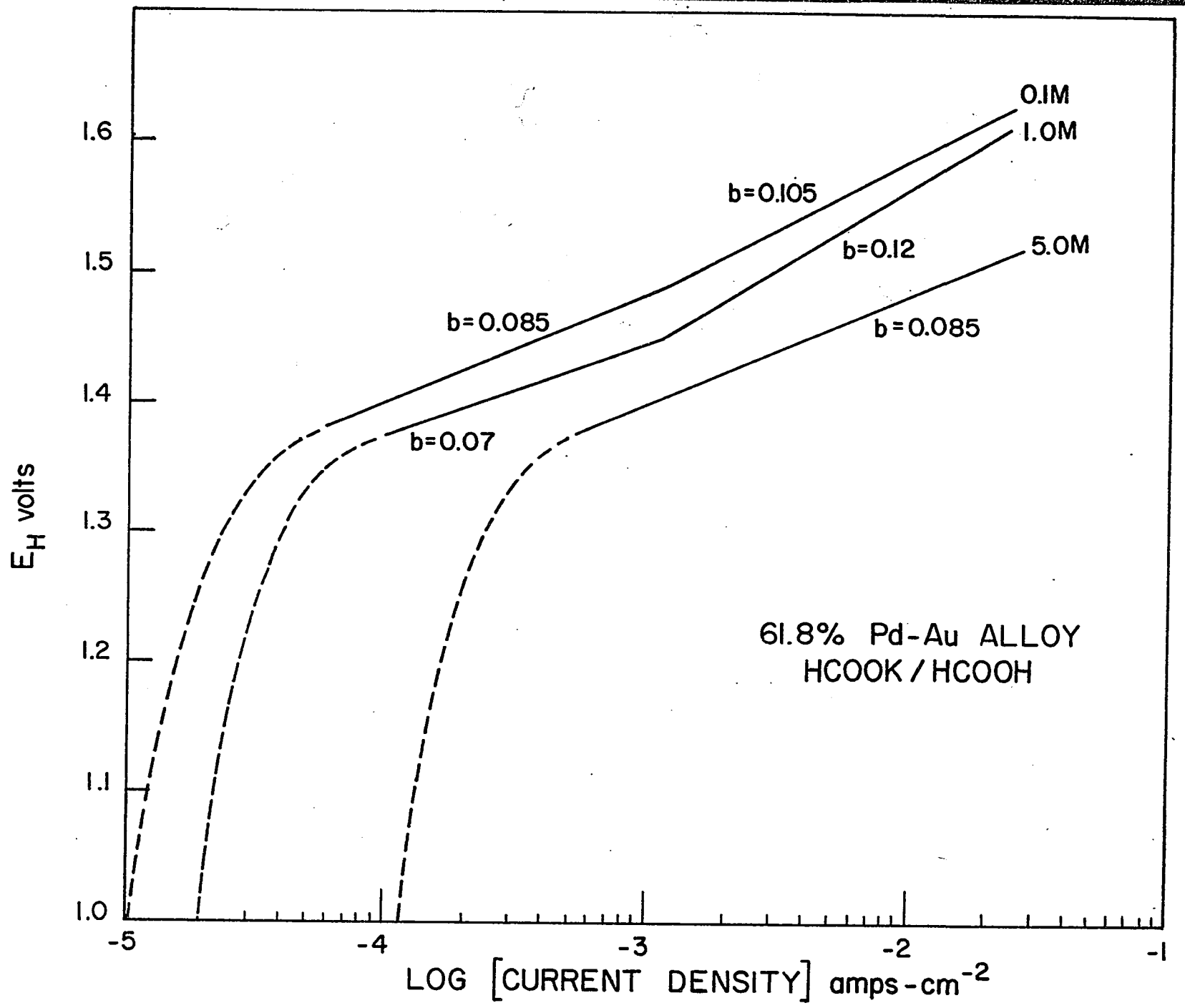
0.1M
1.0M
5.0M
b=0.105
b=0.12
b=0.085
b=0.085
b=0.07
61.8% Pd-Au ALLOY
HCOOK / HCOOH
E_H volts
1.6
1.5
1.4
1.3
1.2
1.1
1.0
-5
-4
-3
-2
-1
LOG [CURRENT DENSITY] amps-cm^{-2}

(iii) Aqueous Formate System at Platinum and Gold

Tafel plots for platinum and gold in this system were obtained by the "steady state" or "slow" method. Measurements were also attempted by the "rapid method"; however, no reproducible results could be obtained, whereas the "slow" method gave excellent reproducibility. Experimental results for both platinum and gold shown in Figures [XVI, XVII] exhibit two potential regions in which linear behavior is observed. It is important to note that a change from a lower to an upper Tafel region occurs at some critical current density (ca. 10^{-3} amps.cm.^{2}) as in the non-aqueous systems. The critical current behavior is thus not especially concerned with potentials required for oxygen evolution as discussed by some previous authors (8,9). A marked hysteresis was observed at both metals in the anode potential-current density behavior obtained under conditions of successively increasing and decreasing constant current. Such hysteresis is not observed in the non-aqueous systems.

Measurements were also attempted on palladium. However, no reproducible results under a variety of experimental conditions (extended pre-electrolysis, method of potential measurement, type of gas bubbled during purification of solutions, etc.) could be obtained.

During all measurements in the aqueous systems, it was observed that the working electrode always remained "bright"

Figure XVI

Tafel plots for formate decarboxylation on Pt in aqueous 1 M HCOOK.

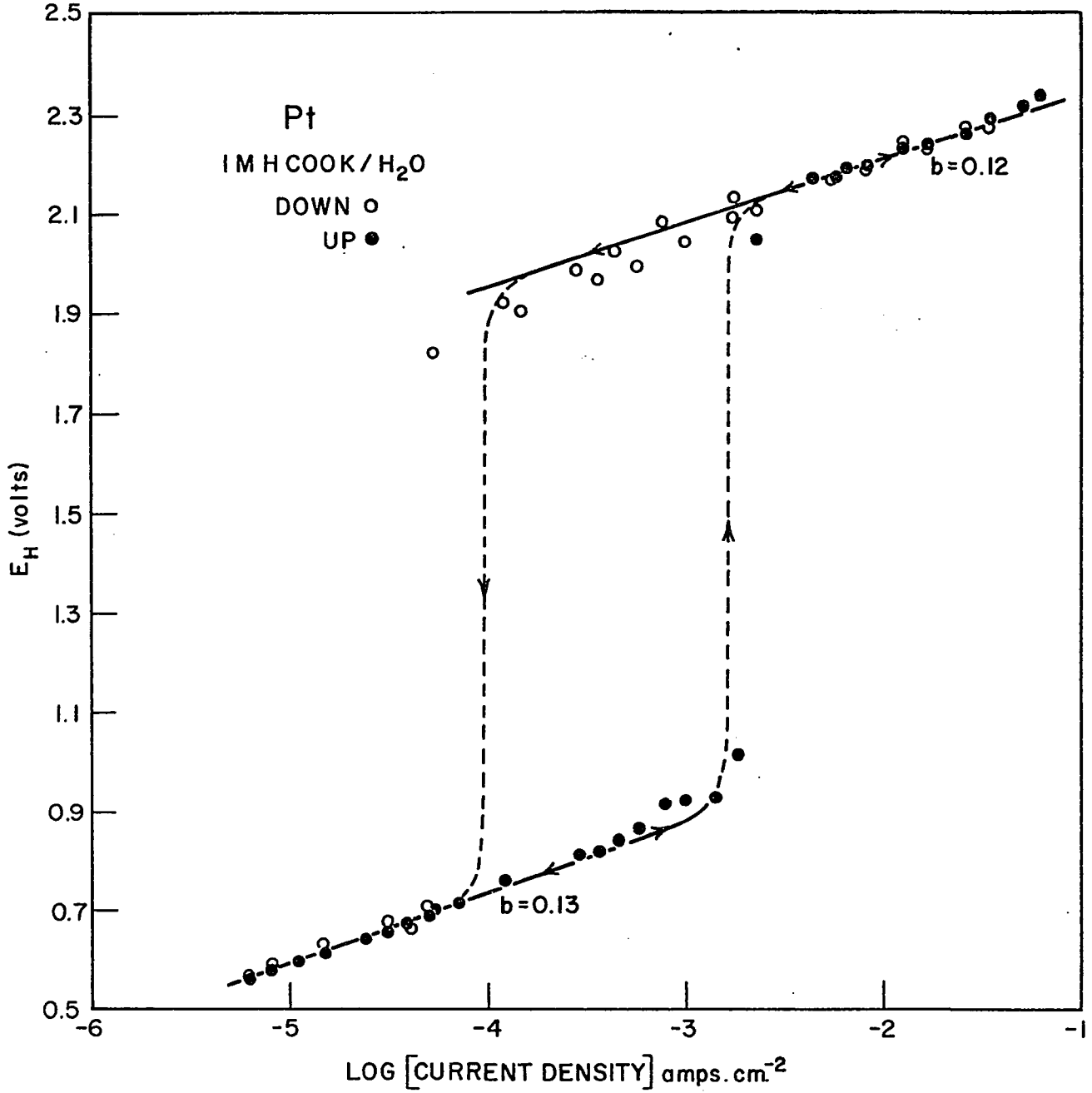
Pt
1M HCOOK / H_2O
DOWN o
UP ●
b=0.12
b=0.13
E_H (volts)
2.5
2.3
2.1
1.9
1.7
1.5
1.3
1.1
0.9
0.7
0.5
-6
-5
-4
-3
-2
-1
LOG [CURRENT DENSITY] amps. cm^{-2}

Figure XVII

Tafel plots for formate decarboxylation on Au in aqueous 1 M $HCOOK_{aq}$

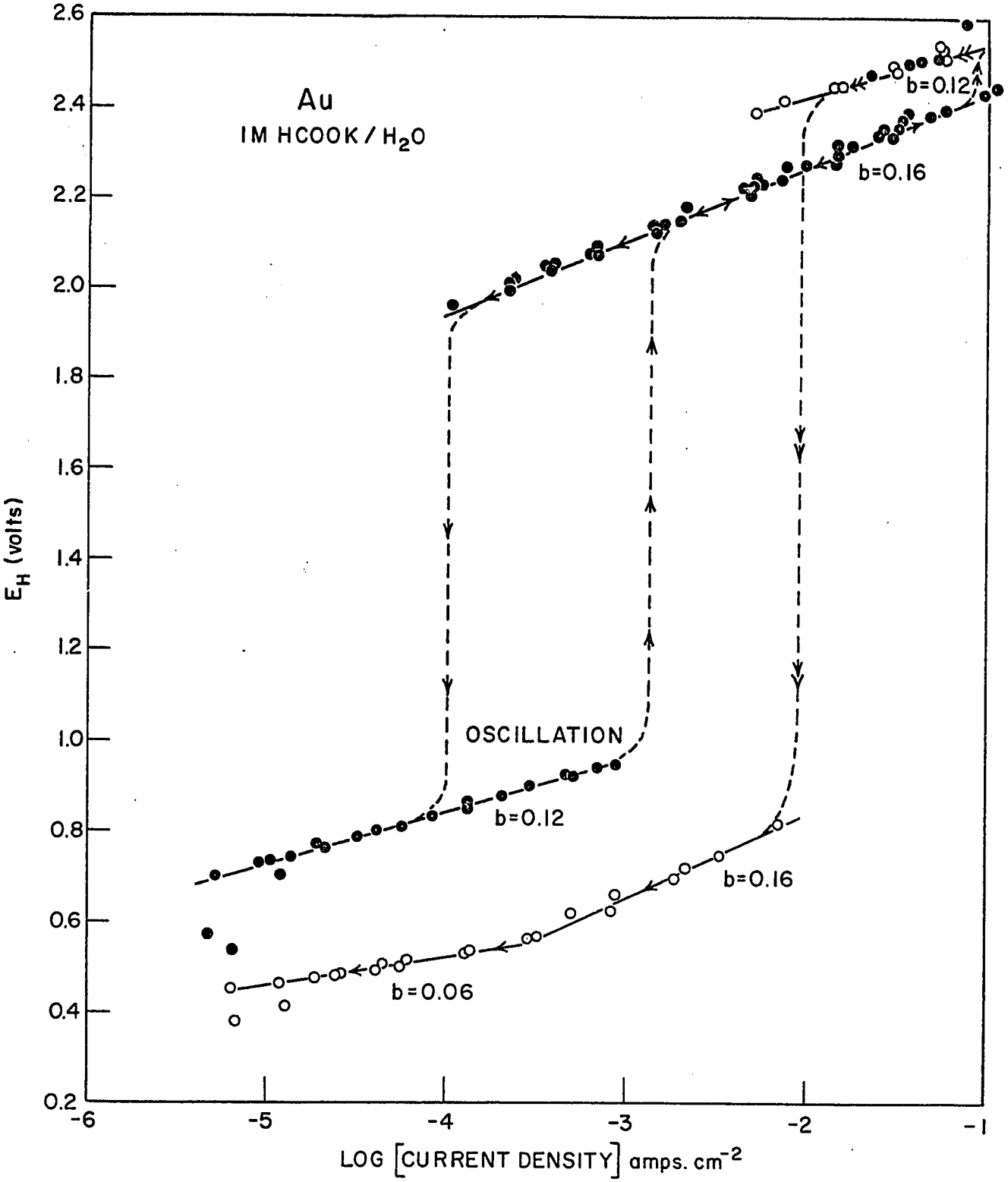
Au
IM HCOOK / H_2O
b=0.12
b=0.16
OSCILLATION
b=0.12
b=0.16
b=0.06
E_H (volts)
LOG [CURRENT DENSITY] amps. cm^{-2}
2.6
2.4
2.2
2.0
1.8
1.6
1.4
1.2
1.0
0.8
0.6
0.4
0.2
-6
-5
-4
-3
-2
-1

with a metallic lustre, except near the highest current densities (ca. 6×10^{-2} amp.cm.$^{-2}$), at which the electrode would turn black due to the formation of a visible anodic film and the current-potential curve would rise to a third short linear Tafel region.

If polarisation measurements were carried out beyond such high current densities, the following behavior was observed:

(α) there was a tendency for a more rapid rise of potential to occur;

(β) upon decrease of current density from these high values, a new second upper region above the first upper region observed with the initially increasing current density, was found;

(γ) with further decrease of current density, a rapid fall of potential (actually a new transition region) occurred to a new lower Tafel region different from that initially observed on the increasing current cycle. This rapid transition occurred at a higher critical current than that corresponding to the normal initial transition region observed with increasing current density in the first part of the run. Experimental results for gold, which demonstrate this type of behavior, are shown in Figure [XVII]. Similar results were also found with platinum. This behavior observed at the quite high current densities was not, however, investigated further owing to its obvious complexity and to the fact that the

principal purpose of the present work was to investigate the non-aqueous media as simpler model systems. It is clear, nevertheless, that further work is desirable for elucidation of this behavior which probably involves formation both of oxide and carboxylate films giving rise to the different types of critical current-potential behavior.

(iv) Aqueous Formate-KOH System at Platinum, Palladium and Gold

The role of oxygen evolution (if any) or oxide film formation in the decarboxylation reaction in aqueous solutions was suggested by the complex behavior observed in the formate decarboxylation kinetics at gold (Figure [XVII]). In order to attempt to facilitate the oxygen evolution process, runs were also carried out in the aqueous formate system (1M HCOOK) in the presence of 1M and 5M KOH. The general result was that the current-potential behavior was simpler than that observed in the absence of KOH and reproducible results could now also be obtained at the palladium electrode as well as at gold and platinum. Tafel plots for platinum, palladium and gold obtained by the steady-state method are shown in Figures [XVIII,XIX,XX] and the Tafel parameters are summarized in Table [V] for 1 and 5 molar KOH solutions with constant formate concentration (1M). In each case, a transition region occurring at some critical current density separates two regions in which linear Tafel behavior was observed. Furthermore, hysteresis in the anode

Figure XVIII

Tafel plots for formate decarboxylation on Pt in aqueous

(a) 1M HCOOK + 1M KOH

(b) 1M HCOOK + 5M KOH.

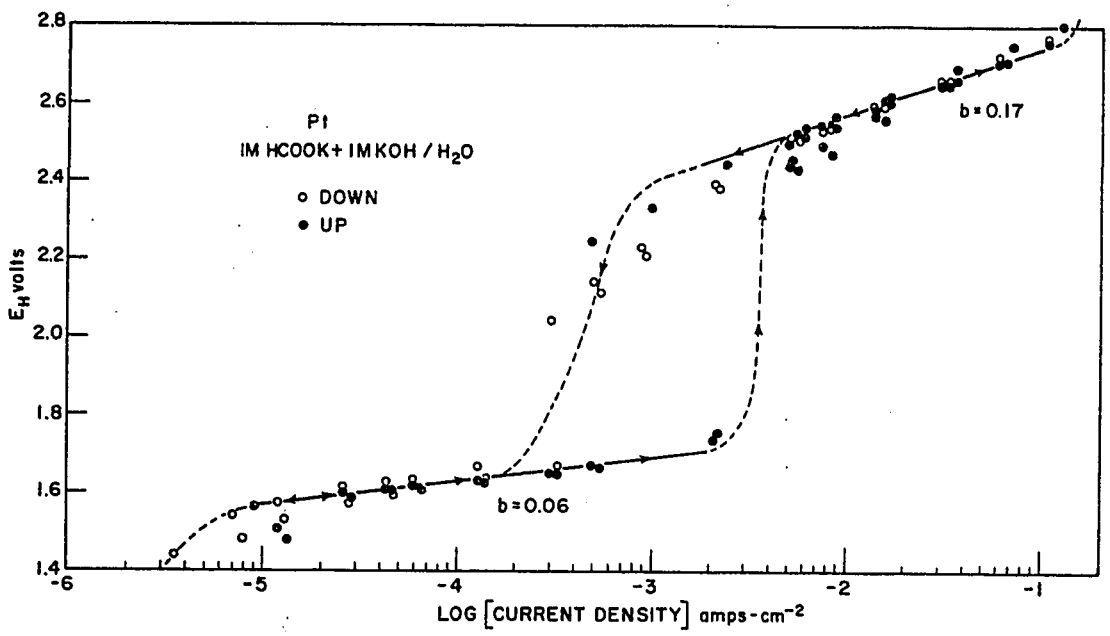
Pt
IM HCOOK + IM KOH / H_2O
o DOWN
• UP
b = 0.17
b = 0.06
E_H volts
LOG [CURRENT DENSITY] amps-cm^{-2}

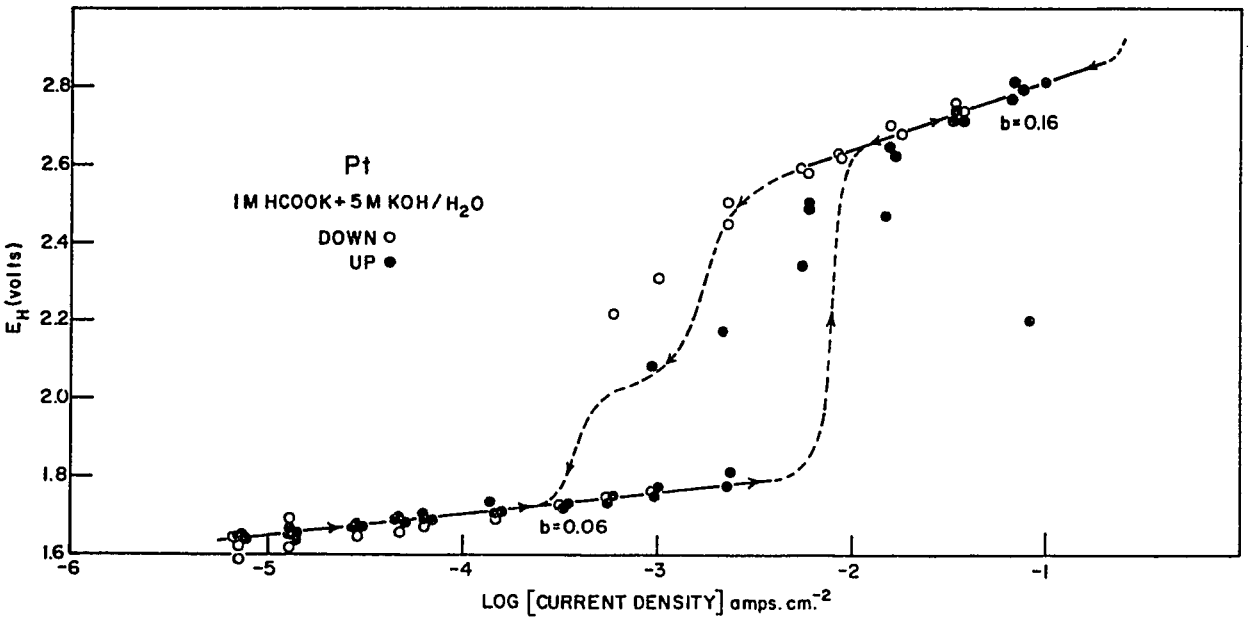
Pt
IM HCOOK + 5 M KOH / H_2O
DOWN o
UP •
b = 0.16
b = 0.06
E_H (volts)
LOG [CURRENT DENSITY] amps. cm.$^{-2}$

Figure XIX

Tafel plots for formate decarboxylation on Pd in aqueous

(a) 1M HCOOK + 5M KOH

(b) 1M HCOOK + 1M KOH.

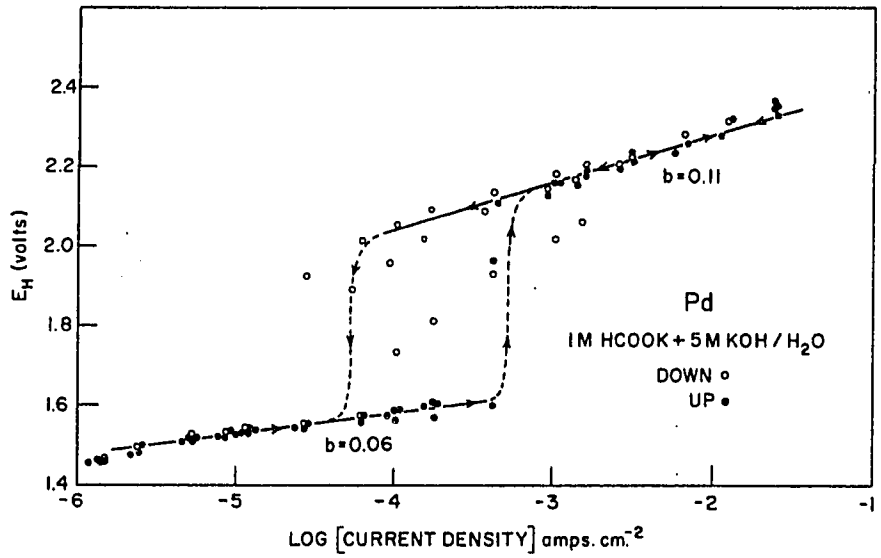
2.4
2.2
2.0
1.8
1.6
1.4
E_H (volts)
b=0.11
Pd
1M HCOOK+5M KOH / H_2O
DOWN ○
UP ●
b=0.06
-6
-5
-4
-3
-2
-1
LOG [CURRENT DENSITY] amps. cm.$^{-2}$

Pd
240 Å

175

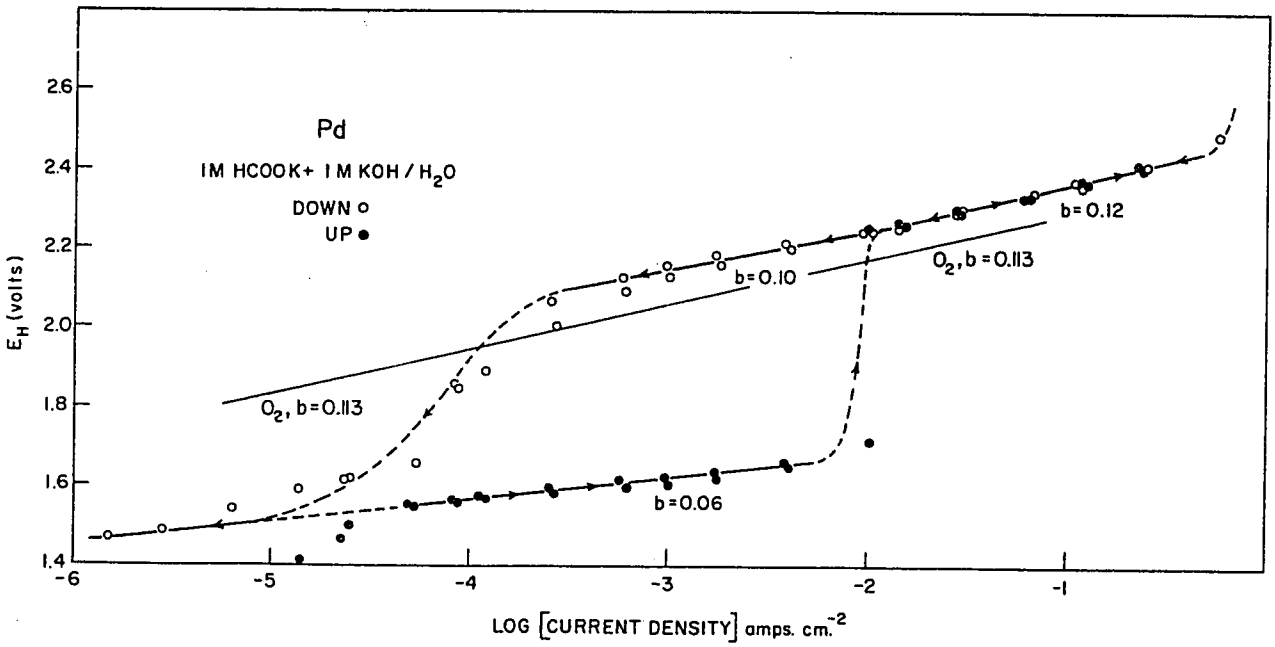
2.6
2.4
2.2
2.0
1.8
1.6
1.4
E_H (volts)
Pd
1M HCOOK+ 1M KOH / H_2O
DOWN ○
UP ●
b=0.12
O_2, b=0.113
b=0.10
O_2, b=0.113
b=0.06
-6
-5
-4
-3
-2
-1
LOG [CURRENT DENSITY] amps. cm.$^{-2}$

Figure XX

Tafel plots for formate decarboxylation on Au in aqueous

(a) 1M HCOOK + 5M KOH

(b) 1M HCOOK + 1M KOH.

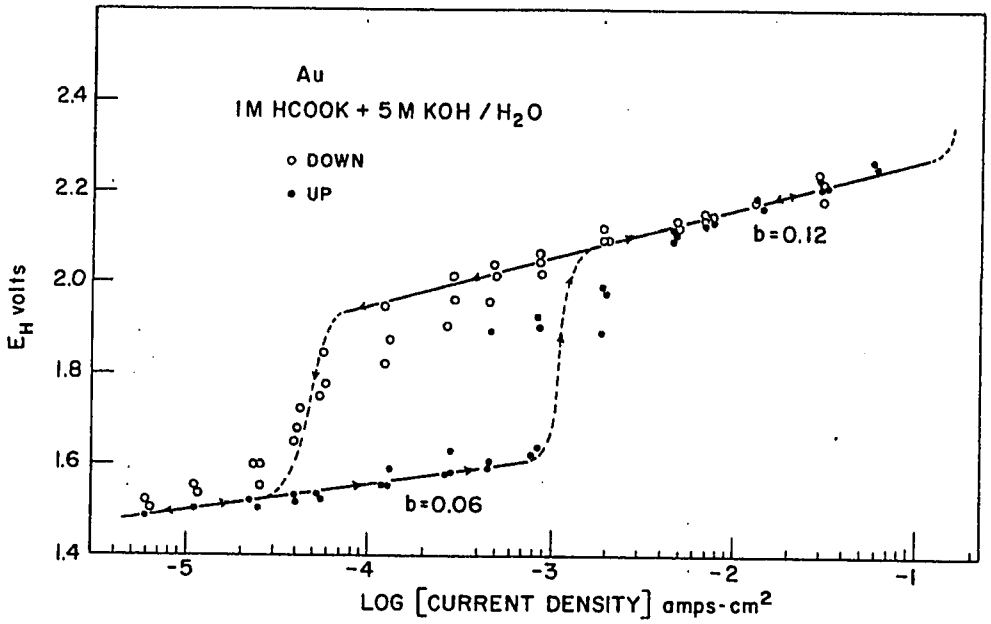
Au
1M HCOOK + 5M KOH / H_2O
o DOWN
• UP
b=0.12
b=0.06
E_H volts
2.4
2.2
2.0
1.8
1.6
1.4
-5
-4
-3
-2
-1
LOG [CURRENT DENSITY] amps-cm^2

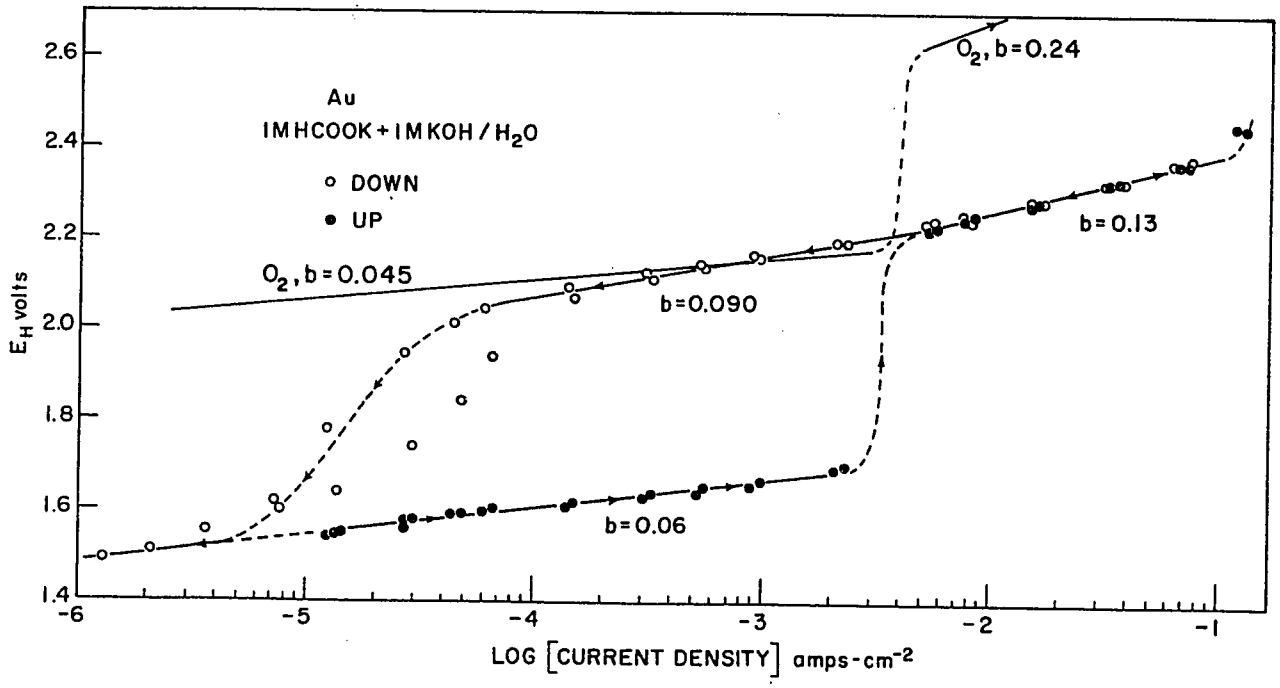
Au
1M HCOOK + 1M KOH / H_2O
o DOWN
• UP
O_2, b=0.24
O_2, b=0.045
b=0.090
b=0.13
b=0.06
E_H volts
2.6
2.4
2.2
2.0
1.8
1.6
1.4
-6
-5
-4
-3
-2
-1
LOG [CURRENT DENSITY] amps-cm^{-2}

potential was observed in the transition region for increasing and decreasing constant current conditions and was most pronounced at gold and palladium (over two decades of current density), and least at platinum (over one decade of current density), in equimolar KOH and formate solutions. At all three metals investigated, a Tafel slope of 0.06 v per decade was observed in the lower current-potential region for both KOH concentrations. In the upper Tafel region a Tafel slope of 0.16 v. was observed at platinum (Figure XVIII) and 0.11 v. for palladium (Figure XIX). Gold (Figure XX) on the other hand, in equimolar KOH-formate solutions, exhibits two linear upper Tafel regions as also found in the non-aqueous systems; the Tafel slope is 0.09 v. in the region where hysteresis was observed in the anode potential and 0.13 v. per decade above the region of hysteresis (See Figure XXb).

In each case it was observed that increasing the concentration of KOH (the concentration of formate being kept constant at 1M) that the lower Tafel region was relatively unaffected by the change in KOH concentration but the upper potential region was shifted significantly towards more positive values of electrode potential (vs. the H_2 electrode in the same solution). The critical current density for the transition was also observed to be shifted to lower values of current density.

Comparison of results obtained in aqueous formate

and aqueous formate solutions containing the KOH, reveals that both the upper and lower Tafel regions are shifted significantly towards higher values of electrode potential, the lower Tafel region being shifted by approximately 900 mv., while the upper region is shifted by approximately 300 mv. towards more positive potentials in the case of platinum but by almost zero mv. in the case of gold. The Tafel slope in the lower region changes from 0.12 in aqueous formate to 0.06 in aqueous formate-KOH solutions in the case of platinum and gold.

(v) Trifluoroacetate-Trifluoroacetic Acid System at Platinum, Palladium and Gold

Experimental results for platinum, palladium and gold are shown in Figures [XXI, XXII, XXIII]. Due to the limited solubility of potassium trifluoroacetate in anhydrous trifluoroacetic acid and its poor electrical conductivity, only one concentration of the salt has been used in this part of the work.

A linear Tafel region extending over several decades of current-density was obtained for platinum (Figure XXI) with a high slope of 0.26 volts per decade; gold (Figure XXIII) shows two characteristic slopes: an initial value of 0.38 changing to a lower slope of 0.23 volts per decade. The Tafel plot for palladium is shown in Figure (XXII) and exhibits two regions, as in the case of gold, having slopes of 0.25 changing to 0.30 volts per decade. It will be noted that these slopes are unusually high in comparison with the normal maximum slope of

Figure XXI

Tafel plot for the Kolbe reaction on Pt in 1M CF_3COOK/CF_3COOH ($5^{\circ}C$).

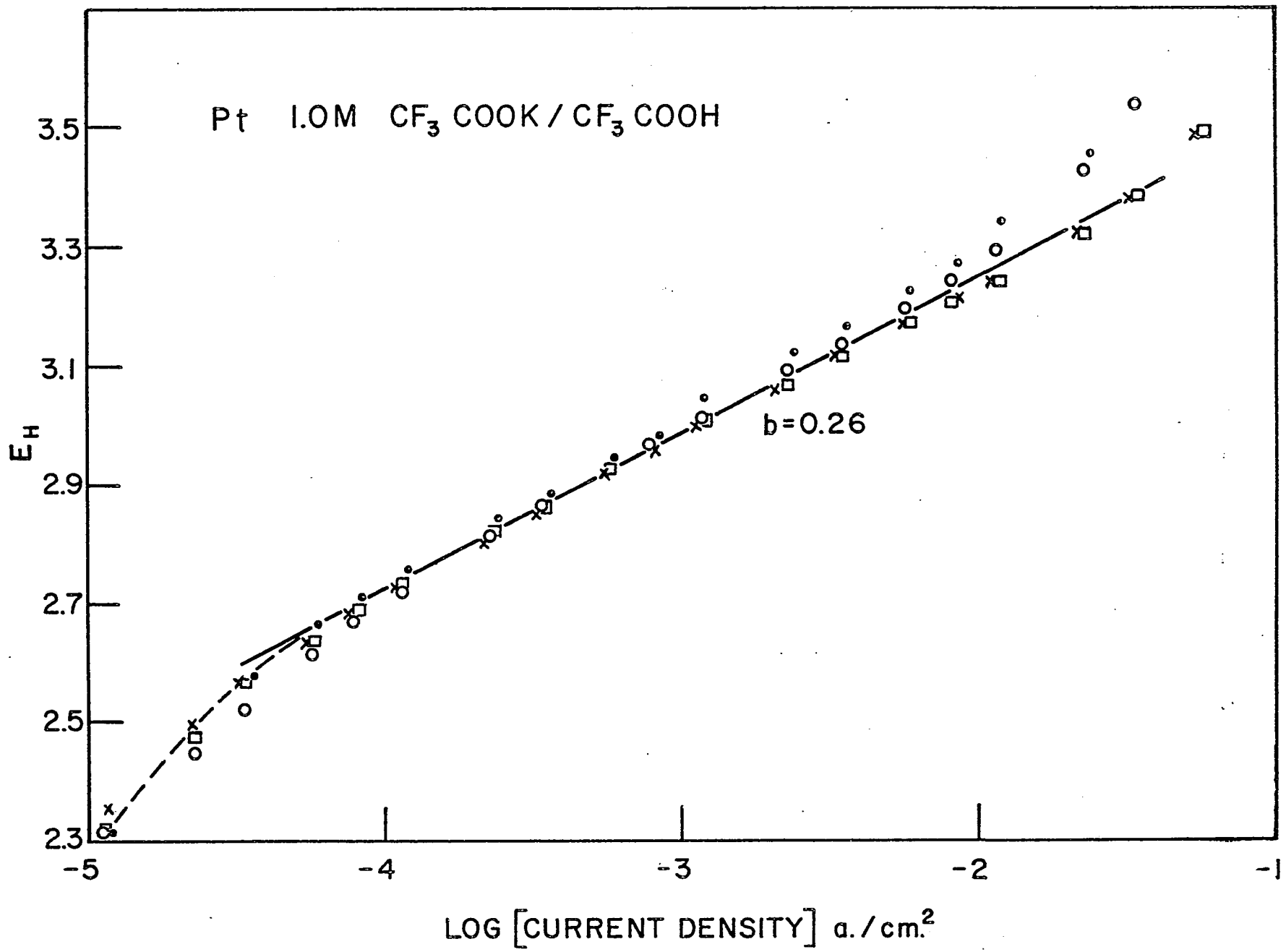
Pt 1.0M CF_3 COOK / CF_3 COOH
b=0.26
E_H
3.5
3.3
3.1
2.9
2.7
2.5
2.3
-5
-4
-3
-2
-1
LOG [CURRENT DENSITY] a./cm.^{2}

Figure XXII

Tafel plot for the Kolbe reaction on Pd in 1M CF_3COOK/CF_3COOH ($5^{\circ}C$).

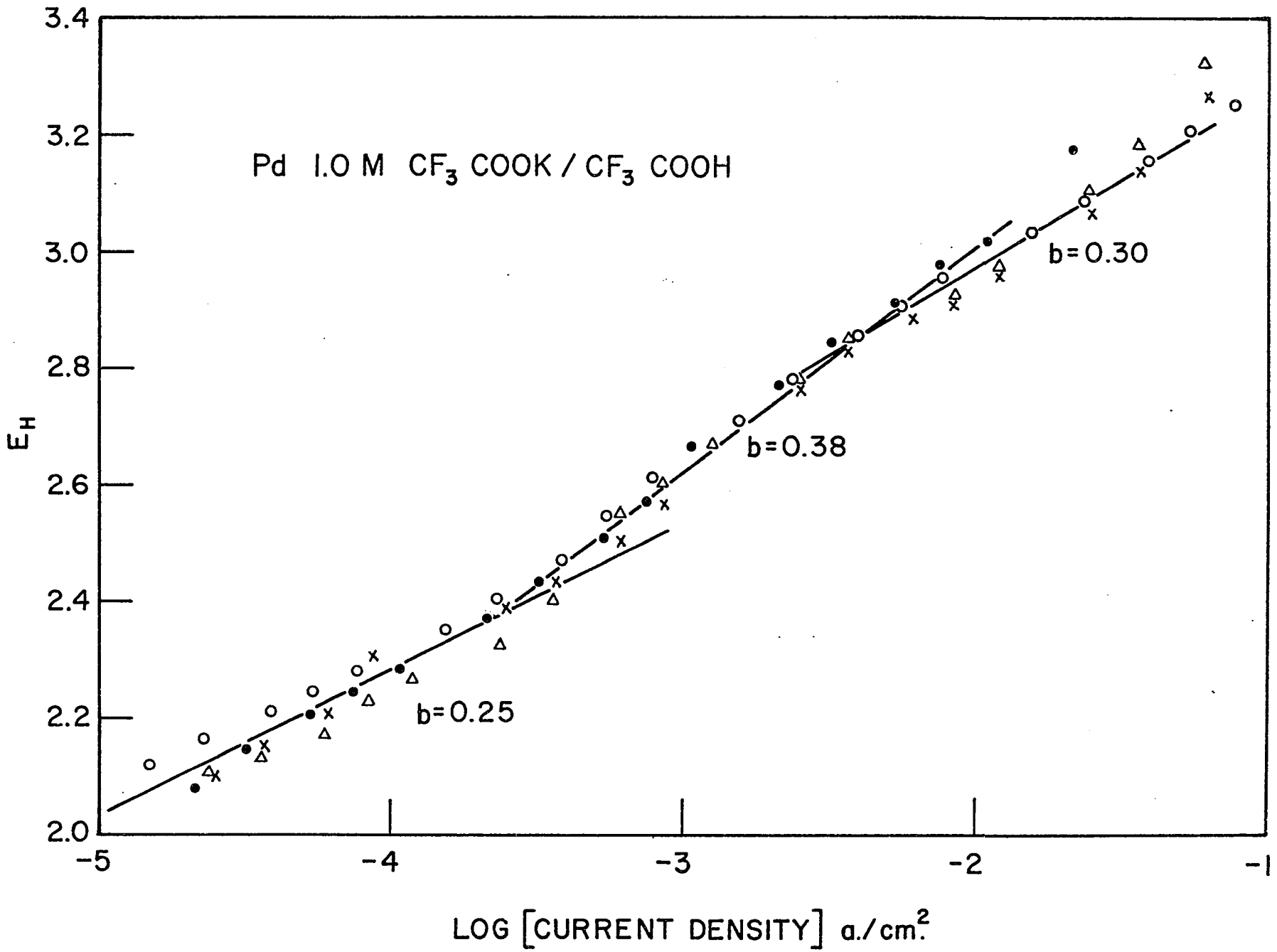
Pd 1.0 M CF_3 COOK / CF_3 COOH
b=0.30
b=0.38
b=0.25
E_H
3.4
3.2
3.0
2.8
2.6
2.4
2.2
2.0
-5
-4
-3
-2
-1
LOG [CURRENT DENSITY] a./cm.^{2}

Figure XXIII

Tafel plot for the Kolbe reaction on Au in 1M CF_3COOK/CF_3COOH (5°C).

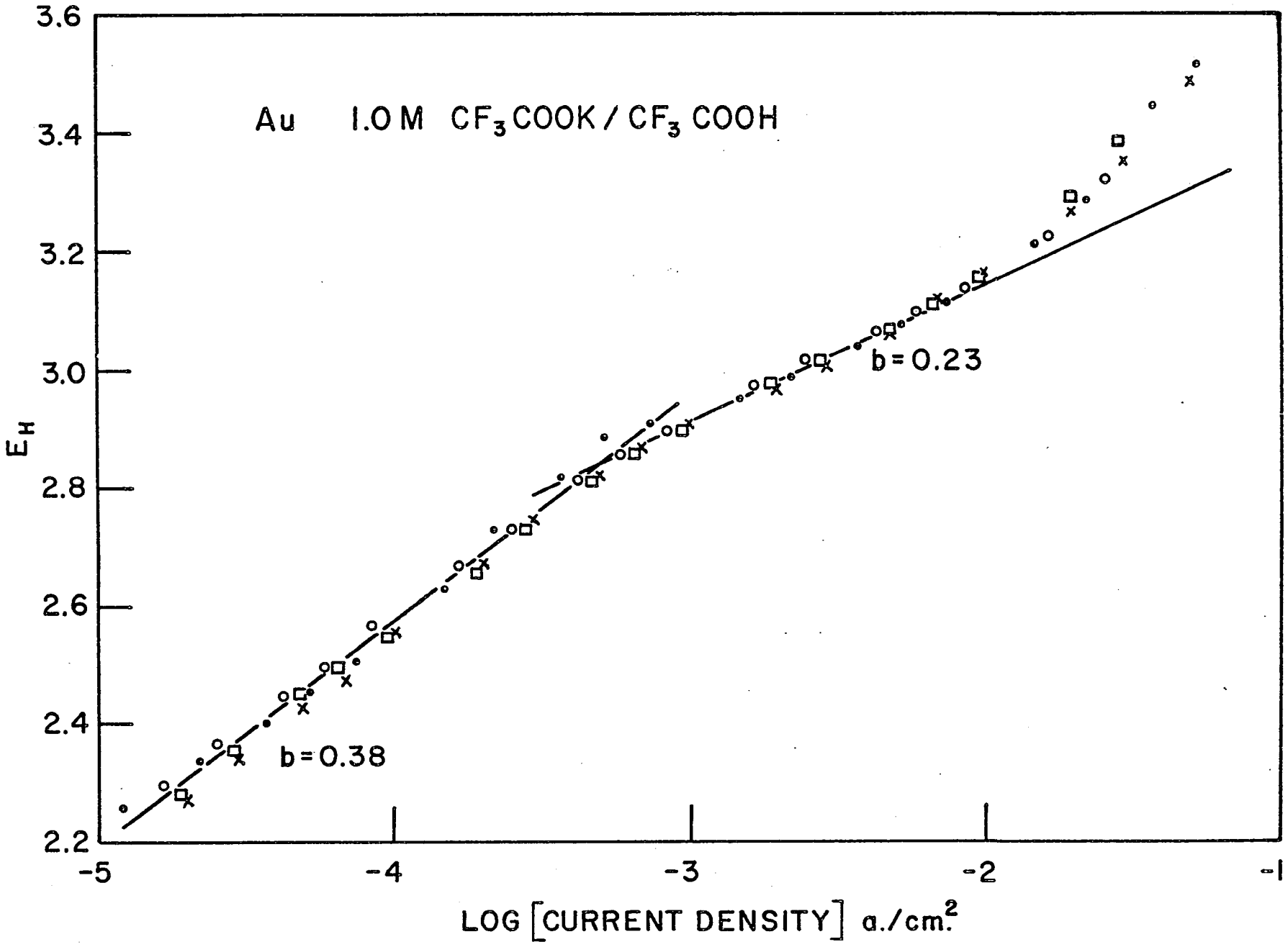
Au 1.0 M CF_3COOK / CF_3COOH
b = 0.23
b = 0.38
E_H
3.6
3.4
3.2
3.0
2.8
2.6
2.4
2.2
-5
-4
-3
-2
-1
LOG [CURRENT DENSITY] a./cm.^{2}

2RT/F for an ionic discharge step proceeding with a symmetry factor of 0.5. Similar high slopes are found in anodic oxygen evolution proceeding at thin oxide films across which there is a significant fall of potential. The present high slopes are well reproducible and are not impurity controlled. From the Figures shown, it is apparent that a lower potential region, below 10^{-5} amps.cm.$^{-2}$ with a sharp transition to an upper region, similar to that observed in the formic acid system, is indicated, and was experimentally confirmed at platinum as, shown in Figure XXIV compared with Pt in the anhydrous formate system. However, this lower region was not investigated for Pd and Au. The Tafel slopes are summarized in Table[VI] but it should be noted that since the data required for the thermodynamic calculation of the reversible potential of the trifluoroacetate decarboxylation reaction are unavailable, the data listed in Table [VI] cannot include the Tafel a constant or of the exchange current.

(vi) Aqueous Trifluoroacetate System at Platinum, Palladium and Gold

Experimental results for platinum, palladium and gold are shown in Figures [XXV-XXVII]. and are similar to those obtained in the system previously discussed in that a transition from a lower to an upper Tafel region is indicated at current densities near 10^{-5} amps.cm.$^{-2}$

It is noteworthy that a linear region extending very

Figure XXIV

Comparison of potential-current density curves on Pt in 1M CF_3COOK and 1M HCOOK in their respective anhydrous acids at 5°C.

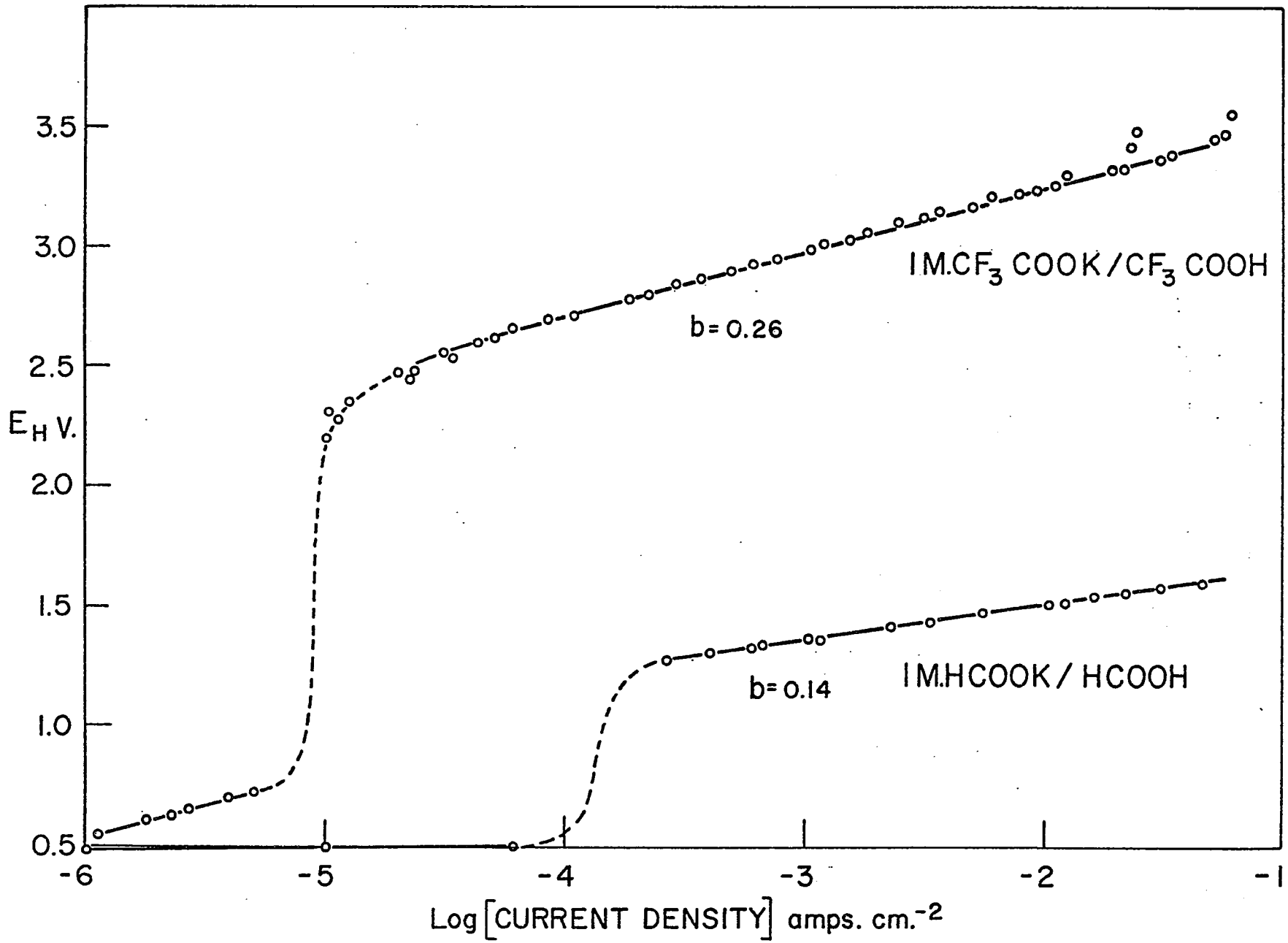
3.5
3.0
2.5
2.0
1.5
1.0
0.5
E_H V.
1M.CF_3 COOK/CF_3 COOH
b= 0.26
1M.HCOOK/ HCOOH
b= 0.14
-6
-5
-4
-3
-2
-1
Log [CURRENT DENSITY] amps. cm.$^{-2}$

Figure XXV

Tafel plots for the Kolbe reaction on Pt in aqueous 1M CF_3COOK (5^oC).

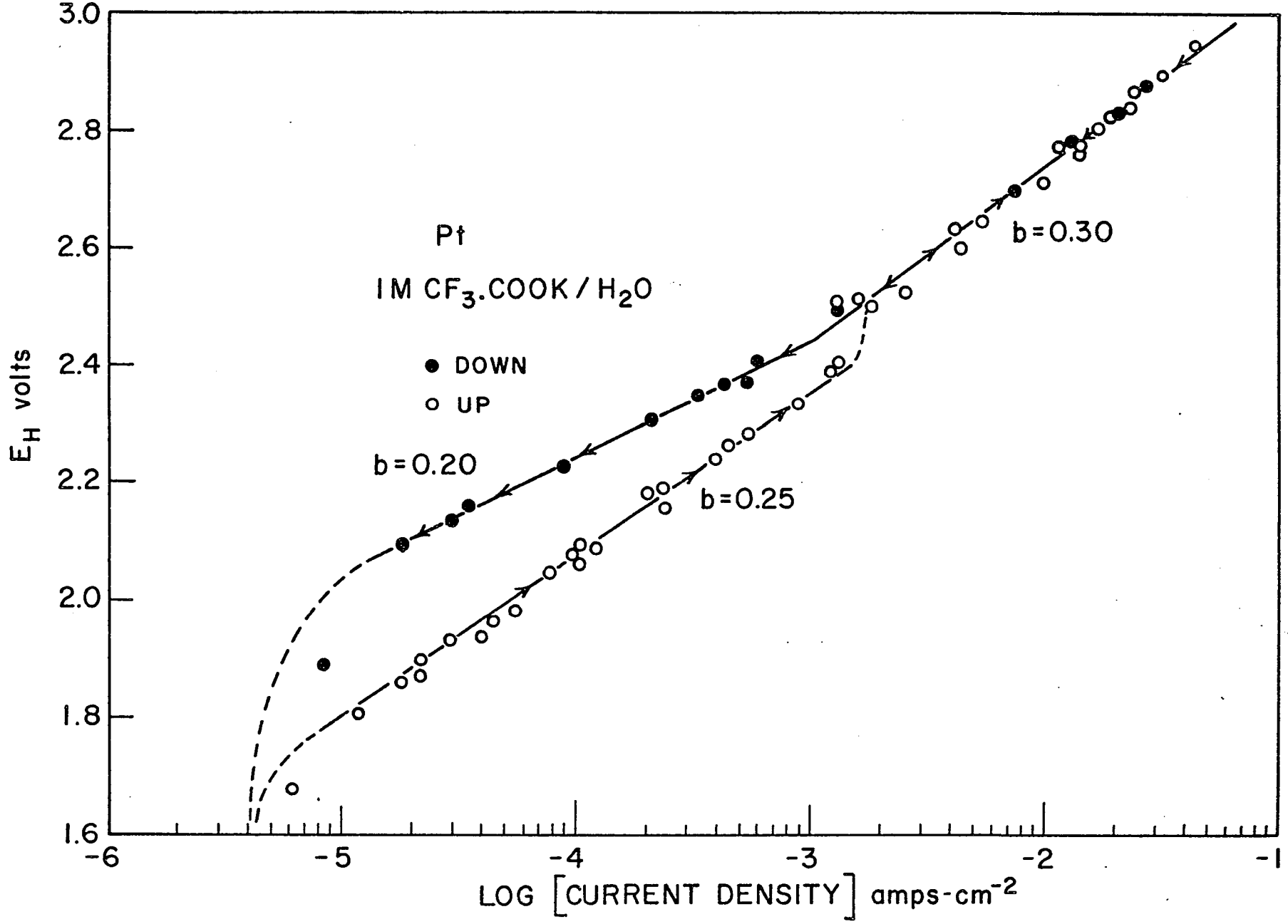
3.0
2.8
2.6
2.4
2.2
2.0
1.8
1.6
E_H volts
Pt
1M CF_3.COOK / H_2O
DOWN
UP
b=0.20
b=0.25
b=0.30
-6
-5
-4
-3
-2
-1
LOG [CURRENT DENSITY] amps-cm^{-2}

Figure XXVI

Tafel plot for the Kolbe reaction on Pd in aqueous 1M CF_3COOK (5°C).

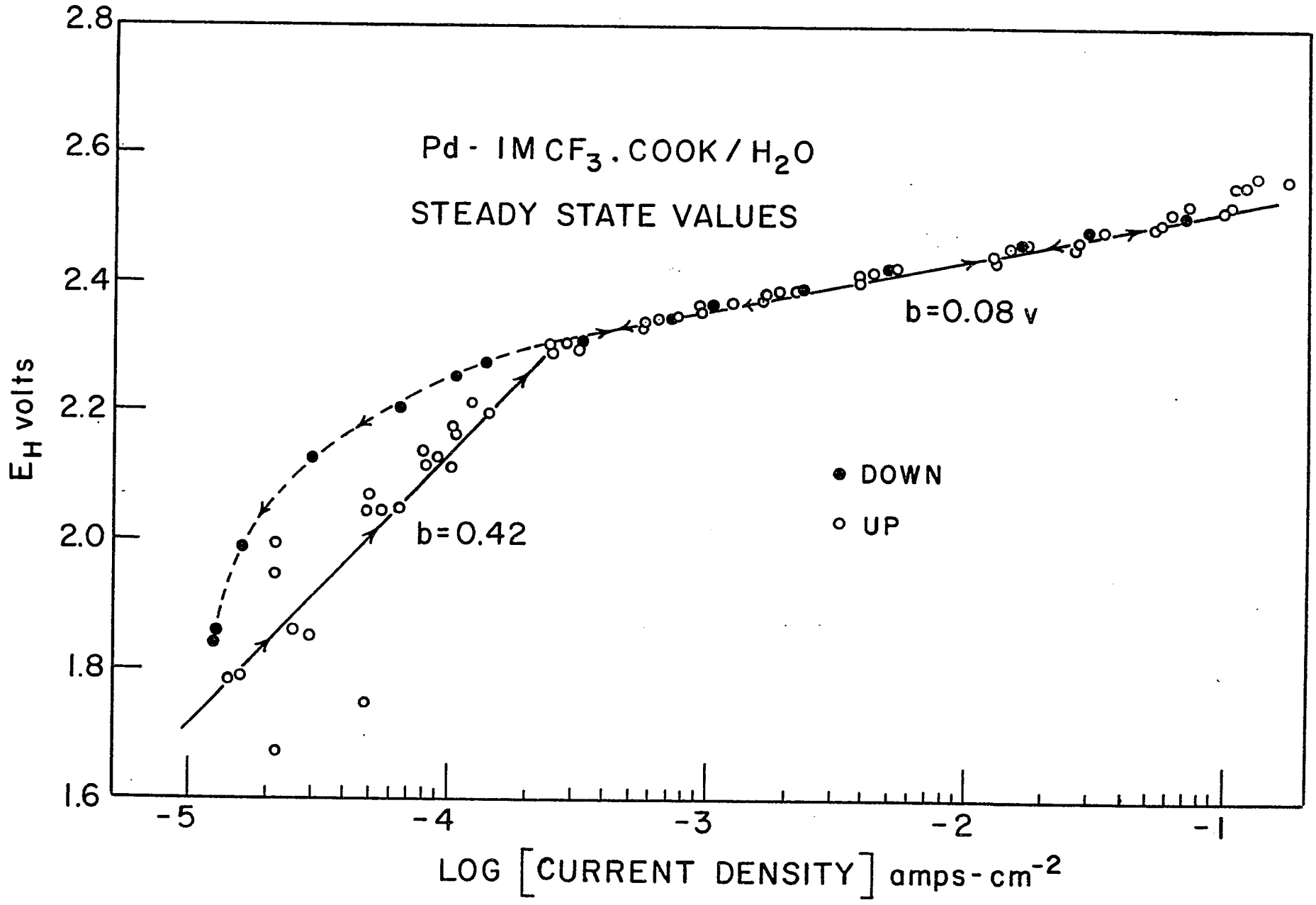
Pd - IM CF_3 . COOK / H_2O
STEADY STATE VALUES
b=0.08 v
b=0.42
DOWN
UP
E_H volts
2.8
2.6
2.4
2.2
2.0
1.8
1.6
-5
-4
-3
-2
-1
LOG [CURRENT DENSITY] amps-cm^{-2}

Figure XXVII

Tafel plot for the Kolbe reaction on Au in aqueous 1M CF_3COOK (5°C).

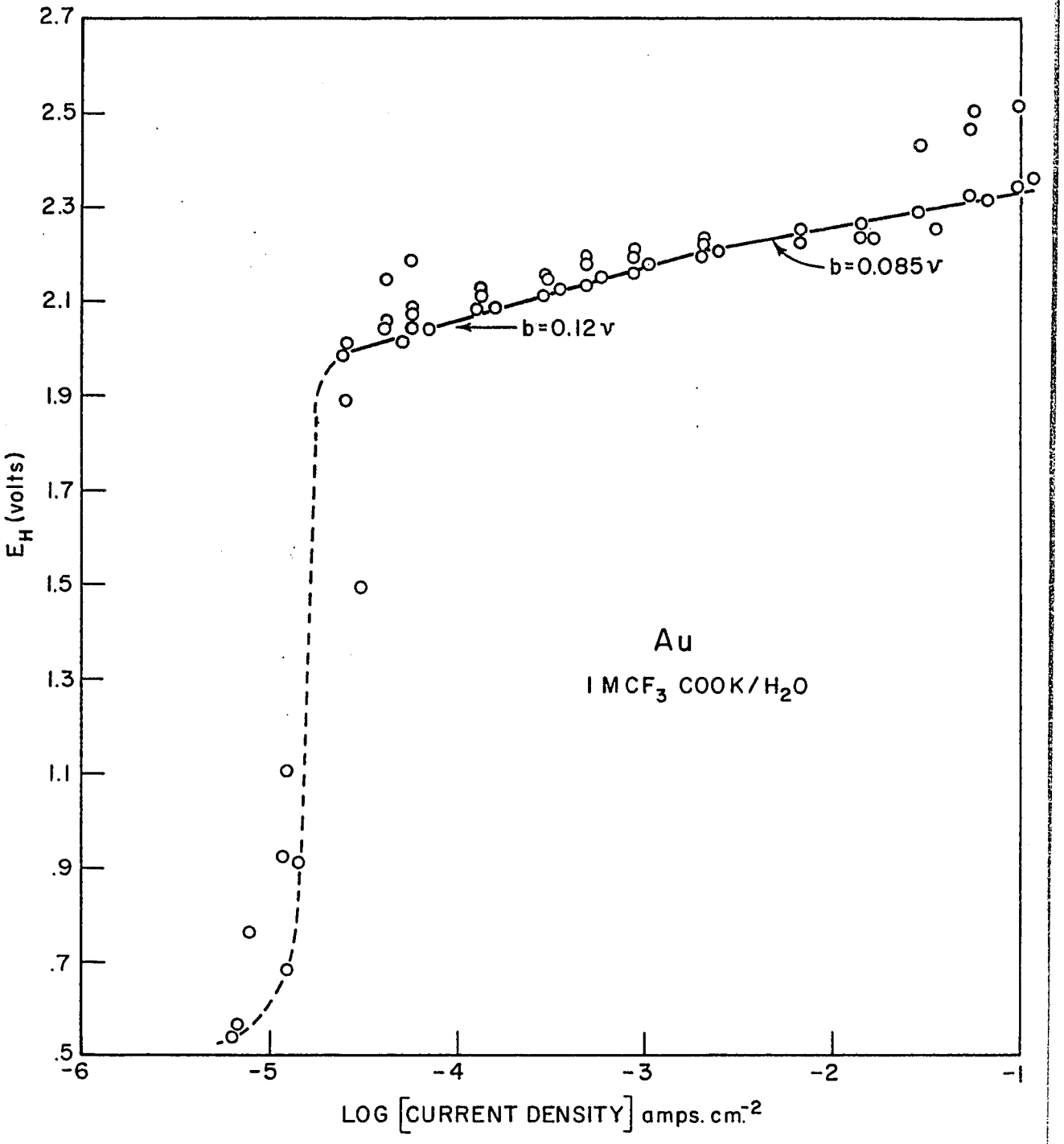
2.7
2.5
2.3
2.1
1.9
1.7
1.5
1.3
1.1
.9
.7
.5
E_H (volts)
-6
-5
-4
-3
-2
-1
LOG [CURRENT DENSITY] amps. cm.$^{-2}$
b=0.12 v
b=0.085 v
Au
1 M CF_3 COOK / H_2O

satisfactorily over several decades of current density was obtained for palladium (Figure XXVI) with a slope of 0.08 volts; platinum (Figure XXV) shows two characteristic slopes, an initial value of 0.20 changing to a higher slope of 0.30 volts per decade. The Tafel plot for gold is shown in Figure [XXVII] and exhibits two linear regions as in the case of platinum, having slopes of 0.12 and 0.085 volts per decade. From the Figures shown, it is apparent that a lower potential region, below 10^{-5} amp.cm.$^{-2}$ similar to that observed in the previous systems discussed is indicated. Tafel slopes are summarized in Table [VI], but for the same reason as that given in the case of the anhydrous system, the reversible exchange current densities cannot be calculated.

(d) Effects of Depolarizers on the Current-Potential Relationship

It was thought at first that the transition from one potential region to another might be due possibly to some depolarizers present in the electrolyte, and more specifically perhaps due to the presence of traces of formaldehyde in the formic acid system. Experimental results with purposely added formaldehyde are shown in Figure [XXVIII]. It can be seen that only the linear region in the lower current density range is affected, being shifted towards higher potentials; the upper region, however, remains unchanged and the transition region is little affected.

Figure XXVIII

Effect of added depolarizer (formaldehyde) on the potential-current density relations at Pd in 1M HCOOK/HCOOH ($5^{o}C$).

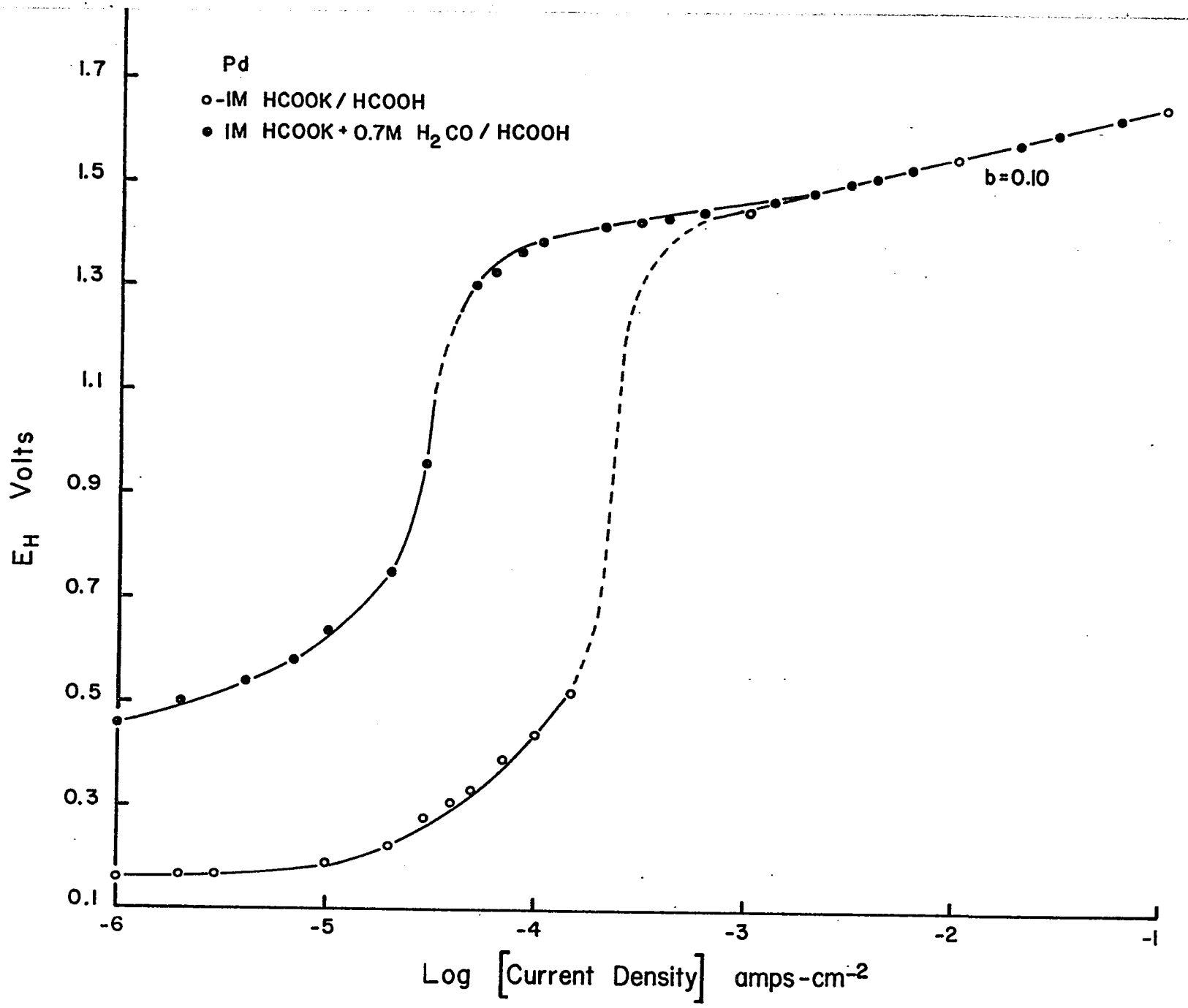
Pd
o-IM HCOOK / HCOOH
• IM HCOOK + 0.7M H_2CO / HCOOH
b=0.10
E_H Volts
1.7
1.5
1.3
1.1
0.9
0.7
0.5
0.3
0.1
-6
-5
-4
-3
-2
-1
Log [Current Density] amps-cm^{-2}

Chemical tests were also carried out for the possible presence of peroxides, peracids and aldehydes but all tests gave negative results. The transition behavior was still observed unchanged in the formic acid system even after the most careful purification of solutions (see Chapter II). Subsequently the same behavior was observed in the trifluoro-acetate-trifluoroacetic system where impurities of the kind which might be present in formic acid would be absent. Similar behavior was also found in the aqueous systems so it was concluded that the "transition" behavior was a general characteristic of the anodic decarboxylation reactions probably connected with the onset of passivation (see Chapters I and IV) and not connected in any way with the possible presence of traces of anodic depolarizers.

In all cases the solutions had been pre-electrolysed for varying periods of time and depolarising impurities should have been removed, if present, during this final purification step. If the transition regions corresponded to limiting diffusion controlled anodic oxidation currents for depolarising impurities, it is readily calculated that such impurities would have had to be present in concentrations of about 10^{-3}-10^{-4} g. equivalent per litre (assuming a diffusion coefficient for impurities of about 10^{-5} $cm.^2$ $sec.^{-1}$). Such a level of depolarising impurities could hardly be present in the purified solutions and should have been detectable in the chemical tests

for likely foreign substances. The whole behavior in the transition region (e.g. occurrence of periodic phenomena, overshoot transients, etc.) is characteristic of passivation with anodic film formation, so we regard this effect as not attributable to impurities in the system. Elsewhere we show direct evidence for anode film formation and calculate the surface coverage by intermediates.

B. POTENTIAL-TIME RELATIONSHIPS UNDER NON-STEADY-STATE CONDITIONS

(a) General

Complementary information on the decarboxylation reaction mechanisms was obtained from galvanostatic d.c. charging potential-time relationships. The type of relation between potential and time is not only dependent on the kinetics of the rate-determining step but is also characteristic of the surface concentration of adsorbed intermediates and/or of anodic film growth, as has been discussed in Chapter I. In this part of the work, all measurements have been carried out at 5°C, using experimental procedures previously described in Chapter II.

(b) Variation of Potential with Time: Variations over Relatively Long Periods of Time

In this section will be described some interesting observations of long period time-variation of electrode potentials made during the course of the current-potential

measurements. The results are sufficiently striking and original (with regard to the decarboxylation reactions) to justify some special description.

In cathodic overpotential measurements, time variations of potential have usually (except, for example, at metals that can take up hydrogen into their lattices) been ascribed to deposition of impurities on active electrocatalytic sites. The time variations observed in the present work were of an altogether different kind and depended critically on current density. At high or low current densities (except at the initial lowest value) the time variations of potential were relatively small (1 mv. $min.^{-1}$ over 20 minutes) and sometimes a more immediate attainment of a steady value was noted. However, near the critical current for the transition region, extended time variations of potential having a characteristic linear-logarithmic dependence upon time were observed in several systems. These effects are analogous to the well known (66,78) behavior observed in electrochemical anodic oxide film formation and passivation and have nothing to do with impurity effects. The behavior observed in the decarboxylation reactions will now be described in more detail.

(i) The Anhydrous Formate-Formic Acid System

Comparison of experimental results obtained by either the "rapid" or the "steady-state" method showed no significant differences in the Tafel slopes obtained and no appreciable

hysteresis was observed in the anode potential behavior for increasing or decreasing current conditions as was the case in the aqueous systems. It was usually observed, however, that as the critical current density was approached by increasing the current density, the electrode potential would "overshoot" and then rapidly return to a final steady value. Similarly with decreasing current density, the potential would "undershoot" and return to the steady value. The magnitude of this transient was found to increase as the critical current density for transition from the lower to the upper Tafel region was approached, and very near to the critical current density, the electrode potential would begin to oscillate (at constant current) about some mean value. Further details of this behavior are described below.

(ii) The Anhydrous Trifluoroacetate-Trifluoroacetic Acid System

In this system, behavior similar to that observed in the anhydrous formate-formic acid system was observed. The Tafel slopes obtained by either polarisation method again showed no significant differences.

(iii) The Aqueous Formate System

Reproducible measurements at platinum and gold electrodes could only be obtained by the "steady state" method due to the more extensive time variation of potential in this

system. The greatest time variation was observed at the beginning of each Tafel region. The variation of potential was logarithmic with time; a typical case is shown in Figure [XXIX] for gold (though the experimental results were not satisfactorily reproducible in the case of palladium, qualitatively similar behavior was observed at all palladium electrodes irrespective of experimental conditions). Two regions of time dependence of potential E were observed; in both cases the potential was linear with the time of polarisation after setting a given constant current. The initial region had a low slope, dE/d log [time], and was followed by a second region having a higher slope before a final more or less steady potential was attained.

In each case, it was also observed that as the critical current density was approached with increasing values of current, the potential would "overshoot" and then recovered logarithmically with time at constant current. Similarly with decreasing current densities the potential would "undershoot" and then recover logarithmically with time to a final steady value. This behavior is shown in Figures [XXX, XXXI] for palladium and gold electrodes.

It was also observed that as the critical current density was approached, with either increasing or decreasing values of current density, the magnitude of the potential "overshoot" or "undershoot", respectively, increased until

Figure XXIX

Variation of potential as a function of logarithmic time on Au in aqueous 1M HCOOK.

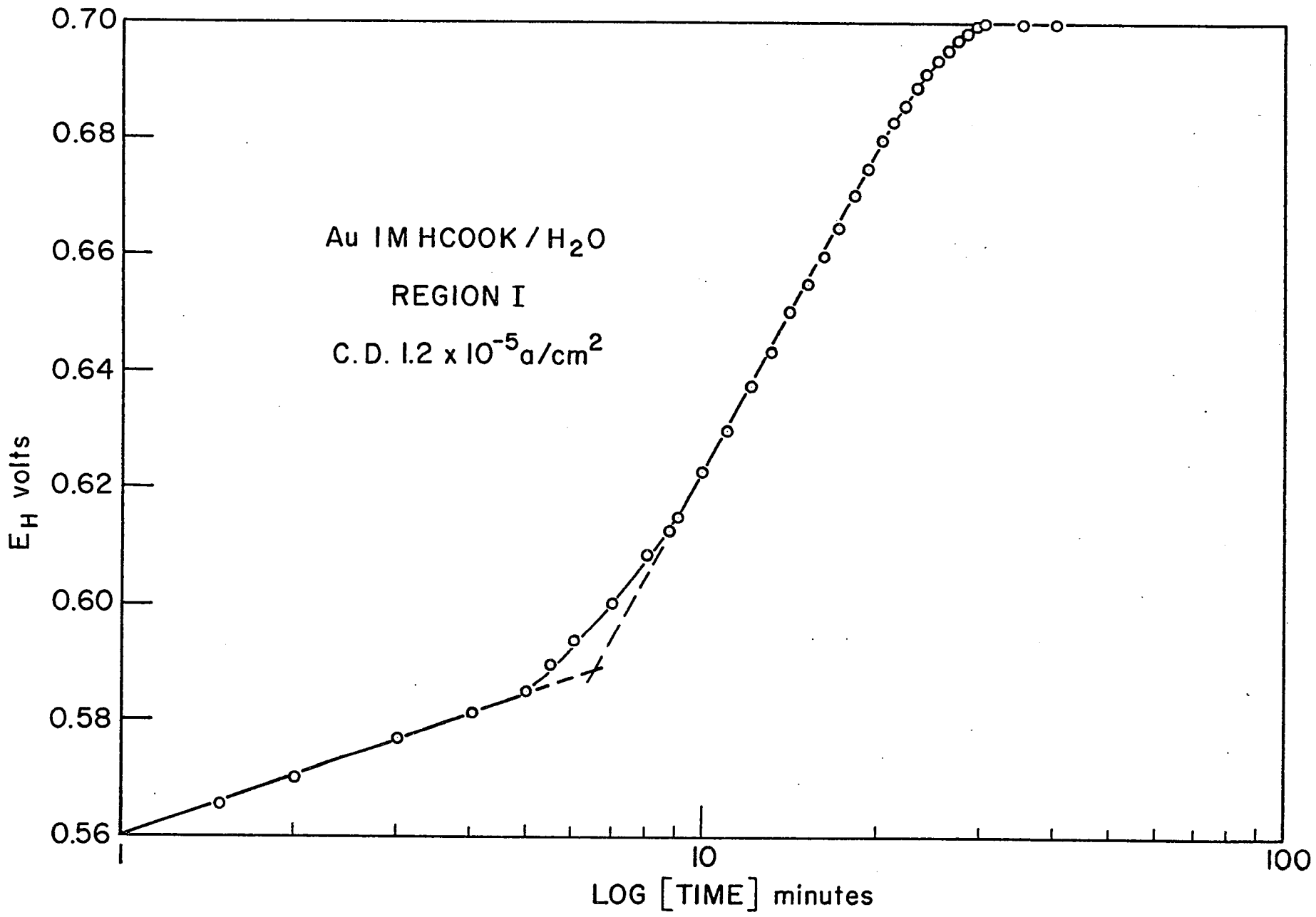
0.70
0.68
0.66
0.64
0.62
0.60
0.58
0.56
E_H volts
Au 1M HCOOK / H_2O
REGION I
C.D. 1.2 x 10^{-5} a/cm^2
1
10
100
LOG [TIME] minutes

Figure XXX

Recovery of potential from "undershoot" at Pd in aqueous 1M HCOOK.

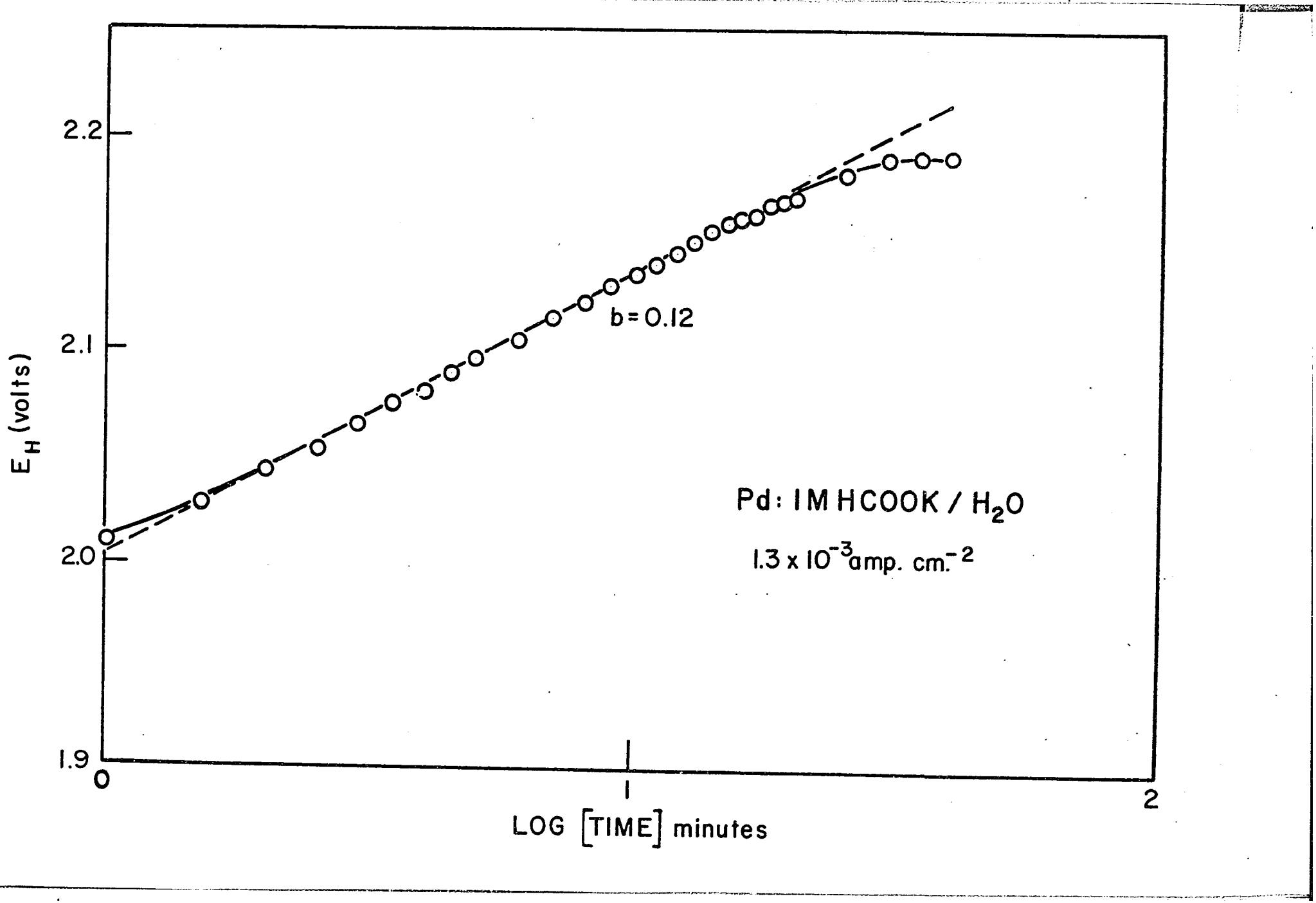
2.2
2.1
2.0
1.9
E_H (volts)
b = 0.12
Pd : 1M HCOOK / H_2O
1.3×10^{-3} amp. $cm.^{-2}$
0
1
2
LOG [TIME] minutes

Figure XXXI

Recovery of potential from "undershoot" at Au in aqueous 1M HCOOK.

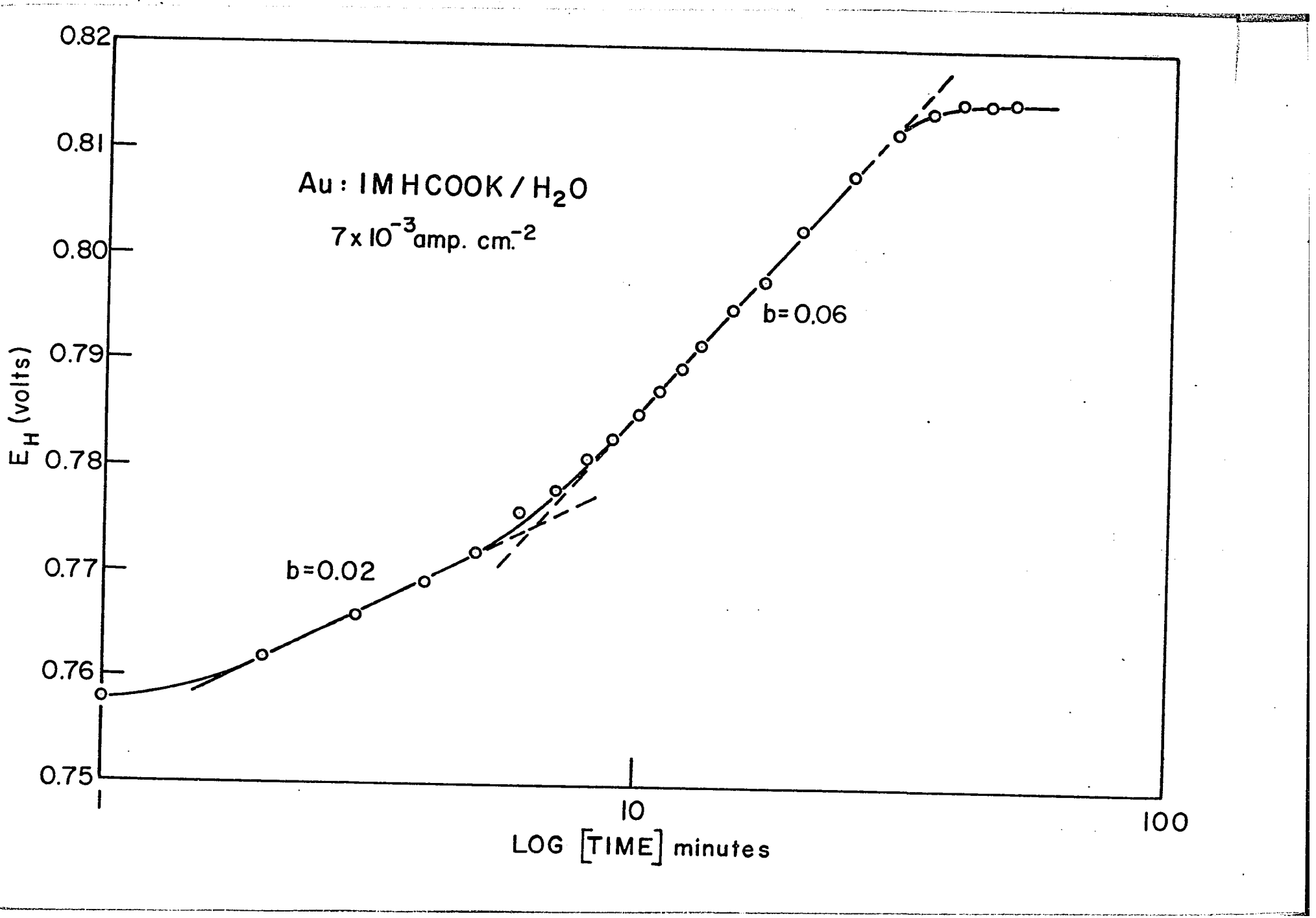
0.82
0.81
0.80
0.79
0.78
0.77
0.76
0.75
E_H (volts)
Au : IM HCOOK / H_2O
7×10^{-3} amp. cm^{-2}
b=0.02
b=0.06
1
10
100
LOG [TIME] minutes

finally, very near the critical current density, the potential would begin to oscillate (see below) before finally reaching the relevant (i.e. upper or lower) potential region where steady behavior was again observed. This behavior in the aqueous formate system is thus exactly analogous to that found in the anhydrous formic acid solution.

(iv) The Behavior in the Aqueous Formate-KOH System

Similar logarithmic time-variation with transient overshoots and periodic phenomena were observed in the aqueous KOH-formate system as in the pure aqueous and non-aqueous formate systems. A typical variation of potential with the logarithm of time at gold is shown in Figure [XXXII] for equimolar KOH-formate solution.

(c) Periodic Behavior

At all electrodes, both in anhydrous and aqueous media, periodic variation in the anode potential near the transition region was observed, as has been mentioned above. The potential would oscillate with increasing amplitude, and decreasing-frequency about a mean potential; suddenly the potential would increase up to values characteristic of the initial part of the upper potential region and then suddenly fall to the original rest potential. The potential would then increase rapidly and begin to oscillate again about the same mean potential as that observed previously. The whole cycle of events then repeated itself sometimes for several hours. A

Figure XXXII

Variation of Potential as a function of logarithmic time at Au in aqueous 1M HCOOK + 1 M KOH.

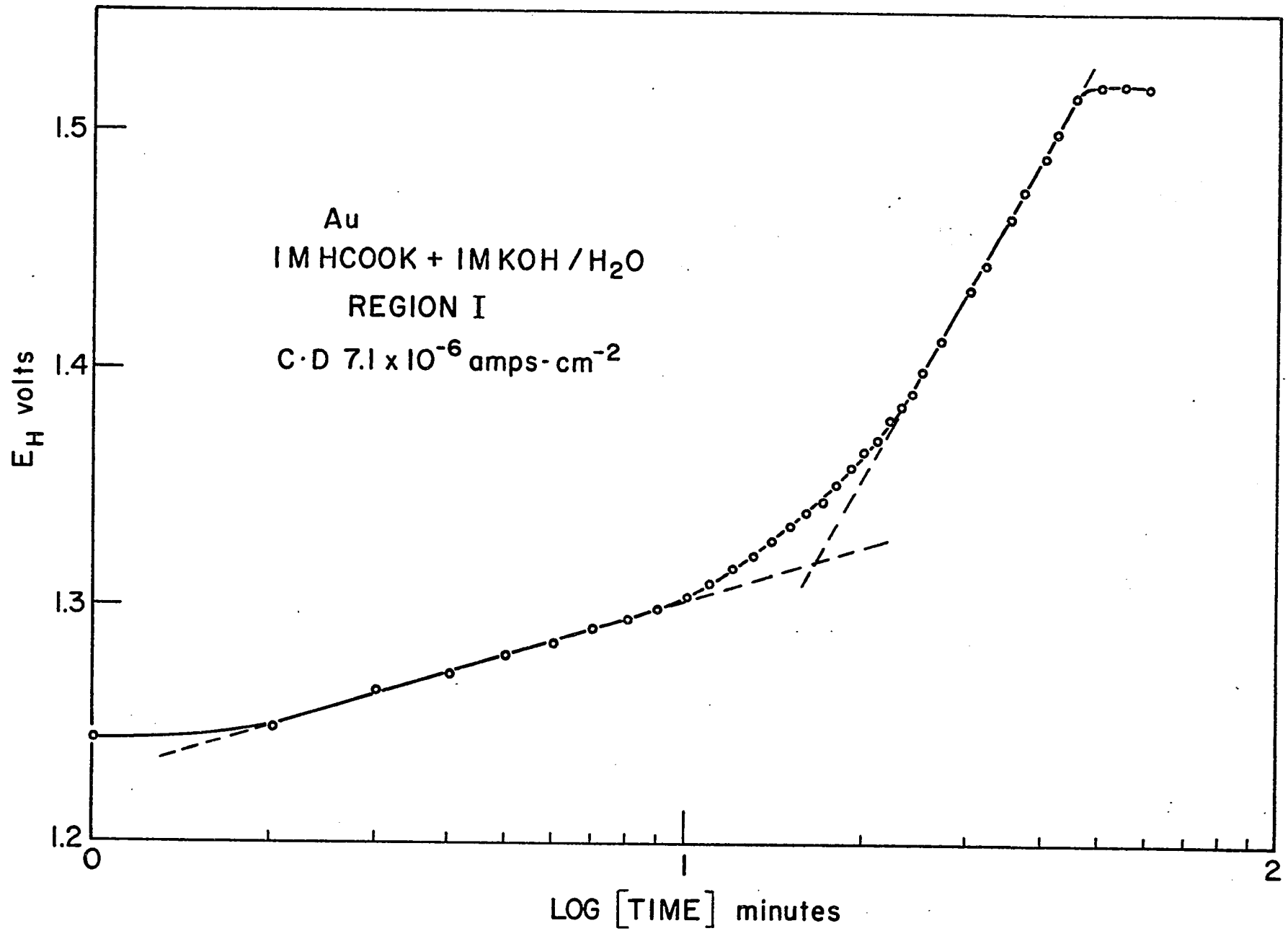
Au
1M HCOOK + 1M KOH / H_2O
REGION I
C·D 7.1 x 10^{-6} amps-cm^{-2}
E_H volts
1.5
1.4
1.3
1.2
0
1
2
LOG [TIME] minutes

typical example of this behavior is shown in Figure [XXXIII]. The oscillations are particularly large, up to 0.7 volts. Although similar periodic phenomena have been observed previously (71-75) in anodic passivation and oxide film formation, the amplitude of the oscillations observed in the above system is much larger than that of any periodic fluctuations previously observed in other systems.

(d) Open-Circuit Decay Behavior

Complementary information on the pseudo-capacitance of the electrode and the related extent of surface coverage of the electrode by adsorbed intermediates or anodic films can be obtained from studies of the kinetics of decay of potential of the initially polarised electrode with time on open-circuit, as discussed by Conway and Bourgault (119). Under conditions where the time variation of potential is important, as in the present work, the decay of electrode potential with time on open-circuit can also offer an alternative method of obtaining kinetically significant Tafel parameters under the conditions previously discussed (120).

(i) E.M.F. Decay in the Anhydrous Formate-Formic Acid System

Typical open-circuit decay curves obtained after interruption of the constant current at various current densities between 10^{-6}-10^{-2} amps.cm.$^{-2}$ from both the upper and

Figure XXXIII

Potential oscillation observed on Pd in 1M $HCOOK/H_2O$.

1 division = 10 mv.

1 division = 15 seconds.

i = 1.7×10^{-4} amp.$cm.^{-2}$

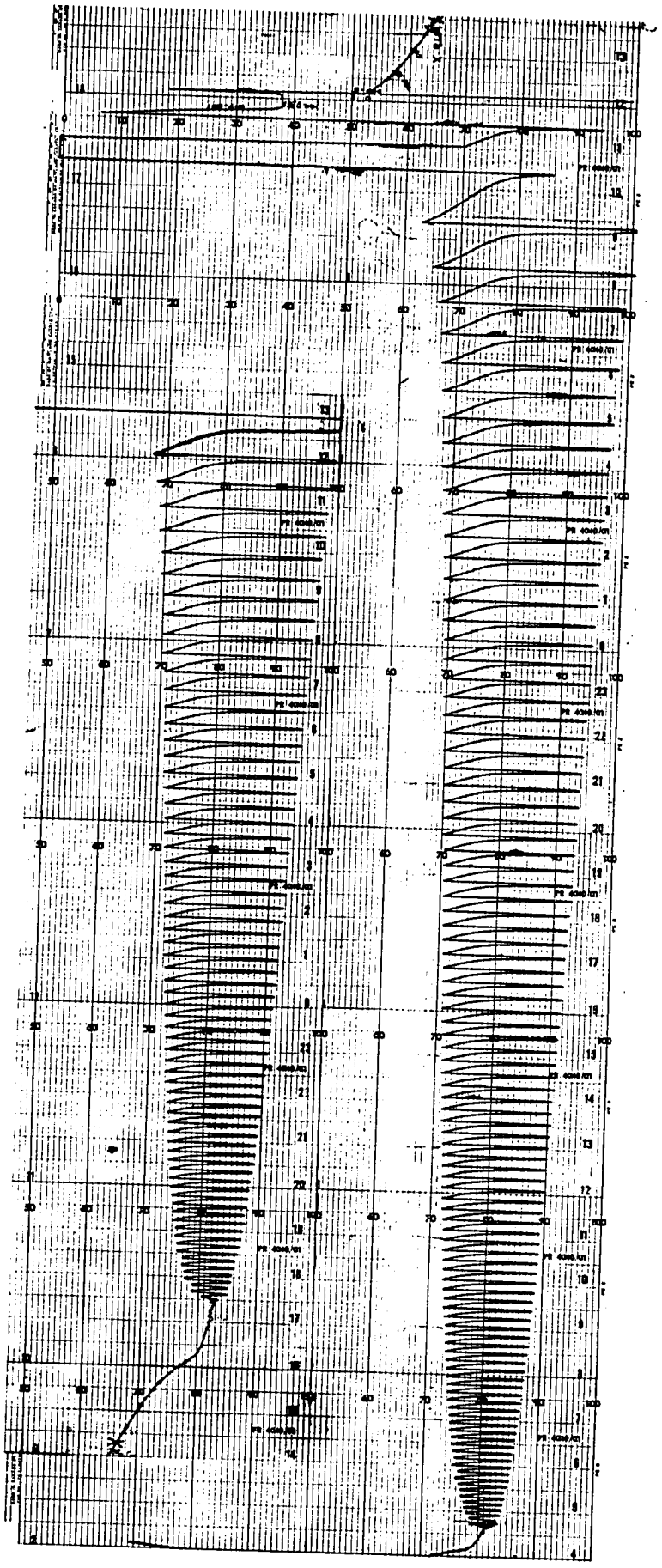

current-potential regions are shown in Figures [XXXIV-XXXVII] for platinum, palladium and gold. Quantitative treatment of these curves will be given in Chapter IV.

(ii) Dependence of Duration of Arrest of Potential During Galvanostatic Discharge on Previous Polarisation Time in the Anhydrous Formate-Formic Acid System

During the open-circuit decay measurements in the formate-formic acid system, it was noted that arrests of potential occurred indicating an appreciable pseudo-capacity associated with surface films of intermediates. These arrests were found to be longer in duration the longer the previous polarisation time, which suggested that they were associated with self-discharge of surface films of an anodic product present in greater amounts (actually probably corresponding to thicker films of the anodic product) the longer the time of previous polarisation at constant current, i.e. the greater the amount of film forming charge that had been passed.

In order to investigate these phenomena more completely, galvanostatic reversed pulse cathodic transients (see Chapter II) were applied to the electrode after various previous extents of anodic polarisation, i.e. after various anodic charges had been passed corresponding to the product of current and time of polarisation. The results of these studies have been expressed either in terms of the delay time Δt in the arrest region of constant reversed (cathodic) current

Figure XXXIV

Decay of potential on open-circuit at Pt
in 1M HCOOK/HCOOH - high current density.(1.2×10^{-2} amp.cm^{-2}).

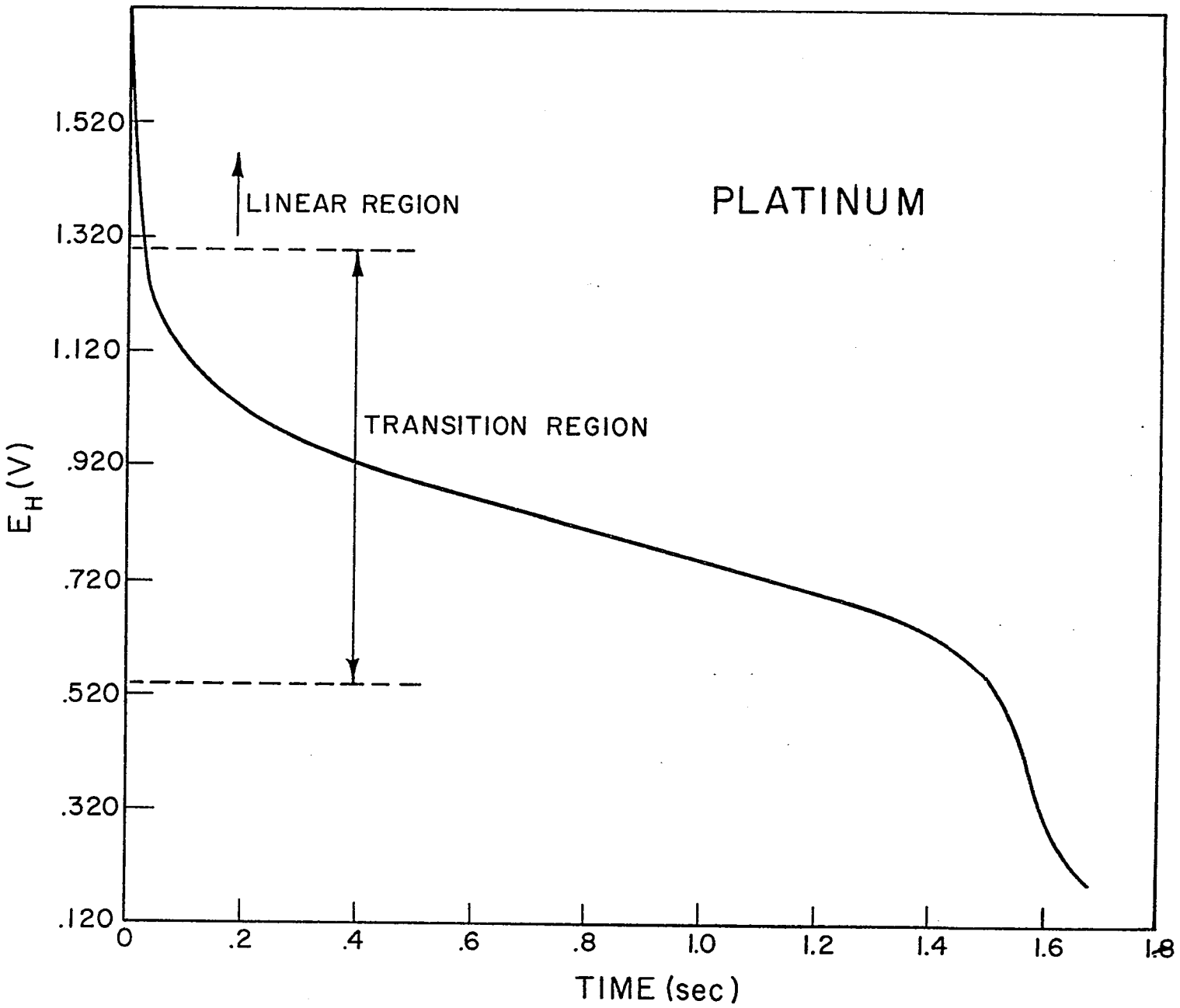
PLATINUM
LINEAR REGION
TRANSITION REGION
1.520
1.320
1.120
.920
.720
.520
.320
.120
E_H (V)
0
.2
.4
.6
.8
1.0
1.2
1.4
1.6
1.8
TIME (sec)

Figure XXXV

Decay of potential on open-circuit at Pd in 1M HCOOK/HCOOH - high current density (9×10^{-3} amp.cm^{-2}).

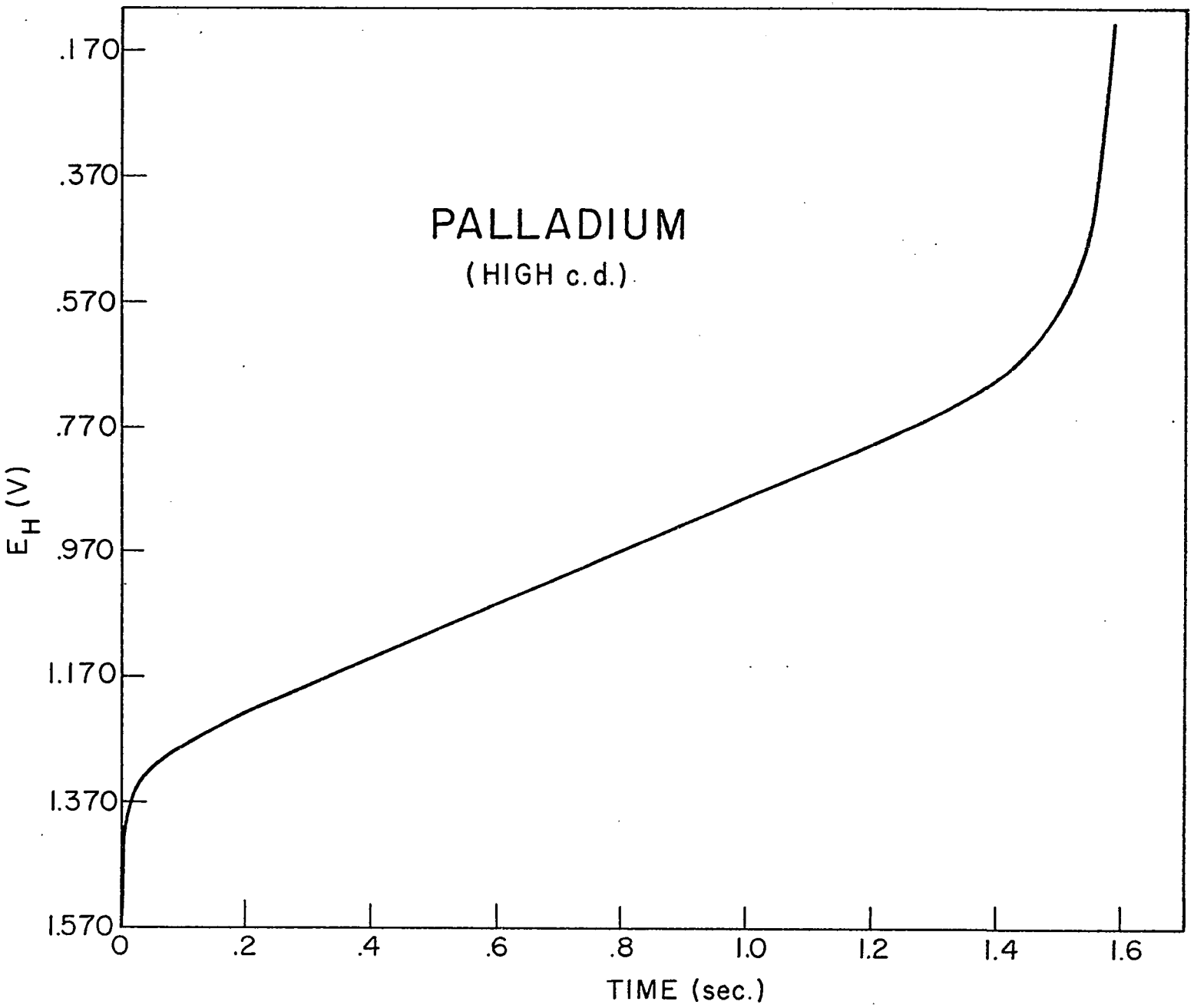
PALLADIUM
(HIGH c.d.)
.170
.370
.570
.770
.970
1.170
1.370
1.570
E_H (V)
0
.2
.4
.6
.8
1.0
1.2
1.4
1.6
TIME (sec.)

Figure XXXVI

Decay of potential on open-circuit at Pd in 1M HCOOH - low current density. (8.4×10^{-6} amp.cm^{-2}).

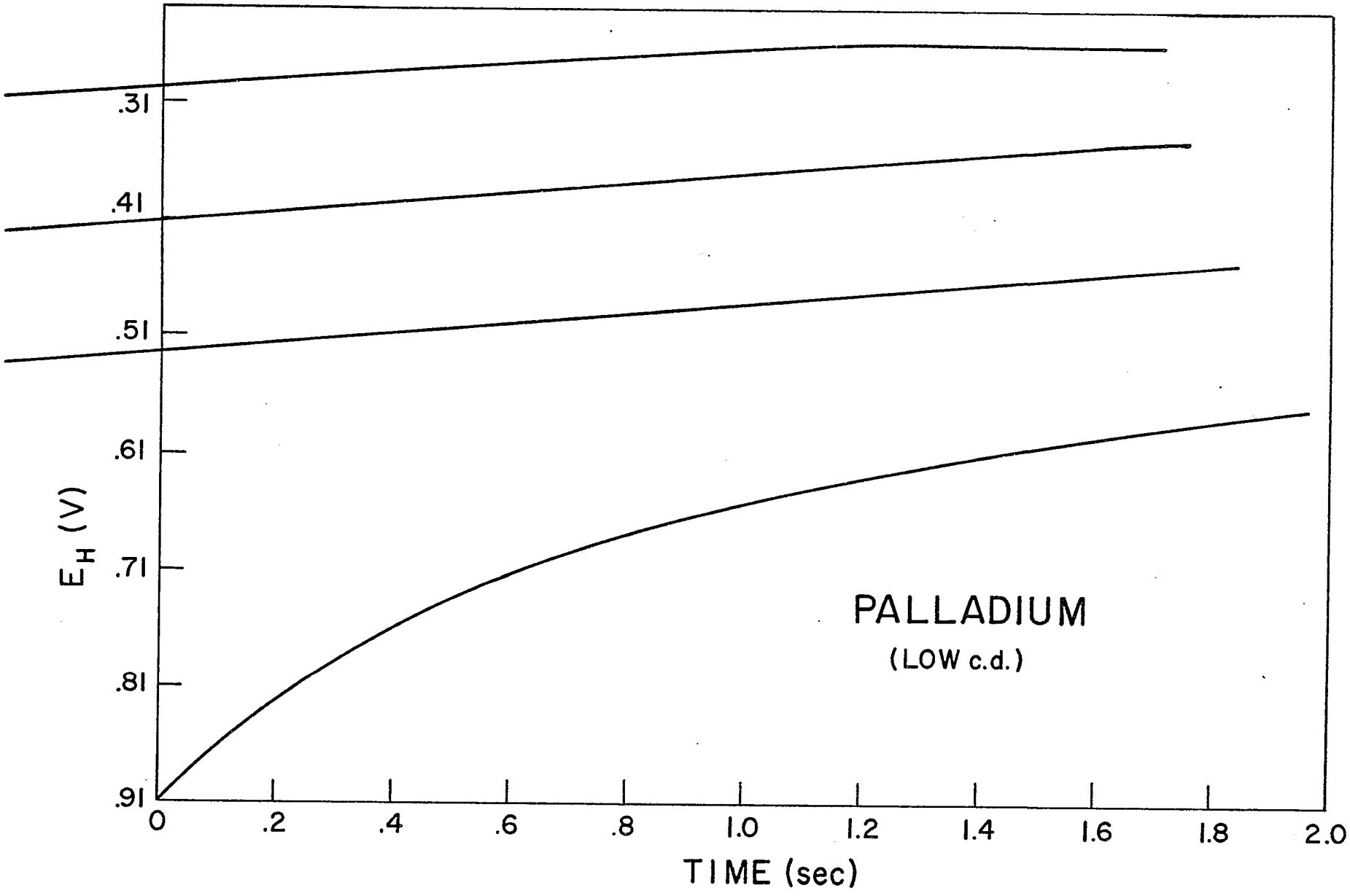
.31
.41
.51
.61
.71
.81
.91
E_H (V)
0
.2
.4
.6
.8
1.0
1.2
1.4
1.6
1.8
2.0
TIME (sec)
PALLADIUM
(LOW c.d.)

Figure XXXVII

Decay of potential on open-circuit at Au in 1M HCOOK/HCOOH - high current density. (3.1×10^{-2} amp.cm^{-2}).

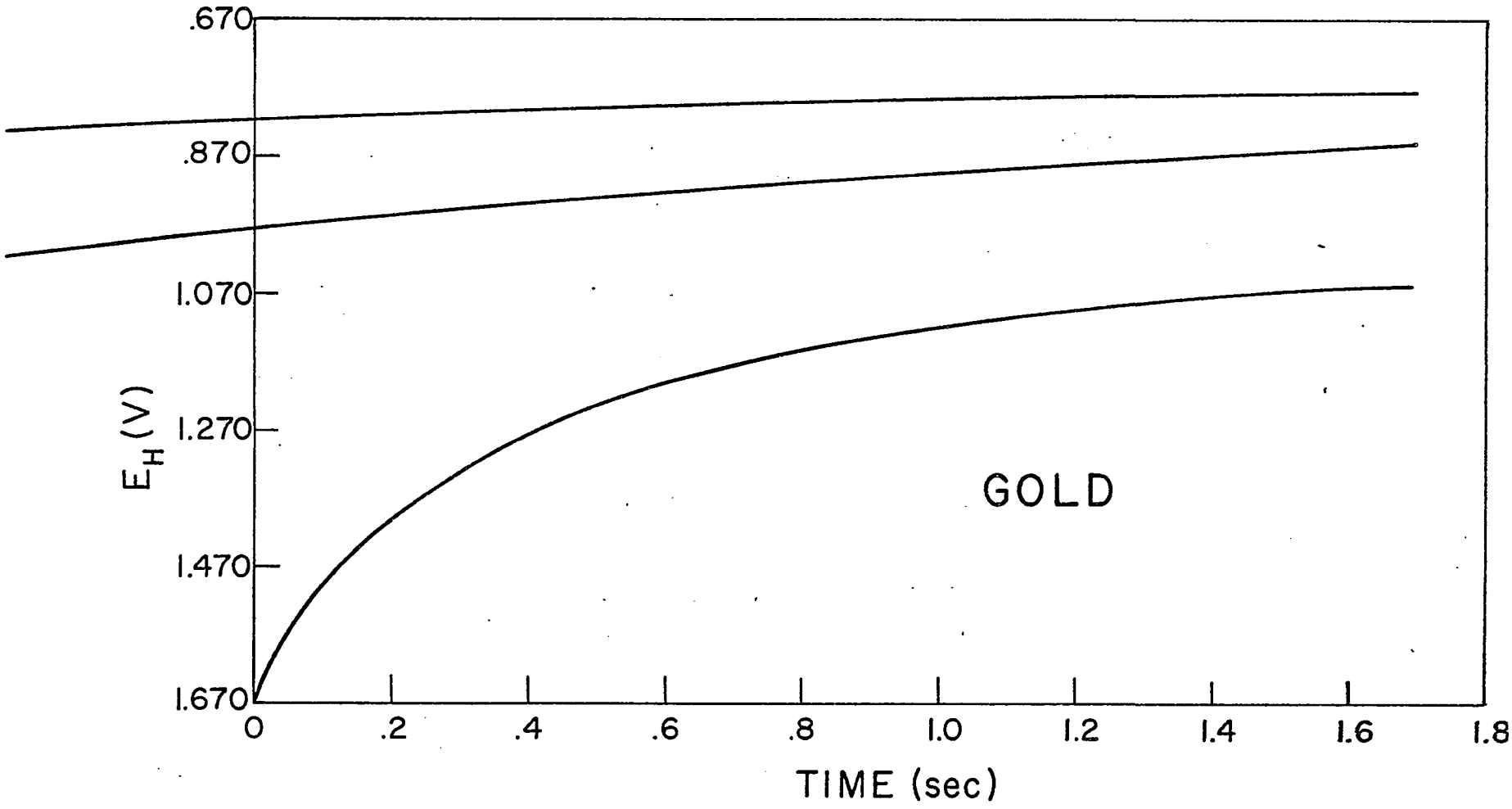
.670
.870
1.070
1.270
1.470
1.670
E_H (V)
GOLD
0
.2
.4
.6
.8
1.0
1.2
1.4
1.6
1.8
TIME (sec)

i or in terms of the charge required to drive the potential down across the arrest region, i.e. the product $i\Delta t$. The latter is then a direct measure of the charge required to remove the film of intermediates between the range of potentials corresponding to the potential arrest. The significance of this approach has been discussed earlier in Chapter I and the details of the experimental method have been discussed in Chapter II.

The extents of arrest expressed either as Δt or $1/\Delta t$, the reciprocal charge, have been plotted for gold, palladium and platinum at various current densities of previous polarisation (these current densities are also numerically the same as those used in the reverse discharge pulse) against the log of the previous anodic polarisation time (i.e. in effect, as a function of the log of the charge previously passed anodically). This type of plot was made on the anticipation that, since the arrest region probably corresponded to reduction of an anodic film, the film would have grown as a function of time at a rate given by one or other of the film growth laws discussed in Chapter I. Square roots plots (cf. equation 7, Chapter I) of the previous polarisation time gave no qualitatively significant result but the logarithmic function of time (cf. equation 13, Chapter I) gave linear regions in a plot of delay of arrest vs log [time of previous polarisation] as shown in Figure [XXXVIII].

Figure XXXVIII

Delay time in the arrest region as a function of logarithmic time of previous anodic polarisation at Pt, Pd and Au in 1M HCOOK/HCOOH.

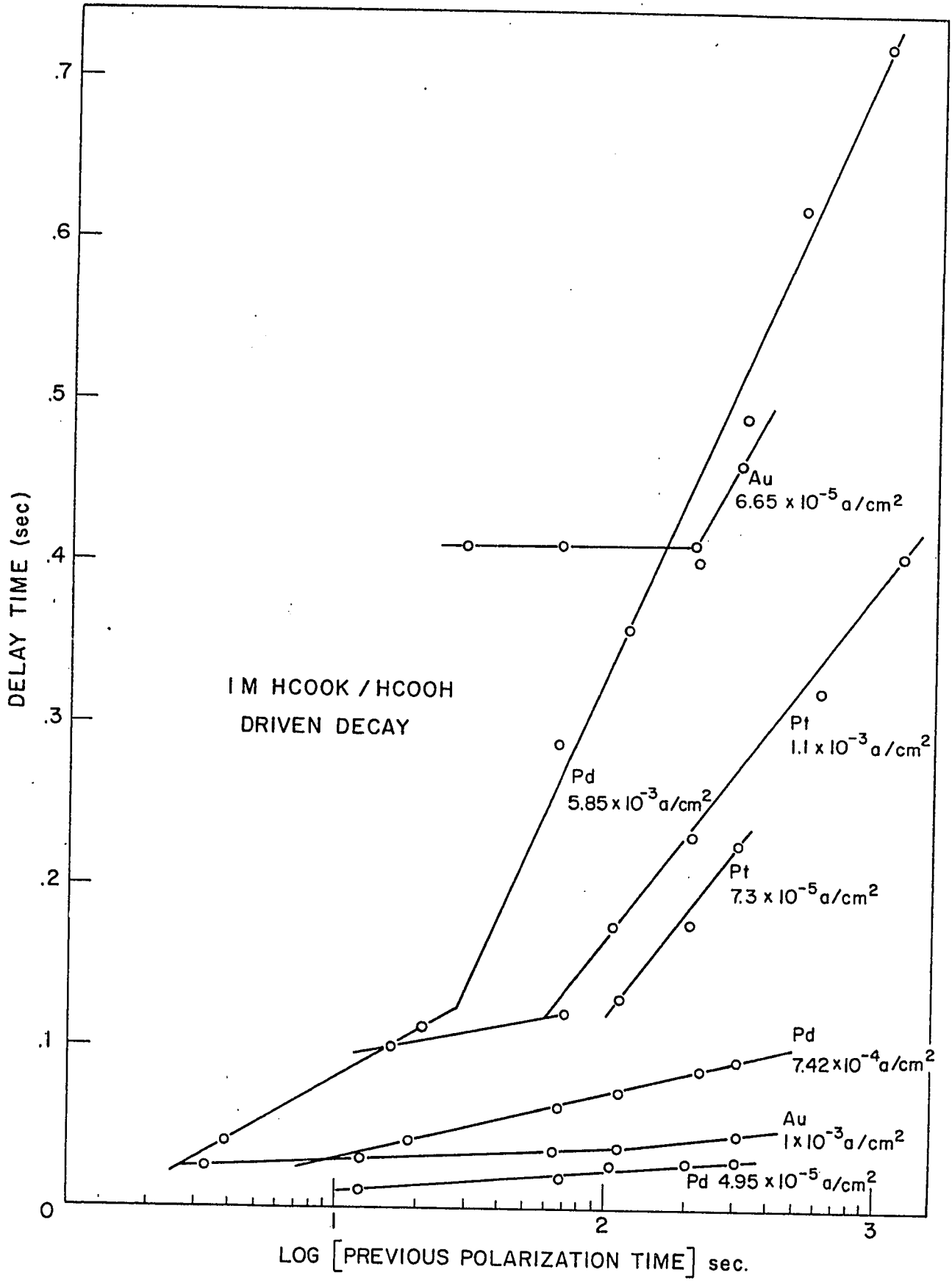
DELAY TIME (sec)
.7
.6
.5
.4
.3
.2
.1
0
1
2
3
LOG [PREVIOUS POLARIZATION TIME] sec.
1 M HCOOK / HCOOH
DRIVEN DECAY
Au
6.65 x 10⁻⁵ a/cm²
Pd
5.85 x 10⁻³ a/cm²
Pt
1.1 x 10⁻³ a/cm²
Pt
7.3 x 10⁻⁵ a/cm²
Pd
7.42 x 10⁻⁴ a/cm²
Au
1 x 10⁻³ a/cm²
Pd 4.95 x 10⁻⁵ a/cm²

Corresponding plots of $1/i\Delta t$, the reciprocal charge associated with the arrest, are shown in Figures [XXXIX, XL, XLI] and show similar linear logarithmic behavior over appreciable ranges of previous anodic polarisation time. Film thickness and pseudo-capacity behavior associated with these anodic films are discussed further in Chapter IV.

In the lower Tafel region (i.e. at current densities below the transition region) the duration of the arrest increases only slowly with prolonged polarisation. However, in the upper Tafel region (i.e. at current densities beyond the transition critical current), an initial region of slow increase is followed by a region where the length of the arrest region increases rapidly with the time of the previous polarisation before the reverse pulse measurement is commenced.

(iii) Arrest Behavior in the Trifluoroacetate-Trifluoroacetic Acid System

Results similar to those reported above for the formate system were observed in the trifluoroacetate-trifluoroacetic acid system at platinum, palladium and gold electrodes. The length of the arrest region (delay times at constant cathodic current) in terms of the charge associated with the arrest region are shown in Figure XLII as a function of logarithmic time of previous anodic polarisation. Pseudo-capacities and extents of coverage by

Figure XXXIX

Reciprocal charge associated with arrest region at Pt as a function of the logarithm of previous anodic polarisation time/in 1M HCOOK/HCOOH.

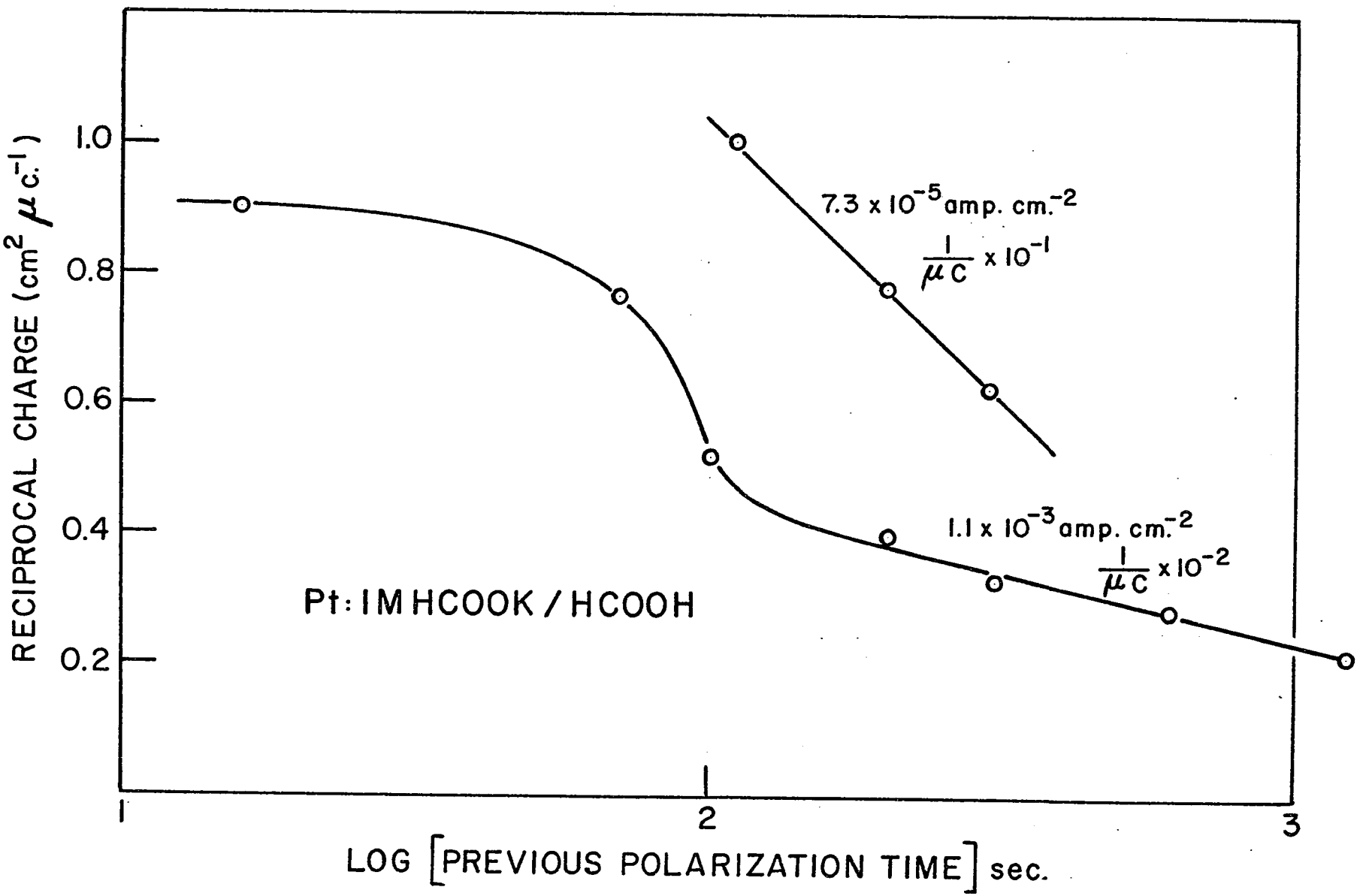
RECIPROCAL CHARGE ($cm^2 \mu c.^{-1}$)
1.0
0.8
0.6
0.4
0.2
1
2
3
LOG [PREVIOUS POLARIZATION TIME] sec.
7.3×10^{-5} amp. $cm.^{-2}$
$\frac{1}{\mu C} \times 10^{-1}$
1.1×10^{-3} amp. $cm.^{-2}$
$\frac{1}{\mu C} \times 10^{-2}$
Pt: 1M HCOOK / HCOOH

Figure XL

Reciprocal Charge associated with arrest region at Pd as a function of the logarithm of previous anodic polarisation time/in 1M HCOOK/HCOOH.

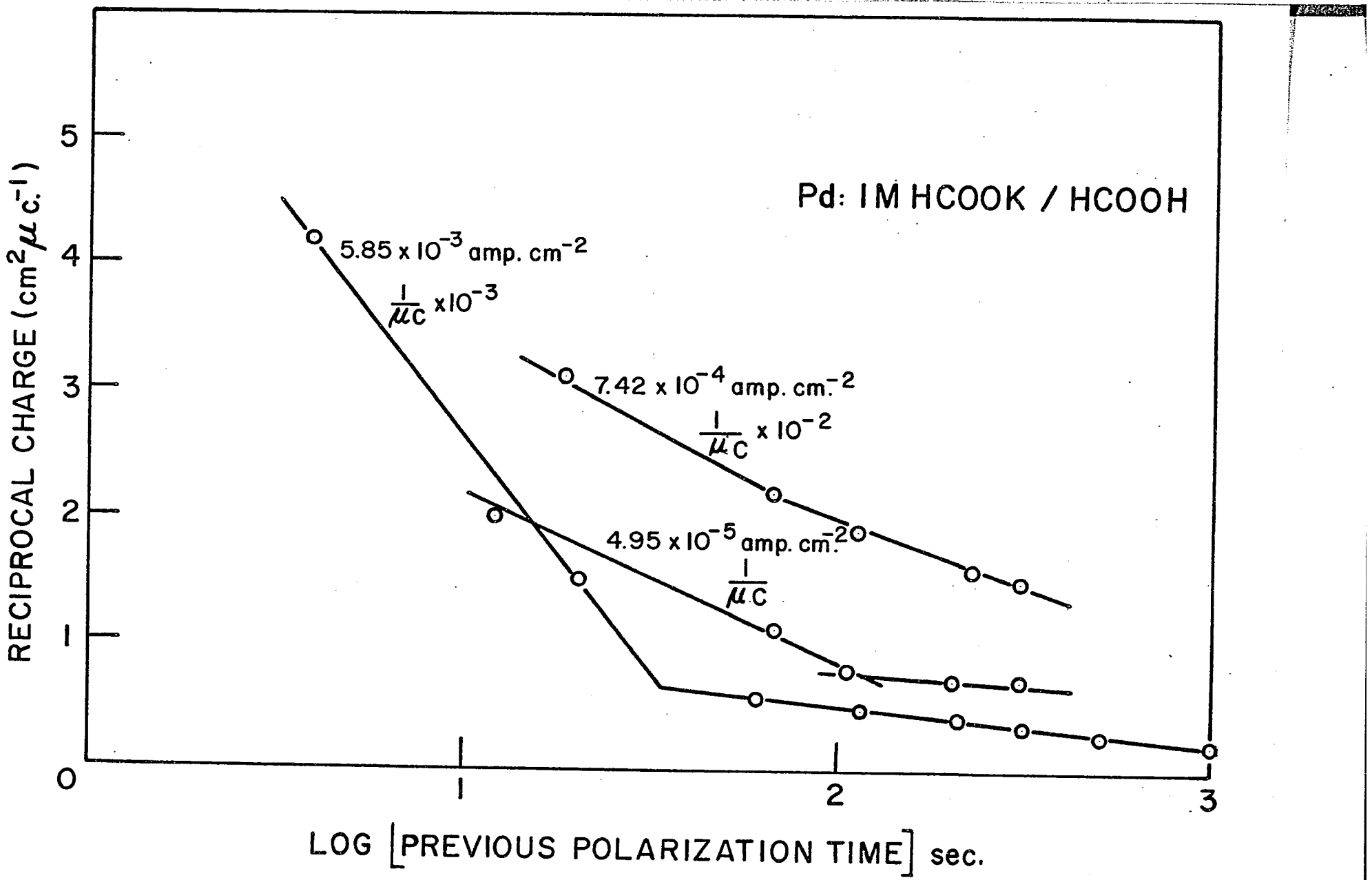
Pd: 1M HCOOK / HCOOH
5.85 x 10⁻³ amp. cm⁻²
1/μC x10⁻³
7.42 x 10⁻⁴ amp. cm⁻²
1/μC x 10⁻²
4.95 x 10⁻⁵ amp. cm⁻²
1/μC
RECIPROCAL CHARGE (cm²μc.⁻¹)
0
1
2
3
4
5
1
2
3
LOG [PREVIOUS POLARIZATION TIME] sec.

Figure XLI

Reciprocal charge associated with arrest region at Au as a function of the logarithm of previous anodic polarisation time in 1M HCOOK/HCOOH.

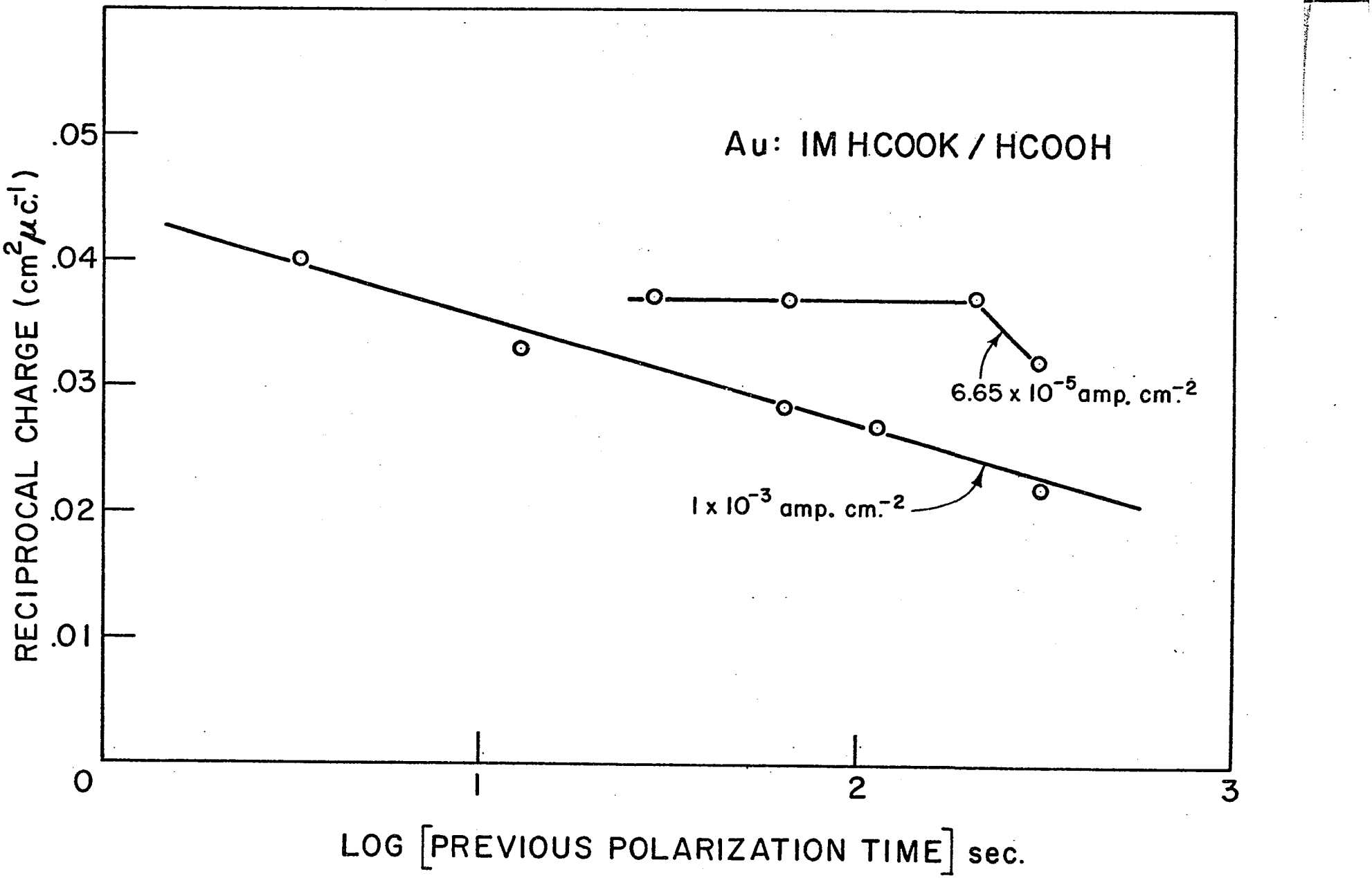
Au: IM HCOOK / HCOOH
6.65 x 10⁻⁵ amp. cm.⁻²
1 x 10⁻³ amp. cm.⁻²
RECIPROCAL CHARGE (cm²μc.⁻¹)
.05
.04
.03
.02
.01
0
1
2
3
LOG [PREVIOUS POLARIZATION TIME] sec.

Figure XLII

Surface charge associated with the arrest region at Pt, Pd and Au in 1M CF_3COOK/CF_3COOH at the current densities indicated in the Figure.

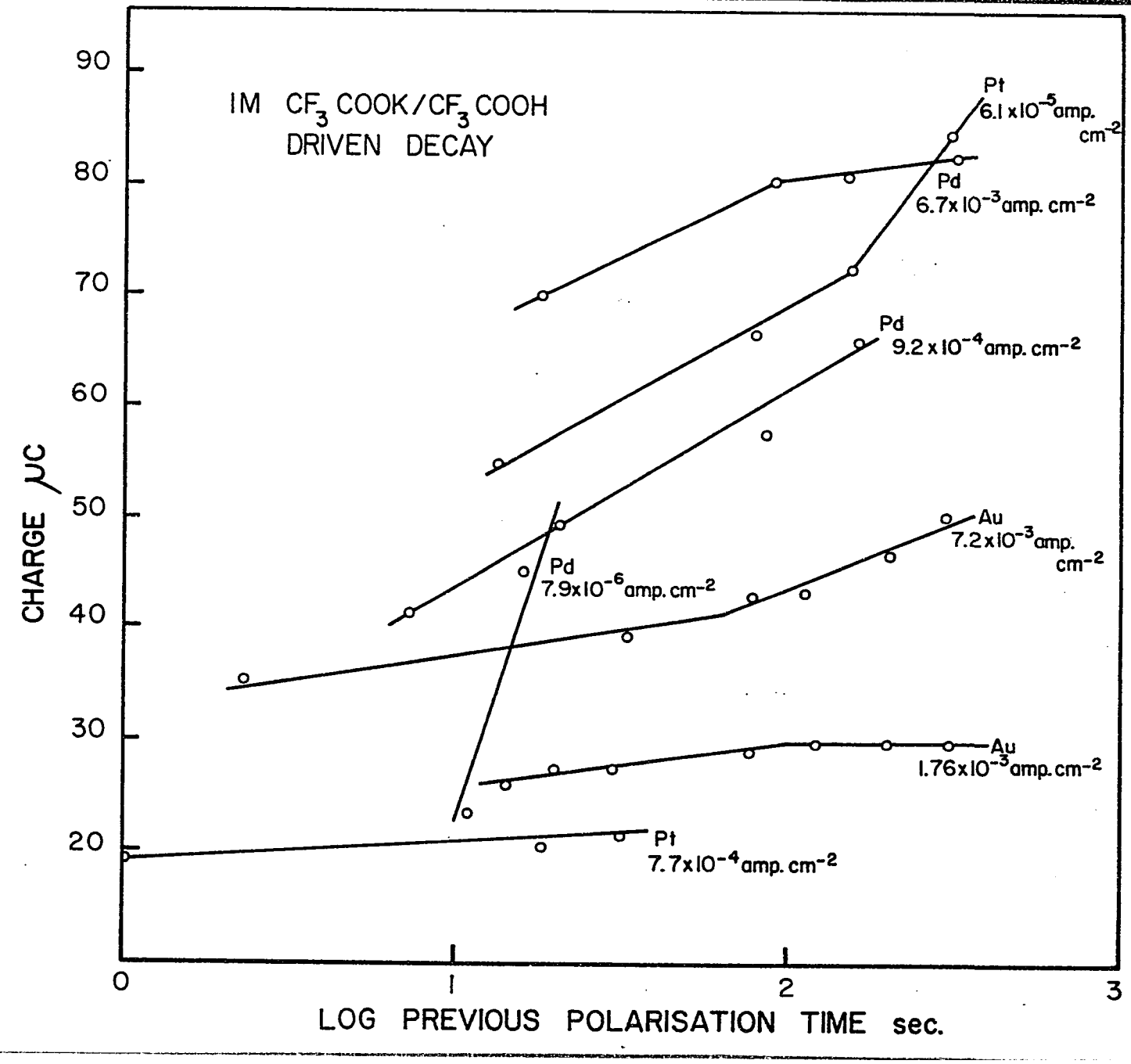
1M CF_3COOK/CF_3COOH
DRIVEN DECAY
Pt
6.1×10^{-5} amp. cm^{-2}
Pd
6.7×10^{-3} amp. cm^{-2}
Pd
9.2×10^{-4} amp. cm^{-2}
Au
7.2×10^{-3} amp. cm^{-2}
Pd
7.9×10^{-6} amp. cm^{-2}
Au
1.76×10^{-3} amp. cm^{-2}
Pt
7.7×10^{-4} amp. cm^{-2}
CHARGE μC
90
80
70
60
50
40
30
20
0
1
2
3
LOG PREVIOUS POLARISATION TIME sec.

intermediates are evaluated and discussed in Chapter IV.

C. DELAYED GAS EVOLUTION AT PALLADIUM IN ANHYDROUS FORMATE FORMIC ACID

An unusual and apparently unique phenomenon was observed during the course of coulombic efficiency studies on palladium. It was observed that following the interruption of anodic current (with normal termination of gas evolution) a delayed "burst" of extra gas was suddenly evolved at the anode. The length of the delay in the evolution of the burst of gas following interruption of polarisation was found to be dependent upon the time of previous polarisation. Simultaneous ciné-photography of the anode and measurement of electrode potential (by means of the oscilloscope) was carried out. In Figure [XLIII] open-circuit decay curves are shown for palladium at two current densities of prior polarisation for the times indicated in the figure. In Figure [XLIV], the duration of the delay of fall of potential in the arrest region as a function of logarithm of previous polarisation time is shown for several current densities. Figure [XLII] shows a comparison between the period of delay in gas evolution as a function of the logarithm of the previous polarisation time, and the corresponding delay in the fall of potential, i.e. the duration of the arrest of potential on open-circuit decay after polarisation at a single current density of 10^{-2} amp.cm.$^{-2}$

Figure XLIII

Open-circuit decay curves at two current densities of prior polarisation at Pd for the times indicated in the Figure.

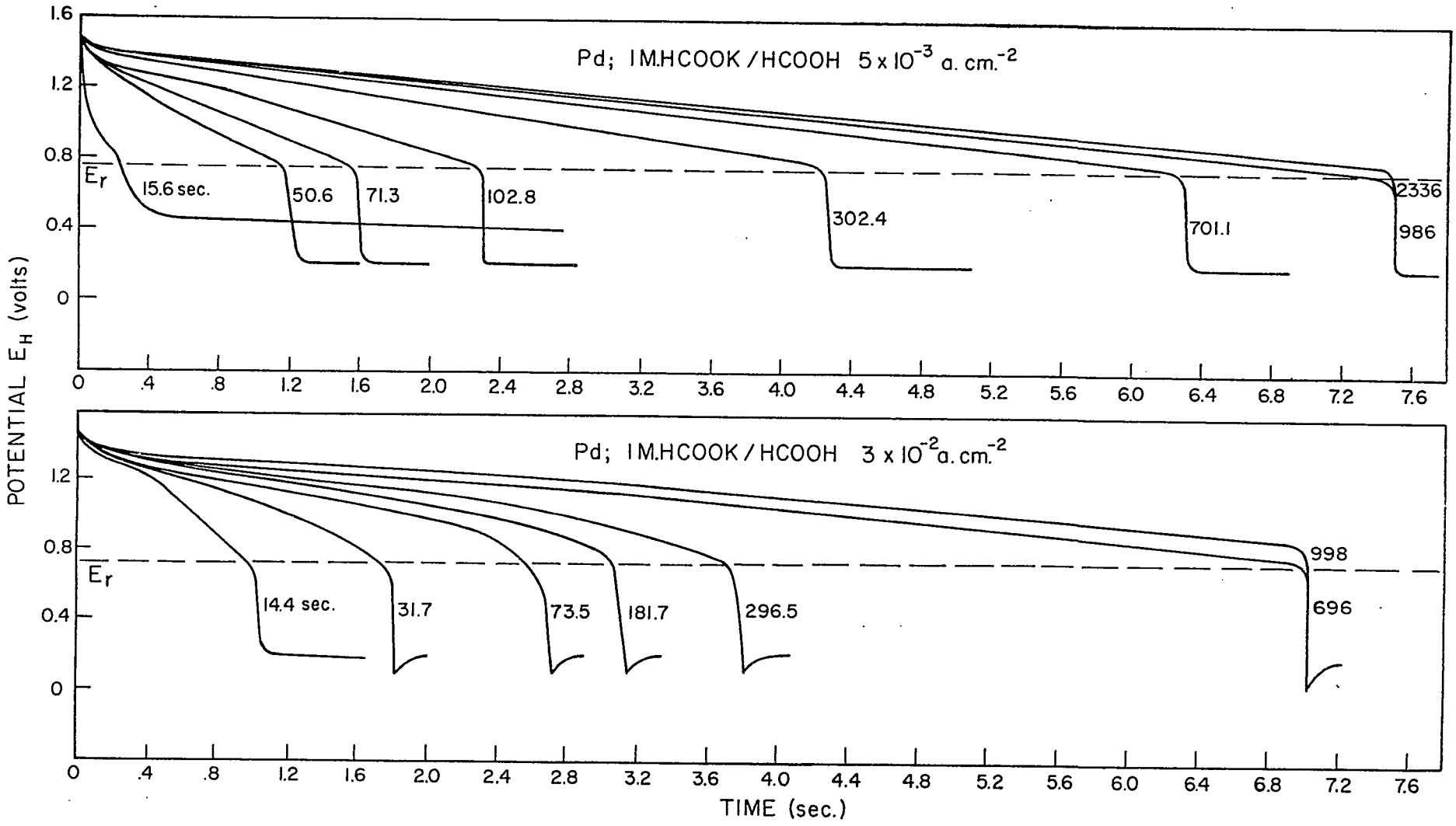
Pd; 1M.HCOOK/HCOOH 5 x 10⁻³ a. cm.⁻²
Pd; 1M.HCOOK/HCOOH 3 x 10⁻² a. cm.⁻²
Er
15.6 sec.
50.6
71.3
102.8
302.4
701.1
2336
986
14.4 sec.
31.7
73.5
181.7
296.5
998
696
POTENTIAL E_H (volts)
TIME (sec.)

Figure XLIV

Delay time in the arrest region as a function of the logarithm of the time of previous polarisation at Pd at several current densities.

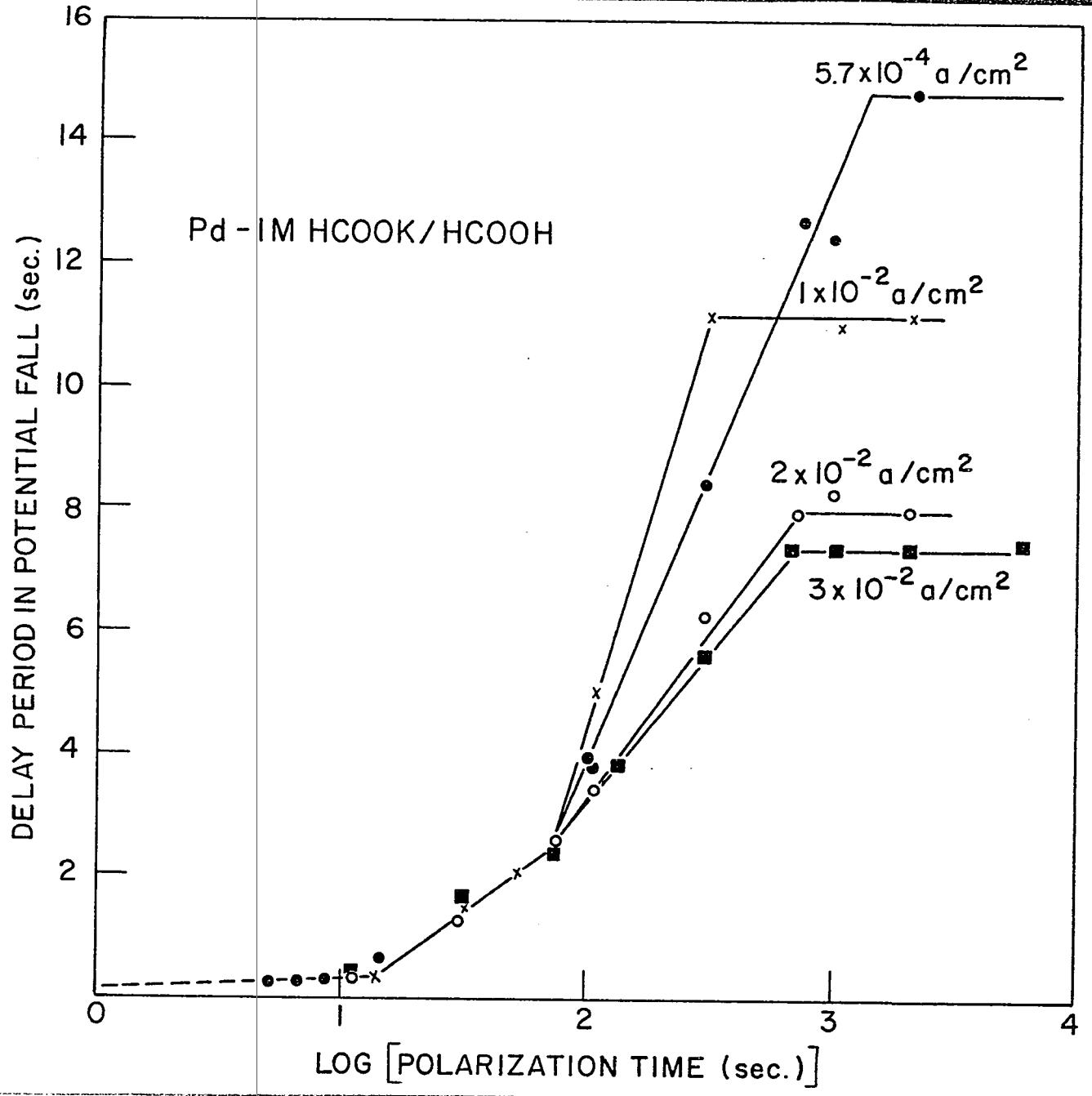
Pd - 1M HCOOK/HCOOH
5.7x10^-4 a/cm^2
1x10^-2 a/cm^2
2x10^-2 a/cm^2
3x10^-2 a/cm^2
DELAY PERIOD IN POTENTIAL FALL (sec.)
LOG [POLARIZATION TIME (sec.)]
0
1
2
3
4
2
4
6
8
10
12
14
16

The two kinds of data plotted in Figure XLV evidently fall on a more or less common line from which it can be concluded that the delay period in gas evolution is identical with the delay in the arrest region of the open-circuit potential-time relation, i.e., the burst of gas appears at a more or less critical potential after a delay period determined by the time required for the electrode potential to fall to that critical potential. Thus, it is seen from Figure XLVI that irrespective of the current density of prior anodic polarisation, the electrode potential at which delayed gas evolution occurs is more or less constant and independent of the actual delay period involved. This suggests that the process of decomposition (of an anodic film) leading to the gas evolution can only occur when a critical electrochemical thermodynamic condition of the film is attained, i.e. after the anode potential has fallen to some potential below that characteristic of the stability of the film substance.

Figure XLV

Relationship of both the delay in open-circuit gas evolution and the potential delay to the period of prior anodic polarisation at 10^{-2} amp.cm.$^{-2}$ o, delayed gas evolution x, potential delay.

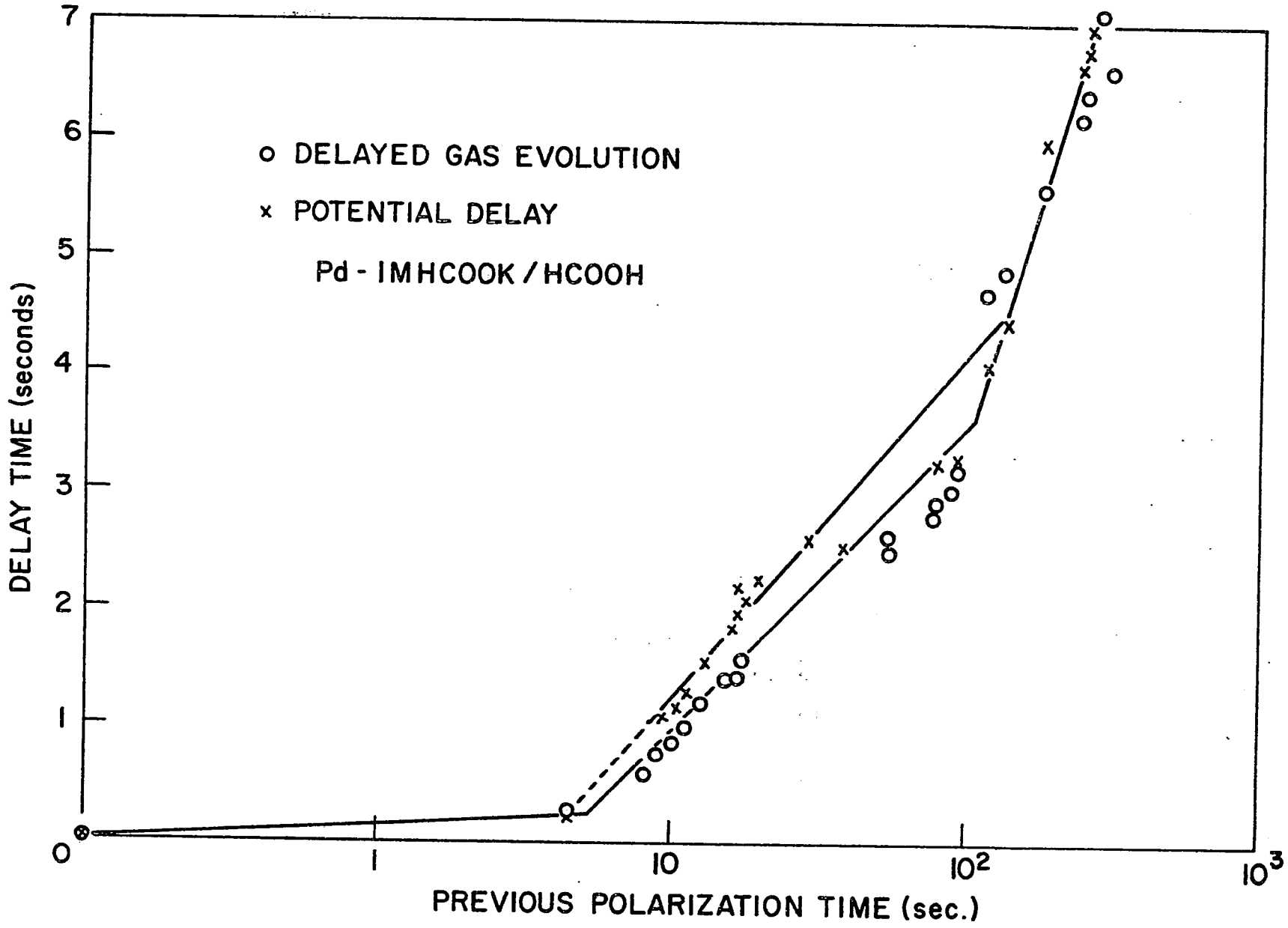
o DELAYED GAS EVOLUTION
x POTENTIAL DELAY
Pd - IMHCOOK / HCOOH
DELAY TIME (seconds)
PREVIOUS POLARIZATION TIME (sec.)
0
1
2
3
4
5
6
7
1
10
10²
10³

Figure XLVI

E.M.F. associated with delayed gas evolution as a function of delay time.

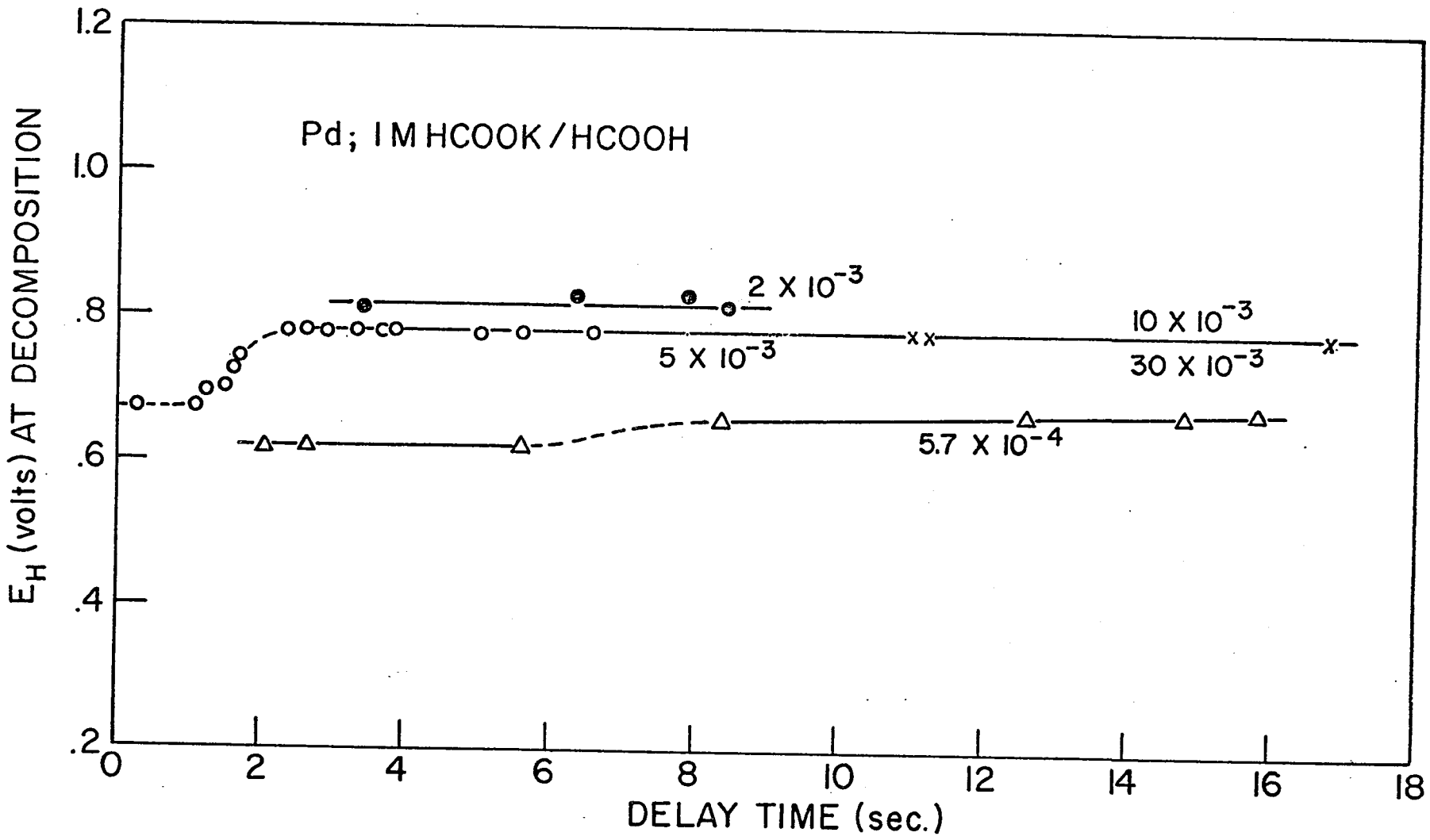
Pd; 1M HCOOK/HCOOH
2 X 10⁻³
5 X 10⁻³
10 X 10⁻³
30 X 10⁻³
5.7 X 10⁻⁴
E_H (volts) AT DECOMPOSITION
DELAY TIME (sec.)
1.2
1.0
.8
.6
.4
.2
0
2
4
6
8
10
12
14
16
18

CHAPTER IV

DISCUSSION

A. GENERAL INTRODUCTION

The aims of the present investigation have been to examine the basic electrochemical behavior of reactions involving anodic decarboxylation by choosing initially two systems in which side reactions are minimised so that the electrochemical kinetics of a single reaction can be studied.

In the first case, we shall examine the mechanism of the apparently simplest anodic decarboxylation that can occur, viz. that of formic acid or the formate ion. No other papers have evidently been published previously on the electrochemical kinetics of this reaction, and other previous work (e.g. 21) has been concerned only with the problem of coulombic yields of CO_2 at the anode, the absence of hydrogen as an anodic product and the production of hydrogen at the cathode. This reaction is ideally suited for electrochemical study since (i) the reaction pathway is very largely the simple decarboxylation to give hydrogen ions and carbon dioxide, and (ii) the reaction is an essential model reaction for studies on the Kolbe reaction itself.

In the second case, a true Kolbe coupling reaction

is examined but one which is virtually free from complications by formation of side products. Such a reaction is that occurring in the electrolysis of trifluoroacetates where C_2F_6, and the stoichiometric quantity of carbon dioxide, are almost exclusively the reaction products. Since the α-carbon atom in the trifluoroacetate ion cannot easily be further oxidised, oxidative side reactions, such as occur in the aqueous acetate case, are absent and the electrochemical mechanism can be examined under ideal conditions.

The approaches made, which have been described in detail in Chapter II, have been as follows: evaluation of the Tafel parameters i_o and b determining the current-potential relationship and examination, where possible, of the significance of these parameters in terms of rate-controlling steps; examination of the role of adsorbed intermediates by galvanostatic charging and open-circuit decay measurements (119) with evaluation of electrode adsorption pseudo-capacitance (102) and surface charge, and discussion of their significance in relation to reaction mechanisms.

The mechanisms of consecutive reactions can always be elucidated more definitively if knowledge of the behavior and concentration of reaction intermediates adsorbed at the surface is available. Steady-state current-potential curves for electrochemical reactions can lead to an understanding

of the reaction mechanism only to a limited extent through evaluation and interpretation of Tafel slopes; non-steady state measurements by means of analysis of transients can lead, in favourable cases, to important complementary information on: (i) the surface coverage of the electrode by reaction intermediates as a function of potential, and (ii) the associated adsorption pseudo-capacitance (102); interpretation of the potential dependence of the latter can then lead to information on the adsorption behavior (e.g. the type of isotherm applying) of the intermediates at the surface.

In the case of anodic film formation, i.e. beyond monolayer adsorption of anodic reaction intermediates, the extent of film growth can be examined as a function of time and current density and also the role of anodic barrier layer films in the reaction can be examined (81,87).

B. THE DECARBOXYLATION OF FORMATE IN PURE FORMIC ACID

(a) Kinetic Parameters

The kinetic parameters i_o (the exchange current) and b, the Tafel slope, which characterise the kinetics of the rate-determining step can be obtained from the current-potential relations in Figures [X-XV]. Evaluation of the exchange current, i_o, requires calculation of the reversible potential for the reaction

$$HCOO^- \longrightarrow CO_2 + H^+ + 2\,e \qquad \text{I}$$

on the hydrogen scale in pure formic acid, since the reaction itself is not practically reversible. The half-cell reactions (European convention) involving the hydrogen electrode are reaction I and

$$H_2 \longrightarrow 2\,H^+ + 2\,e$$

corresponding to the overall cell reaction:

$$HCOOH \longrightarrow CO_{2(g)} + H_{2(g)}. \qquad \text{Ia}$$

The equilibrium constant for reaction Ia is

$$K = \frac{f_{CO_2}\, f_{H_2}}{a_{HCOOH}} \qquad [38]$$

in terms of the fugacities of the gases and the activity of formic acid. The free energy change is

$$\Delta G = \Delta G^o + RT \ln f_{CO_2} f_{H_2} - RT \ln a_{HCOOH} \qquad [39]$$

and the e.m.f. of the hydrogen-formic acid cell is therefore, at unit fugacity (pressure) of the gases (the standard state),

$$E = E^o - \frac{RT}{2F} \ln a_{HCOOH} \qquad [40]$$

The ΔG^o value for reaction Ia was obtained from the standard free energies of formation of HCOOH(liq.) and $CO_{2(g)}$ as 10.62(2) kcal.mole^{-1} (126) for a standard state of unit mole fraction of HCOOH and unit fugacity (atmospheres) of CO_2 (here unit pressure is actually taken). The value of E^o is hence -0.230 v (European convention) on the hydrogen scale

in pure formic acid. The observed current-potential behavior can hence be extrapolated to the theoretical reversible potential and the log $[i_o]$ evaluated or log $[i_o]$ can be calculated from the observed overpotential at a given current density and Tafel slope. Values of i_o and b are summarised in Table IV. The formic acid decarboxylation is seen to be highly irreversible. This result is of current interest in that it offers a quantitative kinetic explanation of the difficulty of obtaining useful rapid oxidation beyond the formate stage to CO_2 encountered in the anodic oxidation of methanol (147).

(b) Reaction Mechanism

No previous studies of the electrochemical mechanism of the reaction have been made, although the possible production of $HCOO^{\bullet}$ radicals as intermediates has been recognized (21). The following steps corresponding to the overall reaction I with formate ions can be envisaged; equivalent steps involving the reactant molecule HCOOH can, of course, be written but involve the same intermediates.

$$M + HCOO^- \longrightarrow HCOO^{\bullet}(M) + e \qquad \text{II}$$

$$HCOO^{\bullet}(M) \longrightarrow CO_2 + H^{\bullet}(M) \qquad \text{III} \qquad \text{Scheme A}$$

$$H^{\bullet}(M) \longrightarrow H^+ + e \qquad \text{IV}$$

where (M) indicates a site on the metal surface to which the

Table IV

Mean Tafel Parameters in Anhydrous HCOOK-HCOOH

(from data for a minimum of ten electrodes).

Temp. 5 ±.1°C

Electrode	Conc. M	b ± 1%	i_0 (calc.)** amps-cm^{-2} ± 40%	Current Density Range
Pt	0.1	0.14	1.2×10^{-15}	1×10^{-4} - 3×10^{-2}
	1	0.14	5.2×10^{-15}	2×10^{-4} - 3×10^{-2}
	5	0.12	3.2×10^{-16}	9×10^{-4} - 1×10^{-1}
Pd	0.1	0.10	1.0×10^{-21}	4×10^{-5} - 2×10^{-2}
		0.12*	1.0×10^{-15}	1.5×10^{-5} - 2.5×10^{-4}
	1	0.10	1.8×10^{-20}	5×10^{-4} - 1×10^{-1}
		0.14*	2.1×10^{-14}	1.5×10^{-5} - 2.5×10^{-4}
	5	0.11	1×10^{-18}	5×10^{-4} - 6×10^{-2}
Au≠	0.1	0.065	5×10^{-31}	1.8×10^{-5} - 3×10^{-4}
		0.13	1.2×10^{-17}	3×10^{-4} - 2.5×10^{-2}
	1	0.065	3.5×10^{-30}	2.5×10^{-5} - 1×10^{-3}
		0.14	4.8×10^{-16}	1×10^{-3} - 5×10^{-2}
	5	0.065	2.0×10^{-29}	5×10^{-5} - 9×10^{-3}
		0.18	2.3×10^{-12}	9×10^{-3} - 6×10^{-2}

(Continued on next page)

Table IV - Continued

22.6% Pd-Au≠	0.1	0.10	1.3×10^{-21}	4.5×10^{-5}	-1.5×10^{-3}
		0.12	1.3×10^{-18}	1.5×10^{-3}	-4.5×10^{-2}
	1	0.07	1.7×10^{-28}	4.5×10^{-5}	-1.6×10^{-3}
		0.09	5.8×10^{-23}	1.6×10^{-3}	-4×10^{-2}
	5	0.07	6.2×10^{-28}	5.5×10^{-5}	-4.5×10^{-2}
44.8% Pd-Au≠	0.1	0.08	1.3×10^{-25}	1.5×10^{-5}	-5.5×10^{-4}
		0.12	1.9×10^{-18}	5.5×10^{-4}	-4.5×10^{-2}
	1	0.07	3.5×10^{-28}	3×10^{-5}	-1.6×10^{-3}
		0.11	3.5×10^{-19}	1.6×10^{-3}	-5×10^{-2}
	5	0.07	1.3×10^{-27}	6×10^{-5}	-4.5×10^{-2}
61.8% Pd-Au≠	0.1	0.085	6.8×10^{-24}	6×10^{-5}	-1.3×10^{-3}
		0.11	4.7×10^{-20}	1.3×10^{-3}	-2.5×10^{-2}
	1	0.07	1.2×10^{-27}	7.5×10^{-5}	-1×10^{-3}
		0.12	1.1×10^{-17}	1×10^{-3}	-2.5×10^{-2}
	5	0.085	6.8×10^{-23}	4.5×10^{-4}	-2.5×10^{-2}

* Intermediate potential region; see Figure XI.

≠ Two slopes in the upper region are observed here; see Figs. XII-XV.

** Based on calculated extrapolations to the theoretical reversible potential $E_H = -0.230$ V w.r.t. the hydrogen electrode in the same solution. The i_o values have been referred to their E_H value at 25°C. From the entropy change in the overall reaction which is approximately 51 e.u. the reversible potential at 5°C will differ from the above value by ca. 21 mV.

ad-species is bound;

or

$$M + HCOO^- \longrightarrow HCOO^{\bullet}(M) + e \qquad II$$

$$HCOO^{\bullet}(M) \longrightarrow CO_2 + H^+ + e \qquad V$$

Scheme B

or

$$M + HCOO^- \longrightarrow M + CO_2 + H^+ + 2e \qquad VI$$

Scheme C

i.e. the overall reaction in one step involving two electrons (see below).

A pathway involving

$$HCOO^{\bullet}(M) \longrightarrow CO_2 + H^{\bullet}(M) \qquad III$$

followed by either

$$2\,H^{\bullet}(M) \longrightarrow H_2 \quad \text{(Kolbe product analogue)}$$

or

$$H^{\bullet}(M) + HCOO^- \longrightarrow H_2 + CO_2 + e$$

is not observed experimentally (even to a trace extent) presumably since if III occurs, the desorption ionisation IV will tend to be very rapid at the high anodic potentials involved, and the steady-state coverage by adsorbed H atoms will be very small.

Radical-ion desorption steps (cf. the case of the hydrogen evolution reaction) such as

$$HCOO^{\bullet}(M) + HCOO^- \longrightarrow (HCOO)_2 + e$$

or recombination of the HCOO• radicals, could lead to diformyl peroxide.* Experimentally peroxides are not detectable, either during or following prolonged electrolysis. Formation of a peroxide $(HCOO)_2$ from HCOO•, followed by its decomposition to the same HCOO• species with subsequent electrochemical CO_2 formation is a kinetically unlikely cyclic process as we have argued in the Introduction.

Step VI (Scheme C) or a radical desorption step such as

$$HCOO^{\bullet}(M) + HCOO^{-} \longrightarrow 2H^{+} + 2CO_2 + 3e$$

are unlikely since they involve more than one electron in a single rate-determining step. Similarly, a step such as

$$HCOO^{-} + H^{\bullet}(M) \longrightarrow 2H^{+} + 2CO_2 + 3e$$

is electrochemically improbable as a single electrochemical step. Schemes A or B are hence the likely pathways in CO_2 evolution and can be regarded as examples of the "discharged ion" theory of decarboxylation (54).

(c) Kinetic Equations for Steps in the Formate Decarboxylation Reaction

(i) Langmuir Conditions

The theoretically predictable Tafel slopes for

---

* No published reports on the existence or stability of diformyl peroxide appear to exist; however, peroxy-formic acid has been reported to be very unstable, losing oxygen rapidly even at 0°C (148).

Langmuir conditions, that is when the coverages by adsorbed intermediates are limitingly low or limitingly high, are readily derived for various rate-determining steps in the above schemes by now well-known principles of analysis of consecutive electrochemical reactions which have been treated in previous theses from this Department and in the literature (32,33). For scheme A we obtain the kinetic equation for reaction II as

$$v_2 = k_2 (1-\theta_F)\, a_F \text{-exp.} - [\Delta G_2^{\neq} - \beta VF]/RT \qquad [41]$$

where the subscripts F^-/and F represent the formate ion and adsorbed formate radical, respectively (the latter at a coverage θ), the remaining terms including β the symmetry factor having thcir usual significance (32,33). Similarly, for succeeding steps in Scheme A

$$v_{-2} = k_{-2}\, \theta_F \exp -[\Delta G_{-2}^{\neq} + (1-\beta)\, VF]/RT \qquad [42]$$

$$v_3 = k_3\, \theta_F\, (1-\theta_H) \exp - [\Delta G_3^{\neq}/RT] \qquad [43]$$

$$v_{-3} = k_{-3}\, \theta_H\, (1-\theta_F) \exp - [\Delta G_{-3}^{\neq}/RT] \qquad [44]$$

$$v_4 = k_4\, \theta_H \exp - [\Delta G_4^{\neq} - \beta VF]/RT \qquad [45]$$

We now examine limiting cases, assuming as usual limitingly low ($\theta < 0.1$) or limitingly high ($\theta \longrightarrow 1$) surface coverages by intermediates (109,119).

When the ion-discharge step II is rate-determining and subsequent steps rapid, θ_F and θ_H will be small and we obtain

$$v_2 = k_2 a_{F^-} \exp. - [\Delta G_2^{\neq} - \beta VF]/RT \qquad [46]$$

Assuming $\beta \doteq 1/2$ as usual, the Tafel slope is obtained as

$$dV/d \ln i_2 = 2\ RT/F. \qquad [47]$$

In a similar manner, the limiting Tafel slopes for the remaining steps, if rate-determining, can be obtained and are summarised below for the conditions noted.

Scheme A:

a)	Ion discharge step II.	2RT/F
b)	First order decomposition of HCOO•(M) [III] with II in quasi-equilibrium and surface coverage of HCOO•(M) potential-dependent.	RT/F
c)	HCOO•(M) approaching full coverage and its surface concentration consequently potential independent.	Limiting current
d)	H•(M) ionisation step IV (steps II and III in quasi-equilibrium) - unlikely to be rate-controlling at high anodic potentials.	2RT/3F
	H•(M) ionisation at full coverage by H• (unlikely to be rate-controlling at high anodic potentials).	2RT/F

Scheme B

a)	Ion discharge II (as in scheme A)	2RT/F
b)	HCOO•(M) ionisation and decomposition	
	(i) Full coverage by HCOO•(M)	2RT/F
	(ii) Potential-dependent coverage with II in quasi-equilibrium.	2RT/3F

(ii) Temkin Conditions

The kinetic treatment in terms of the Langmuir adsorption isotherm, i.e. when the heat of adsorption of significantly adsorbed intermediates is assumed to be independent of coverage, is only satisfactory when applied to cases where the degree of surface coverage by adsorbed intermediates is either limitingly low or tending to unity. Experimentally, Frumkin et al. (138-140) had recognized some years ago in the case of the hydrogen evolution reaction that coverages by H in that reaction were intermediate in value (i.e. $0.1 < \theta < 0.9$), and that experimental results in the hydrogen evolution reaction could be explained satisfactorily by taking into account a linear decrease in the heat of adsorption with coverage i.e. using the Temkin adsorption isotherm (135) which involves an energy of adsorption term linearly dependent upon coverage. Several more recent studies have given similar experimental results for the behavior of adsorbed hydrogen at certain electrodes (95,110) and for coverage of oxide electrodes by adsorbed oxygen-containing species (33,119). The importance of coverage effects has also been demonstrated in determining the dependence of exchange currents on the heat of adsorption of H at metals (141) and in determining the isotopic relative electrochemical rates of H_2 and D_2 production (142).

Thomas (127) has recently examined the kinetics of

the hydrogen evolution reaction for the case where a linear variation in the heat of adsorption for intermediate coverage conditions ($0.2 < \theta < 0.8$, "Temkin" conditions) is considered and gives rise to a coverage dependent heat of activation. Under certain conditions, the latter term predominantly determines the rates of steps involving adsorption and desorption of H radicals on the electrode surface.

A more general case has recently been considered by Conway and Gileadi (102) for the kinetics of consecutive reactions involving more than two consecutive steps (as in electrochemical oxygen evolution) and hence for cases where the electrode may be appreciably covered simultaneously by more than one adsorbed intermediate.

The linear decrease of the heat of adsorption with coverage may be written (127)

$$\Delta H_\theta = \Delta H_o - r\theta \qquad [48]$$

where r is a constant energy term determining the variation of heat of adsorption with coverage, ΔH_θ and ΔH_o are the heats of adsorption at finite and zero coverage, respectively. In a series of consecutive electrochemical reactions where more than one adsorbed intermediates may be present on the electrode surface, relations analogous to equation [48] have been postulated. The exact form of these relations depends, however, on the model chosen to represent the

fall of heats of adsorption with coverage.*

If *à priori* heterogeneity** of surface sites is assumed (127) with no specificity of surface sites for adsorption of any one of the intermediates, the energy of adsorption for a given species will only depend on the number of sites remaining beyond the total coverage θ_T; we can then write in general, as shown previously, for the case of two intermediates A and B, equations of the form

$$\Delta H_A = \Delta H_A^o - r_A\theta_T$$
$$\Delta H_B = \Delta H_B^o - r_B\theta_T \qquad [49]$$

analogous to equation [48].

An alternative model which has been proposed (102) is based on surface induction effects (128) associated with a change of the work function of the metal, which in part determines the energy of chemisorption; the change in work function arises from the presence of the dipole double-layer set up by the chemisorbed species. The equations analogous to [48] and [49] for species A and B may then be written (102)

---

* The use of these and other models involving, for example, two dimensional interactions, viz. dipole-dipole repulsion, ion-ion interaction at the surface and "London" dispersion forces, have been discussed elsewhere (102) and will be considered in detail in a thesis shortly to be presented by Gileadi; the models based on two-dimensional molecular interactions in the interphase do not lead to a linear variation of ΔH with θ as observed experimentally, and the interactions are too small to account for the observed fall of ΔH with θ, in the range of intermediate ($0.1 < \theta < 0.9$) coverages.

** The term used by Boudart (128); "intrinsic heterogeneity" would be a better term to use.

$$\Delta H_A = \Delta H_A^o - (r_A\theta_A + r_B\theta_B)$$
$$\Delta H_B = \Delta H_B^o - (r_B\theta_B + r_A\theta_A) \qquad [50]$$

in which it is assumed that the variation of the heat of adsorption of the species A or B will depend, to a first approximation, on the sum of two terms involving the respective dipole double-layer surface potential contributions from each species. It is important to note that the same terms determine the variation of the heat of adsorption of both A and B with coverage by A and B, and for convenience we can hence write $r_A\theta_A + r_B\theta_B$ as $f(\theta)$.

In the present case of the formate decarboxylation, we show later in this Chapter that the surface coverage by the electrochemically formed intermediates ($HCOO^{\bullet}$) varies from some small value up to full coverage. In a number of non-electrochemical heterogeneous reactions, the Langmuir isotherm has been used as a basis for interpretation of the kinetics (e.g. in the case of ethylene hydrogenation studied by Langmuir (143) and Hinshelwood (144)) although chemisorption of reactants is rarely associated with a constant energy of adsorption, and coverages by adsorbed reactants are often appreciable. Such a treatment corresponds to the limiting ones given above for the various reaction steps in the formate decarboxylation.

However, in order to make as complete and exact

an analysis as possible of theoretically predictable results, we now examine cases where effects of coverage by the intermediates on their respective heats of adsorption are significant and introduce these effects in the free energies* of activation of the various steps in the formate decarboxylation reaction.

Following the previous application by Conway and Gileadi (102) of Boudart's treatment (128) of surface induction effects to electrochemical reactions where a linear decrease of the heat of adsorption with coverage is assumed, we obtain for reaction II in scheme A

$$v_2 = k_2(1-\theta_F)\, a_{F^-} \exp. - [\Delta G_2^{\neq} - \beta VF + \alpha f(\theta)]/RT \qquad [51]$$

where the subscripts F^- and F again represent the formate ion and adsorbed formate radical, respectively, the latter at a coverage θ_F; $f(\theta)$ represents the term $r_F\theta_F + r_H\theta_H$, similar to that used previously to allow for the variation of the heat of adsorption of F and H with coverage; α and β are symmetry factors (109), where β is probably identical with $1-\alpha$ since the effects of potential on the initial state curve for the ion in solution and the electron in the metal, will be analogous

---

* In introducing the $r\theta$ terms from equations [49] or [50] into the kinetic equations, we make the same assumption as Parsons (141) or Thomas (127) that the changes of apparent standard free energy of adsorption with coverage parallel the changes of heat of adsorption with coverage. This is probably a justifiable assumption in strong chemisorption if adsorbent adsorbate vibrations are strong and change little with coverage, so that changes of vibrational entropy contributions with coverage are unimportant.

to the effect of change of adsorption energy in the final state curve. Similarly, for other steps in the reaction scheme A

$$v_{-2} = k_{-2}\,\theta_F \exp.-[\Delta G^{\neq}_{-2} - (1-\alpha)\,f(\theta) + (1-\beta)\,f(\theta)]/RT \quad [52]$$

$$v_3 = k_3\,\theta_F(1-\theta_H) \exp.-[\Delta G^{\neq}_{3} = \alpha f(\theta) + (1-\alpha)\,f(\theta)]/RT \quad [53]$$

$$v_{-3} = k_{-3}\,\theta_H(1-\theta_F) \exp.-[\Delta G^{\neq}_{-3} - \alpha f(\theta) + (1-\alpha)\,f(\theta)]/RT \quad [54]$$

and

$$v_4 = k_4\,\theta_H \exp. - [\Delta G^{\neq}_{4} - \alpha f(\theta) - \beta VF]/RT \quad [55]$$

We now examine limiting cases assuming that at appreciable coverages sufficient to influence the exponential terms ("Temkin" conditions) the pre-exponential coverage terms are of the order of magnitude of unity and will not be very potential dependent (cf. 127) compared with the exponential terms in potential. If II, the ion discharge step, were rate-determining we obviously obtain the same result as in the Langmuir case, namely

$$dV/d \ln i_2 = 2RT/F \quad [56]$$

When III is rate-determining and II can be regarded as in quasi-equilibrium, the above approximations regarding the relative values of the exponential and pre-exponential terms in coverage lead to

$$VF = f(\theta) + K_2 \quad [57]$$

where K_2 is a constant at constant solution composition and temperature, and θ_H is small (since IV will tend to be fast under these conditions and particularly at the high anodic potentials involved here). By substituting $f(\theta)$ from equation [57] into equation [53], we obtain

$$v_3 = k' \theta_F \exp. - [\Delta G_3^{\neq} - \alpha VF + (1-\alpha) VF]/RT$$

$$= k' \theta_F \exp. - [\Delta G_3^{\neq} - (2\alpha-1)VF]/RT \qquad [58]$$

It is important to note that following substitution for $f(\theta)$, the resulting rate equation is independent of the form of the $f(\theta)$ since $f(\theta)$ is always substituted in terms of VF through the equation derived for equilibrium in a pre-rate determining step (equation [57]). When $\alpha = 1/2$, the rate of a step such as III at intermediate coverage conditions will be practically independent of potential; as a result, the slope will tend to infinity and a limiting current will be observed. A slight potential dependence may, in fact, arise since the rate of III is proportional to the pre-exponential term in surface concentration of the adsorbed formate radicals, and hence to the coverage, the latter being a linear function of potential according to equation [57].

Finally for the unlikely case of IV being rate-determining at potentials substantially anodic to the hydrogen electrode potential, and with II and III in quasi-equilibrium,

$$v_4 = k_4' \theta_H \exp. - [\Delta G_4^{\neq} - \alpha VF - \beta VF]/RT$$

$$= k_4' \theta_H \exp. -[\Delta G_4^{\neq} - (\alpha + \beta)VF]/RT \qquad [59]$$

the Tafel slope is hence

$$\frac{dV}{d \ln i_4} = \frac{RT}{F} \quad \text{assuming } \alpha = \beta = 1/2 \qquad [60]$$

In scheme B, the result for II is the same as above and for V rate-determining

$$v_5 = k_5 \theta_F \exp. - [\Delta G_5^{\neq} - \beta VF - \alpha f(\theta)]/RT \qquad [61]$$

so that with II in quasi-equilibrium, and equation [57] applying again, we may write

$$v_5 = k_5 \theta_F \exp. - [\Delta G_5^{\neq} - \beta VF - \alpha VF]/RT \qquad [62]$$

which gives the Tafel slope

$$\frac{dV}{d \ln i_5} = \frac{RT}{F} \quad \text{with } \alpha = \beta = 1/2. \qquad [63]$$

If we assume <u>à priori</u> heterogeneity of surface sites as in previous papers (102,127), we obtain for reaction II in scheme A,

$$v_2 = k_2(1-\theta_F)a_F \exp. - [\Delta G_2^{\neq} - \beta VF + \beta r_1 \theta_T]/RT \qquad [64]$$

where r_1 is a term similar to that used previously (127) to allow for the variation of heat of adsorption of F with coverage, β is the usual symmetry factor (109) and the remaining terms are as defined previously. Similarly

$$v_{-2} = k_{-2}\,\theta_F \exp. - [\Delta G^{\neq}_{-2} + (1-\beta)VF - (1-\beta)r_1\theta_T]/RT \quad [65]$$

For step III which involves H as well as "F" radicals, we must write

$$v_3 = k_3\,\theta_F(1-\theta_H) \exp. - [\Delta G^{\neq}_{3} - \beta r_1\theta_T + (1-\beta)r_2\theta_T]/RT \quad [66]$$

and

$$v_{-3} = k_{-3}\,\theta_H(1-\theta_F) \exp.-[\Delta G^{\neq}_{-3} - \beta r_2\theta_T + (1-\beta)r_1\theta_T]/RT \quad [67]$$

where r_2 is a term similar to r_1, but referring to the variation of heat of adsorption of H with coverage. The velocity of reaction IV is similarly given by

$$v_4 = k_4\,\theta_H \exp. - [\Delta G^{\neq}_{4} - \beta VF - \beta r_2\theta_T]/RT \quad [68]$$

since this step only involves one adsorbed entity H in its initial state.

Proceeding in a similar manner to that adopted previously for evaluation of Tafel slopes using the surface induction model, we obtain the same result as for Langmuir conditions or for the induction model for II, that is when the ion-discharge step is rate-determining, viz. $dV/d \ln i_2 = 2RT/F$.

When III is rate-determing, and II can be regarded as in quasi-equilibrium, so that now (cf. equation [57])

$$VF = r_1\theta_T + K_2 \quad [69]$$

Then assuming, as discussed previously, that θ_H is small, substituting for θ_T from equation [69] and neglecting the pre-

exponential term in θ gives

$$v_3 = k' \exp. - [\Delta G_3^{\neq} + (\frac{r_2 - r_1}{2r_1})VF]/RT \qquad [70]$$

so that the Tafel slope is

$$\frac{dV}{d \ln i_3} = \frac{RT}{F} \left(\frac{2r_1}{r_1 - r_2}\right) \qquad [71]$$

When reaction IV is rate-determining and with II and III in quasi-equilibrium, substituting for θ_T then gives

$$v_4 = k' \exp. - [\Delta G_4^{\neq} - \beta VF - \beta \frac{r_2}{r_1} VF]/RT$$

or

$$= k' \exp. - [\Delta G_4^{\neq} - (\frac{r_1 + r_2}{r_1}) \beta VF]/RT \qquad [72]$$

and the Tafel slope is hence

$$\frac{dV}{d \ln i_4} = \frac{2RT}{F} \left(\frac{r_1}{r_1 + r_2}\right) \quad (\beta = 1/2) \qquad [73]$$

In scheme B, the results for II will, of course, be the same as above (equation [65]) and for V rate-determining

$$v_5 = k_5 \theta_F \exp. - [\Delta G_5^{\neq} - \beta VF - \beta r_1 \theta_T]/RT \qquad [74]$$

with II in quasi-equilibrium, and equation [69] applying

$$v_5 = k_5 \theta_F \exp. - [\Delta G_5^{\neq} - 2 \beta VF]/RT \qquad [75]$$

so that

$$\frac{dV}{d \ln i_5} = \frac{RT}{F} \quad (\beta = 1/2) \qquad [76]$$

except for limitingly full coverage by $HCOO^{\bullet}(M)$ when the Langmuir result will any case apply ($dV/d \ln i_5 = \frac{2RT}{F}$).

As in the previous published calculations of Conway and Bourgault (33) and Conway and Gileadi (102), it is evident that the slopes deduced will depend on the values assumed for r_1 and r_2; however, it is seen from the equations deduced above for the intrinsic heterogeneity model that we only require the ratio r_2/r_1. Since reaction IV will tend to be very rapid at the high anodic potentials normally attained in this reaction, even at low current densities, $\theta_H \rightarrow 0$ so that $\theta_T \rightarrow \theta_F$. In the case of the radicals "F" and H, we note that their areas are quite different and from Courtauld space-filling models it may be calculated that the area of "F" is about 14.2 ($\pm$ 1) $\mathring{A}^2$ and that of H (e.g. for one atom of H per surface hexagonal hole or per surface metal atom) about 6($\pm$ 0.5) $\mathring{A}^2$. We also suggest that for purely steric reasons the effective value of r_1 will be some 2.5 times larger than that of r_2 and we may anticipate that if r_1 and r_2 are also associated with two-dimensional dipole-layer induction effects (128) in the interphase, r_1 will be greater than r_2 owing to the greater surface dipole moment, since presumably the adsorbed $HCOO^{\bullet}$ will be appreciably more polar than the adsorbed H. The steric effect in the ratio of effective r_1 and r_2 values arises since, if reaction III were

allowed to proceed for a unit surface fully covered with "F" to produce the equivalent coverage by H (assuming no further antecedent reactions), the latter species would, in fact, only cover approximately 1/2.5 of the surface. Thus, when any "F" radical decomposes it effectively locally creates for the resulting H a relatively uncovered region of the surface.

We may hence anticipate values of r_1 about 3 to 4 times r_2; $dV/d \ln i_3$ will hence be in the range 3 RT/F to 2.7 RT/F; when $r_1 \gg r_2$, $dV/d \ln i_3 = 2RT/F$ as a minimum value. The observed slopes lower than 2RT/F cannot therefore be explained by taking, for example, $r_1 \ll r_2$ since negative values of the Tafel slope then result, which have no physical significance; and for the special and probably unlikely case of $r_1 = r_2$, we obtain a limiting current as in the case of the induction model. The observed lower slopes of ca. RT/F at Au and the Pd-Au alloys, (see Figs. XII-XV) hence cannot be explained in terms of reaction III proceeding at appreciable coverages under "Temkin" conditions.

Similarly, the limiting values for the case of IV being rate-determining are: (i) RT/2F for $r_1 = r_2$ (ii) RT/F when $r_1 \gg r_2$ and (iii) if $r_1 \ll r_2$ the current-potential curve would tend to a limiting potential.* Since the r values may differ, the intrinsic heterogeneity model allows the

* Limiting potentials, in contrast to limiting currents, are unusual. However, a case of this behavior has been observed by Hoare and Schuldiner (145) in the case of the hydrogen evolution reaction at the β-palladium-hydrogen electrode.

possibility of some variation of Tafel slopes from the limiting values discussed above.

The Tafel slopes deduced above under Langmuir and Temkin conditions are summarised in Table V. Comparison with the experimental behavior will be discussed following section (c) below.

In the above kinetic treatment for intermediate coverage conditions, we may note that the form of the model chosen to account for the linear variation of adsorption energy is important in the deduction of kinetic current-potential relations and Tafel slopes. The results given by the two models are only identical under certain limiting conditions. At present, owing to the lack of experimental evidence, we cannot unequivocally state which of the two models is more correct. Gas phase adsorption studies involving two components (i.e. N and H at iron (128)) appear to favour the induction model. A more complete and hence physically more correct representation probably lies somewhere between the two models considered, i.e. both induction and intrinsic heterogeneity effects are important. In the present case, the surface induction model is favoured since no assumptions as to the magnitude of the r values or the extent of surface coverage by a particular adsorbed species when two or more surface intermediates may be present on the surface

Table V

Theoretically Predicted Tafel Slopes for the Formate Decarboxylation Reaction

Steps	Langmuir Conditions $\theta < 0.1; \theta \rightarrow 1$		Intermediate coverage conditions ($0.2 < \theta < 0.8$)			
			Induction model		Heterogeneity model	
	Tafel Slope	Limiting conditions	Tafel Slope	Limiting conditions	Tafel Slope	Limiting conditions
$HCOO^- \xrightarrow{II} HCOO^\bullet + e$	$\frac{2RT}{F}$	Rate constants for following steps relatively large so that $\theta_F \rightarrow 0$	$\frac{2RT}{F}$	Rate constants for following steps relatively large so that $\theta_F \rightarrow 0$	$\frac{2RT}{F}$	Rate constants for following steps relatively large so that $\theta_F \rightarrow 0$
$HCOO^\bullet \xrightarrow{III} H^\bullet + CO_2$	$\frac{RT}{F}$ or Limiting current	II in equilibrium coverage by $HCOO^\bullet(M)$ potential dependent; $HCOO^\bullet(M)$ approaching full coverage but potential independent	Limiting current	II in quasi-equilibrium	$\frac{2RT}{F}\left(\frac{r_1}{r_1 - r_2}\right)$; Limiting current $2RT/F$	II in quasi-equilibrium; $r_1 = r_2$; $r_1 \gg r_2$; No physical significance to $r_1 < r_2$
$H^\bullet \xrightarrow{IV} H^+ + e$	$\frac{2RT}{3F}$ or $\frac{2RT}{F}$	II and III in quasi-equilibrium; $H^\bullet(M)$ coverage approaching full coverage	RT/F	II and III in quasi-equilibrium	$\frac{RT}{F}\left(\frac{r_1}{r_1 + r_2}\right)$; RT/F; limiting potential	II and III in quasi-equilibrium; $r_1 = r_2$; $r_1 \gg r_2$; $r_1 \ll r_2$

(Continued on next page)

Table V - Continued

V $HCOO^{\bullet} \longrightarrow H^{+}$ $+ CO_2 + e$	2RT/F or 2RT/3F	Full coverage by $HCOO^{\bullet}(M)$ II in quasi-equilibrium and $HCOO^{\bullet}(M)$ coverage potential dependent	RT/F	II and III in quasi-equilibrium	RT/F	II in quasi-equilibrium

is required. Furthermore the exact nature of the f(θ) (linear or non-linear relations will lead to the same results) will not influence the theoretical results. Experimentally in the present system, a significant degree of electro-polishing occurs particularly at current densities below the critical current density and hence it seems reasonable to assume that surface heterogeneities are reduced considerably (but not necessarily eliminated on an atomic scale) before any significant coverage by adsorbed intermediates occurs in the decarboxylation reaction.

Barrier layer film effects which are important in determining the kinetics of some anodic reactions (87,130) are evidently not significant in the present reaction since the maximum Tafel slopes observed are not abnormally high. There is more possibility, however, of the role of such effects in the Kolbe reaction itself and in aqueous solutions (see below).

(d) Discussion of Galvanostatic Transients

Some possibility for distinction between the various mechanisms envisaged above is afforded by the galvanostatic charging method. It is seen that at appreciable current densities (Figs. XLVII-XLIX) there is a significant arrest amounting to 200-250 μ-coulombs cm^{-2} at platinum or gold and up to 1770 μ-coulombs cm^{-2} both on

Figure XLVII

Anodic charging curves for gold and palladium electrodes at various current densities in 1M HCOOK/ 100% HCOOH (5°C), starting at the potentials indicated

a)	Au					
1.	7×10^{-6}	a.cm.$^{-2}$	180 mv.	0.05	v. cm.$^{-1}$	0.2 sec. cm.$^{-1}$
2.	1.7×10^{-5}	a.cm.$^{-2}$	180 mv.	0.2	v. cm.$^{-1}$	1 sec. cm.$^{-1}$
3.	6×10^{-5}	a.cm.$^{-2}$	180 mv.	0.2	v. cm.$^{-1}$	1 sec. cm.$^{-1}$
4.	9×10^{-4}	a.cm.$^{-2}$	180 mv.	0.2	v. cm.$^{-1}$	0.1 sec. cm.$^{-1}$
b)	Pd					
1.	1.2×10^{-5}	a.cm.$^{-2}$	160 mv.	0.1	v. cm.$^{-1}$	0.2 sec. cm.$^{-1}$
2.	1.4×10^{-4}	a.cm.$^{-2}$	160 mv.	0.2	v. cm.$^{-1}$	0.2 sec. cm.$^{-1}$
3.	4.07×10^{-4}	a.cm.$^{-2}$	160 mv.	0.2	v. cm.$^{-1}$	0.2 sec. cm.$^{-1}$
4.	2.33×10^{-3}	a.cm.$^{-2}$	160 mv.	0.2	v. cm.$^{-1}$	0.2 sec. cm.$^{-1}$

Pd

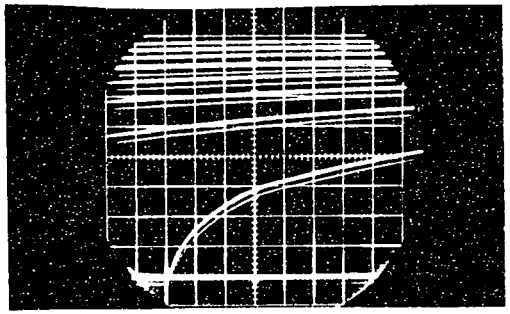

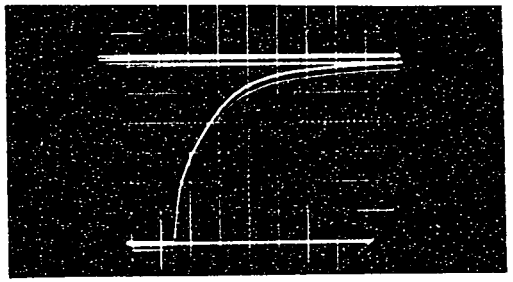

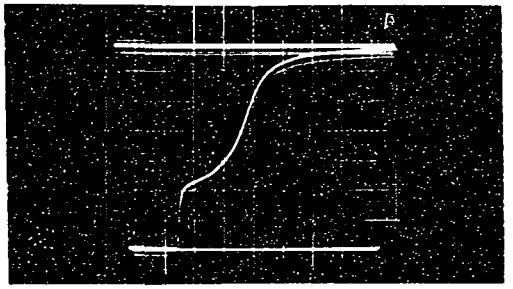

Pd

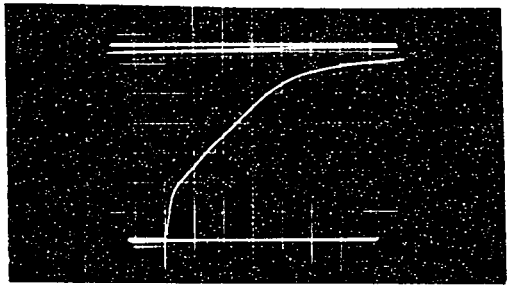

4

1

2

3

Au

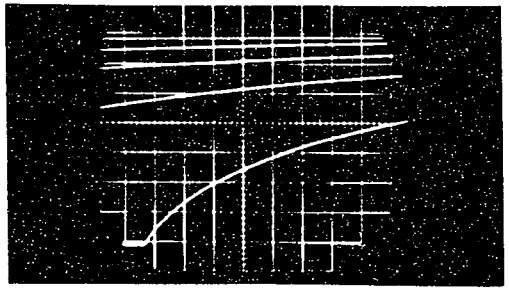

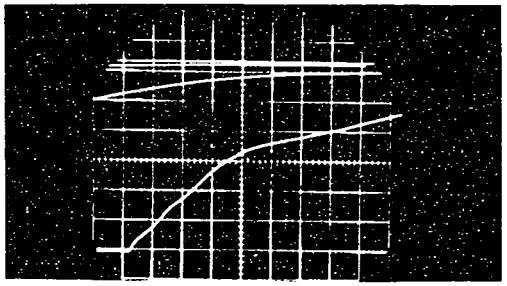

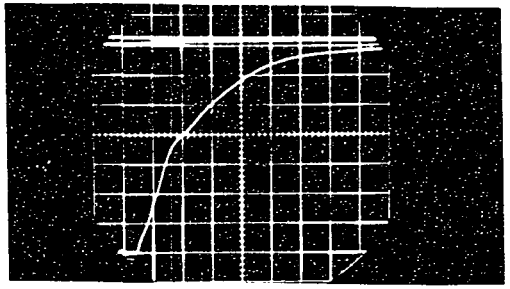

Au

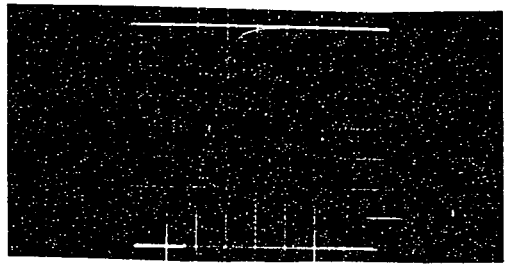

4

Figure XLVIII

Cathodic reverse pulse discharge curves for gold electrodes at various current densities in 1M HCOOK/ 100% HCOOH (5°C), starting at the potentials indicated

a) Au

1.	7.1×10^{-6} a.cm.$^{-2}$	560 mv.	0.2 v. cm.$^{-1}$	0.5 sec. cm.$^{-1}$
2.	2.7×10^{-5} a.cm.$^{-2}$	1355 mv.	0.2 v. cm.$^{-1}$	0.5 sec. cm.$^{-1}$
3.	6×10^{-3} a.cm.$^{-2}$	1420 mv.	0.2 v. cm.$^{-1}$	0.5 sec. cm.$^{-1}$
4.	3.1×10^{-4} a.cm.$^{-2}$	1460 mv.	0.2 v. cm.$^{-1}$	0.2 sec. cm.$^{-1}$

b) Pt

1.	2.4×10^{-5} a.cm.$^{-2}$	1110 mv.	0.2 v. cm.$^{-1}$	0.2 sec. cm.$^{-1}$
2.	2.7×10^{-4} a.cm.$^{-2}$	1165 mv.	0.2 v. cm.$^{-1}$	0.2 sec. cm.$^{-1}$
3.	7.8×10^{-4} a.cm.$^{-2}$	1360 mv.	0.2 v. cm.$^{-1}$	50 msec. cm.$^{-1}$
4.	1.8×10^{-3} a.cm.$^{-2}$	1410 mv.	0.2 v. cm.$^{-1}$	50 msec. cm.$^{-1}$
5.	4.5×10^{-3} a.cm.$^{-2}$	1480 mv.	0.2 v. cm.$^{-1}$	50 msec. cm.$^{-1}$

Au

1

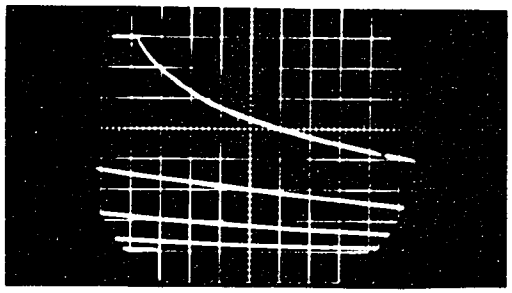

2

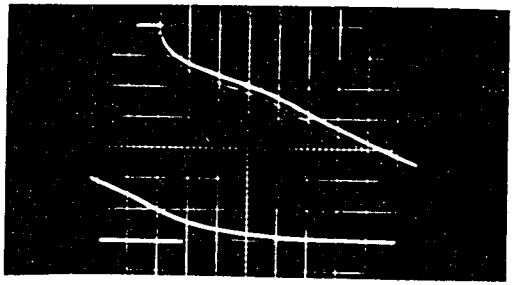

3

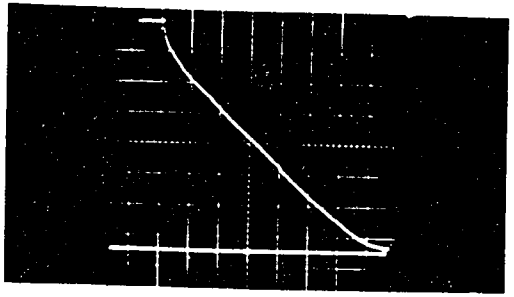

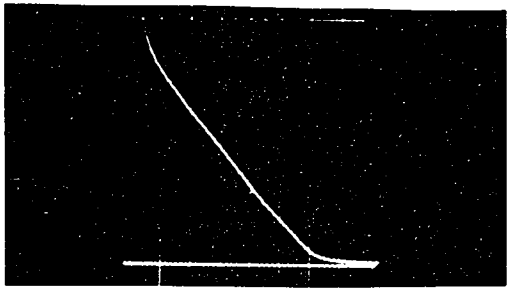

4

Pt

1

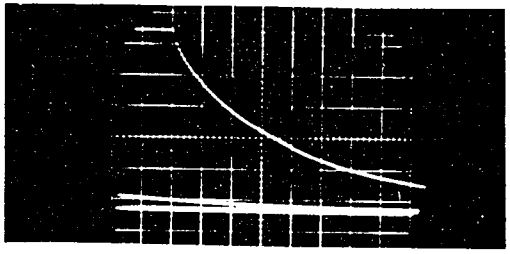

2

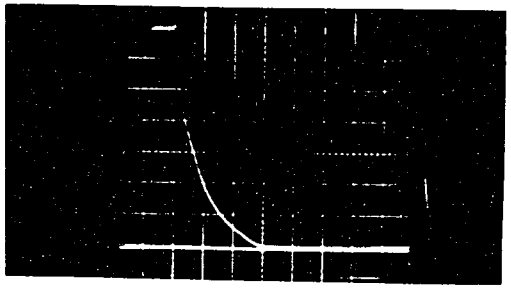

3

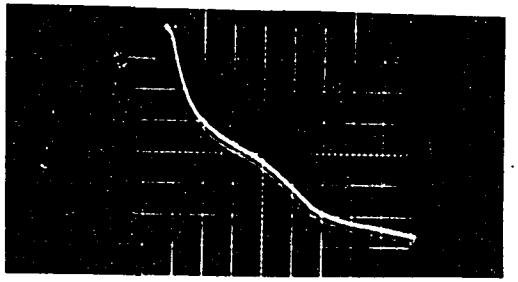

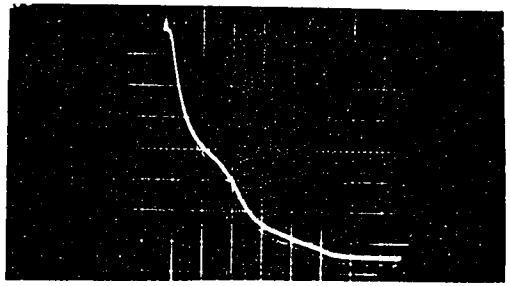

4

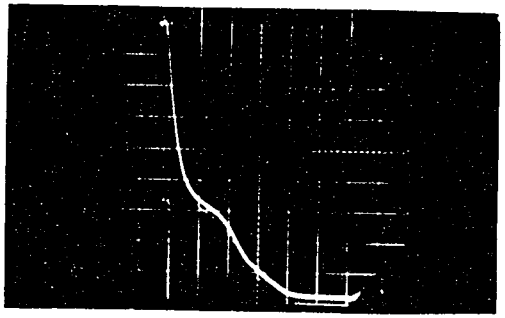

5

Figure XLIX

Cathodic discharge transients as a function of time of previous anodic polarisation, starting at the potentials indicated

Pd 1M HCOOK/HCOOH 5°C

1.	5.9×10^{-3} a.cm.$^{-2}$	3.9 sec.	1115 mv.	50 msec.cm.$^{-1}$	0.2 v.cm.$^{-1}$
2.	5.9×10^{-3} a.cm.$^{-2}$	20.6 sec.	1295 mv.	50 msec.cm.$^{-1}$	0.2 v.cm.$^{-1}$
3.	5.9×10^{-3} a.cm.$^{-2}$	65.6 sec.	1395 mv.	50 msec.cm.$^{-1}$	0.2 v.cm.$^{-1}$
4.	5.9×10^{-3} a.cm.$^{-2}$	118 sec.	1400 mv.	50 msec.cm.$^{-1}$	0.2 v.cm.$^{-1}$
5.	5.9×10^{-3} a.cm.$^{-2}$	505 sec.	1415 mv.	0.1 sec.cm.$^{-1}$	0.2 v.cm.$^{-1}$
6.	5.9×10^{-3} a.cm.$^{-2}$	1050 sec.	1560 mv.	0.2 sec.cm.$^{-1}$	0.2 v.cm.$^{-1}$

[Note change in time scale in (4), (5) and (6)].

Au 1M HCOOK/HCOOH 5°C

1.*	6.65×10^{-5} a.cm.$^{-2}$	29.2 sec.	1410 mv.	0.5 sec.cm.$^{-1}$	0.2 v.cm.$^{-1}$
2.*	6.65×10^{-5} a.cm.$^{-2}$	66.5 sec.	1410 mv.	0.5 sec.cm.$^{-1}$	0.2 v.cm.$^{-1}$
3.	1.1×10^{-3} a.cm.$^{-2}$	212 sec.	1480 mv.	20 msec.cm.$^{-1}$	0.2 v.cm.$^{-1}$
4.	1.1×10^{-3} a.cm.$^{-2}$	310 sec.	1480 mv.	50 msec.cm.$^{-1}$	0.2 v.cm.$^{-1}$

[*Note almost constant capacity of 160 μF cm.$^{-1}$ ca. 1.0 v.]

Pt 1M HCOOK/HCOOH 5°C

1.	1.1×10^{-3} a.cm.$^{-2}$	15.9 sec.	1420 mv.	50 msec.cm.$^{-1}$	0.2 v.cm.$^{-1}$
2.	1.1×10^{-3} a.cm.$^{-2}$	105 sec.	1430 mv.	50 msec.cm.$^{-1}$	0.2 v.cm.$^{-1}$
3.	1.1×10^{-3} a.cm.$^{-2}$	310 sec.	1410 mv.	50 msec.cm.$^{-1}$	0.2 v.cm.$^{-1}$

Au

1

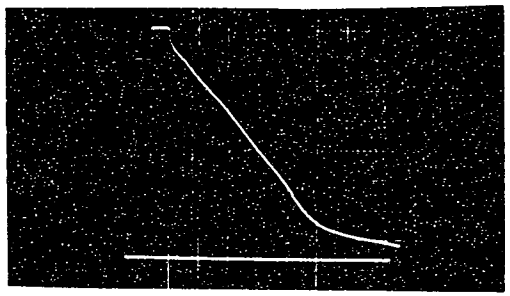

2

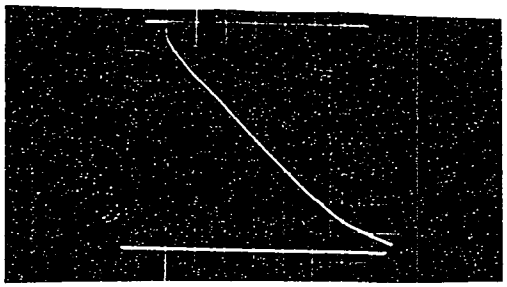

Au

3

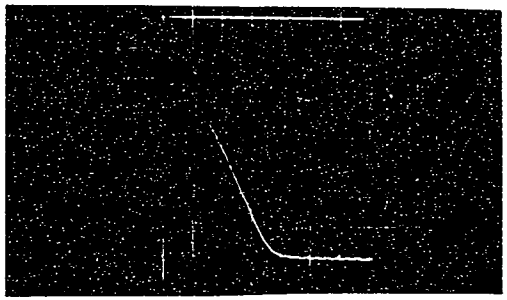

4

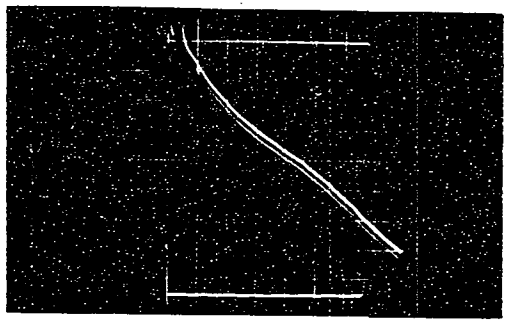

Pt

1

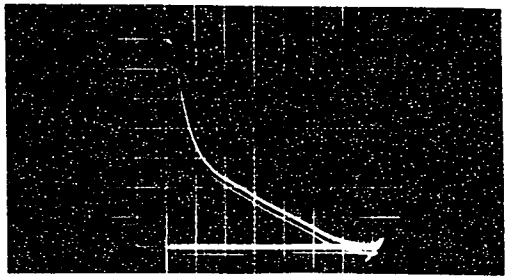

2

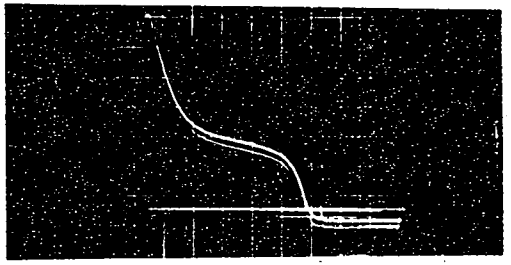

3

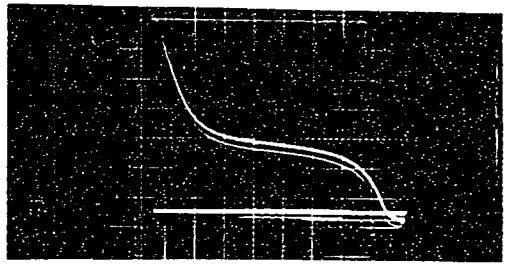

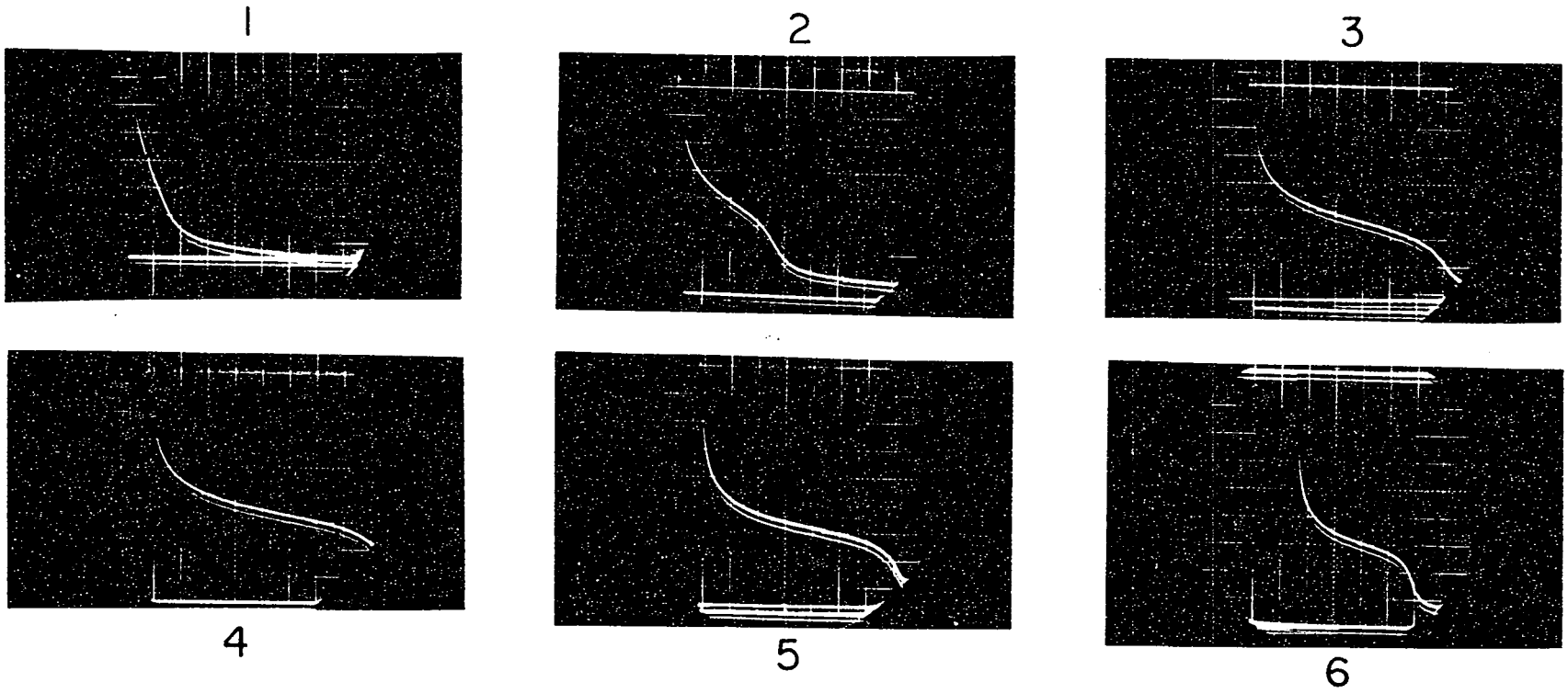
1
2
3
Pd
Pd
4
5
6

charging and forced discharge transients (and also implicit in the open-circuit decay curves) at appreciable current densities at Pd (123,131). The charging arrest cannot be a diffusion controlled transient since (i) the arrest is seen both on the reverse transient and on open-circuit decay; and (ii) at the current densities used, the transition time for $HCOO^-$ oxidation can be calculated from a form of the familiar Sand relation (146)

$$C_e - C_o = 1.129 \frac{i}{ZF} \sqrt{\frac{t}{D}} \qquad [77]$$

where C_o is the concentration in the bulk of the solution (in moles $cm.^{-3}$), C_e the concentration at the surface of the electrode and D the diffusion coefficient of the electrochemically active species.

Assuming a value for the diffusion coefficient of 5×10^{-6} cm^2 sec^{-1}, the bulk concentration C_o as 1M (10^{-3} mole cm^{-3}), and $i = 10^{-3}$ amp.cm^{-2} (the current corresponding to the limiting current in the present case) the transition time ($t = \tau$), at which C_e becomes equal to zero and $i = i_{lim}$ is hence

$$\tau = \frac{(5 \times 10^{-6})(96,500)^2(10^{-3})}{(1.129)^2 (10^{-3})^2}$$

$$= 3.9 \times 10^4 \text{ seconds.}$$

The transition times for diffusion controlled $HCOO^-$ oxidation are thus some 10^3 - 10^4 times larger than that

observed experimentally (1-5 seconds), hence the limiting current is not diffusion controlled.

The magnitude of the arrests at platinum and gold correspond to an initial coverage of about one monolayer by some more or less reversibly removable adsorbed species, presumably produced in the discharge step. The calculation is based on the assumed area of the $HCOO^{\bullet}$ radical of 14.2 A^{o2} (from Courtauld models) as mentioned above. It is reasonable to assume that the adsorbed species associated with the arrest in the transient is the chemisorbed $HCOO^{\bullet}$ radical discussed above; it is unlikely to be $H^{\bullet}$ since any adsorbed $H^{\bullet}$ would tend to be removed at a very high rate (ca. $10^{10}\ \theta_H$ amp.cm.$^{-2}$) at the high anodic potentials (ca. 1-1.5 v) encountered so that its steady state coverage in the anodic reaction could, as we have argued previously, hardly be significant and certainly not experimentally measureable in a slow transient such as that observed here. The charging results therefore indicate an appreciable coverage, presumably by $HCOO^{\bullet}$ radicals; it may hence be concluded that, at least for the upper potential region [Figs. X-XV], discharge from or to which gives the arrest in the transients, a radical desorption step is the rate-determining process, i.e. either process III (scheme A) or V (scheme B) is involved.

Reaction III gives a Tafel slope $dV/d \ln i_3 = RT/F$

under "Langmuir" conditions with $\theta_{HCOO^{\bullet}}$ potential dependent; under "Temkin" conditions, III gives a limiting current or a slope 2RT/F $(\frac{r_1}{r_1-r_2})$ on the induction or heterogeneity models, respectively. Reaction V gives a slope 2RT/F for full coverage by $HCOO^{\bullet}$, while for potential-dependent coverage conditions a slope of 2RT/3F for "Langmuir" adsorption is predicted. A slope of RT/F is indicated by both models when "Temkin" conditions apply. The slope 2RT/3F (see Table IV) is <u>not</u> observed experimentally under any of the conditions examined, but slopes of approximately RT/F and 2RT/F are found for Au and the Pd-Au alloys (in the upper potential region) while slopes of about 2RT/F are found for Pt and Pd. At gold, the change of slope from a low to a higher value (RT/F $\longrightarrow$ 2RT/F) with increasing current density is explicable formally in terms either of a transition from one rate-determining step to another in a consecutive reaction sequence, or in terms of a transition from "Langmuir" to "Temkin" conditions (e.g. for reaction III or V); the corresponding change for reaction V is from 2RT/3F (Langmuir) to RT/F (Temkin) to 2RT/F (Langmuir, full coverage). The first transition (2RT/3F $\longrightarrow$ 2RT/F) is not observed. We believe the latter type of transition in slope (viz. RT/F to 2RT/F) may be applicable in the present case, since a second <u>consecutive</u> step (e.g. IV) is not plausible in this scheme. Alternatively III (Langmuir) followed by V

(at full coverage) - which is in reality a related path involving the same initial state - is also consistent with the results for gold and some of the alloys. It is important to note that only in the case of gold does the fractional coverage not attain unity (see p.188 and Fig. LIII) at the top of the transition region. The Temkin slope of RT/F can therefore continue above the transition region until at some higher current density, full coverage is attained and the Langmuir slope of 2RT/F applies, as observed. In the case of the alloys, no significant trend of i_o values with electron d-band configuration is observed. This is probably due to the fact that anode films are involved and the kinetics are determined by the properties of these films rather than the underlying metals. Similar conclusions were reached in the case of the oxygen evolution reaction at Pd-Au alloys (87).

For Pt or Pd, the results are consistent with III (Temkin with $r_1 \gg r_2$) or V (full coverage) over the whole current density range in the upper region. We have outlined plausible reaction mechanisms here consistent with the experimental behavior. Further conclusions will be drawn following a quantitative discussion of the behavior of the probable intermediates as deduced from a study of the e.m.f. decay behavior.

(e) Significance of the Transition Region in the Current-Potential Curves

The sharp transitions from a lower to an upper region in the current-potential curves (cf. Fig. X-XV) observed in the present system suggested that a phenomenon similar to passivation with anodic film formation (as observed in oxygen evolution (87)) was occurring in the decarboxylation reaction. In the present work in non-aqueous formic acid, no oxygen evolution or oxide film formation is possible and we must presume that the passivation behavior is associated with formation of a film of "formate" or formate radicals on the electrode surface. This is supported by observations of: (i) periodic fluctuations of potential (see Fig. XXXVIII) at constant current density near the critical current for transition in the current-potential plot. Such periodic phenomena are characteristic of changes of an anode surface from an active to a passive, back to an active state, etc., and are well known in the anodic oxidation of metals (73,74,75) and (ii) "overshoot"and "undershoot" transients in the potential as the current is suddenly increased or decreased, respectively, when near the critical current.

Typical curves obtained galvanostatically for anodic charging and reverse cathodic discharge after polarisation are shown in Figures XLVII-XLIX, which are photographic copies

of actual oscilloscope photographs. For the three metals, platinum, palladium and gold studied in the present work, there is clear evidence of an arrest in the charging and discharging transients corresponding to the charge associated with a film of adsorbed intermediates produced in the anodic reaction. The arrests appear only after moderate and high anodic polarisation and confirm that the transition behavior in the current-potential plot is associated with a critical condition for formation of an anodic product (i.e. an anodic passive film) on the electrode surface, which can be removed either by a self-discharge process (33,119) on open-circuit or by a reverse cathodic pulse, as with adsorbed H or O (138,139). The transition behavior, which shows all the characteristics of a "passivation" phenomenon, may thus be directly ascribed to formation of a monolayer of adsorbed reaction intermediates. Quantitative proof of monolayer formation under certain conditions is indicated by the results to be discussed below.

Following our initial observations reported in a preliminary paper (123,131), we believe that the above results from discharging and charging experiments constitute the first direct proof of the role of an extensive layer of adsorbed intermediates in electrochemical decarboxylation reactions. Similar adsorbed intermediates are formed in the case of the Kolbe reaction itself (with CF_3COO^-) and will be discussed later.

(f) The Charge and Pseudo-Capacity Associated with Adsorbed Intermediates Calculated from Open-circuit Decay Transients

The determination of electrode capacitance from the initial rate of decay of potential, V (free of ohmic and/or concentration polarisation effects) on open-circuit following polarisation at a current density i_i is well known (93,132) and is based on the assumption that the electrode reaction continues on open-circuit by a self-discharge process, which at the moment of current interruption has the same rate as that corresponding to the initial polarising current density, i.e.

$$-C \left(\frac{dV}{dt}\right)_{i_i} = i_i \qquad [78]$$

so that the initial total capacitance (i.e. the adsorption pseudo-capacitance plus the ionic double-layer capacitance) can be calculated. The capacitance as a function of potential, V, could then, in principle, be obtained (133) by using various initial polarising current densities (119) corresponding to various initial overpotentials.

The kinetics of e.m.f. decay are normally expressed (93,119,133) by an equation of the form

$$i = -C_V \frac{dV}{dt} = i_o \exp V/b. \qquad [79]$$

at any potential, where b is the Naperian Tafel slope, and $i_o \exp [V/b]$ is, in fact, the self-discharge current passing

at the overpotential V.

We propose that this treatment can be extended over the whole of the e.m.f. decay curve provided that the current-potential relationship is known over the same range of potentials. We need not assume that the mechanism of the reaction remains the same throughout the e.m.f. decay (it may or may not). However, it is necessary to assume as usual (93,119,133) that on open-circuit whatever process is rate-determining in steady-state polarisation at any potential V, is also rate-determining in the self-discharge process at the same potential.

From equation [79], it is clear that the capacity at any potential during open-circuit decay of potential is given by

$$C_V = - \frac{i_o \exp[V/b]}{dV/dt} \qquad [80]$$

The charge q associated with the electrode surface and corresponding to the capacity, C_V, is given by

$$dq = C_V dV \qquad [81]$$

If C_V is principally an adsorption pseudo-capacitance (see below), the charge Δq associated with a change of coverage θ by the intermediates between two potentials V_1 and V_2 can be obtained by substituting for C_V from equation [80] in equation [81] and integrating over the potential range

$$\Delta q = - \int_{V_1}^{V_2} \frac{i_o \exp[V/b]dV}{dV/dt} \qquad [82]$$

where we keep the term dV/dt in the denominator for convenience in order to evaluate $i_o \exp[V/b]dV/dt$ experimentally and integrate the equation graphically over a range of values of potential. The value of Δq obtained obviously corresponds to the change of charge associated with a change of coverage by the intermediates as the potential is changed from V_1 to V_2. If C_V corresponds to a pseudo-capacity associated with the adsorption of reaction intermediates (102,109,125), it will usually be large (109,119) compared with the ionic double-layer capacity when the coverage θ by intermediates is $0.2 < \theta < 0.8$. Hence integration in equation [82] over the potential region of appreciable values of C_V will give, to a close approximation, the actual value of q (as a function of potential) associated with the adsorbed intermediates and hence θ the extent of coverage, if we assume that one electron is required for Faradaic discharge to produce each adsorbed HCOO• group and also assume an effective molecular area (14.2 Å^2 as above) for the adsorbed species, as discussed previously (pp. 178).

The above treatment has been applied quantitatively to the evaluation of the pseudo-capacity and coverage associated with the adsorbed species in the formate decarboxylation, particularly near the critical current or transition region where we suspect that formation of a passivating layer is occurring. Values of dV/dt have been obtained from decay curves (see Fig. XXXIV-XXXVII) using the prism and set-square method

accurate to ± 1%, and values of $i_o \exp [V/b]$ from the experimental current-potential relationships (see Figs. X-XII). The potentials in the transition region, at a given current density, are not well defined owing to their variation with time (here potentiostatic current-potential studies might be more satisfactory). In this transition region, however, the current density is approximately constant (and any uncertainty in its variation over about 0.5-1.0 v. in this region is quite small), so that the capacity is principally determined by dV/dt which varies very much more over this range of potential in the transition region, and can be evaluated precisely from the decay curves. At the top and bottom of the transition region, where the current varies more with potential than in the transition region itself, the current-potential relation is defined experimentally with normal precision, so that the capacities can be evaluated again with satisfactory accuracy.

The capacity curves evaluated using equation [82] over the transition region are shown in Figures L-LII as a function of the overpotential for the overall reaction Ia and the integral charges associated with this region are shown in Figure LIII for platinum, palladium and gold.

(g) Interpretation of the $HCOO^*$ Adsorption Pseudo-Capacitance Behavior

The significance of adsorption pseudo-capacitance has been discussed elsewhere (119,141) in relation to the extent

Figure L

Capacity curves for the formate decarboxylation in the transition region as a function of overpotential (1M HCOOK/100%:HCOOH; 5°C. From open-circuit decay and Tafel line parameters).

Platinum - high current density ($i = 1.2 \times 10^{-2}$ amp.cm^{-2}).

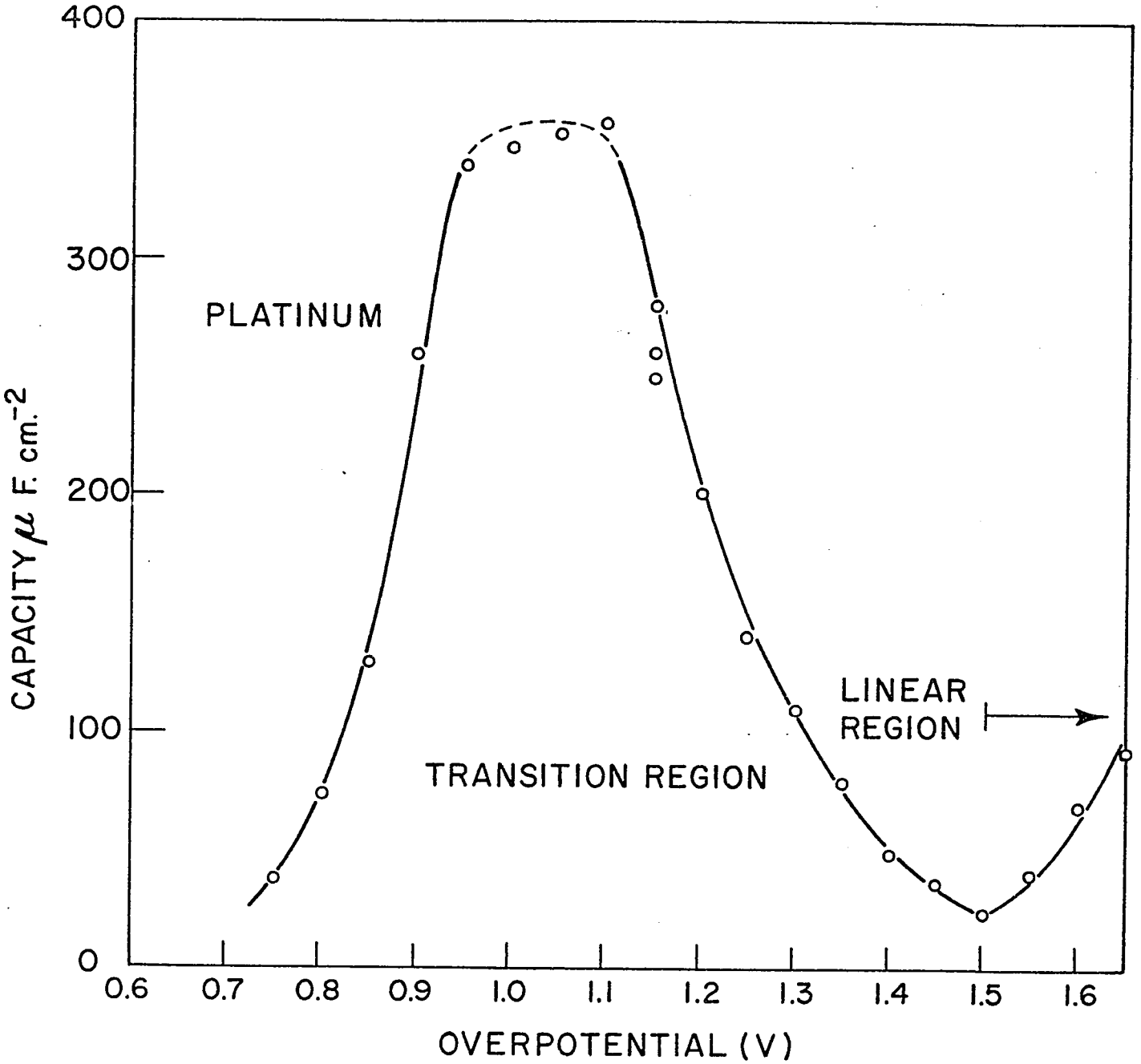
400
300
200
100
0
CAPACITY μ F. cm.-2
PLATINUM
TRANSITION REGION
LINEAR
REGION
0.6
0.7
0.8
0.9
1.0
1.1
1.2
1.3
1.4
1.5
1.6
OVERPOTENTIAL (V)

Figure LI

Capacity curves for the formate decarboxylation in the transition region as a function of overpotential (1M HCOOK/100% HCOOH; 5°C. From open-circuit decay and Tafel line parameters).

Palladium (a) low current density ($i = 1.5 \times 10^{-5}$ amp.cm^{-2})

(b) high current density ($i = 9 \times 10^{-3}$ amp.cm^{-2}).

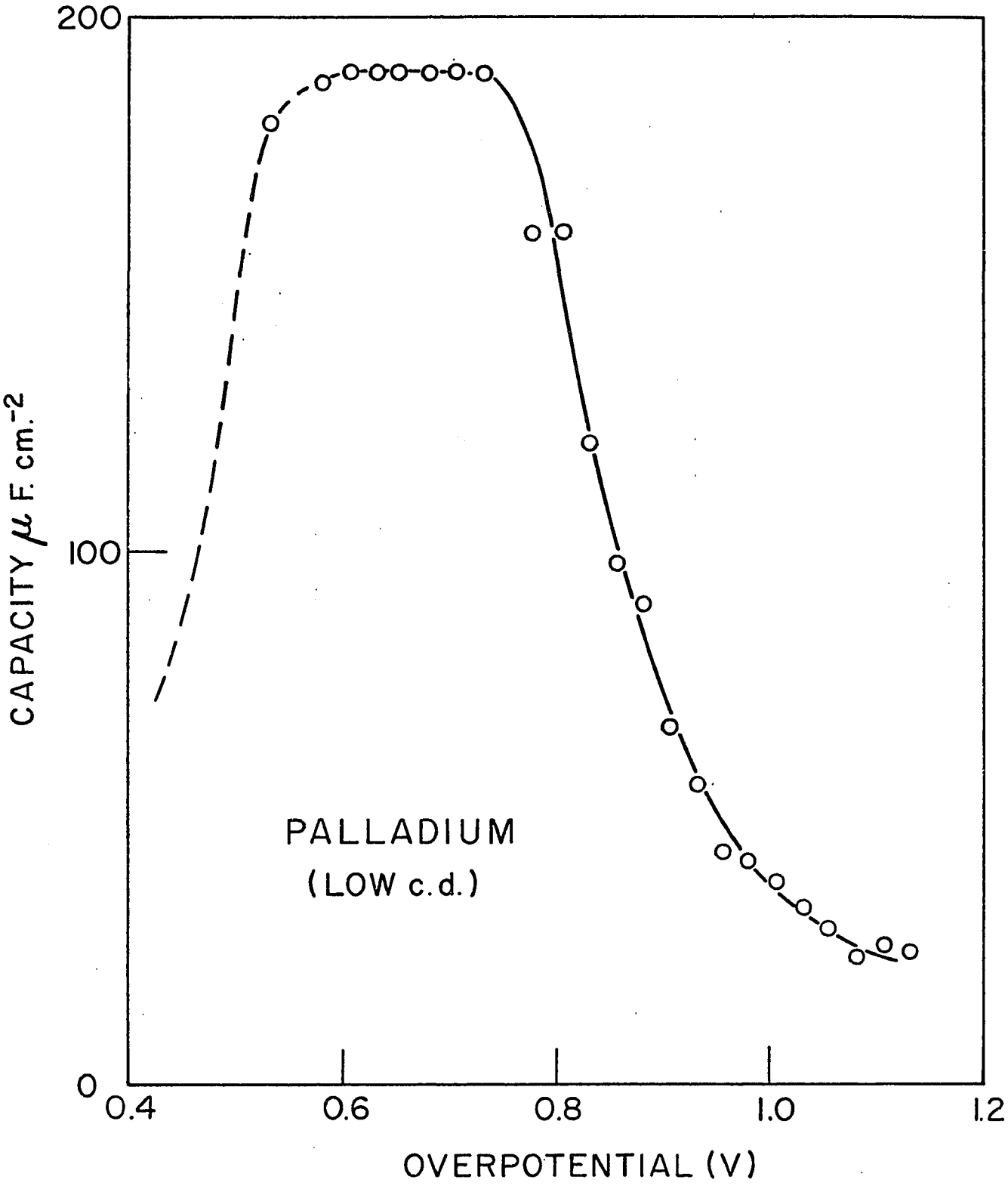
200
100
0
CAPACITY μ F. cm.-2
PALLADIUM
(LOW c.d.)
0.4
0.6
0.8
1.0
1.2
OVERPOTENTIAL (V)

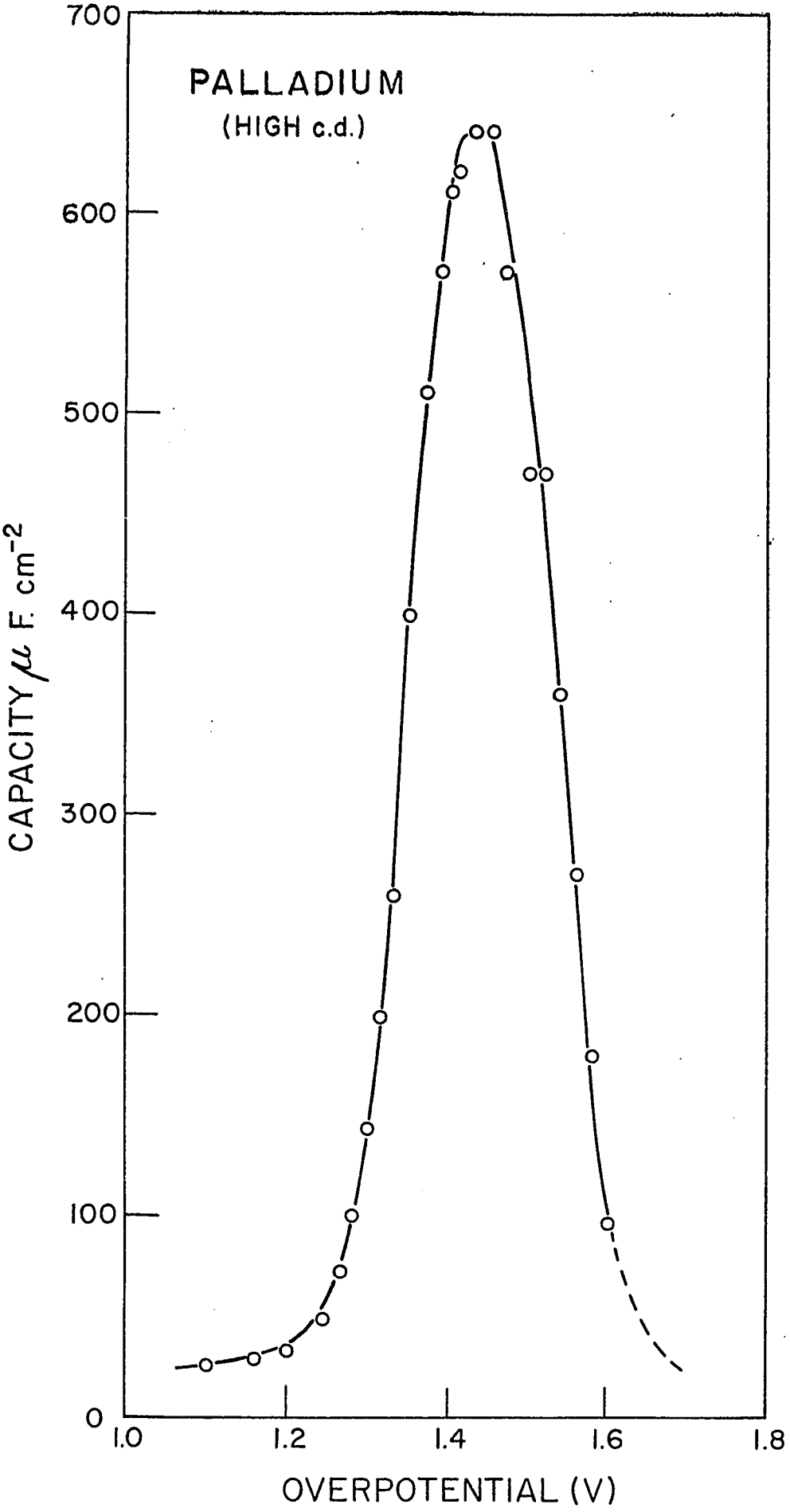
PALLADIUM
(HIGH c.d.)
700
600
500
400
300
200
100
0
CAPACITY μ F. cm⁻²
1.0
1.2
1.4
1.6
1.8
OVERPOTENTIAL (V)

Figure LII

Capacity curves for the formate decarboxylation in the transition region as a function of overpotential (1M HCOOK/100% HCOOH; 5°C. From open-circuit decay and Tafel line parameters).

Gold (a) low current density ($i = 9 \times 10^{-4}$ amp.cm^{-2})

(b) high current density ($i = 3.1 \times 10^{-3}$ amp.cm^{-2}).

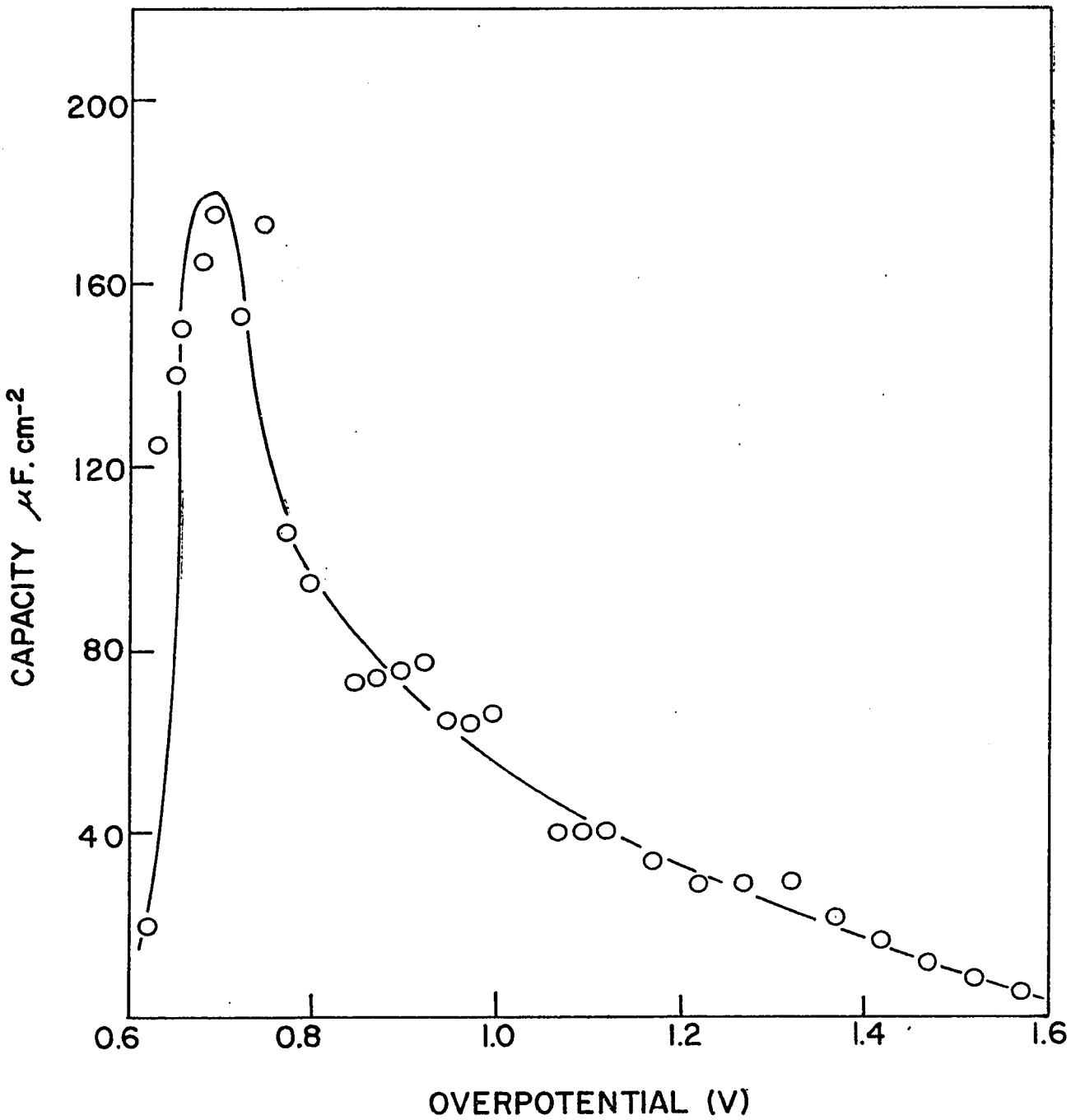
200
160
120
80
40
CAPACITY μF. cm-2
0.6
0.8
1.0
1.2
1.4
1.6
OVERPOTENTIAL (V)

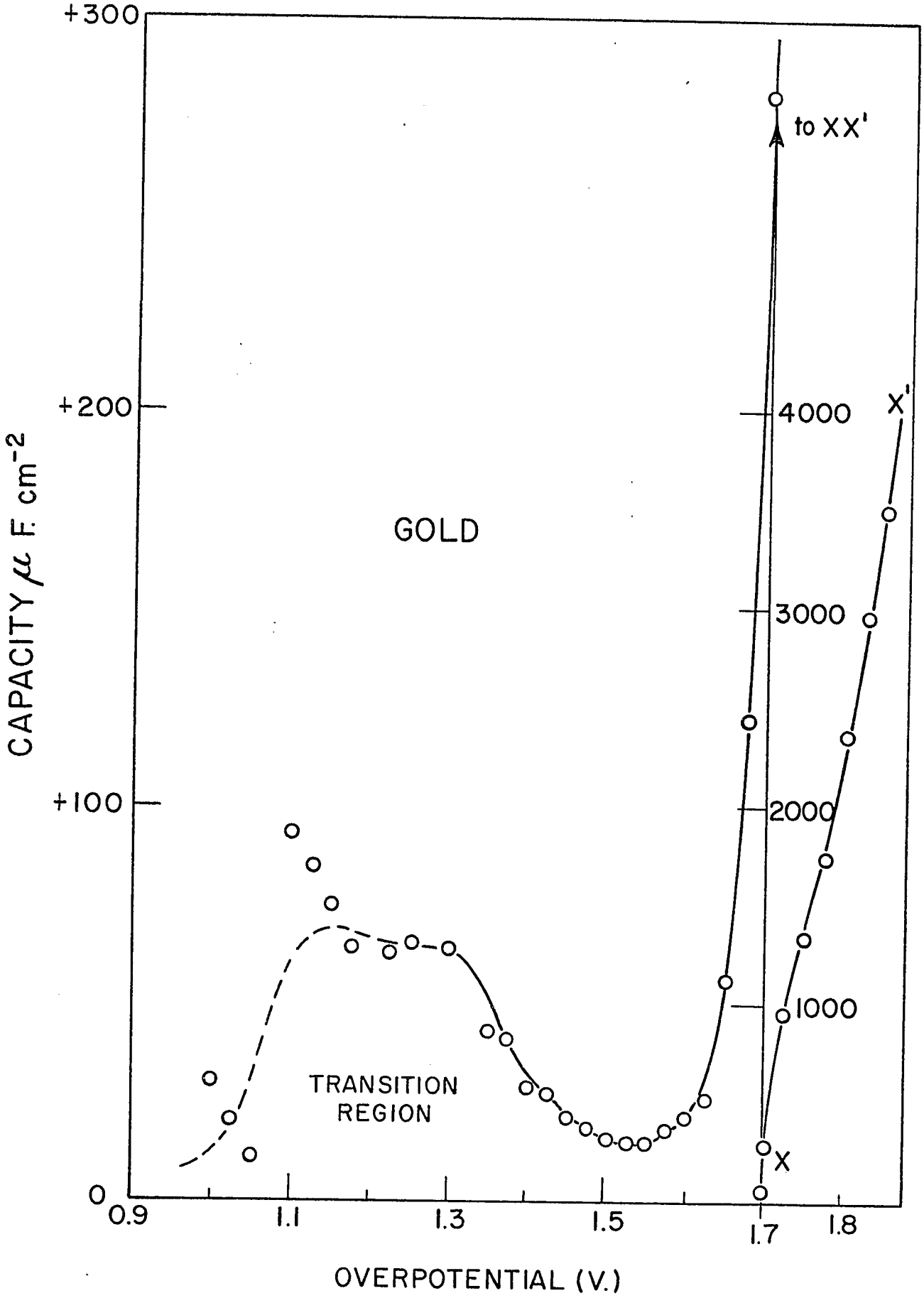
+300
+200
+100
0
CAPACITY μ F. cm⁻²
GOLD
TRANSITION
REGION
to XX'
X'
X
4000
3000
2000
1000
0.9
1.1
1.3
1.5
1.7
1.8
OVERPOTENTIAL (V.)

Figure LIII

Integral charges associated with the adsorbed species, deduced from Figs. L-LII. ($\theta_{HCOO^{\bullet}} = 1$ corresponds to 113 μc. $cm.^{-2}$ for a real to apparent area factor of unity).

(A) - Palladium ($i = 9 \times 10^{-3}$ amp.cm^{-2})

(B) - Platinum ($i = 4.5 \times 10^{-3}$ amp.cm^{-2})

(C) - Gold. ($i = 9 \times 10^{-4}$ amp.cm^{-2}).

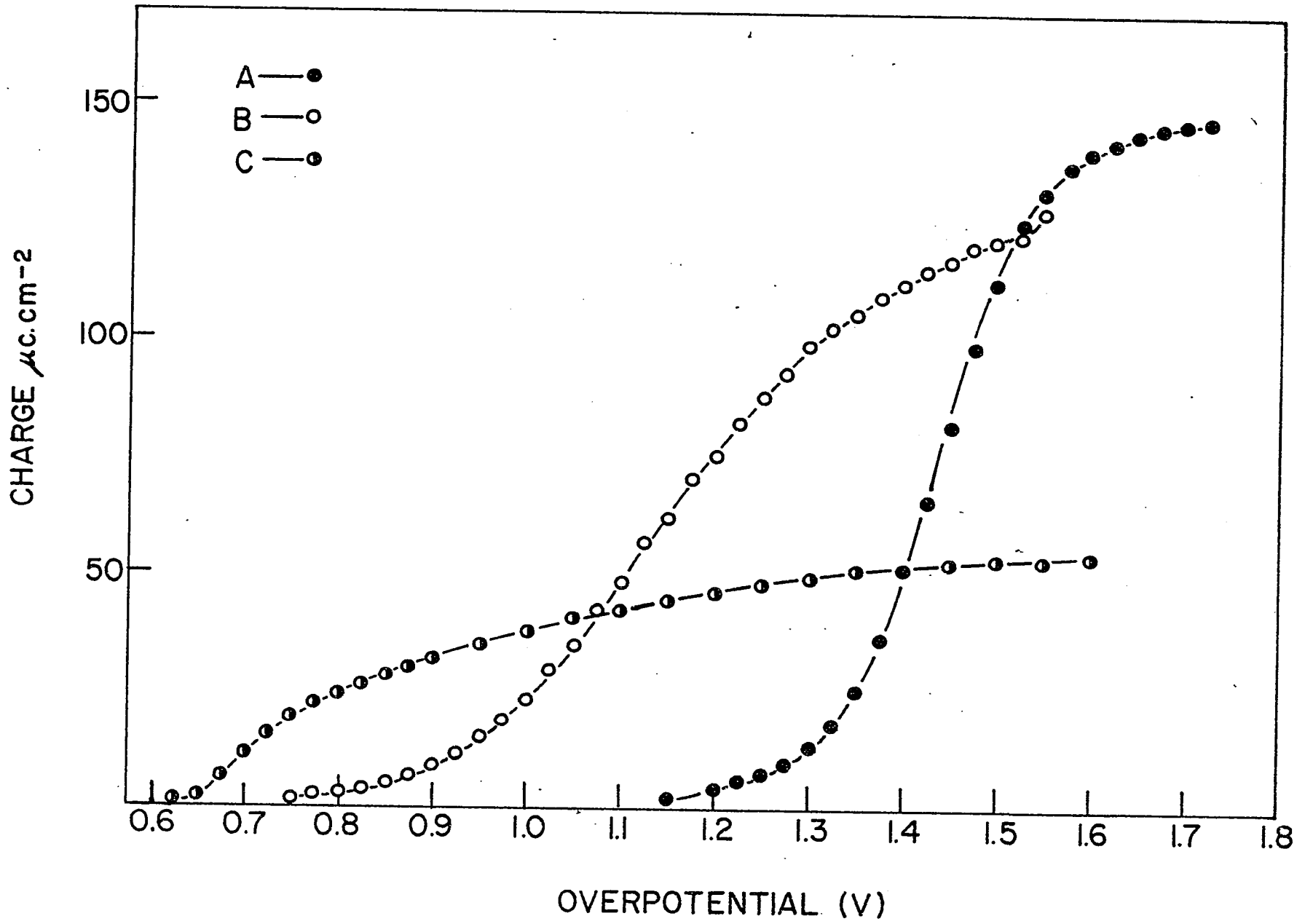
A
B
C
150
100
50
CHARGE μc.cm⁻²
0.6
0.7
0.8
0.9
1.0
1.1
1.2
1.3
1.4
1.5
1.6
1.7
1.8
OVERPOTENTIAL (V)

of surface coverage by intermediates, and to the type of adsorption isotherm applying to the adsorption of the electrochemically active intermediate. The consequences of coverage-dependent activation energies discussed in the section on reaction mechanisms, have been also considered (102) in relation to the pseudo-capacitance associated with adsorbed intermediates, in particular with regard to the extent of potential dependence of the pseudo-capacitance.

We examine the case for conditions where appreciable values of the pseudo-capacitance are due only to one species, viz., $HCOO^{\bullet}$, i.e. when reaction III is the slow step and II is hence/in quasi-equilibrium. The surface is then covered only by $HCOO^{\bullet}$ species and $f(\theta)$ in equation [50] becomes simply $r_F\theta_F$. If reaction II is in quasi-equilibrium,

$$k_2 (1-\theta_F)\, a_{F^-} \exp.-[\Delta G_2^{\neq} - \beta VF + \alpha r_F\theta_F]/RT = k_{-2}\, \theta_F \exp. - [\Delta G_{-2}^{\neq} - (1-\alpha)\, r_F\theta_F + (1-\beta)VF/RT \qquad [83]$$

so that by taking logarithims and solving for the potential V we obtain

$$V = \frac{RT}{F} \ln \left(\frac{\theta_F}{1-\theta_F}\right) + r_F\theta_F/F + K_2' \qquad [84]$$

where K_2' is a constant at constant composition and temperature. The pseudo-capacity associated with adsorbed $HCOO^{\bullet}$ formation is then given by

$$\frac{k'}{C} = \frac{dV}{d\theta} \equiv \frac{RT}{F} \frac{d}{d\theta} (\ln \theta_F/1-\theta_F) + \frac{r_F}{F} \qquad [85]$$

This equation, as has been shown previously* (102), involves a "Langmuir" term in $\theta_F/1-\theta_F$ and a "Temkin" term in r_F arising, respectively, from the pre-exponential and the exponential terms in θ_F in the rate equations for the forward and backward directions of reaction II, at equilibrium. Equation [85] can hence be written, as shown by Conway and Gileadi (102),

$$\frac{1}{C} = \frac{1}{C_T} + \frac{1}{C_L} \qquad [86]$$

or

$$C = \frac{C_T C_L}{C_T + C_L} \qquad [87]$$

from which it is seen that the two pseudo-capacity contributions combine in "series"** to determine the overall adsorption pseudo-capacitance.

The potential dependence of C for various values of r has been evaluated in the general case (102) by calculating C as a function of θ and θ as a function of V using equations

---

* A discussion and full deduction of this and preceding equations which lead to the pseudo-capacity will shortly be presented in a thesis by Gileadi and will be published in a paper at present in press (Transactions of the Faraday Society).

** The overall pseudo-capacitance itself is, of course, combined in parallel with the ionic double-layer capacity. Under conditions when the adsorption pseudo-capacity is of kinetic significance, the ionic double layer capacity is normally regarded as relatively insignificant, except at high values of r when $C \rightarrow C_T$.

similar to equations [84] and [85].

The capacity curve for C as a function of over-potential at palladium has almost the correct shape (102,109) for the case of Langmuir adsorption (r = 0) of the intermediates. Its maximum value is however too low (particularly bearing in mind that the real/apparent area factor for the metal surface must be rather greater than one) since for the adsorption of formate radicals, the maximum theoretically expected "Langmuir" value (from equation [85]) is $k'F/4RT$, where k' is the charge associated with the formation of a monolayer of adsorbed intermediates ($\theta_{HCOO\bullet} = 1$),. In the present case for a molecular area of 14.2 $\mathring{A}^2$ for HCOO• (from space-filling Courtauld models) $k' = 113\ \mu c.cm^{-2}$ so that the theoretical value for $C_{MAX.}$ is hence 1100 $\mu F.cm.^{-2}$ for the present reaction. The actual observed capacity behavior as a function of over-potential fits the general equation (equation [85]) deduced previously (102) taking into account the finite variation of heat of adsorption of HCOO• with coverage (127,135) through the term r which will be evaluated below.

At palladium, two transition regions are observed in the current-potential plot (Figure XI) for 1M and 5M potassium formate in anhydrous formic acid. Correspondingly, two pseudo-capacity regions arise as shown in Figures LI, LII.

The lower region pseudo-capacity exhibits a wider range of potential dependence than the upper one which approaches ideal Langmuir (cf. Figure LI) behavior the most closely in the present series of results.

The corresponding data for platinum and gold, and for the lower current densities at palladium, indicate that the pseudo-capacitance is less potential dependent and has lower values. This is as expected theoretically (102) since the more the pseudo-capacity originates from a Temkin term involving a linear dependence of coverage upon potential (corresponding to a constant pseudo-capacity) the lower will be its maximum value and the wider its range of potential dependence.

(h) Surface Charge and Coverage by Intermediates

The integral surface charges associated with adsorbed intermediates over the transition region may be calculated by applying equation [82] and the apparent coverages estimated by assuming a molecular area of 14.2 $\mathring{A}^2$ (p. 178) for the $HCOO^{\bullet}$ radical. The integral charges calculated for the transition region from the experimental current-voltage and e.m.f. decay curves are shown in Figure LIII for platinum, palladium and gold as a function of overpotential.

The results indicate that the potential-dependence of coverage depends on the metal, i.e. different r values are involved.

From the observed capacity curve (Figures L-LII)

and the charge as a function of potential, a value of r_1 may be obtained by comparison of the experimental maximum capacities with that calculated for the case of ideal Langmuir pseudo-capacity. Alternatively r can be evaluated from equation [85] if the real to apparent surface area can be determined.

At palladium a value of $r_1 = 3$ Kcal.mole^{-1} is obtained. The data for platinum indicate a larger value of r_1 (viz. 7 Kcal/mole) since C and q (or θ) are potential dependent over a wider range of potentials than for the case of Pd or for the ideal Langmuir case. Since, in both of these cases, the θ values vary from around 0.1 to unity, but different r_1 values are found for the same reaction, (and hence presumably for the same intermediates) we conclude that r_1 may be predominantly determined by heterogeneity of energies of adsorption at various sites rather than by two-dimensional interaction effects within the adsorbed layer. It is recognised, however, that different orientations of the adsorbed species at Pt and Pd could also lead to different two dimensional interactions and hence to different r_1 values. The linear variation of heat of adsorption with coverage assumed in this treatment and elsewhere (127,135) is, as we have discussed above, actually best accounted for in terms of the model discussed by Boudart (128) and based on induced heterogeneity effects through the surface potential arising from the adsorbed layer and its effect

on the electronic work function of the metal.

(i) Coverage Effects and Conclusions on Mechanism of the Reaction in Pure Formic Acid

The above discussion gives rather direct quantitative evidence regarding the behavior of the adsorbed intermediates, which we must presume to be HCOO• radicals. It is clear that the transition associated with the sharp change of potential, must be ascribed to filling up of the surface by the adsorbed HCOO• species. This suggests that the primary discharge of formate ions is not the rate-controlling step, as we have deduced previously. Beyond a certain critical current, decomposition of the radicals can no longer support the current and a limiting current is observed. This suggests that the rate-controlling reaction at low current densities is

$$HCOO^{\bullet} \longrightarrow H^{\bullet} + CO_2$$

which gives a limiting current corresponding to the "transition behavior", rather than

$$HCOO^{\bullet} \longrightarrow H^{+} + CO_2 + e$$

which is always potential dependent. Once the transition region is completed, further potential dependent reaction can continue by

$$HCOO^{\bullet}_{\theta \to 1} \longrightarrow H^{+} + CO_2 + e$$

at the higher current-densities with a Tafel slope of 2RT/F

(see p. 189) as observed experimentally. The transition behavior, which shows all the characteristics of a "passivation" phenomenon, (to be discussed further below in the light of other experimental observations) may thus be directly ascribed to formation of a monolayer of adsorbed reaction intermediates. The corresponding "active" region is that at low current-densities i.e. below the transition current-densities, where we have shown, in fact, (p. 94) that some attack of the electrode occurs and the coulombic yields of CO_2 are appreciably less than those expected for the quantitative occurrence of the formate decarboxylation.

Beyond the transition region at higher current densities, the pseudo-capacity again increases with increasing potential (or current-density) and time owing to formation of thicker films as discussed below and shown in Figures L, LII.

(j) The Phenomenon of Delayed Gas Evolution

During the course of electrochemical kinetic studies on the formate decarboxylation reaction, a remarkable phenomenon was observed. During the steady-state electrolysis of potassium formate in pure anhydrous formic acid at platinum, palladium and gold, the only gas evolved is carbon dioxide. On interrupting the current at platinum and gold electrodes, the gas evolution ceases rapidly in the normal way. However, on interrupting the current at a palladium electrode, the gas

evolution initially ceases, but is then followed by a further burst of gas from the surface after a delay period of up to 5 seconds, this gas evolution occurring in the complete absence of current flow. The effect is quite reproducible and is best observed at current densities greater than 10^{-2} amp.cm^{-2} in 5M solutions of potassium formate in formic acid at 5°C. Although carbon dioxide is evolved at platinum and gold with the same current efficiency as at palladium, the delayed gas evolution was not observed and the effect hence arises from some property of the palladium anode, all other conditions being identical. No hydrogen (the Kolbe analogue product) is evolved for reasons which have been discussed previously (p. 164), since it would ionise extremely rapidly at the high anodic potentials reached in the reaction. Hence it is improbable that hydrogen produced in the decarboxylation step and taken up into the surface regions of the palladium is responsible for the effect, and in fact the coulombic yields of carbon dioxide gas by continuous and repeatedly interrupted polarisation are identical within experimental error and no hydrogen is detectable by chemical or gas chromatographic methods of analysis under either set of conditions of polarisation. The gas evolved with delay on open-circuit is hence almost certainly CO_2.

The delay time in the gas evolution after the external current is interrupted is found to be a function of the

time of previous anodic electrolysis up to periods of about five minutes (Figure XXXVIII) This suggests that the anodic electrolysis forms a relatively thick film of a surface palladium formate* (possibly non-stoichiometric (119)) at the electrode, and, after net current ceases to flow, this film breaks down autocatalytically with evolution of carbon dioxide. The breakdown appears to occur at a more or less critical potential independent of the previous polarising current density as shown in Fig. (XLVI). This potential may hence be a quasi-thermodynamic potential for the normally unstable palladium formate species. The formation of this film appears to be analogous to that of passive films formed anodically, for example, in aqueous solutions at nickel and iron. Galvanostatic charging and open-circuit decay curves for the polarised palladium electrodes indicate , as we have discussed previously and below (p . 212), the formation of surface films as shown in Figures XLVII, XLIX. The pseudo-capacity associated with the film formed at palladium after appreciable times of anodic polarisation is much greater (ca. 10 times) than that at platinum or gold (Figures XXXIX-XLI) where no delayed gas evolution is observed, and this is consistent

* No stable palladium formate compounds appear to exist and this is consistent with the present observations that such a compound, if formed under anodic strongly oxidizing conditions, decomposes as soon as the potential has fallen to lower anodic values.

with the ten times smaller film thickness (or charge) observed at the platinum or gold electrodes in the same system; this is evidently the reason why the delayed decomposition is observed at palladium although it may still occur, but not be visible at platinum or gold. We believe that the effect at palladium is larger than at the other metals since palladium is less noble than platinum or gold, so that palladium has a greater susceptibility to anodic oxidation.

The period of arrest, or delay, in the e.m.f. decay curve, in fact, is directly related to the delay in the open-circuit gas evolution (determined by ciné-photography) as shown in Figure XLV; both effects appear to be related to the thickness of the anodically formed layer. Less spectacular self-discharge effects with non-delayed evolution of oxygen occurring over much longer periods of time are known in oxide electrode systems (119,120). Visible delayed gas evolution effects are not observed when the true Kolbe reaction is proceeding i.e. in the electrolysis of trifluoroacetate in anhydrous trifluoroacetic acid, although galvanostatic charging curves again indicate formation of surface films but of thicknesses much less than those found at palladium in the potassium formate-formic acid system.

(k) Anodic Film Formation

Following the observation (123) of a delayed gas evolution in the e.m.f. decay at palladium electrodes described

above, and which was dependent on the time of previous anodic polarisation, a number of experiments were carried out to evaluate, by cathodic galvanostatic discharge, the extent of film formation in the anodic decomposition of formate in 100% formic acid as a function of the time and current density of previous polarisation. The results for palladium, gold and platinum are shown in Fig. XXXVIII in terms of the delay time in the arrest region of the galvanostatic cathodic discharge transients as a function of the logarithm of the time of previous anodic polarisation. In Figs. XXXIX, XL and XLI the corresponding charges associated with the arrest region are plotted reciprocally in terms of the log of the previous anodic polarisation time and in Fig. XLIV are shown typical arrests on open-circuit after anodic polarisation of Pd for various times. Choice of the logarithmic plot was suggested by theories of film growth (80) in which, under high-field conditions (i.e. with thin films as in the present case), with metal ion transfer from the metal into the anodic film the rate-controlling process in film growth, a reciprocal relation should exist between film thickness and the logarithm of time of growth. In the present case, the thickness is assumed to be proportional to the charge associated with the film. In the formate case, this charge amounts to about 113 $\mu c.cm^{-2}$ per monolayer of $HCOO^{\bullet}$ (area 14.2 $\overset{\circ}{A}^2$). The parabolic growth law (90) in which the film thickness should vary with the square root of time of growth for low-field

conditions, when metal ion diffusion in the film is rate-controlling for film growth, does not fit the present results so well as the reciprocal log plot.

At palladium the charge associated with the arrest region increases with time of anodic polarisation and reaches about 4000 $\mu c.cm.^{-2}$ or about 35 layers in thickness. If this were a layer of a palladium formate which decomposed on open-circuit, about 0.01 ml. of CO_2 would be liberated at a 10 $cm.^2$ electrode. This is presumably the gas which is observed in the delayed gas evolution (123). The film growth rate cannot be directly related to the current passing, since most of the current is associated with the overall Faradaic process of CO_2 evolution in the formate electrolysis; only a small fraction of the total current is evidently involved in increasing the anode film thickness with time. The maximum charge of about 4000 $\mu c.cm.^2$ at the palladium electrode is just sufficient to produce a visible gas evolution if the layer is a formate of palladium (see above) which decomposes to give CO_2 auto-catalytically after a delay period or, equivalently, after the electrode potential has fallen to a critical value (123). No delayed gas evolution is seen at platinum or gold or in the Kolbe reaction itself and this is consistent with the ten times smaller film thickness (or charge) observed at the platinum electrode (Fig. XXXIX) in the same formate/formic

acid system.

(1) Periodic Phenomena and Passivation

The periodic phenomena observed and referred to above on p. 191 probably do not differ in nature from those well known in the anodic oxidation of metals, and no new light is shed on the mechanisms involved as this was beyond the scope of the present studies. However, a few points can be discussed generally, as such phenomena have not previously been reported for oxidation in non-aqueous media where oxide films cannot be formed.

The periodic phenomena observed are probably related to a critical condition of passivation and formation of a carboxylate film ($HCOO^{\bullet}(M)$) in the present case), oscillation occurring when the system can exist in two possible states neither of which is permanently stable.

Evidently further work is required than the scope of the present investigation permitted in order to elucidate the mechanism of these phenomena more definitively.

The theory of periodic phenomena and unstable steady states has been discussed by Franck (75) in relation to the nerve excitation problem and to periodic passivation of iron. Since this phenomenon was observed only incidentally in the present work, we do not propose to examine its explanation further except to point out that observation of this behavior, which is well known in oxide film passivation of metals,

supports our contention that the transition behavior observed in the formate and Kolbe decarboxylation reactions is really a metal passivation process.

C. DECARBOXYLATION OF FORMATE IN AQUEOUS SOLUTION

In order to compare qualitatively the kinetic behavior of the formate decarboxylation reaction under aqueous conditions with that under the idealised conditions in the wholly non-aqueous formate-formic acid system, a number of runs were performed in 1M aqueous solutions of potassium formate and in solutions containing 1M and 5M KOH. The latter was used to stabilize the pH and also purposely to attempt to facilitate simultaneous oxygen evolution or oxide film formation in the aqueous systems and thus to examine their effects, if any, on the decarboxylation reaction. The purpose of this part of the work was to attempt to provide some basis with the simple formate reaction for the more complex side oxidation reactions associated with oxygen evolution that have been observed by other authors in the aqueous Kolbe reaction with acetate. The experimental approaches in this section of the work were similar to those described in Chapter II.

(a) Kinetic Parameters

The standard reversible potential, E^{o}, for the aqueous formate decarboxylation reaction was calculated for the reaction

$$HCOO^{-} \rightleftharpoons 2H^{+} + CO_2 + 2e$$

from available thermodynamic data (126); values are recorded

in Table VI for the various aqueous solutions used. Apparent exchange current densities, i_o, based on the reversible potentials (Table VI) are recorded in Table VII, and were estimated from the experimentally determined total current Tafel lines* (Figures XVI-XX) as discussed previously (p. 159).

The runs in aqueous formate and aqueous formate-KOH solutions (Figures XVI-XX) all demonstrate well defined transition regions and the lower potential region is better developed than in non-aqueous solution since the limiting transition current density is higher than it is in the formate-formic acid (100%) system (section A above). At palladium, gold and platinum, the lower Tafel region consistently has a slope of 0.06 (RT/F) and the upper regions slopes of about 0.12 (2RT/F) or slightly larger.

Typical transition behavior (i.e. potential oscillation) were also observed in the aqueous system as in the non-aqueous system.

(b) Significance of Tafel Slopes

Coulombic yield measurements for the anodic formate decarboxylation reaction in aqueous solution given in Table III show that some oxygen (as well as CO_2) is evolved under aqueous conditions. Hence the interpretation of the observed electrochemical behavior in terms of the steps which have been deduced

* Corrections for the O_2 co-current do not seriously affect the slopes of the current potential plots except for gold where the current efficiencies are quite low.

Table VI

Reversible Potentials for the Reaction $HCOOH \rightleftarrows 2H^+ + CO_2 + 2e$ on the Hydrogen Scale in the Same Solution Indicated

a)	1 M aq. HCOOK	E_H =	-0.047 v.
b)	1 M aq. HCOOK + 1M aq. KOH	E_H =	+0.105 v.
c)	1 M aq. HCOOK + 5M aq. KOH	E_H =	+0.125 v.

Data are calculated from thermodynamic data for 25°C. Standard state HCOOH = unit activity, 1 atm. pressure of CO_2 and H_2. The reversible potential of the reaction shown depends on KOH concentration since the extent of hydrolysis of the potassium formate by $H_2O + HCOO^- \rightarrow HCOOH + OH^-$ depends on KOH activity. The reversible potentials calculated for 5°C will differ from the above values by approximately 17 mV since the standard entropy change for the reaction HCOOH (aq.) $\rightleftarrows CO_2 + H_2$ is approximately 43 e.u.

Table VII

Mean Tafel Parameters for the Aqueous Formate Decarboxylation Reaction (5°C)

(Minimum of ten Electrodes in two Solutions)

Electrode	Concentration	b ± 1% (v)	i_o amp.cm^{-2} (± 40%)	Current Density Range (amp. cm^{-2})
Pt	1M HCOOK/H_2O	0.13(lower)	1×10^{-10}	6×10^{-6} - 1×10^{-2}
		0.12(upper)	1.7×10^{-21}	2×10^{-4} - 5×10^{-2}
Au	"	0.12(lower)	3.9×10^{-11}	5×10^{-6} - 1×10^{-3}
		0.16(upper)	3.9×10^{-17}	1.5×10^{-4} - 5×10^{-2}
Pt	1M HCOOK + 1M KOH/H_2O	0.06(lower)	4×10^{-30}	9×10^{-6} - 2×10^{-3}
		0.17(upper)	3.2×10^{-17}	1.5×10^{-3} - 1.1×10^{-1}
Pd	"	0.06(lower)	4×10^{-29}	1.5×10^{-6} - 5×10^{-3}
		0.12(above hysteresis)	1.3×10^{-20}	1.5×10^{-2} - 5×10^{-1}
		0.10 (in hysteresis region)	4×10^{-24}	2.5×10^{-4} - 1.5×10^{-2}
Au	"	0.06(lower)	8×10^{-26}	1.5×10^{-6} - 2.5×10^{-3}
		0.13(above hysteresis region)	4×10^{-19}	5×10^{-3} - 1.1×10^{-1}
		0.09(in hysteresis region)	6×10^{-26}	5×10^{-5} - 5×10^{-3}

Continued on next page.

Table VII - continued

Pt	1M HCOOK + 5M KOH/H_2O	0.06(lower)	5×10^{-31}	$7 \times 10^{-6} - 3 \times 10^{-3}$
		0.16(upper)	2×10^{-18}	$5 \times 10^{-3} - 2 \times 10^{-1}$
Pd	"	0.06(lower)	1×10^{-29}	$2 \times 10^{-6} - 4 \times 10^{-4}$
		0.11(upper)	2×10^{-22}	$8 \times 10^{-5} - 2.5 \times 10^{-2}$
Au	"	0.06(lower)	2×10^{-28}	$5 \times 10^{-6} - 9 \times 10^{-4}$
		0.12(upper)	1×10^{-19}	$6 \times 10^{-5} - 5 \times 10^{-2}$

Note: Exchange currents are calculated with respect to the reversible potential estimated from the thermodynamic free energy for 25°C - see Table VI.

The apparent i_o values for Au are based on the overall current. The values given are hence correct to within about a half of one order of magnitude bearing in mind the current efficiency of the reaction at gold. This uncertainty is not seriously different from that involved in the extrapolation to the reversible potential. At Pt and Pd the error is correspondingly less.

previously for the anhydrous formate system and which may be involved in the overall reaction (reaction I), cannot be made with the same certitude except, perhaps, at the highest current densities. In considering the role of simultaneous reactions of formate decomposition and oxygen evolution, it must be borne in mind that formation of formate radicals at the surface will almost certainly modify the oxygen evolution kinetics, and vice versa, and the present results show that formation of O-containing species (e.g. $OH^{\bullet}$ or $O^{\bullet}$) substantially inhibits the formate kinetics and hence no simple relationship between the kinetics of the reactions, when they occur together, can be proposed. At intermediate current densities, e.g. in the case of gold (Table III) oxygen evolution is appreciable and occurs simultaneously with CO_2 evolution.*

(c) Galvanostatic Transients and Reaction Mechanism

(i) Film Formation

The reversed pulse cathodic transients for the formate reaction in aqueous and in aqueous alkaline solutions (1M KOH) shown in Figures LIV indicate that the reaction proceeds at anodic films of appreciable thickness (5-20 monolayers). In general, at the three metals Pt, Pd and Au the

* This may account for the fact that side oxidation reactions in the acetate Kolbe reaction are more extensive at Au than at other metals, e.g. 60% yields of methanol can be obtained in the "Kolbe electrolysis" at gold.

Figure LIV

Galvanostatic reversed pulse cathodic discharge curves for the aqueous formate decarboxylation (5°C):

(a) Pt, 1M $HCOOK/H_2O$

(1) 6.8×10^{-4} a.cm.$^{-2}$ (159 sec.) 0.1 v.cm.$^{-1}$, 20 msec.cm.$^{-1}$
Over all q = 95 μc.cm.$^{-2}$ (no arrest capacity).

(2) 1.1×10^{-2} a.cm.$^{-2}$ (67.1sec.) 0.2 v.cm.$^{-1}$ 10 msec.cm.$^{-1}$
C = 1900 μF. q = 495 μc.cm.$^{-2}$

(3) 4.2×10^{-2} a.cm.$^{-2}$ (175 sec.) 0.5 v.cm.$^{-1}$ 5 msec.cm.$^{-1}$
Two regions of arrest; $q_1 \doteq 645$ μc.cm.$^{-2}$, $q_2 = 600$ μc.cm.$^{-2}$

(b) Pd, 1M $HCOOK/H_2O$

(1) 8.5×10^{-4} a.cm.$^{-2}$ (328 sec.) 0.1 v.cm.$^{-1}$ 10 msec.cm.$^{-1}$
C = 40 μF., q = 30 μc.cm.$^{-2}$

(2) 7.5×10^{-3} a.cm.$^{-2}$ (164 sec.) 0.2 v.cm.$^{-1}$ 10 msec.cm.$^{-1}$
C = 660 μF; q = 525 μc.cm.$^{-2}$

(3) 5.3×10^{-2} a.cm.$^{-2}$ (162 sec.) 0.5 v.cm.$^{-1}$ 20 msec.cm.$^{-1}$
Note complex structure (reproducible) developed at high c.d. This behavior is <u>not</u> observed in 100% formic acid at comparable c.d.
$q_1 \doteq 1500$ μ.c.cm.$^{-2}$ (note undershoot)
$q_2 \doteq 2200$ μc.cm.$^{-2}$
$q_3 \doteq 1700$ μc.cm.$^{-2}$

(c) Pd, 1M HCOOK, 1M KOH/H_2O

(1) 5×10^{-5} a.cm.$^{-2}$ (152 sec.) 0.1 v.cm.$^{-1}$ 0.1 sec. cm.$^{-1}$
(little arrest region).

(2) 9.9×10^{-4} a.cm.$^{-2}$ (154 sec.) 0.5 v.cm.$^{-1}$ 0.2 sec. cm.$^{-1}$
$q_1 \doteq 400$ μc.cm.$^{-2}$
$q_2 \doteq 400$ μc.cm.$^{-2}$ (approx. potential-independent region).

(3) 8.6×10^{-3} a.cm.$^{-2}$ (345 sec.) 0.5 v.cm.$^{-1}$ 50 msec.cm.$^{-1}$
$q_1 \doteq 1290$ μc.cm.$^{-2}$ (note undershoot)
$q_2 \doteq 1720$ μc.cm.$^{-2}$
q_3 - uncertain

(d) Au, 1M HCOOK/H_2O

(1) 1.4×10^{-4} a.cm.$^{-2}$ (309 sec.) 0.1 v.cm.$^{-1}$ 0.1 sec. cm.
(no arrest region).

(2) 5.7×10^{-2} a.cm.$^{-2}$ (166 sec.) 0.5 v.cm.$^{-1}$ 10 msec.cm.$^{-1}$
Complex arrest behavior.

(e) Au, 1M HCOOK, 1M KOH/H_2O

(1) 3.7×10^{-5} a.cm.$^{-2}$ (501 sec.) 0.2 v.cm.$^{-1}$ 0.2 sec.cm.$^{-1}$
No arrest region.

(2) 2.6×10^{-4} a.cm.$^{-2}$ (504 sec.) 0.5 v.cm.$^{-1}$ 0.5 sec.cm.$^{-1}$
Mean C $\doteq$ 7800 μF; q = 780 μc.cm.$^{-2}$

(3) 6.4×10^{-3} a.cm.$^{-2}$ (514 sec.) 0.5 v.cm.$^{-1}$ 50 msec.cm.$^{-1}$
Mean C $\doteq$ 400 μF; q = 1920 μc.cm.$^{-2}$

(f) Pt, 1M HCOOK; 1M KOH/H_2O

(1) 3×10^{-4} a.cm.$^{-2}$ (436 sec.) 0.1 v.cm.$^{-1}$ 0.1 sec.cm.$^{-1}$

C = 700 μF; q = 210 μc.cm.$^{-2}$

(2) 8.7×10^{-4} a. cm.$^{-2}$ (327 sec.) 0.2 v.cm.$^{-1}$ 0.2 sec.cm.$^{-1}$

(3) 6×10^{-2} a.cm.$^{-2}$ (526 sec.) 0.5 v.cm.$^{-1}$ 5 msec.cm.$^{-1}$

C variable but large; total q = 1590 μc.cm.$^{-2}$

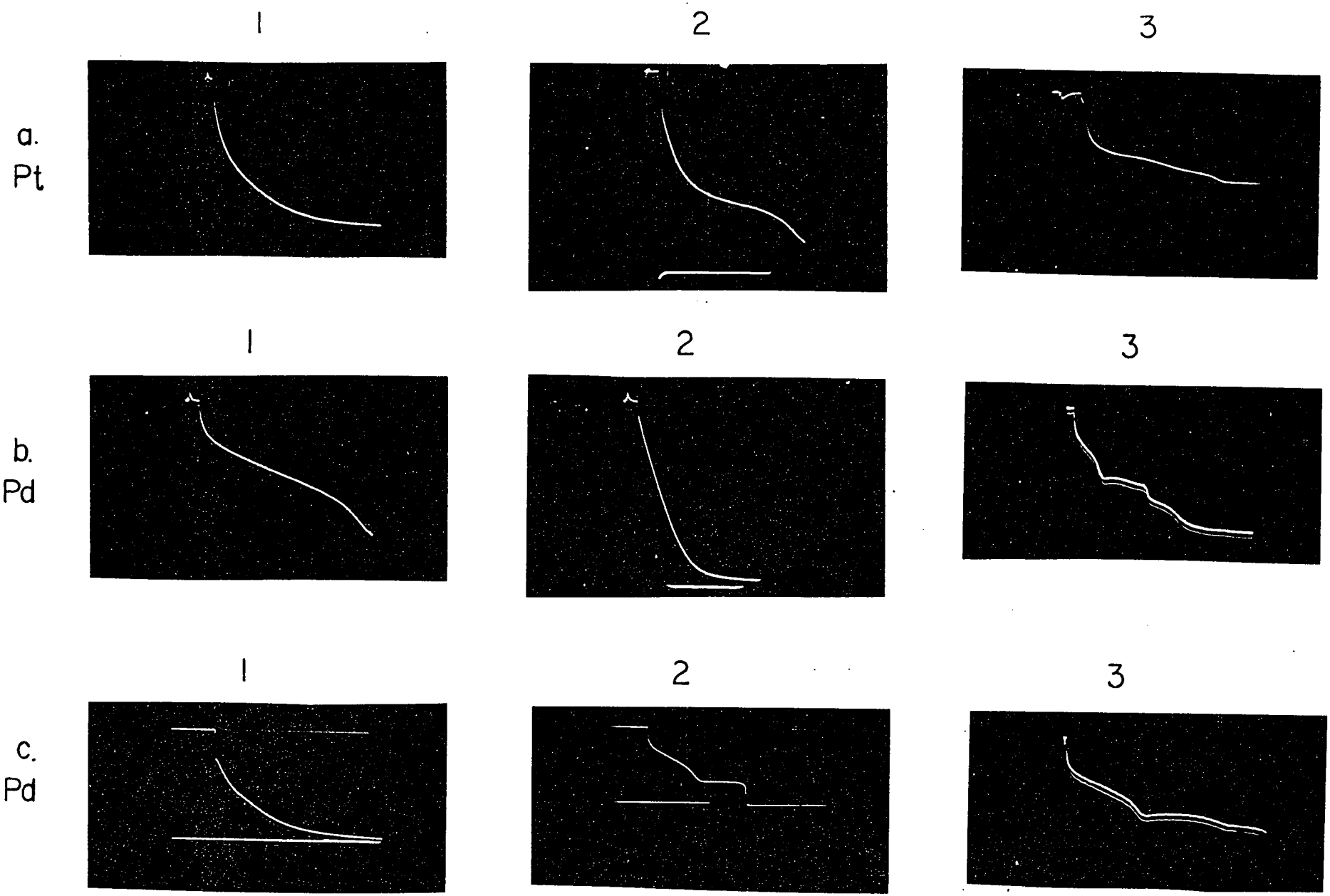
1
2
3
a.
Pt
1
2
3
b.
Pd
1
2
3
c.
Pd

d. Au

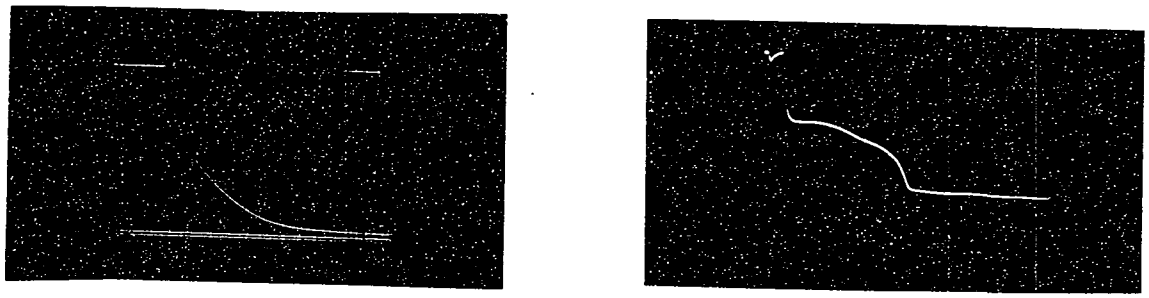

e. Au

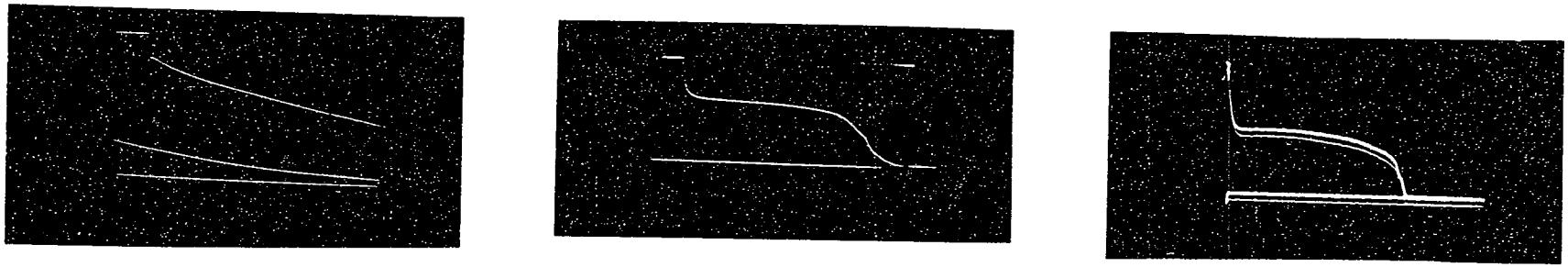

f. Pt

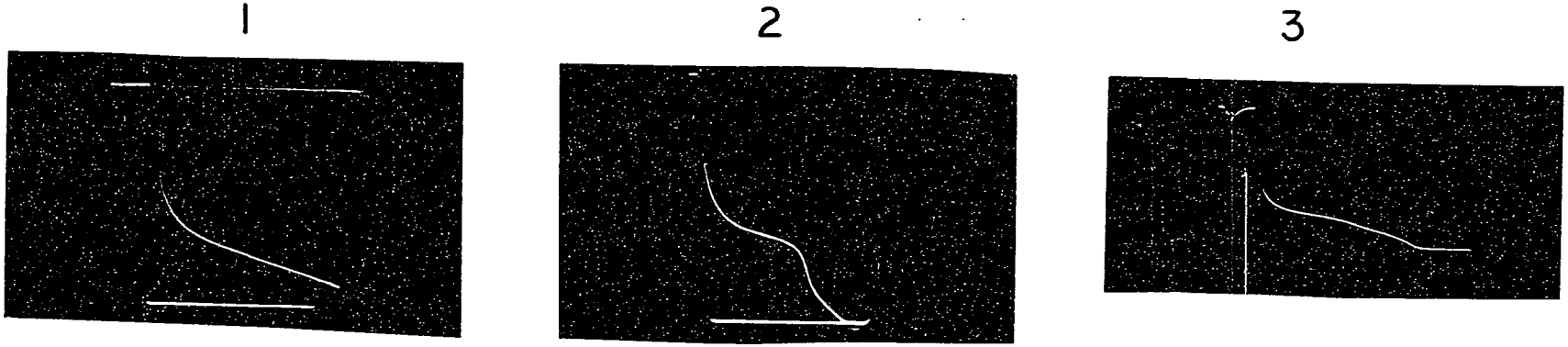

film thickness increases with current density (as also at Pd in 100% formic acid). With all three metals, and particularly with Pd, the arrest behavior in the aqueous and aqueous-KOH media is more complex than in the pure formic acid system. At palladium, three distinct arrest regions are developed at the higher current densities which suggest relatively thick (20-30 layers) anodic films in various oxidation states of the metal, or possibly both oxide and formate film formation over different potential ranges. Some evidence for this is seen in the current density-potential curve (Figure XVI) for platinum, where at the highest current densities the behavior of the current with decreasing potential is quite different from that found for increasing current if the polarisation has not reached the highest values. The critical potentials referred to in previous work on the Kolbe reaction itself (29,122,131) are, we believe associated with the upper potential region (or related critical currents for film formation) in the film-forming region of the transients. In the non-aqueous solutions a critical film-forming region occurs at a certain limiting current and it is evidently this condition for film formation or "passivation" which has been regarded as necessary for occurrence of the Kolbe reaction at appreciable efficiencies. Actually, under non-aqueous conditions (in the CF_3COOH system) this film formation is not a pre-requisite since we have found that the Kolbe coupling

reaction (see section D) also occurs at currents below the critical current, i.e. in the lower Tafel region. However, in aqueous solutions, it is usually found (8,9,122) that some oxygen evolution precedes Kolbe coupling, so it appears that the electrode requires to be "passivated" by a carboxylate film (possibly on top of an oxide film e.g. see Figures LIV (b) and (c) for the formate case) before significant coupling can occur. Presumably, so long as a film of reactive oxygen-containing species (e.g. OH• or O•) is present at the interface, some oxidative degradation of discharged alkyl carboxylate radicals (in the case of the Kolbe reaction) tends to occur leading to "Hofer-Moest" products. We suggest that only when this film is superceded by a complete carboxylate film does the coupling reaction occur efficiently. In the 100% trifluoroacetic or formic acid systems, no oxide film formation can occur (for example, no double arrests are seen in the transients) and the decarboxylation reaction occurs only on a simple film of the adsorbed carboxylate at high current density, and on a partially covered metal surface (see below) at current densities below the critical current.

(d) Time Dependence of Potential

In the polarisation measurements made in determining the current-potential behavior, it was observed that near the transition region (with either increasing or decreasing currents), there was considerable time-variation of electrode

potential which was not observed at lower or higher current densities (i.e. above or below the transition region). As the current was either suddenly increased or decreased the potential would "overshoot" or "undershoot", respectively, before attaining its final steady value. Similar behavior has been observed previously in the anodic oxygen evolution reaction (87) and at barrier-layer film electrodes (130). The phenomenon is characteristic of slow adjustment of space charge in a barrier-layer film when the field across the film is suddenly changed. Typical plots of the logarithmic change of potential with time near the transition region and of e.m.f. recovery after undershoot are shown in Figures XXX, XXXII.

The build-up curves are similar to those found in the anodic evolution of oxygen at platinum and are probably associated with the same type of process (76), viz. deactivation of sites on the metal surface by adsorption of an intermediate product (probably $HCOO^{\bullet}$ in the present case) of one of the steps in the reaction. The logarithmic recovery following "overshoot" or "undershoot", also observed in the oxygen evolution reaction (87) at palladium, is probably associated with a first order readjustment of space charge (30) in the multilayer semiconducting film following a sudden change of field as the current density (or potential) is changed.

(e) <u>The Role of Oxygen in the Reaction in Aqueous Media</u>

It is of interest that addition of KOH in the aqueous

formate decarboxylation reaction diminishes the "height" of the transition region. Inspection of the curves (Figures XVI-XX), indicates that this is mainly due to a shift of the lower Tafel line to higher overpotentials (or lower exchange currents: see Table VII) in the presence of KOH. This effect, which is very marked, is seemingly general since it is observed at Pt, Au and also Pd, although the reproducibility of the results in pure aqueous formate solutions is bad at the latter metal. We suggest that this striking effect arising upon addition of the KOH is due either to adsorption of OH^- ions competitive with that of $HCOO^\bullet$ radicals or to facilitation of formation of an oxide film* in the lower Tafel region; the overall process in this region is not, by any means, wholly oxygen evolution and the Tafel parameters for this region, if they were calculated for oxygen evolution with respect to the reversible oxygen potential, are not at all comparable with those which have been reported elsewhere for oxygen evolution at gold or palladium (87) in pure 1M KOH solutions, or which are available (76) for platinum. The process in the lower slope region is hence not simply oxygen evolution or oxide film formation, as is also apparent from the significant evolution of CO_2 (in the absence

* The galvanostatic results, shown in Fig. LV indicate, for example, complex film formation in the aqueous formate decarboxylation reaction, as we have mentioned above.

of KOH). The data of MacDonald and Conway (87) for oxygen evolution at Au and Pd in 1M aq. KOH are shown in Figures XIX and XX for comparison. It is evident from these Figures that the formate decarboxylation at Au in the presence of 1M KOH proceeds over most of the current density range at potentials less than those for the oxygen evolution reaction in 1M KOH in the absence of formate. In the case of Pd, which shows no transition region in the oxygen evolution Tafel line (87), it will be noted that a transition region is developed (as in the non-aqueous solutions) in the formate/KOH system. This transition region, and that probably at Au in the formate solution, is hence not specifically connected with the oxygen evolution process.

The results discussed above demonstrate that in aqueous media the decarboxylation reactions are more complex than in non-aqueous media and probably involve surface films both of oxide and carboxylate species. In the aqueous system, although no simple relationship between the kinetics of the two reactions can be proposed when they occur together, galvanostatic results do indicate that film formation, similar to that observed in the non-aqueous system is occurring; however, with two processes occurring the decay curves are complicated. In the non-aqueous system, where no complicating reactions due to oxide film growth or oxygen evolution can occur, we have shown that the transition region

corresponds, in most cases, to filling up the surface with adsorbed radicals. The lower Tafel line in the aqueous formate system, which is below the normal molecular oxygen evolution potential (but the possibility of formation of adsorbed oxygen on the surface is not excluded) probably corresponds to the rate-determining step

$$HCOO^{\bullet} \longrightarrow H^{\bullet} + CO_2.$$

associated with the unimolecular decomposition slope of RT/F (reaction III, see part A) and observed experimentally. The upper region then probably corresponds to discharge of the formate radicals (reaction VI) at high coverage, or further discharge of formate ions on to the multi-layer or film of adsorbed formate, e.g. in a manner analogous to the oxygen evolution reaction which usually occurs on an oxide layer rather than on the metal surface itself.

D. THE MODEL REACTION WITH TRIFLUOROACETATE (the true Kolbe Reaction)

(a) Kinetic Parameters

Exchange current densities, i_o, could not be evaluated for the overall trifluoroacetate Kolbe reaction

$$2CF_3COO^{-} \longrightarrow C_2F_6 + + 2CO_2 + 2e \qquad \text{I}$$

owing to the lack of the appropriate thermodynamic data. The experimentally determined Tafel slopes, however are

summarised in Table VIII showing the current density range over which they arise.

(b) Reaction Mechanism

By analogy with the reaction with formate, we may envisage the following steps in the overall reaction I

$$CF_3COO^- \longrightarrow CF_3COO^{\bullet}(M) + e \qquad II$$

$$CF_3COO^{\bullet}(M) \longrightarrow CF_3^{\bullet}(M) + CO_2 \qquad III$$

$$2CF_3^{\bullet}(M) \longrightarrow C_2F_6 \qquad IV$$

Side reactions could lead to the production of the peroxide $(CF_3COO)_2$ or the ester CF_3COOCH_3; the coulombic yields (Table II), however, indicate that these side reactions, if present at all, are insignificant, although adsorbed peroxide could be an intermediate which quantitatively decomposes to CO_2 and C_2F_6. A reaction involving two ions, decarboxylation, coupling and two-electron transfer in one step is unlikely. The above scheme is hence believed to be the most reasonable pathway on which to base a more definitive treatment of reaction mechanism; also the steps postulated are consistent with other known radical processes in the gas phase (46) and in solution (42-45). At full coverage by $CF_3COO^{\bullet}$ in III, a potential-dependent radical ion desorption paths such as

Table VIII

Experimental Tafel Parameters for the Trifluoroacetate-Trifluoroacetic System

(Minimum of ten Electrodes in two Solutions)

1M CF_3COOK/CF_3COOH (5^oC)

Electrode	b ± 1% (v)	Current Density Range amps.cm^{-2}
Pt	0.26	$7 \times 10^{-5} - 5 \times 10^{-2}$
Pd	0.25	$1 \times 10^{-5} - 5 \times 10^{-4}$
	0.38	$5 \times 10^{-4} - 5 \times 10^{-3}$
	0.30	$5 \times 10^{-3} - 8 \times 10^{-2}$
Au	0.38	$1 \times 10^{-5} - 7 \times 10^{-4}$
	0.23	$7 \times 10^{-4} - 2 \times 10^{-2}$
1M CF_3COOK/H_2O (5^oC)		
Pt	0.25(up)	$8 \times 10^{-6} - 1.5 \times 10^{-3}$
	0.20(down)	$1 \times 10^{-5} - 1 \times 10^{-3}$
	0.30(upper)	$1 \times 10^{-3} - 5 \times 10^{-2}$
Pd	0.42(up)	$1 \times 10^{-5} - 3 \times 10^{-4}$
	0.08(upper)	$3 \times 10^{-4} - 9.5 \times 10^{-2}$
Au	0.12	$2 \times 10^{-5} - 2 \times 10^{-3}$
	0.085	$2 \times 10^{-3} - 1 \times 10^{-1}$

$$CF_3^{\bullet} + CF_3COO^- \rightarrow C_2F_6 + CO_2 + e \qquad V$$

or

$$CF_3COO^{\bullet} + CF_3COO^- \rightarrow C_2F_6 + 2CO_2 + e \qquad VI^*$$

may also be envisaged, analogous to the reaction $H^{\bullet} + H^+ + e \rightarrow H_2$ in the hydrogen evolution reaction.

(c) Kinetic Equations for Steps in the Trifluoroacetate-"Kolbe" Reaction

(i) Langmuir Conditions

The limiting Tafel slopes for the above steps under Langmuir conditions (32,33) can be obtained by a treatment analogous to that given for the formate decarboxylation and with those for the well known cases of hydrogen and oxygen evolution. The limiting Tafel slopes are hence $dV/d \ln i_2 = 2RT/F$ (assuming $\beta = 0.5$); $dV/d \ln i_3 = RT/F$ or a limiting current (i.e. $dV/d \ln i_3 \rightarrow \infty$) as the coverage by $CF_3COO^{\bullet}$ approaches unity; $dV/d \ln i_4 = RT/2F$ or a recombination controlled limiting current as the coverage by $CF_3^{\bullet}$ tends to unity. For reactions V or VI, when $\theta_{CF_3COO^{\bullet}}$ is potential independent at full coverage the Tafel slope would be $dV/d \ln i_5 = 2RT/F$; and for $\theta_{CF_3COO^{\bullet}}$ potential dependent, with II and III in quasi-equilibrium we obtain the Tafel slope as $2RT/3F$.

---

* While VI is a possible alternative desorption step, it is clear that this is probably not exclusively the desorption pathway since, in the acetate case, CH_3 radicals produced in the Kolbe reaction have been shown to initiate polymerisation (see page 22 and refs. 63-65) as well as $CH_3COO^{\bullet}$ radicals. Reaction II followed by VI cannot hence be an exclusive pathway.

The step corresponding to reaction IV in the formate decarboxylation (pp. 5), viz. ionization of H and decarboxylation in one step, is unlikely here since this would lead to the formation of the carbonium ion CF_3^+ which presumably will give CF_3COOCF_3 (or CF_3OH in water) as a final product. This pathway is insignificant as shown by the nature of the observed products and coulombic yields (Table II).

(ii) Temkin Conditions

The corresponding rate-equations under conditions where coverage dependent activation energies (102,127) must be considered in the kinetics will now be examined.
We obtain for the ion-discharge step II

$$v_2 = k_2 (1-\theta_A) a_A - \exp.- [\Delta G_2^{\neq} - \beta VF + \alpha f(\theta)]/RT \qquad [88]$$

as in the corresponding formate case in which surface induction effects due to adsorbed intermediates are considered to be the origin of the assumed linear variation of heats of adsorption with coverage.

The rate of the back reaction is given by

$$v_{-2} = k_{-2}\, \theta_A \exp - [\Delta G_{-2}^{\neq} + (1-\beta)VF - (1-\alpha)\, f(\theta)]/RT \qquad [89]$$

where θ_A is the coverage due to $CF_3COO^{\bullet}$ and $f(\theta)$ represents the terms $(r_A\theta_A + r_M\theta_M)$ similar to those defined in the formate case where the subscripts A and M now refer to the variation in the heat of adsorption with coverage by adsorbed

$CF_3COO^\bullet$ and $CF_3^\bullet$, respectively. The remaining terms have their usual significance.

Similarly

$$v_3 = k_3 \theta_A (1-\theta_M) \exp.- [\Delta G_3^{\neq} - \alpha f(\theta) + (1-\alpha) f(\theta)]/RT \quad [90]$$

$$v_{-3} = k_{-3} \theta_M (1-\theta_A) \exp. - [\Delta G_{-3}^{\neq} + (1-\alpha) f(\theta) - \alpha f(\theta)]/RT \quad [91]$$

and

$$v_4 = k_4 \theta_M^2 \exp. - [\Delta G_4^{\neq} - 2\alpha f(\theta)]/RT \quad \text{for activated} \quad [92]$$

(cf. Thomas (127)). adsorption of C_2F_6 as $2CF_3^\bullet$ and for non-activated adsorption the rate is given by

$$v_4 = k_4 \theta_M^2 \exp. - [\Delta G_4^{\neq} - 2 f(\theta)]/RT \quad [93]$$

We now examine limiting cases, assuming as previously (127) that at coverages sufficient to influence the exponential terms, the pre-exponential terms are of the order of unity. If II, the ion-discharge step, were rate-determining and subsequent steps rapid, so that $\theta_A \longrightarrow 0$, Temkin conditions will be inapplicable; we are then simply left with the Langmuir result for limitingly low conditions of surface coverage which leads to a Tafel slope of $dV/d \ln i_2 = 2RT/F$.

If III were rate-determining, the quasi-equilibrium condition for step II gives

$$VF = f(\theta) + K_2 \quad [94]$$

where K_2 is a constant at constant temperature and solution composition, as in the formate case.

Substituting $f(\theta)$ from equation [94] into equation [90] and neglecting pre-exponential terms in θ, we obtain

$$v_3 = k' \exp - [\Delta G_3^{\neq} - \alpha VF + (1-\alpha)VF]/RT \qquad [95]$$

which gives a limiting Tafel slope* i.e. $dV/d \ln i_3 \rightarrow \infty$ with $\alpha = 1/2$.

For reaction IV rate-determining, with II and III in quasi-equilibrium, we obtain, by combining equations [94], [92] and [93],

$$v_4 = k' \exp. - [\Delta G_4^{\neq} - 2\alpha VF]/RT \qquad [96]$$

for activated adsorption of C_2F_6, and for non-activated adsorption

$$v_4 = k' \exp. [\Delta G_4^{\neq} - 2VF]/RT \qquad [97]$$

The corresponding Tafel slopes are then

$$\frac{dV}{d \ln i_4} = \frac{RT}{F}; \quad \frac{dV}{d \ln i_4} = \frac{RT}{2F}, \text{ respectively.} \qquad [98]$$

Finally, when step V is rate-determining, the rate is given by

---

* The step III following the discharge of the trifluoroacetate ion, does not, as in the formate decarboxylation reaction, involve terms in $f(\theta)$, following substitution for $f(\theta)$ from equation [94] since they cancel out, so that the rate of such steps under Temkin conditions will be practically independent of potential. A slight dependence may be observed since the rate is proportional to coverage which is a linear function of potential (cf. equation [94]).

$$v_5 = k_5 \theta_M a_A - \exp. - [\Delta G_5^{\neq} - \beta VF - \alpha f(\theta)]/RT \qquad [99]$$

for activated adsorption of C_2F_6 as $2CF_3^{\bullet}$, and

$$v_5 = k_5 \theta_M a_A - \exp. - [\Delta G_5^{\neq} - \beta VF - f(\theta)]/RT \qquad [100]$$

for the non-activated adsorption case.

With II and III in quasi-equilibrium we obtain from equations [94], [99] and [100].

$$v_5 = k' \exp. - [\Delta G_5^{\neq} - \beta VF - \alpha VF]/RT \qquad [101]$$

and the Tafel slope as

$$\frac{dV}{d \ln i_5} = RT/F \quad \text{for activated adsorption when } \alpha = \beta = 1/2,$$

and

$$v_5 = k' \exp. - [\Delta G_5^{\neq} - \beta VF - VF]/RT \qquad [102]$$

for the non-activated adsorption case, so that

$$\frac{dV}{d \ln i_5} = 2RT/3F \quad \text{for non-activated adsorption when } \beta = 1/2.$$

Both Tafel slopes are seen to be identical with those obtained under Langmuir limiting conditions (Table IX).

By analogy with the treatment given above and for the formate decarboxylation reaction, the Tafel slopes for the above steps assuming à priori heterogeneity of surface sites are

$$\frac{dV}{d \ln i_2} = \frac{2RT}{F}; \quad \frac{dV}{d \ln i_3} = \frac{2RT}{F} \frac{r_1}{r_1 - r_2}$$

Table IX

Theoretically Predicted Tafel Slopes for the Model Reaction with Trifluoroacetate

Step	Langmuir Conditions $\theta < 0.1$; $\theta \to 1$		Intermediate coverage conditions ($0.2 < \theta < 0.8$)			
			Induction model		Heterogeneity model	
	Tafel Slope	Limiting conditions	Tafel Slope	Limiting conditions	Tafel slope	Limiting conditions
II $CF_3COO^- \rightarrow CF_3COO^\bullet + e$	$\frac{2RT}{F}$	Rate constants for following steps relatively large so that $\theta_A \to 0$	$\frac{2RT}{F}$ $\therefore$ inapplicable	$\theta_A \to 0$	$\frac{2RT}{F}$ $\therefore$ inapplicable	$\theta_A \to 0$
III $CF_3COO^\bullet \rightarrow CF_3^\bullet + CO_2$	$\frac{RT}{F}$ or Limiting	$\theta_A = f(V)$ $CF_3COO^\bullet$ approaching unity and potential independent	Limiting current	II in quasi-equilibrium	$\frac{2RT}{F}\frac{r_1}{r_1-r_2}$ Limiting current $r_1 = r_2$ $2RT/F$ $r_1 \gg r_2$ No physical significance to Tafel slope $r_1 \ll r_2$	II in quasi-equilibrium
IV $2CF_3^\bullet \rightarrow C_2F_6$	$\frac{RT}{F}$ or Limiting current	II and III in quasi-equilibrium and coverage by $CF_3^\bullet$ potential dependent Coverage by $CF_3^\bullet$ approaching unity and potential independent	$\frac{RT}{F}$ or II and III in quasi-equilibrium $\frac{RT}{F}$ for activated adsorption of C_2F_6		$\frac{RT}{2F}\frac{r_1}{r_2}$ II and III in quasi-equilibrium or $\frac{RT}{F}\frac{r_1}{r_2}$ for activated adsorption of C_2F_6 $\frac{RT}{2F}$ or $\frac{RT}{F}$ $r_1 = r_2$ tending to a limiting current $r_1 \gg r_2$ tending to a limiting potential $r_1 \ll r_2$	

(Continued on next page)

(Table IX - Continued)

V $CF_3^{\bullet}+CF_3COO^- \rightarrow$ $C_2F_6+CO_2+e$	$\frac{2RT}{F}$ or $\frac{2RT}{3F}$	II and III in quasi-equilibrium coverage by $CF_3^{\bullet}$ approaching unity and potential independent Coverage by $CF_3^{\bullet}$ potential dependent	$\frac{2RT}{3F}$ or $\frac{RT}{F}$	II and III in quasi-equilibrium for activated adsorption of C_2F_6	$\frac{2RT}{F}\frac{r_1}{r_1-2r_2}$ or $\frac{2RT}{F}\frac{r_1}{r_1+r_2}$ $\frac{2RT}{3F}$ or $\frac{RT}{F}$ $\frac{2RT}{F}$ or $\frac{2RT}{F}$ tending to a limiting potential	II and III in quasi-equilibrium for activated adsorption of C_2F_6 $r_1 = r_2$ $r_1 \gg r_2$ $r_1 \ll r_2$
VI $CF_3COO^{\bullet}+$ $CF_3COO^- \rightarrow$ $C_2F_6+2CO_2+e$	$\frac{2RT}{F}$ $\frac{2RT}{3F}$	II in quasi-equilibrium coverage by $CF_3COO^{\bullet}$ approaching unity and potential independent Coverage by $CF_3COO^{\bullet}$ potential dependent	$\frac{2RT}{3F}$ or $\frac{RT}{F}$	II in quasi-equilibrium for activated adsorption	$\frac{2RT}{3F}$ $\frac{RT}{F}$	II in quasi-equilibrium for activated adsorption

as in the corresponding formate reaction, where r_1 now refers to the change of adsorption energy of $CF_3COO^\bullet$ with coverage and r_2 to the corresponding changes for $CF_3^\bullet$. The limiting values of the Tafel slope for reaction III are (i) limiting current ($r_1 = r_2$), i.e. $dV/d \ln i_3 \rightarrow \infty$ and (ii) $2RT/F$ ($r_1 \gg r_2$); when $r_1 \ll r_2$ the Tafel slope is negative and hence no physical significance can be attached to this condition.

At any coverage by $CF_3^\bullet$, step IV will be associated with a slope of $RT/2F.\ r_1/r_2$ or $RT/F\ r_1/r_2$ for conditions of non-activated and activated adsorption, respectively, of $CF_3^\bullet$ from C_2F_6 (cf. the hydrogen case (127)) if the coverage by $CF_3COO^\bullet$ is appreciable. The alternate termination step (V) yields Tafel slopes of

$$\frac{dV}{d \ln i_5} = \frac{2RT}{F} \cdot \frac{r_1}{r_1 + 2r_2} \quad \text{and} \quad \frac{dV}{d \ln i_5} = \frac{2RT}{F} \frac{r_1}{r_1 + r_2}$$

for non-activated and activated adsorption of C_2F_6, respectively. The limiting values are (i) $2RT/3F$ or RT/F with $r_1 = r_2$ (ii) $2RT/F$ in both cases and (iii) for $r_1 \ll r_2$ the current voltage curve will tend to a limiting potential (cf. p. 179). The Tafel slopes derived above for the various conditions are summarised in Table IX.

(d) <u>Galvanostatic Transients for the Potassium Trifluoroacetate-Trifluoroacetic Acid (100%) System</u>

The qualitative features of the transients (Fig. LV)

Figure LV

Galvanostatic reversed pulse discharge curves for the Kolbe reaction with trifluoroacetate in 100% trifluoroacetic acid (5°C):

(a) Pt, anhydrous CF_3COOH, 1M CF_3COOK

(1) 7.3×10^{-6} a.cm.$^{-2}$ (166 sec.) 0.2 v.cm.$^{-1}$; 0.1 sec.cm.$^{-1}$ (no arrest region).

(2) 6×10^{-3} a.cm.$^{-2}$ (314 sec.) 0.5 cm.$^{-1}$; 10 msec.cm.$^{-1}$ C = 264 μF; q = 90 μc.cm.$^{-2}$

(b) Pd, anhydrous CF_3COOH, 1M CF_3COOK.

(1) 7.9×10^{-6} a.cm.$^{-2}$ (304 sec.) 0.1 v.cm.$^{-1}$; 0.2 sec.cm.$^{-1}$ C = 83 μF; q = 40 μc.cm.$^{-2}$

(2) 9.2×10^{-4} a.cm.$^{-2}$ (164 sec.) 0.2 v.cm.$^{-1}$; 20 msec.cm.$^{-1}$ C = 171 μF; q = 83 μc.cm.$^{-2}$

(3) 6.7×10^{-3} a.cm.$^{-2}$ (326 sec.) 0.5 v.cm.$^{-1}$ 10 msec.cm.$^{-1}$ C = 400 μF; q = 100 μc.cm.$^{-2}$

(c) Au, anhydrous CF_3COOH, 1M CF_3COOK.

(1) 6×10^{-5} a.cm.$^{-2}$ (204 sec.); 0.5 v.cm.$^{-1}$; 0.2 sec.cm.$^{-1}$ C = 64 μF; q = 96 μc.cm.$^{-2}$

(2) 1.8×10^{-3} a.cm.$^{-2}$ (309 sec.); 0.5 v.cm.$^{-1}$ 20 msec.cm.$^{-1}$ C = 70 μF; q = 88 μc.cm.$^{-2}$

(3) 7.2×10^{-3} a.cm.$^{-2}$ (304 sec.); 0.5 v.cm.$^{-1}$; 5M sec.cm.$^{-1}$ C = 82 μF; q = 72 μc.cm.$^{-2}$ (intermediate region at inflection gives capacity approx. 200 μF.cm.$^{-2}$).

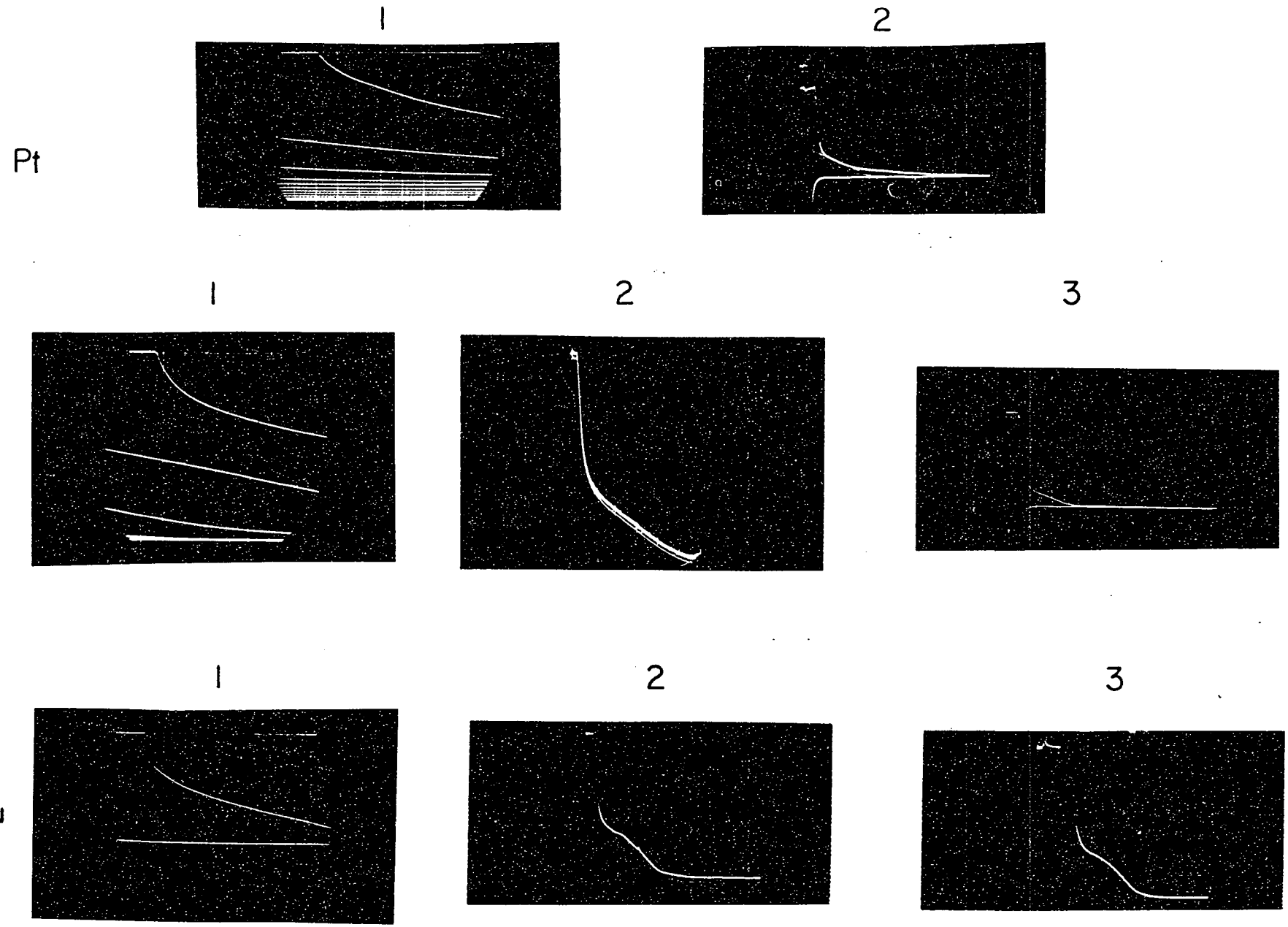
1
2
Pt
1
2
3
Pd
1
2
3
Au

were similar to those observed in the formate-formic acid system except that the arrests were generally much shorter at a given current density indicating a rather lower surface concentration of adsorbed species. The galvanostatic reversed pulse cathodic transients for the anhydrous trifluoroacetate system at the three metals Pt, Pd and Au consistently indicate short arrests of about 30-100 μ coulombs cm^{-2} of apparent electrode area* which, with an area of the species $CF_3COO^{\bullet}$ taken as 25 $\mathring{A}^2$ from Courtauld models, corresponds to apparent fractional coverages of about 0.36-1.7; with a real apparent area factor (cf. 136) of about 3, these coverages would all become <u>less</u> than a monolayer. Also, a similar build-up of an adsorbed layer with time of polarisation (Figure XLII) is observed as in the formate-formic acid system, but the limiting thickness does not exceed that corresponding to 50-80 μcoulombs cm^{-2}, i.e. a monolayer.* This is further confirmation that for the trifluoroacetate reaction in anhydrous trifluoroacetic acid, the process occurs on a more or less completely filled surface at current-densities above that for the transition behavior, or passivation (typical transition phenomena as discussed in the formate case are also observed), and barrier-

---

* A monolayer of $CF_3COO^{\bullet}$ (25 $\mathring{A}^2$) corresponds to about 66 μ coulombs cm^{-2} of real area.

layer films of appreciable thickness are therefore not involved. These conclusions reached here in regard to surface coverage will be seen subsequently to be of importance in the discussion of the kinetics. The detailed data, obtained from cathodic reversed pulse discharge transients, for surface charge, coverage and mean pseudo-capacity are summarised in Table X. Extended polarisation prior to discharge increases the coverage and pseudo-capacity somewhat as seen from the Table; the capacity and coverage also depend on current density (or potential) as expected.

(e) Significance of Tafel Slopes for the Kolbe Reaction

(i) Trifluoroacetate-Trifluoroacetic Acid (100%) System

The observed slopes Figures XXI-XXIII above the transition region are consistently above 2RT/F and approach values between 0.24 v and 0.38 v (i.e. about 4RT/F or 6RT/F). Slopes higher than 2RT/F can, in principle, be explained in terms of barrier layer films as discussed previously for processes at anodic oxide films (81,87); under such conditions the slope is proportional to the thickenss of the film and the transfer coefficient for a single electron charge transfer step becomes a/D where a is the half-jump distance or barrier half-width (see Figure II) and D is the thickness of the film. The observed slopes thus would correspond, as in the oxygen evolution reaction at gold and palladium-gold alloys (87),

Table X

Surface Charge q_s, coverage θ and Mean Pseudo-Capacity C in the Trifluoroacetate Reaction

(from cathodic reversed pulse discharge transients)

i $a.cm.^{-2}$	E_H v.	q_s ($\mu c.cm.^{-2}$)	θ	C $\mu F.cm.^{-2}$	Previous Polarisation time (sec).
Pd 1M CF_3COOK/CF_3COOH system					
7.9×10^{-6}	0.960	23	0.36	47	75.6
	1.030	45	0.70	80	159
	1.070	40	0.76	83	304
9.15×10^{-4}	1.860	41	0.64	147	7.2
	2.070	58	0.89	122	87.5
	2.120	83	1.02	171	164
6.7×10^{-3}	2.310	70	1.1	185	18.1
	2.340	80	1.25	259	91.2
	2.345	80	1.25	244	163
	2.345	100	1.25	400	326
Pt 1M CF_3COOK/CF_3COOH system					
7.7×10^{-4}	2.050	20	0.31	82	188
	2.050	22	0.33	86	311
6.05×10^{-3}	2.13	54	1.1	362	13.6
	2.14	67	1.3	211	78
	2.13	74	1.4	255	159
	2.13	90	1.7	276	310
	2.13	90	1.7	264	314

(Continued on next page)

Table X - Continued

Au 1M CF_3COOK/CF_3COOH					
1.76×10^{-3}	2.91	26	0.41	85	14.8
	2.93	27	0.43	75	19.1
	3.02	29	0.45	107	78
	3.04	30	0.47	142	121
	3.05	30	0.47	113	204
7.15×10^{-3}	3.175	36	0.56	97	2.3
	3.200	39	0.61	197	33
	3.215	43	0.67	295	79
	3.220	43	0.67	143	115
	3.220	47	0.72	111	203
	3.220	72	0.78	82	304

Notes on Table X

1. θ values are based on an area of 25 $\AA^2$ for the $CF_3COO^\bullet$ radical assuming no free area between groups. The corresponding effective molecular area for a square lattice arrangement will be $4/\pi$ times larger and value of the charge for $\theta = 1$ will be $4/\pi$ times smaller.
2. The values quoted in this table are all calculated for the apparent electrode area.
3. θ and mean C values are calculated from the arrest region in the cathodic discharge transients.
4. The derived data recorded in this table were calculated from measurements on 10 x enlargements of the oscilloscope photographs.

to a film thickness of the order of two to three monolayers.

Coulombic yields are satisfactory and amount to 96% of the theoretical yield based on reaction I. Also the correct ratio of C_2F_6 (except for small traces of CF_4 [less than 2%] at low current densities) to CO_2 for passage of two Faradays is observed in CO_2 saturated solutions (see Table II). It is on account of the observation of the high coulombic yields that the kinetics in pure trifluoroacetic acid can be discussed almost exclusively in terms of the overall reaction I above.

The appreciable coverages observed are inconsistent with reaction II being rate-determining and indicate a relatively slow desorption step. The recombination slopes RT/2F (or RT/F) for IV are not observed under any conditions so that it can be stated fairly unambiguously that the radical coupling reaction IV cannot be rate-determining. The nature of the products does not indicate a carbonium ion desorption mechanism, so that III or V are probably the only rate-determining steps which can be formulated in accordance with all the experimental data. The coverage results indicate appreciable values of θ so that the kinetic treatment for appreciable coverages ($\theta \doteqdot 0.5$) must probably be preferred. For reaction III rate-determining, Tafel slopes of $\frac{2RT}{F}\frac{r_1}{r_1-r_2}$ and a limiting current are predicted by the heterogeneity and induction models, respectively. All observed slopes for the non-aqueous system are much greater than 2RT/F ($\beta \doteqdot 1/2$). In

terms of the intrinsic heterogeneity model, the high slopes observed could in principal (but see below) be explained with values of r_1 which are about 1.2-2 times r_2; thus for $r_2 = 1/2\ r_1$ the Tafel slope is 4RT/F and with $r_2 = \frac{2}{3}\ r_1$ the slope is 6RT/F. As in the formate case, it is reasonable to assume that r_1 for the adsorption of the bulky polar $CF_3COO^\bullet$ group is greater than that for the small $CF_3^\bullet$ group. As we have mentioned above, it should be noted that high anodic slopes could, in principle be explained on the basis of charge transfer across barrier layer films (81,87) as in the formation of anodic oxide layers in oxygen evolution. However, for the present reaction, with the observed real fractional coverages of less than unity in most cases, this explanation is inconsistent with the experimental data as it implies a barrier film thickness D of at least four to six times the half-jump distance a ($\beta \doteq a/D$). It will be noted that the high slopes always occur <u>above</u> the transition region, that is, where the surface, as in the formate case, is probably already more or less filled by the trifluoroacetoxy radicals. In such a case, the "Temkin" slopes deduced for reaction III are actually inapplicable since the coverage by $CF_3COO^\bullet$ is either high or unity (Langmuir conditions) and hence potential independent. A potential-dependent desorption step such as V (or VI) proceeding on the more or less completely covered surface appears therefore to be indicated as the likely mechanism in the upper Tafel region. The metal

solution interface can then be represented as a complex double-layer with a potential difference across the layer of $CF_3COO^\bullet + CF_3^\bullet$ radicals and a further potential difference across the usual ionic double-layer. The potential profile will hence be as qualitatively shown in Figure LVI, i.e. with a surface dipole double-layer and an ionic double-layer beyond its limit at the interface with the solution. The effective symmetry factor is then appreciably less than 0.5 if the activated state in the charge transfer desorption reaction V falls within the limits of the ionic double-layer and an appreciable fraction of the total metal-solution p.d. falls across the dipole double-layer.* The same effects need <u>not</u> arise in the formate reaction where the rate of decomposition of the adsorbed radical layer itself can be potential dependent at high coverage by the reaction

$$HCOO^\bullet \longrightarrow CO_2 + H^+ + e \qquad \text{VI}$$

as discussed previously. This is consistent with the normal (ca. 2RT/F) slopes observed in the upper Tafel region in the formate decomposition.

(ii) <u>Significance of the Transition Region and Critical Potential in the Kolbe Reaction</u>

Since different mechanisms for an overall electrode

* This model is actually a variant of the barrier-layer model except that no separate process of potential dependent activated transport of charge-carriers within a film of significant thickness is involved.

Figure LVI

Schematic representation of surface layer at electrode with adsorbed trifluoroacetate radicals.

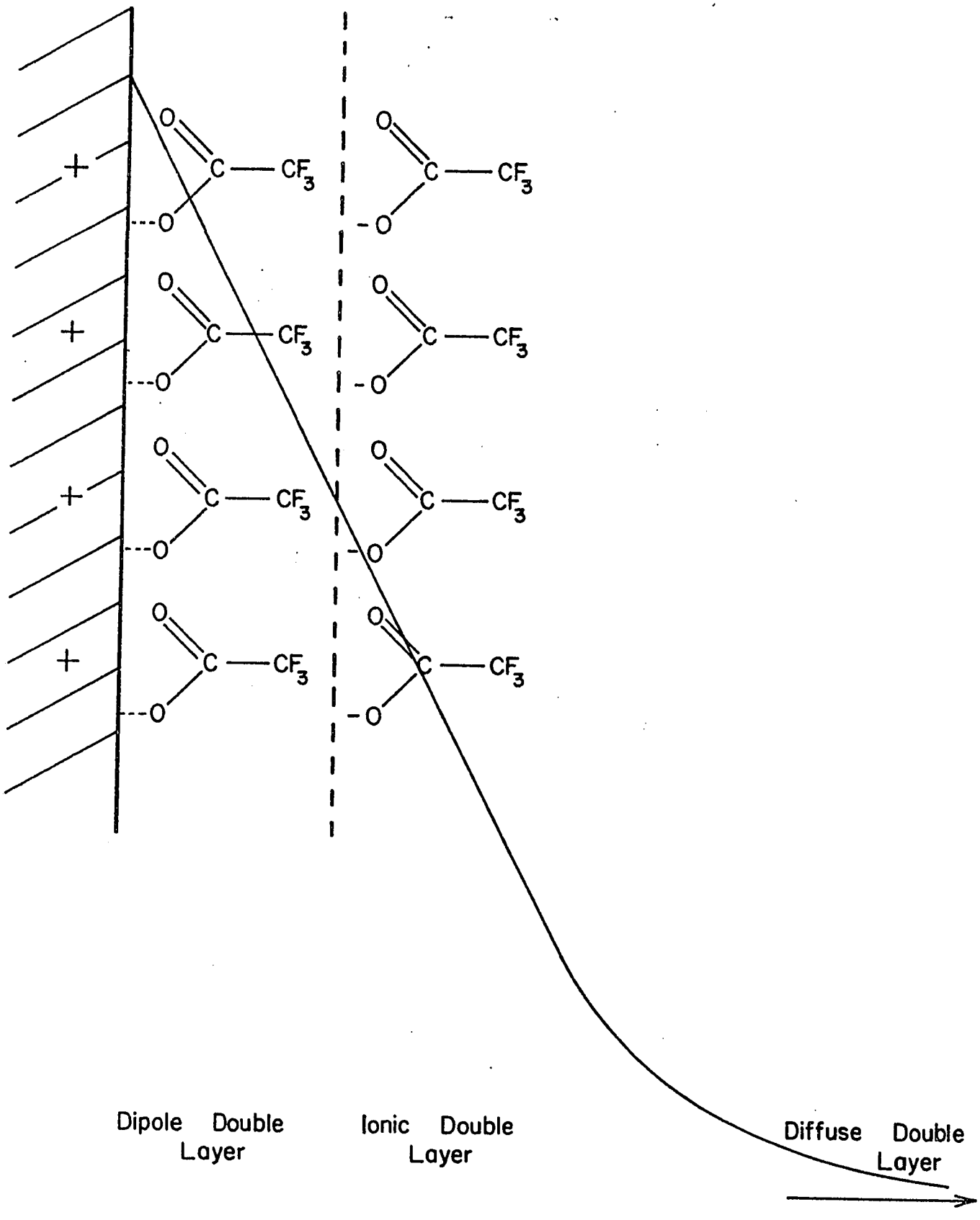
Dipole Double Layer
Ionic Double Layer
Diffuse Double Layer

reaction usually have a different dependence of rate upon the potential, the mechanism which is favoured at one potential at a given electrode might no longer be favoured at a different potential. In this manner a change in the mechanism of an overall reaction may occur as the potential is varied. We have suggested above (Section c.1) that in the lower potential region, as the potential is increased, the relevant rate-determining step can no longer maintain the current being passed so that a limiting current is eventually attained. Further increase of current can then only occur if the electrode potential then increases rapidly as the surface concentration of intermediates, (in this case the adsorbed carboxylate radicals RCOO•) builds up until a potential is reached at which some other mechanism in the overall electrode reaction can proceed at a rate sufficient to carry higher current for the overall reaction. This can be understood by considering Figure LVII.

The lines I and II represent hypothetical Tafel lines for two different alternative reaction mechanisms occurring, respectively, on the relatively bare and the completely covered surface. The overall rate of the reaction will be governed by the faster reaction;* thus in region I, reaction I will tend to occur much faster than reaction II at the same

---

* This is analogous to the treatment given in the case of alternative and consecutive reactions which has been discussed elsewhere (119,120).

Figure LVII

Schematic representation of a change of mechanism for the case of coverage dependent alternative reactions.

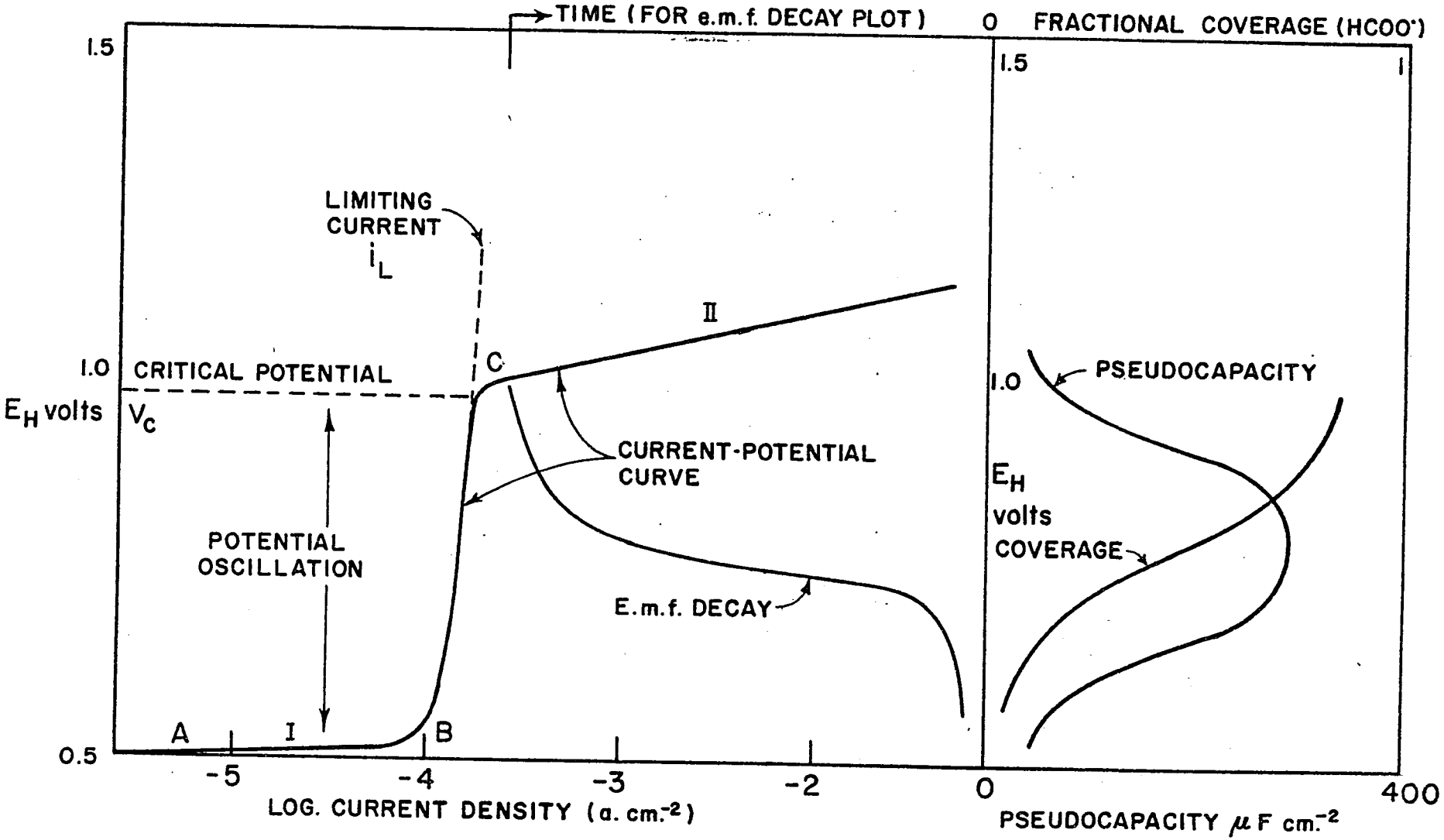
TIME (FOR e.m.f. DECAY PLOT)
0 FRACTIONAL COVERAGE (HCOO⁻)
1.5
1.0
0.5
E_H volts
LIMITING CURRENT
i_L
CRITICAL POTENTIAL
V_C
II
C
CURRENT-POTENTIAL CURVE
POTENTIAL OSCILLATION
E.m.f. DECAY
A
I
B
-5
-4
-3
-2
LOG. CURRENT DENSITY (a. cm.⁻²)
1.5
1.0
I
PSEUDOCAPACITY
E_H volts
COVERAGE
0
400
PSEUDOCAPACITY μF cm.⁻²

potential since the exchange current i_{o_I} will be greater than $i_{o_{II}}$ for the lines I and II, respectively, and reaction II is in any case fictitious below the current i_L unless hysteresis occurs in the current-potential relation. However as the rate increases and the point B is approached, the rate-determining reaction in region I can for example, if it is a first order decomposition step, no longer maintain the current and a limiting current or transition region is observed. The potential then increases, the rate remaining almost constant, until the point C is reached where some other new potential-dependent reaction mechanism II, now controlling the kinetics of the overall reaction, can occur at a rate sufficient to carry increased currents even though $i_{o_I} > i_{o_{II}}$ since the rate-determining step in region I has a limiting current (or rate).

For this reason we believe that a critical current density rather than a critical potential determines the course of the Kolbe or formate decarboxylation reactions, since it is only because the rate-determining step in region I reaches a limiting current that the potential can rise to the region II at which some other rate-determining mechanism can occur which can be driven at the appreciable rates, e.g. 10^{-2}-10^{-1} a.cm.$^{-1}$, normally necessary for reasonably rapid collection of Kolbe product gases. The critical potential itself (the top of the transition region) appears to have no special significance for

formation of the dimeric Kolbe product, however, (as claimed by Pande and Shukla) since we observe the coupled product C_2F_6 below the transition region in the trifluoroacetate reaction as well as above it.

At potentials beyond V_C (corresponding to the position C) the potential dependent reaction II provides an alternative kinetically easier current pathway than reaction I proceeding almost independent of potential at the limiting rate $i_{L_{(I)}}$. The "critical potential" is then simply defined by the intersection of the limiting current-potential relation for step I with the normal linear logarithmic relation for the potential dependent rate of step II.

In the formate case, the step II which is alternative to step I is then the reaction

$$HCOO^{\bullet}(M) \longrightarrow H^{+} + CO_2 + e$$

where the current density corresponds to the unimolecular decomposition step

$$HCOO^{\bullet} \longrightarrow H^{\bullet} + CO_2$$

proceeding at $\theta_{HCOO^{\bullet}} \longrightarrow 1$.

In the trifluoroacetate case the limiting process at low current densities would be the step*

* This step is consistent with the deduction of Wilson and Lippincott (53) that a first order decomposition of $CH_3COO^{\bullet}$ (in the acetate case) is involved.

$$CF_3COO^{\bullet} \longrightarrow CF_3^{\bullet} + CO_2$$

analogous to that above for the formate case but the continuing potential-dependent process leading to the upper Tafel lines of high slope (4RT/F to 6RT/F) would be either of the desorption steps

$$CF_3^{\bullet} + CF_3COO^{-} \longrightarrow C_2F_6 + CO_2 + e$$

or

$$CF_3COO^{\bullet} + CF_3COO^{-} \longrightarrow C_2F_6 + 2CO_2 + e$$

as we have discussed previously.

E. REACTIONS IN AQUEOUS SOLUTION

Several experiments were carried out in aqueous solutions of potassium trifluoroacetate in order to compare qualitatively the kinetic behavior under idealised conditions in the wholly non-aqueous trifluoroacetate system with that in the aqueous solutions more usually used in conducting the Kolbe reaction.

The runs in aqueous CF_3COOK exhibit slopes greater than 2RT/F (0.25-0.30 v) in the upper region only at platinum electrodes, (Figure XXV), while at palladium or gold (Figures XXVI, XXVII) the slopes are between 0.08 v and 0.12 v There is usually hysteresis near the transition region, between the results obtained for increasing and decreasing polarising currents suggesting irreversibility in the film forming process. At platinum, (Figure XXV) there appears to be a small second transition region at a current density of 2×10^{-3} amp.cm^{-2}

possibly corresponding to that mentioned for the aqueous acetate case by Dickenson and Wynne-Jones (122). This is not observed at palladium or gold.

During the course of polarisation measurements, visible (oxide) film formation was always observed to occur. Coulombic yield measurements on the gaseous products showed, in fact, that oxygen was the principal product (87-95%) at Au and Pd with only ca. 5% CO_2 and very little C_2F_6. At Pt, Kolbe yields up to 25% with O_2 were observed. As in the aqueous formate case discussed previously, no simple relationship between the kinetics of the two reactions, when they occur together can be proposed. The kinetics of both reactions will be altered considerably when they occur simultaneously, as we have shown in the formate case and as has been shown for the case of oxygen evolution in the presence of acetate ions (49). Evidently at Au and Pd, oxide films of appreciable thickness and stability are formed and almost completely inhibit the trifluoroacetate discharge.

F. COMPARISONS WITH RECENT WORK

The current-potential measurements obtained in the present investigation follow the pattern indicated by previous workers in other systems e.g., with acetate (29,122), while the results on the presence of oxygen in the anode gas from decarboxylation in aqueous solutions are in general agreement with the results of previous investigations on the Kolbe reaction in aqueous solutions of aliphatic acids and confirm the complexity of the reaction in aqueous solutions where side reactions can be appreciable.

Most of the previous work has been concerned (i)

with characterisation of the variety of products which are normally found in the aqueous Kolbe reaction and (ii) with postulation of reaction steps that could explain the origin of such products. Virtually no rigorous electrochemical kinetic analysis of possible steps in the Kolbe reaction has been given previously, including the recent work of Dickenson and Wynne-Jones (122). Similarly, for the formate decarboxylation reaction, no previous experimental or theoretical electrochemical kinetic work has been done, the only previous studies, as we have mentioned above, being concerned with qualitative aspects of the reaction, such as the lack of hydrogen production at the anode.

In the earlier studies on the Kolbe reaction, it has been observed that the Kolbe products are only observed in appreciable yield when some critical potential has been reached, and this has been considered to be the potential at which carboxylate ions begin to be discharged (27,28). In the light of the present work, this conclusion must now be considered to be incorrect since we have shown by galvanostatic studies and pseudo-capacitance measurements that the transition region corresponds to adsorption on the electrode surface of discharged carboxylate ions. A similar conclusion has been reached for the aqueous acetate case (122). Furthermore, the reversible potentials for the reaction are much less anodic than the critical potentials so that the carboxylate ions must be discharged at a finite rate at all potentials more anodic than

the reversible potential.

Pande and Shukla (29) in a recent paper have stated that this critical potential represents the potential at which discharged carboxylate ions split into an alkyl radical and carbon dioxide, thus

$$RCOO^{\bullet} \longrightarrow R^{\bullet} + CO_2$$

Below the critical potential, the entire carboxylate radical is considered to take part in any possible reaction with the solvent, OH radicals or simultaneously produced atomic oxygen.

The conclusions reached by Pande and Shukla, we believe, are misleading since olefin formation and saturated hydrocarbons possessing half the number of carbon atoms of the main Kolbe products are found (56,58,60), as the authors have themselves observed, before the critical potential is reached so that it is difficult to understand the origin of such products unless in fact the $RCOO^{\bullet}$ radicals do split to produce $R^{\bullet}$ radicals which then form the observed non-dimeric Kolbe products by H-abstraction or disproportionation reactions.

Pande and Shukla have postulated mechanisms to account for the observed products, which appear to contradict the experimental results. The authors state that the reaction

$$RCOO^{\bullet} \longrightarrow R^{\bullet} + CO_2$$

can only occur in the upper potential region, and that the

alkyl radical can then either couple with another alkyl radical to give the Kolbe product, or react with the carboxylic acid to give a saturated hydrocarbon containing one carbon atom less than the starting material by abstracting hydrogen from the carboxyl group, thus

$$R^{\bullet} + RCOOH \longrightarrow RH + RCOO^{\bullet}$$

Olefin formation is ascribed to a reaction between a hydroxyl radical and a carboxylate radical, thus

$$CH_3CH_2CH_2COO^{\bullet} + OH^{\bullet} \longrightarrow CH_3\text{-}CH_2\text{=}CH_2 + H_2O + CO_2$$

The mechanisms postulated by Pande and Shukla for the Kolbe reaction and some side reactions cannot be upheld on the basis of experimental results of several authors. In fact, it appears that Pande and Shukla are unaware of several publications on the Kolbe reaction (their latest reference being to work done in 1936) as we have discussed in the Introduction.

Experimentally it has been shown (56,57) by isotopic substitution that methane formation in the electrolysis of aqueous acetate solutions arises when the methyl radical abstracts hydrogen from the α-carbon atom in the acetate ion, thus

$$CH_3^{\bullet} + CH_3COO^{-}/D_2O \longrightarrow CH_4 + {}^{\bullet}CH_2COO^{-}$$

and that the isotopic composition of the reaction products was determined solely by the isotopic composition of the acetate

ion and not by that of the solvent water.

Similarly, isotopic substitution studies have shown (56,60) that olefins are formed from alkyl radicals by splitting of the hydrogen atom originally in the β-position to the carboxylate group. The formation of olefins and paraffins containing one carbon atom less than the starting material was shown (60) to occur by disproportionation of the resulting alkyl radicals, i.e. in the case of butyrates

$$2CH_3CH_2CH_2^{\bullet} \longrightarrow CH_3CH{=}CH_2 + CH_3CH_2CH_3$$

Hence the reaction between a hydroxyl radical and a carboxylate radical as postulated by Pande and Shukla (29) in olefin formation is not confirmed experimentally. The formation of saturated hydrocarbons containing one carbon atom less than the starting material (see above) also cannot be upheld on the basis of previous work as we have discussed above; in the case of the triluforoacetate-trifluoroacetic system, the Kolbe product has been observed at low current densities below the "critical potential" as we have discussed earlier.

Since the present experimental studies were completed, Dickenson and Wynne-Jones (122) have published some new results for the aqueous acetate system which have been mentioned above. The experimental approaches have been similar to those described here and which we had described (124) and published (123) prior to the date of submission of their results.

Their experimental results agree with ours in so far as it is concluded that adsorbed carboxylate radicals are important in the Kolbe reaction as we have discussed above. The authors, however, postulate no detailed electrochemical mechanisms for the reactions occurring (in their case in aqueous acetate solution) and do not consider the theoretical electrochemical kinetics of possible steps in the reaction. The experimental results, i.e. Tafel lines and e.m.f. decay curves, show the complexity of the reaction when aqueous solutions are employed and several concomitant processes (i.e. oxide film formation, oxygen evolution and the Kolbe reaction) can occur simultaneously.

Dickenson and Wynne-Jones (122) have considered the transition region and their conclusions which were only qualitative agree with the quantitative deductions we have made about the behavior of adsorbed discharged carboxylate radicals in relation to the origin of the transition region. The authors attribute the upper potential region to the difficulty of discharging carboxylate ions onto a surface <u>covered</u> with adsorbed carboxylate radicals. This implies that charge transfer across a barrier layer film is difficult as in the oxygen evolution reaction (81,87) where anodic barrier oxide layers are formed. If this were the case, the Tafel slopes observed by Dickenson and Wynne-Jones in the aqueous acetate system should have much higher values than those actually observed (2RT/F).

As we have discussed previously (p. 148), if a charge transfer barrier is present, the transfer coefficient α_T for the process occurring at the electrode has the form $\alpha_T = \alpha_s\alpha_f/\alpha_s+\alpha_f$ where α_f and α_s are the transfer coefficients for the film and surface oxidation reactions, respectively. Hence for any reasonable values of the transfer coefficients Tafel slopes appreciably greater than 2RT/F should have been observed.

In the present investigation, we have concluded on the basis of a detailed electrochemical kinetic treatment and quantitative capacitance measurements that the upper potential region arises because of a change of mechanism, as we have discussed previously (pp. 247-253).

The mechanism of charge transfer across barrier layer films is still speculative as little is known concerning the structure or semi-conducting properties of these films. In the aqueous system, the situation is even more complicated as evidenced by the decay transients (see Figure LIV) observed in the present investigation and by Dickenson and Wynne-Jones (122) where the formation of at least two types of layers is indicated, i.e. one due to an oxide film and one to adsorbed discharged carboxylate radicals.

It is clear that the electrochemical aspects of the Kolbe reaction in aqueous media can be elucidated completely only when much more is known about competitive anodic processes,

especially with regard to the mechanism of the oxygen evolution reaction in the presence of foreign ions such as aliphatic carboxylates, which can be discharged at significant rates over the same range of potentials as oxygen is anodically evolved.

CLAIMS TO ORIGINAL RESEARCH

In the present work, a considerable degree of originality is claimed since the formate decarboxylation reaction has never previously been studied with regard to its electrochemical kinetics or with regard to the behavior of adsorbed intermediates in this reaction. Similarly, in the case of the Kolbe reaction itself, the present work constitutes the first attempt to analyse the observed electrochemical kinetic behavior (for conditions where the reaction pathway is unambiguous) in quantitative kinetic terms related to plausible consecutive reaction schemes.

More specific claims are as follows:

1) The formate decarboxylation has been studied in both non-aqueous and aqueous solutions at various metals as a model reaction for the Kolbe electrosynthesis.

2) It is shown that the reaction proceeds by a pathway involving a process analogous to passivation with a reproducible critical limiting current behavior associated with completion of a monolayer of reaction intermediates ($HCOO^{\bullet}$ radicals). This limiting behavior is shown to be succeeded by another potential dependent process at higher current densities. The overall reaction has been shown to be simply the decarboxylation

$$HCOO^{-} \longrightarrow H^{+} + CO_2 + 2e.$$

3) The kinetic parameters for the current-potential behavior observed in the formate reaction at various metals have been deduced for aqueous and non-aqueous solutions, including the respective exchange currents.

4) Theoretical kinetic deductions for the current-potential behavior for the various possible consecutive reaction steps have been made and were based both on Langmuir and Temkin adsorption behavior of the reaction intermediates.

5) The type of isotherm applying to the reaction intermediates ($HCOO^{\bullet}$) in the formate reaction was experimentally deduced by a new method of calculation of adsorption pseudo-capacitance as a function of potential, obtained from a quantitative analysis of polarisation and e.m.f. decay curves.

6) On the basis of the above calculations, the origin of the transition region in the formate and Kolbe decarboxylation reactions was deduced and assignments of reaction mechanism were made.

7) The role of oxygen evolution in the aqueous formate decarboxylation reaction was investigated and is discussed in relation to the kinetics of oxygen evolution itself at the metals studied.

8) A unique phenomenon of autocatalytic delayed gas evolution was observed during the work and its origin elucidated by quantitative comparison of gas evolution delay times with the arrests observed in the open-circuit e.m.f. decay behavior.

9) Similar approaches have been made to the Kolbe reaction itself with trifluoroacetate in both non-aqueous and aqueous solutions at various metals. The system chosen gives minimal side reactions so that the kinetics can be examined with little ambiguity regarding the pathway of the reaction in non-aqueous media.

10) Theoretical kinetic deductions for the current-potential behavior for various consecutive reaction steps in the trifluoroacetate reaction have been made and were based both on Langmuir and Temkin adsorption behavior of the reaction intermediates.

11) The behavior of adsorbed intermediates has been examined as in the formate case, by d.c. transient studies.

REFERENCES

1. M. Faraday, Pogg. Ann., 33, 438 (1834).
2. H. Kolbe, Liebieg Ann., 69, 257 (1849).
3. E.J. Corey, R.R. Saurs and S. Swann, J. Am. Chem. Soc., 99, 5826 (1957).
4. K. Mislow and W.C. Meluck, J. Am. Chem. Soc., 78, 5920 (1956).
5. B.C.L. Weedon, Quart. Rev., 6, 380 (1952).
6. M.J. Allen, Organic electrode processes, Rheinhold Publishing Corporation, New York, 1958, pp. 95-115.
7. C.J. Brockman, Electro-organic chemistry, John Wiley and Sons, New York, 1926, pp. 23-78.
8. S. Glasstone and A. Hickling, J. Chem. Soc., 1878 (1934).
9. S. Glasstone and A. Hickling, J. Chem. Soc., 820 (1936).
10. S.N. Shukla and O.J. Walker, Trans. Faraday Soc., 27, 692 (1931).
11. H. Hofer and M. Moest, Annalen., 323, 285 (1902).
12. J. Petersen, Z. Elektrochem., 18, 710 (1912).
13. S. Swann, Trans. Electrochem. Soc., 56, 457 (1929).
14. F. Fichter and R.E. Meyer, Helv. Chim. Acta, 17, 535 (1934).
15. F. Fichter and T. Holbro, Helv. Chim. Acta, 20, 333 (1937).
16. F. Fichter and H. Stenzel, Helv. Chim. Acta, 22, 970 (1939).
17. D.A. Fairweather, Proc. Roy. Soc., (Edin.), 45, 23 (1925).
18. R.P. Linstead, B.R. Shephard and B.C.L. Weedon, J. Chem. Soc., 3624 (1952).

19. F. Fichter, H. Stenzel and E. Beglinger, Helv. Chim. Acta, 21, 375 (1938).

20. M. Matsui and K. Kizaki, Mem. Coll. Sci. Kyoto, 16A, 297 (1933).

21. E. Baur, Helv. Chim. Acta, 11, 372 (1928).

22. F. Swarts, Bull. Soc. Chim. Belg., 42, 102 (1933).

23. K. Hopfgartner, Monatsh., 32, 523 (1911).

24. J. Salause, Bull. Soc. Chim. France, 37, 522 (1925); Compt. rend., 180, 662 (1925).

25. D.A. Fairweather and O.J. Walker, J. Chem. Soc., 3111 (1926).

26. G.E. Svadkovskaya and S.A. Voitkevich, Uspekki Khimii, S.S.S.R., 29, 161 (1960).

27. S.N. Shukla and O.J. Walker, Trans. Faraday Soc., 27, 722 (1931).

28. G. Preuner and E.B. Ludlam, Z. Physikal. Chem., 59, 682 (1907).

29. G.S. Pande and S.N. Shukla, Electrochimica Acta, 4, 215 (1961).

30. S. Glasstone and A. Hickling, Trans. Electrochem. Soc., 75, 333 (1939).

31. E. Yeager and F. Hovorka, J. Electrochem. Soc., 98, 14 (1951).

32. J. O'M. Bockris, J. Chem. Phys., 24, 817 (1956).

33. B.E. Conway and P.L. Bourgault, Can. J. Chem., 37, 292 (1959); 38, 1557 (1960); 40, 1690 (1962).

34. M.J. Allen, Loc. cit. ref. 6, pp. 99.

35. G. Thiessen, Rec. Chem. Prog., 21, 243 (1960).

36. C. Schall, Z. Elektrochem., 3, 83 (1896).

37. F. Fichter, Trans. Electrochem. Soc., 75, 309 (1939).

38. F. Fichter, ibid., 56, 8 (1929).

39. F. Fichter, Organische electrochemie, Dresden, 1942.

40. F. Fichter and R. Zumbrunn, Helv. Chim. Acta, 10, 869 (1927).

41. F. Fichter and H. Buess, Helv. Chim. Acta, 18, 445 (1935).

42. M.S. Kharasch, J.L. Rowe and W.H. Urrey, J. Org. Chem., 16, 905 (1951).

43. M. Levy, M. Steinberg and M. Szwarc, J. Am. Chem. Soc., 76, 5978 (1954).

44. A. Rembaum and M. Szwarc, J. Am. Chem. Soc., 77, 3486 (1955).

45. C. Walling, Free radicals in solution. John Wiley and Sons, New York, 1957, pp. 581.

46. E.W.R. Steacie, Atomic and free radicals reactions, Rheinhold Publishing Corporation, New York, 1954.

47. S. Goldschmidt, W. Leicher and H. Haas, Annalen, 577, 153 (1952).

48. S. Goldschmidt and M. Minsinger, Chem. Ber., 87, 956 (1954).

49. J. O'M. Bockris, Nature, 159, 401 (1947): Disc. Faraday Soc., 1, 229 (1947).

50. T.I. Boresova and V.I. Veselovskii, Zhur. Fiz. Khim., 27, 1195 (1953).

51. M. Haissinsky and M. Cotton, Compt. rend., 224, 392, 467 (1947).

52. M. Haissinsky, J. Chim. phys., 44, 181 (1947).

53. C.L. Wilson and W.J. Lippincott, J. Am. Chem. Soc., 78, 4290 (1956); J. Electrochem. Soc., 103, 672 (1956).

54. A. Crum-Brown and J. Walker, Annalen, 261, 107 (1891).

55. S.N. Shukla and O.J. Walker, Trans. Faraday Soc., 28, 457 (1932).

56. P. Holeman and K. Clusius, Z. Physikal. Chem., 35B, 261 (1937).

57. K. Clusius and W. Schanzer, Z. Physikal. Chem., 192A, 273 (1943).

58. W. Schanzer and K. Clusius, Z. Physikcal. Chem., 190A, 241 (1941).

59. N.L. Bauld, Ph.D. Thesis, Univ. of Illinois, Urbana, Illinois, 1959.

60. A. Kruis and W. Schanzer, Z. Physikal. Chem., 191A, 301 (1942).

61. M. Ya. Fioshim and Yu B. Vasil'ev, Doklady Akad. Nauk., S.S.S.R., 134, 879 (1960).

62. C.L. Wilson and T. Hayashi, Abstracts of Papers Presented at the 126th Meeting of the American Chemical Society, New York. 1954. pp. 78.

63. L.F. Fieser, R.C. Clapp and W.H. Daudt, J. Am. Chem. Soc., 22, 2052 (1942).

64. W.B. Smith and H.G. Gilde, J. Am. Chem. Soc., 31, 5325 (1959).

65. W.B. Smith and H.G. Gilde, J. Am. Chem., Soc., 32, 659 (1960).

66. T.P. Hoar, Modern aspects of electrochemistry, ed. J.O'M. Bockris, Butterworths Scientific Publications New York. 1959. Vol. II, Chapter IV.

67. Y.M. Kolotyrkin, I.C.P.M., 1957. Z. Elektrochem., 62, 664 (1958).

68. U.R. Evans, Nature, 126, 130 (1930).

69. U.R. Evans, I.C.P.M., 1957. Z. Elektrochem., 62, 619 (1958).

70. Fr. Flade, Z. Physikal. Chem., 76, 513 (1911).

71. E.S. Hedges, J. Chem. Soc., 1533 (1926).

72. E.S. Hedges, J. Chem. Soc., 1029 (1929).

73. K.F. Bonhoeffer and H. Gerischer, Z. Elektrochem., 52, 149 (1948).

74. R.S. Cooper and J.H. Bartlett, J. Electrochem. Soc., 105, 115 (1958).

75. U.F. Franck, Z. Elektrochem., 62, 649 (1958); Z. Physikal. Chem., 3, 183 (1955).

76. J.O'M. Bockris and A.K.M. Shamshul Huq, Proc. Roy. Soc., 237A, 277 (1956).

77. M. Brieter, C.A. Knorr and W. Volkl, Z. Elektrochem., 59, 681 (1955).

78. L. Young, Anodic oxide films, Academic Press, New York, 1961.

79. N.F. Mott, Trans. Faraday Soc., 36, 1 (1940); 43, 429 (1947).

80. N. Cabrera and N.F. Mott, Repts. Prog. in Phys., 12, 163 (1948-49).

81. R.E. Meyer, J. Electrochem. Soc., 107, 847 (1960).

82. D.A. Vermilyea, Acta Met., 1, 282 (1953).

83. L. Young, Trans. Faraday Soc., 50, 159 (1954).

84. C.P. Bean, T.C. Fisher and D.A. Vermilyea, Phys. Rev., 101, 551 (1956).

85. J.F. Dewald, J. Phys. Chem. Solids, 2, 22 (1957).

86. J.F. Dewald, J. Electrochem. Soc., 102, 1 (1955).

87. J.J. MacDonald and B.E. Conway, Proc. Roy. Soc. (London) in press (1962).

88. B.E. Conway, Trans. Roy. Soc., (Can.), 49, 19 (1960).

89. A.N. Frumkin, Acta Physicochim., 18, 23 (1943).

90. A.N. Frumkin, Diac. Faraday Soc., 1, 57 (1947).

91. A. Hickling and F.W. Salt, Trans. Faraday Soc., 38, 474 (1942).

92. J.O'M. Bockris and E.C. Potter, J. Electrochem. Soc., 99, 169 (1952).

93. H.B. Morley and F.E.W. Whetmore, Can. J. Chem., 34, 359 (1956).

94. P.L. Bourgault, Ph.D. Thesis, University of Ottawa, Ottawa, Ontario. 1961. pp. 156.

95. M.A.V. Devanathan, J.O'M. Bockris and W. Mehl, J. Electroanalytical Chem., 1, 143 (1959-60).

96. J.O'M. Bockris, Modern aspects of electrochemistry, Butterworths Scientific Publications, New York. 1959. Vol. 1, Chapter IV.

97. R. Parsons, Trans. Faraday Soc., 47, 1332 (1951).

98. U.F. Franck, Z. Naturf., 4a, 378 (1949).

99. T.P. Bowden, Proc. Roy. Soc., 125A, 446 (1929).

100. J.A.V. Butler and G. Armstrong, Proc. Roy. Soc., 137A, 604 (1932).

101. A. Hickling and D. Taylor, Trans. Faraday Soc., 44, 262 (1948).

102. B.E. Conway and E. Gileadi, Trans. Faraday Soc., in press (1962).

103. H.A. Laitinen and G. Enke, J. Electrochem. Soc., 107, 773 (1960).

104. W.R. Busing and W.J. Kauzmann, J. Chem. Phys., 20, 1129 (1953).

105. A.N. Frumkin and A. Slygin, Acta Physicochim., 5, 819 (1936).

106. K. Rosenthal, P. Dolin and B.V. Erschler, Acta Physicochim., 21, 213 (1946).

107. J.J. McMullen and N. Hackerman, J. Electrochem. Soc., 106, 341 (1959).

108. P. Ruetschi, J.B. Ockerman and R. Amlie, J. Electrochem. Soc., 107, 325 (1960).

109. J.O'M. Bockris and H. Kita, J. Electrochem. Soc., 108, 676 (1961).

110. M.A.V. Devanathan and M. Selvaratnam, Trans. Faraday Soc., 56, 1820 (1960).

111. R.R. Driesbach and R.A. Martin, Ind. Eng. Chem., 41, 2875 (1949).

112. R.E. Buckles and J.F. Mills, J. Am. Chem. Soc., 75, 552 (1953).

113. A.M. Azzam, J.O'M. Bockris, B.E. Conway and H. Rosenberg, Trans. Faraday Soc., 46, 918 (1950).

114. J.O'M. Bockris, B.E. Conway and W. Mehl, J. Sci. Instr., 33, 400 (1956).

115. J.O'M. Bockris, Disc. Faraday Soc., 1, 229 (1947).

116. E.C. Potter, Electrochemistry. Cleaver-Hume Press Ltd., London. 1956. pp. 14.

117. J.O'M. Bockris and B.E. Conway, Trans. Faraday Soc., 45, 989 (1949).

118. B.E. Conway, E.M. Beatty and P.A.D. DeMaine, Electrochimica Acta, 7, 39 (1962).

119. B.E. Conway and P.L. Bourgault, Trans. Faraday Soc., 58, 593 (1962).

120. P.L. Bourgault, Ph.D. Thesis, University of Ottawa, Ottawa, Ontario. 1961. pp. 14.

121. H. Gohr and E. Lange, Z. Elektrochem., 63, 673 (1958).

122. T. Dickenson and W.F.K. Wynne-Jones, Trans. Faraday Soc., 58, 382, 388 and 400 (1962).

123. B.E. Conway and M. Dzieciuch, Nature, 189, 914 (1961).

124. B.E. Conway and M. Dzieciuch, Abstracts of the Meeting of the Electrochemical Society, Chicago; J. Electrochem. Soc., 107, 760 (No. 199) (1960).

125. A. Eucken and B. Weblus, Z. Elektrochem., 55, 114 (1951).

126. W.L. Latimer, Oxidation potentials, 2nd ed., Prentice Hall, New York. 1952.

127. J.G.N. Thomas, Trans. Faraday Soc., 57, 1603 (1961).

128. M. Boudart, J. Am. Chem. Soc., 74, 3556 (1952).

129. G. Halsey and H.S. Taylor, J. Chem. Phys., 15, 624 (1947).

130. L. Young, Proc. Roy. Soc., A263, 395 (1961).

131. B.E. Conway and M. Dzieciuch, Proc. Chem. Soc., (London) 121 (1962).

132. V.E. Past and Z.A. Jofa, Zhur. Fiz. Khim., 33, 913 (1955).

133. G. Armstrong and J.A.V. Butler, Trans. Faraday Soc., 29, 1261 (1933).

134. B.E. Conway, M. Dzieciuch and E. Gileadi, Electrochimica Acta, in course of publication.

135. M.I. Temkin, Zhur. Fiz. Khim., 15, 296 (1941).

136. J.O'M. Bockris and B.E. Conway, J. Chem. Phys., 28, 707 (1958).

137. A. Hickling, Disc. of the Faraday Soc., 1, 227 (1947); and contributions in discussion, pp. 248-251.

138. A.N. Frumkin and A. Slygin, Acta Physicochim., 3, 791 (1935).

139. A. Slygin and B.V. Ershler, ibid., 11, 45 (1959).

140. A.N. Frumkin, P. Dolin and B.V. Ershler, ibid., 13, 779 (1949).

141. R. Parsons, Trans. Faraday Soc., 54, 1053 (1958).

142. B.E. Conway, Proc. Roy. Soc., A256, 128 (1960).

143. I. Langmuir, Trans. Faraday Soc., 17, 621 (1921).

144. C.N. Hinshelwood, Kinetics of Chemical Change, Oxford. 1940. pp. 187-190.

145. J. Hoare and S. Shuldinger, J. Electrochem. Soc., 102, 485 (1955).

146. H.J. Sand, Phil. Mag. 1, 45 (1901); see also J.A.V. Butler, Electrical phenomena at interfaces, Methuen and Co. Ltd., London, 1951. pp. 190-198.

147. L.R. Griffith, R.P. Buck, R.T. MacDonald and M.J. Schlatter, Proceedings-Fifteenth Annual Power Sources Conferences PSC. 1961. pp. 16.

148. A.V. Tobolsky and R.B. Mesrobian, Organic peroxides, Interscience Publishers Inc., New York. 1954. pp. 34.